INFORMATION TO USERS

This manuscript has been reproduced from the microfilm master. UMI films the text directly from the original or copy submitted. Thus, some thesis and dissertation copies are in typewriter face, while others may be from any type of computer printer.

The quality of this reproduction is dependent upon the quality of the copy submitted. Broken or indistinct print, colored or poor quality illustrations and photographs, print bleedthrough, substandard margins, and improper alignment can adversely affect reproduction.

In the unlikely event that the author did not send UMI a complete manuscript and there are missing pages, these will be noted. Also, if unauthorized copyright material had to be removed, a note will indicate the deletion.

Oversize materials (e.g., maps, drawings, charts) are reproduced by sectioning the original, beginning at the upper left-hand corner and continuing from left to right in equal sections with small overlaps. Each original is also photographed in one exposure and is included in reduced form at the back of the book.

Photographs included in the original manuscript have been reproduced xerographically in this copy. Higher quality 6" x 9" black and white photographic prints are available for any photographs or illustrations appearing in this copy for an additional charge. Contact UMI directly to order.

UMI

A Bell & Howell Information Company
300 North Zeeb Road, Ann Arbor MI 48106-1346 USA
313/761-4700 800/521-0600

EFFECTS OF CLIMATIC VARIABILITY ON THE ACTIVE LAYER AND PERMAFROST

A

THESIS

Presented to the Faculty of the University of Alaska

in Partial Fulfillment of the Requirements

for the Degree of

DOCTOR OF PHILOSOPHY

By

Vladimir E. Romanovsky, B.S., M.S., Ph.D.

Fairbanks, Alaska

May 1996

EFFECTS OF CLIMATIC VARIABILITY ON THE ACTIVE LAYER AND PERMAFROST

By

Vladimir E. Romanovsky

RECOMMENDED:

Dist. Prof. D. M. Hopkins

Prof. W. F. Weeks

Prof. G.D. Wendler

Prof. J. P. Zarling

Prof. T. E. Osterkamp, Chairman, Advisory Committee

Prof. P. W. Layer, Head, Dept. of Geology and Geophysics

APPROVED:

Prof. P. B. Reichardt, Dean, College of Natural Sciences

Prof. Joe Kan, Dean of the Graduate School

4-25-96

Date

ABSTRACT

This thesis represents a collection of papers on the response of the active layer and permafrost to climatic variations on different time scales.

Quantitative estimates of the amplitudes of the Milankovich rhythms in several regions of the Russian permafrost zone were used in numerical simulations of permafrost dynamics. The results of modeling explained many aspects of the permafrost distribution and its vertical structure within Russia.

Spatial and temporal variability of the air, ground surface and permafrost temperatures were also analyzed using daily temperature data (upper 0.9 m) from 1986-1993 and results of annual temperature measurements in boreholes (nominally 60 m) from 1983-1995 at three sites in the Prudhoe Bay region of Alaska.

Three numerical models which are based on different numerical methods and are used for calculations of the ground thermal regime were compared with each other, with analytical solutions, and with temperature data. Several approximate analytical solutions for the temperature regime and thickness of the active layer were introduced.

The calculations were used to estimate the interannual variability of the thermal properties of soils which appear to be a result of interannual variations of the average water content during the summer in the upper part of the active layer. Precise temperature data together with computer modeling provided essential new information on dynamics of unfrozen water content in the ground in natural undisturbed conditions during freezing and the subsequent cooling of the active layer. A layer with unusually large unfrozen water content was found to exist at the depth of freeze-up.

The same set of data was used to reconstruct daily permafrost temperatures from 1986-1993 for all depths down to 55 m. Mean annual temperature profiles for each year of 1987-1992 show significant interannual variations within the upper 40 m in a good agreement with published data.

A numerical model of the temperature field in permafrost near its southern limits was developed to study the influence of short-term climatic variations (with periods of 300 and 90 years) on permafrost dynamics.

TABLE OF CONTENTS

LIST OF FIGURES

LIST OF TABLES

ACKNOWLEDGMENTS

I would like to acknowledge the expert guidance and assistance of my thesis advisor and chairman of my advisory committee, Prof. T. E. Osterkamp. His scholarship, colleagueship and friendship provided a source of inspiration and sustained me during difficult times. I owe him an inestimable debt of gratitude.

I extend my very grateful appreciation to the other committee members: Prof. D. Hopkins, Prof. W. Weeks, Prof. G. Wendler and Prof. J. Zarling for their generous assistance to me during my study in the Geophysical Institute and the Department of Geology and Geophysics, University of Alaska, Fairbanks.

I would like to thank Dr. L. Goodrich, Dr. G. Guymon, Prof. J. Gosink, and Dr. N. Seregina for providing their original models which were used in these studies. I would like also to thank Dr. K. Hinkel for his high quality temperature data from Barrow which were used in our studies with his permission.

I wish to acknowledge and thank the UAF Center for Global Change and Arctic System Research, its Director Prof. G. Weller and Associate Director P. Anderson for their interest in my research and for financial support.

I am grateful to my Russian colleagues from the Moscow State University: Prof. N. N. Romanovsky, Prof. L. N. Maximova, Prof. L. S. Garagulya and Dr. N. V. Seregina for their helpful discussions concerning the interactions of permafrost and climatic changes.

A special thanks is expressed to my wife, Noel, for her understanding, encouragement and love during my graduate studies.

This research has been supported by the Polar Earth Sciences Program, Office of Polar Programs, National Science Foundation and by the State of Alaska.

CHAPTER 1

Introduction

Air and ground temperature conditions, snow cover, and the active layer are important conditions and components of land-atmosphere interactions in the Arctic and their investigation is one of the primary thrusts of arctic system research. Permafrost occupies extensive areas in the Arctic. Northern ecological systems depend on permafrost conditions, which also directly influence human activities. At the same time, permafrost is one of the physical elements in the landscape most sensitive to climatic change. Therefore, study of the interactions between permafrost and climate, especially during the period of possible climatic warming, is one of the most important aspects of arctic system research.

The predicted climatic warming associated with projected increases in greenhouse gas concentrations in the atmosphere will be most pronounced in the Arctic and should be detectable there first (Nelson et al., 1993). General circulation models project global mean equilibrium temperature increases of between 1.8°C and 5.2°C for a doubling of preindustrial CO_2 concentrations. The temperature rise in Arctic regions may be 2 to 3 times greater than the global average. Climatic warming will significantly influence permafrost conditions and, as a result, stability of roads, buildings and pipelines. Virtually all surface activities associated with the development of natural resources will be effected.

The fate of permafrost (whether it degrades or aggrades) is controlled by climatologic, biologic, hydrologic, geologic, and oceanographic factors through their influence on the flow of heat and mass (moisture and solutes) to and from the permafrost table. Consequently, there is a need for developing a better understanding of how the

climate, biota (primarily vegetation), hydrology, geology, and the ocean influence heat and mass flow processes at the ground surface, within the active layer, and at the permafrost table. Warming air temperatures would generate a somewhat different change at the surface of the permafrost because of the effects on heat balance of the material between the permafrost and the atmosphere. In the continuous permafrost zone, the effect on the permafrost would be to warm it and possibly, to change the depth of the active layer (Osterkamp, 1982; Osterkamp and Lachenbruch, 1990; Nelson et al., 1993).

Permafrost is linked to the atmosphere by the intervening active layer, vegetation, and snow cover which vary strongly with time and location. Consequently, it is important to develop a better understanding of the spatial and temporal behavior of the active layer and upper permafrost to seasonal, annual, and multi-year changes in climate. Dynamics of the permafrost distribution and the active layer thickness influence significantly the hydrology and hydrogeology of the arctic land as well as its geomorphology. Together these conditions influence characteristics of the biota and form particular landscape types so that permafrost dynamics determines changes in the ecosystem as a whole.

Another very important application for results discussed in this thesis is an interaction between the carbon cycle and permafrost and active layer variations. This interaction is an essential element in the positive feedback mechanism in the natural global system "Terrestrial Permafrost - Land - Atmosphere." Warming of the permafrost environment could change the balance between carbon accumulation and decomposition processes and substantially disrupt the equilibrium of the natural carbon cycle. Large amounts of carbon and methane are stored in permafrost below the annually thawed active layer. This organic matter frozen in permafrost is not presently involved in the carbon cycle. Warming may accelerate the rate of decomposition, which is limited now by low temperatures, and thaw deeper layers of formerly frozen organic soils, making them available for decomposition. Some experimental evidence exists indicating that

arctic tundra and boreal forests are changing from a carbon dioxide sink to a source (Kolchugina and Vinson, 1993; Oechel et al., 1993; Oechel and Vourlitis, 1994). For the case of strong temporal variations in active layer thicknesses the results of measurements of greenhouse gas fluxes will be naturally time dependent.

Monitoring the ground temperatures and active layer thicknesses and characteristics is also necessary for assessing changes in the environment (Barry et al., 1994), which directly influence the conditions and quality of human life and activity in the circumpolar north. Active layer thicknesses are particularly important because of their direct effects on engineering constructions.

To predict the behavior of the active layer in connection with the predicted climatic warming, it is necessary to understand active layer thawing and freezing under natural conditions which vary significantly from year to year. It was discovered (Osterkamp et al., 1994; Romanovsky and Osterkamp, 1995a; Osterkamp and Romanovsky, 1996) that this natural interannual variability in the active layer characteristics has the same order of magnitude as the predicted long-term warming. On the other hand, the measured long-term changes in the active layer characteristics can be interpreted as a sensitive indicator of global change in the Arctic.

Predicted anthropogenic climatic warming will interfere with natural climatic variations. These variations are well known for the time scales of tens and hundreds thousands of years (ice age rhythms during the Pleistocene-Holocene time). There are lines of evidence in geothermal and paleoclimatic data that the same kind of rhythmical variations with much shorter periods also exist (Shnitnikov, 1957; Maximov, 1972; Sergin, 1975; Khotinsky, 1977; Kovalenko et al., 1987; Rozanov 1987; Hubrechts et al., 1989; Romanovsky et al., 1991a; Romanovsky and Maximova, 1991; Currie, 1993; Osterkamp et al., 1994; Kazantsev, 1994; Pavlov, 1994; Safanda et al., 1994; Romanovsky and Osterkamp, 1995a). The periods of such variations are about 2000-1500, 300-200, 100-90, 40, 22, and 11 years. However, there has been very little study of these rhythms. Currently, there is no conclusive theory of these variations, though

such a theory is necessary for an explanation of their derivation and for forecasting of middle- and short-term climatic changes.

Results of studies of the long- and short-term climatic variations and their effects on permafrost are discussed in Chapter 2 and later in Chapters 7 and 8. Long-term variations were studied using the basic principles of Milankovitch global climate change theory and harmonic analysis with cycle periods of 200, 100, 41, 21, and 11 thousands years (ka). These harmonics were combined in an attempt to refine the paleotemperature variations in different regions of Russia from the late Pleistocene to the present. This long-term model was tested with a series of computer simulations of perennial freezing and thawing that showed good agreement with reconstructions of paleopermafrost distribution and with its present vertical structure. These studies provided also an explanation for the two-layer permafrost structure which is very common for some regions of the permafrost zone in Russia. Short-term climatic cycles can be studied using meteorological data and the permafrost temperature measurements in drill holes.

Predicted climatic changes in the near future can significantly alter the Arctic environment during the next half century but the amplitude of these changes and their impact on the quality of human life in the Arctic are unknown. Numerical modeling is one of very few methods which can provide information on the direction and consequences of global changes. Most of the current GCM's are unable to reliably predict regional climatic changes resulting from a global-scale change (Hewitson and Crane, 1992; Hewitson, 1994). One of the reasons given for this is an insufficient consideration of land-atmosphere interactions. While in "classic" GCM's only snow albedo has been included, recent models take into account more complete information about surface conditions (snow cover characteristics, ground temperature, active layer thicknesses and characteristics, and surface and ground hydrology) (Cohen and Rind, 1991; Verseghy, 1991; Giorgi *et al.*, 1993; Marshal and Oglesby, 1994; Marshall et al., 1994; Giorgi, 1995; Lynch et al., 1995). For this reason, the accuracy of calculations of

the active layer thicknesses and characteristics and the thermal regime of the active layer and near-surface permafrost become very important.

Numerical modeling of the active layer and near-surface permafrost temperature fields dynamics is also an important component of engineering design in the Northern regions. The significant role of permafrost relates to the dependence of its mechanical and physical properties on the temperature (especially if the temperature is close to 0°C). These properties change dramatically if permafrost becomes unstable and starts to melt (Osterkamp and Lachenbruch, 1990).

Application of any numerical models to investigation of natural processes has to be justified by some kind of verification. Usually these verifications for thermal models are confined to comparison with analytical solutions for some simple cases with constant initial and boundary conditions (e.g. Neumann solution). Seldom are computer models verified using measured temperature data or compared to each other running with the same set of input data. In Chapter 3, three numerical models for the ground thermal regime calculations based on different numerical methods and different treatments of freezing and thawing are compared with each other, with analytical solutions, and with measured temperature data.

Developing an understanding of land-atmosphere interactions in arctic ecosystems requires information on the response of the thermal regime of the active layer and near-surface permafrost to seasonal and climatic changes. This information is also useful for investigating surface geological processes related to permafrost (thermokarst development, frost heaving, ice wedge formation, mass wasting) (Washburn, 1980), for the design and construction of engineering works in permafrost regions (Esch and Osterkamp, 1990; Osterkamp and Lachenbruch, 1990), and for extracting information on past climate from permafrost temperature profiles (Lachenbruch and Marshall, 1986). On a regional scale, changes in the active layer and near-surface permafrost can be used as an indicator of global change (Nelson et al., 1993). Permafrost is linked to the atmosphere by the intervening active layer, vegetation,

and snow cover which vary strongly with time and location. Consequently, it is important to develop a better understanding of the spatial and temporal behavior of the active layer and upper permafrost to seasonal, annual, and multi-year changes in climate.

Active layer measurements in northern Alaska, Canada and Russia have a long history. However, there is little information about the temperature regime and long-term variations in active layer thicknesses. Evidence for a cyclic variation of the upper permafrost temperatures with a period of 10-11 years was obtained from temperature measurements in shallow (nominally 60 m) drill holes in the Prudhoe Bay region (Osterkamp et al., 1994; Osterkamp and Romanovsky, 1996). The existence of the rhythmic variability of the mean annual permafrost temperatures with periods of 9-13 and about 40 years was also reported by Kazantsev (1994) for the Russian Far East and North-East of Russia.

Chapter 4 presents the results of the field temperature measurements, including air and surface temperatures, as well as ground temperatures down to about the 1 m depth. The measurements were made every four hours for six years (1986-1992) on the Coastal Plain of the Alaskan Arctic adjacent to the Beaufort Sea in the Prudhoe Bay region. The sites are along the Dalton Highway south from Prudhoe Bay and include West Dock, Deadhorse, and Franklin Bluffs (Figure 5.1). The main purpose of these measurements was to develop a long-term continuous data base for investigating the thermal response of the active layer and near-surface permafrost to changes in climate. Analyses of these data can provide an understanding of the importance of the air temperature and surface conditions on the active layer and permafrost temperatures. Since the permafrost can usually be treated as a conductive medium, a determination of the surface temperature history is a key element in predicting it's future thermal regime.

It is very helpful to use simple analytical solutions in studies of the effects of climatic variations and changes in the natural conditions at the ground surface on the temperature regime of the active layer and near-surface permafrost and on the active layer thicknesses. The discussion of these methods which had been developed earlier but

were refined in our studies starts in Chapter 4 with an introduction of an analytical solution which allows for calculations of the thermal offset in the active layer. Results of comparisons between this solution and numerical calculations and measured data is also included in Chapter 4. This discussion continues in Chapter 5, where the modified Kudryavtsev's method for calculations of maximum active layer thicknesses is introduced. This method is compared also with a numerical solution, with measured data, and with other analytical solutions.

The main concern of Chapter 5 is seasonal thaw processes. Seasonal thawing of the ground as a thermodynamical process is determined by certain thermal parameters. The primary parameters are the temperature regime at the ground surface (especially during the summer), thermal properties of the ground to the depth of 15 to 20 m (thermal conductivity and heat capacity), and water and ice content within the active layer. The natural factors which determine the values of these parameters are the air temperature (mean annual temperatures and the range of their seasonal variations), precipitation, snow cover characteristics (snow depth and thermal conductivity), type of vegetation and its thermal characteristics, soil composition, drainage conditions and others (Kudryavtsev et al., 1974).

Results of analyses and interpretation of the active layer and near-surface permafrost temperature regime using the measured temperatures at the ground surface in the Prudhoe Bay region as input data are discussed in Chapter 5. The data include the annually measured temperatures in the deeper boreholes (about 60 m) at the same sites. Chapter 5 is concerned with the thawing portion of the annual cycle, specifically how seasonal thawing progresses and methods for determining the maximum depth of the active layer. The available data were used to calibrate a finite element thermal model which was then applied to simulate seasonal thawing and temperature field dynamics in the active layer and near-surface permafrost.

Chapter 6 continues the discussion of the processes related to seasonal thawing and freezing of the active layer in the Alaskan Arctic which was started in previous

Chapters, concentrating on the thermal processes and unfrozen water behavior in the ground during freezing and following cooling of the active layer.

The dynamics of active layer freezing are important for the cryogenic structure of the frozen active layer and near-surface permafrost because the rate and proportion of freezing from the top and from the bottom of the active layer determine the growth of ice lenses. This is true especially in the case of progressive formation of syngenetic permafrost (Shur, 1988). For this reason, it is necessary to know which part of the active layer was freezing downward from the ground surface and which part was freezing upward from the permafrost table.

Characteristics of freezing of the active layer and ice lens formation determines the physical, chemical and mechanical properties of the frozen soils and their behavior as a foundation for engineering works. The processes of frost heaving and subsequent settlement of the ground during the thawing are determined by the freezing regime of the active layer.

The freezing regime of the active layer significantly influences the physical, mechanical and thermal properties of soils when unfrozen water is present in frozen ground. These properties become strongly temperature dependent over a wide range of the negative temperatures. The problems related to the presence of unfrozen water in frozen soils have been investigated in the laboratory (Nersesova and Tutunov, 1957; Lovell, 1957; Tsytovich, 1973; Anderson et al., 1973; Anderson and Tice, 1973; Ershov et al., 1979; Black and Tice, 1988; Tice et al., 1988). At the present time, precise high frequency temperature measurements in the active layer and near-surface permafrost have been collected. These data, along with advanced computer models of the freezing and thawing processes, provide new opportunities to study the unfrozen water content *in situ* in frozen soils and its dynamics during the year.

Application of this technique to the measured temperature data from the Prudhoe Bay region and Barrow is discussed in Chapter 6. This provides essential new information on the dynamics of the unfrozen water content in the ground in natural

undisturbed conditions during freezing of the active layer, which show unexpectedly large amounts of unfrozen water at low temperatures.

The results of joint interpretation of two data sets from the active layer and near-surface permafrost and from deeper boreholes in the permafrost are reported in Chapter 7, which links the seasonal and interannual variations of the temperatures in the upper 1 m of soils with the temperature regime in permafrost to the 50-60 m depth. These data sets included precise temperature profiles (resolution 0.001°C and accuracy 0.01°C) obtained from 1983 to 1995 in these drill holes at three sites south from Prudhoe Bay; West Dock, Deadhorse, and Franklin Bluffs. In addition, high frequency (4 h time interval) measurements of temperatures (resolution 0.01°C and accuracy 0.1 to 0.2°C) in the air, at the ground surface, in the active layer and permafrost (down to 0.7-0.9 m) from 1986 to 1993 at the same sites are used in this Chapter. These sites are well suited to investigate long-term variations in active layer and permafrost conditions. Special care was taken to minimize the thermal disturbance in the drill holes and to the ground surface surrounding the sites.

In previous publications (Osterkamp et al., 1994; Romanovsky and Osterkamp, 1995a), these two sets of data were used separately. The primary problem in using the permafrost temperature profiles, which were measured only once per year, is the gap in information on annual and interannual permafrost temperature variations within the depth of annual temperature changes, typically 20 to 25 m. This lack of information makes it difficult to relate the deeper permafrost temperature changes with the temperature variations at the permafrost surface. The problem was resolved through the use of computer simulations of the dynamics of the permafrost temperature field which allowed reconstruction of the ground temperatures for all times from 1986 to 1993 and for all depths.

In Chapter 8, the possibilities of theoretical investigations of the reaction of permafrost within complex geological structures and for inhomogeneous surface conditions to the short-term climatic variations are discussed.

One-dimensional models of temperature fields are used most often when studying the effect of geological structure and climate on the formation and dynamics of permafrost and the temperature field in the ground. Numerous examples are known, however, when the measured temperatures cannot be explained by a one-dimensional conductive model. In this case the conclusion is often that the temperature field is not one-dimensional and its formation is affected by horizontal inhomogeneities. The latter are most frequently due to the geological structure of the grounds and temperature conditions on their surface. An attempt is made in this chapter to analyze the impact of such inhomogeneities on the temperature field. Such an analysis is most interesting for non-stationary temperature fields, i.e. when the natural climate dynamics is taken into consideration. The latter was expressed as the superposition of the different time scale temperature variations at the ground surface.

A numerical permafrost temperature model was developed for the southern Siberia region to study the influence of these rhythmic climatic changes on the dynamics of permafrost. The mathematical model was represented as a two-dimensional heat conduction problem for a moist substrate for complex geological structures and inhomogeneous surface conditions. Calculations of the dynamics of the temperature fields and permafrost boundaries were made to evaluate this model. The results of modeling showed that the two-dimensional temperature field along some profiles (particularly at sites with complex geological structures) contain much more information about past permafrost dynamics than temperature profiles from single boreholes. The joint use of both the field temperature data along profiles, and numerical modeling can provide a more detailed explanations of the present permafrost structure and more accurate forecasts of permafrost changes in the future.

CHAPTER 2

Paleotemperature Reconstruction for Freeze -Thaw Processes During the Late Pleistocene Through the Holocene

V. E. Romanovsky, L. N. Maximova and N. V. Seregina, 1991. Paleotemperature Reconstruction for Freeze -Thaw Processes During the Late Pleistocene Through the Holocene. In *Proceedings of the International Conference on the Role of Polar Regions in Global Change*, University of Alaska, Fairbanks, vol. **2**, 537-542.

2.1 Abstract

Variations in ground surface temperatures for different regions of the USSR were studied using the basic principles of Milankovitch global climate change theory and harmonic analysis with cycle periods of 200, 100, 41, 21, and 11 thousands years (ka). The amplitude of these cycles has been calculated based on the following assumptions: (1) Climatic rhythms are represented as sinusoidal variations of temperature with periods of 200 (T′), 100 (T1), 41 (T2), 21 (T3) and 11 (T4) ka. (2) Minima of harmonics T′ and T2 occurred between 25 and 26 ka ago, while minimum of period T3 occurred between 22 and 23 ka ago; in addition, maxima of periods T1 and T4 were 5 ka ago. (3) Northern hemisphere deviations from present-day temperatures during the last cold epoch were up to 9°C in high latitudes, ice-free areas and 5°C for lower latitudes; during the last warm epoch, these values were 4°C and 2°C, respectively.

Harmonics T2, T3 and T4 were combined in an attempt to refine the paleotemperature variations in different regions of the USSR from the late Pleistocene to the present. This long-term model was tested with a series of computer simulations

of perennial freezing that showed good agreement with reconstructions of paleopermafrost distribution and with its present vertical structure.

A model of surface temperature change was developed for middle- and short-term climate fluctuations. For this, temperature fluctuations with periods of 2000-1500, 300-200, 100-90, 40, 22 and 11 years are assumed. Cycles of 100, 40, 22, and 11 years can be studied from meteorological data.

The middle- and short-term cycles are the most important for understanding and predicting permafrost dynamics, especially in the southern extremes of permafrost distribution. However, 300-200 and 2000-1500 year cycles cannot be studied using meteorological data. Fluctuations of mountain glaciers offer a means of studying these long-term cycles.

2.2 Introduction

The difficulty with permafrost paleoreconstructions is a shortage of knowledge about chronological sequences of the climatic events during the late Pleistocene and Holocene. There was not enough data for the mathematical modeling of the permafrost dynamics because of the need to discover climatic rhythms and to fully describe such rhythms quantitatively (period, amplitude, phase).

The present-day permafrost structure formed, in general, during the late Pleistocene and Holocene. Therefore, this time period (approximately 100 ka) is the most important for the modeling of the history of the formation of permafrost. The most difficult problem is the reconstruction of the temperature conditions on the ground surface during this time period. However, there presently are some fundamental elaborations about global climatic changes that allow this problem to be solved quantitatively. It is important to assume the existence of dramatic climate oscillations during the Pleistocene with the background of general climate cooling during the Cenozoic. According to the Milankovitch theory, the long-term changes (with periods

of tens and hundreds thousands of years) are associated with fluctuations in the amount of solar energy striking the Earth's surface caused by periodic changes in the Earth's orbital drive.

The knowledge of middle- and short-term climate variations is important, especially for applications to engineering predictions. The periods of such variations likely are 2000-1500, 300-200, 100-90, 40, 22, and 11 years. There has been very little study of these rhythms. Currently, there is no conclusive theory of these variations. Such a theory is necessary for an explanation of their derivation and for forecasting of middle- and short-term climate changes. The study of glacier dynamics may be used for this purpose.

2.3 The Study of Long -Term Climate Variations

The study of the long-term variations allowed the discovery of a general tendency for climate changes during the late Pleistocene and Holocene for different regions of the permafrost zone in the USSR. The paleotemperature curves (Figures 2.1A and 2.2) have been calculated in accordance with established practice (Maximov, 1972; Sergin, 1975; Zubakov, 1986; and others). Assuming simple sinusoidal form of the T2, T3 and T4, the summary paleotemperature curve *T(t)* can be written as

$$T(t) = A_2 \sin(\frac{2\pi}{P_2}t + \varphi_2) + A_3 \sin(\frac{2\pi}{P_3}t + \varphi_3) + A_4 \sin(\frac{2\pi}{P_4}t + \varphi_4) \qquad (2.1)$$

The length of periods (P_2 , P_3 , P_4) and the values of phase lags (φ_2 , φ_3 , φ_4) of the T2, T3, and T4 harmonics are known from the Milankovich theory, the only unknowns are the amplitudes (A_2 , A_3 , A_4) of these rhythms. To estimate their values, three equations are necessary.

Based on this assumption and assumptions presented in the abstract of this paper (see page 11), a system of equations was derived yielding the amplitudes of the

T2, T3, and T4 harmonics and enabling construction of the summary paleotemperature curves *T(t)* (Maximova and Romanovsky, 1985, 1988):

$$\begin{aligned} T(t)\big|_{t=t_{min}} - T(t)\big|_{t=t_0} &= a \\ T(t)\big|_{t=t_{max}} - T(t)\big|_{t=t_0} &= b \\ \frac{dT(t)}{dt}\bigg|_{t=t_{max}} &= 0 \end{aligned} \qquad (2.2)$$

where $T(t)$ is the total temperature as a function of time, t_{max} and t_{min} are the time of the last thermal maximum and minimum, t_0 is the present time, and a and b are temperature deviations from the present-day values during the periods of these minimum and maximum. The amplitudes of T′ and T1 harmonics were assumed to equal 1°C.

The climatic variations in the late Pleistocene and Holocene obtained from the curves are in agreement with the consensus opinion of the paleoclimatic peculiarities of that time. The paleotemperature curve (Figure 2.1B) illustrates principal climatic events of the late Pleistocene - Holocene and their time interval corresponding to the isotopic oxygen profile of ice from boreholes at the Vostok station in Antarctica (Gordienko et al., 1983) and to its paleogeographic interpretation. Figure 2.1C shows movement of the ice-sheet margin between Indiana and Quebec during the last major climatic cycle and the general mean-global temperature curve according to Imbrie and Imbrie (1986). Both examples are in agreement with the reconstructed for the south of East Siberia paleotemperature curve (Figure 2.1A).

From the curve obtained for the highlands of southeastern Siberia over an interval of 160 ka, the following events can be identified (Zubakov, 1986): the Riss-Wurmian thermochron 130-117 ka ago with climatic warming about 100-90 ka (95-80 ka by the isotopic oxygen curve), a dramatic cooling about 75 ka (75-70 ka by the

isotopic oxygen curve), an intra-Wurmian rise in temperatures with a peak about 48 ka, and late Wurmian cooling 33-15 ka (with a minimum 27-24 ka by the isotopic oxygen curve), and climatic warming in the Holocene 15 ka ago.

The summary curves obtained (Figure 2.2) confirm the known facts on the rise in the amplitude of climatic changes from southeastern to northwestern USSR, as well as the Holocene thermal maximum lagging behind in the same direction (Khotinsky, 1977). The earlier terms of the thermal maximum in East Siberia, as compared with the European North and West Siberia, can be explained by the laws governing the changes in individual rhythm amplitudes in these regions. In accordance with the Milankovitch theory of climatic fluctuations, there are significant latitudinal differences in the T2 and T3 rhythms: the former dominates at high latitudes but near 45°N its amplitude approaching zero, while the amplitude of the T3 rhythm increases towards the south.

According to the solutions obtained, the amplitude of the T2 rhythm decreases from 8-9.5°C in the European North down to 2.5°C in the Far East. The amplitude of the T3 rhythm increases from 1°C in northern West Siberia to 1.5-2°C in the Transbaikal region. The total range of climatic variations and the time of their maximum manifestation varies accordingly. Thus, in northern West Siberia (the Ob' River basin) where the amplitude of the T2, T3, and T4 rhythms equals 7.2°C, 1.2°C, and 0.5°C, respectively, the total amplitude of temperature variations reaches 16°C and the Holocene thermal maximum dates around 4.5-6.5 ka ago. In the Transbaikal region, where the least difference between the T2 and T3 rhythms and T4 rhythm is practically lacking, the summary total amplitude of climatic variations is twice as small and the Holocene thermal maximum has the earliest dating from 10-11 to 8 ka ago. Such an early beginning of the maximum is acknowledged by the investigators of the region (Yendrikhinsky, 1982). One can refine the thermal maximum time in the Holocene by superposing the middle-term rhythm (2-1.5 ka) of Shnitnikov (1957) on the curves obtained.

The process of ground freezing in the late Pleistocene glacial epoch and thawing during the Holocene temperature maximum in the Baikal rift zone depressions were studied in accordance with these temperature variations. This region was chosen for experimental examination of the hypothetical temperature variations because of a number of circumstances. The position of depressions, extending latitudinally, allows the changes in surface temperatures due to the displacement of geographical zones to be ignored. The landscapes of lacustrine-alluvial plains in the depression floors over the investigated period of time (80 ka) changed insignificantly (Belova, 1985). This permits the supposition that the dynamics of the temperature field in the ground were determined practically by climatic variations. Two permafrost horizons have been identified in the depressions; the late Pleistocene and the Holocene (Zamana, 1980). They can occur independently, constitute a two-stage section (Upper-Angara and Barguzin depressions), and merge into a single frozen series (Chara depression).

The appropriate examples of models are given in Figure 2.3. The presence of the two-stage section has made it possible to compare the estimated and actual depths of ground freezing and thawing at three levels: the bottom of the Holocene horizon, as well as the top and bottom of the late Pleistocene frozen ground. The corresponding actual data are for the depths from 30-50 m to 80-110 m, 70-150 m, and 130-300; maximum thickness of the relict permafrost horizon amounts to 150-200 m, but in the regions with high present-day temperatures this horizon is intensively degrading and is only several meters thick.

Ground freezing and thawing have been simulated numerically using the program for solution of Stefan's multifront problem developed at the Department of Geocryology, Moscow State University (Seregina, 1989; Romanovsky et al., 1991b).

Comparison of the computed data and factual data yields positive results. This, in the opinion of the authors, justifies the attempt of refining the paleotemperature variations in different regions of the USSR for the late Wurm-Holocene by summing up the harmonics T1, T2, T3 and T4.

2.4 Study of the Middle-and Short-Term Climate Variations

The model of long-term cycles describes only a general tendency of the permafrost to form and change its main features in space and time over large regions of the permafrost zone.

For engineering application, it is more important to establish the dynamic of the permafrost and its temperature field on concrete sites through relatively short time intervals (from ten to one hundred years). The depth of such changes may be relatively small (not more than 50-100 meters). It is possible only if some regularity of middle- and short-term climate changes is known. So the problem is to arrange middle-term (with periods of hundreds and a few thousand years) and short-term (with periods of tens and a few hundred years) climatic cycles.

The long-term meteorological data can be used for identification of the short-term climate changes without understanding their derivations. As an example of such a possibility, Figure 2.4 shows selected temperature data dating back to 1530 for the north face of the Alps (Huybrechts et al., 1989). It is possible to recognize from these data several rhythms with periods of 300, 400, 40 and perhaps 22 years. The amplitudes of these rhythms are approximately 0.4°C, 0.4°C and 0.5°C, respectively. It seems that the amplitudes of the 40 and 22 years rhythms are not constant, but change with time.

Figure 2.5 shows changes in the average temperature of the northern hemisphere (Imbrie and Imbrie, 1986). This graph shows that two rhythms with periods of 100 and 40 years can be recognized, and these rhythms have approximately the same phases over the whole northern hemisphere.

The difficulty of the solution of the middle-term climate change problem is the absence at the present time of some common theory about the derivation of such changes (like the theory of Milankovitch for the long-term cycles). However, there is

good knowledge of natural phenomena that are sensitive to climate change. One such phenomenon is mountain glaciers.

2.5 The Possibility and Difficulty of Using Mountain Glaciers for Climatic Rhythms Prediction

It is obvious that mountain glaciers react on global long-term climate changes. However, it is difficult to study long-term changes using glacier data because following the advance of the glaciers, geomorpholoigical and geological features of the previous glacial deposits are destroyed. Therefore, we know glacier dynamics in response to climate change for only the last 20,000 years, i.e. during the last period of deglaciation of mountain glaciers. The last deglaciation is a stable process of common retreat of the mountain glaciers, in general, over at least the whole northern hemisphere. This process has been continuing in Alaska since 12 to 15 thousands years ago (Calkin, 1988). In Europe and in the USSR, deglaciation of mountain glaciers has continued for the last 13 to 14 thousand years (Maximov, 1972). Deglaciation is a complex process. With a background of general retreat of the glaciers, there are the rhythmical retreat-advance movements of the shorter periods. The total number of such cycles for glaciers in Europe and the Soviet Union is 7 over the last 12 thousand years, and 5 cycles over the last 8 thousand years for Alaska. Therefore, there are the rhythmical changes of climate with a period of 1500-2000 years. Sometimes, it is possible to recognize the shorter "inner" rhythms in glacier movement, but there is not sufficient data for final conclusions.

More detailed study of concrete glaciers allows the establishment of the presence of such rhythms. However, it is difficult to generalize such data from several glaciers because the phases of the short-term changes of the positions of the glacier fronts are different. Even over the same region and neighboring glaciers, it is possible that one of them is retreating and another is advancing.

The cause of such glacier behavior is the presence of positive and negative feedbacks in the system Glacier-Local Mainland-Atmosphere-Ocean. The result of the feedback effect is the apparently random reaction of glaciers of different size, geometry, stability, and location to the same global climatic changes.

2.6 Conclusions

Climate changes have the character of oscillation. The study shows that surface temperature changes can be described as some superposition of separate harmonic oscillations with different periods (from tens of years to hundreds of thousands of years and more).

The main rhythms are synchronic at least for the whole northern hemisphere. The peculiarity of manifestations of summary surface temperature changes, including different times of thermal maximum and minimum during the late Pleistocene and Holocene over the different regions of the permafrost zone can be explained exclusively through differences in the distinct harmonic amplitudes for these regions. Mountain glacier movements can be used in the analysis of middle and short-term climate changes, but the presence of the feedback mechanisms must be taken into account.

The short-term changes can be studied through long-term meteorological records. At the present time in the field of geocryology, there is a need for a prediction mechanism and a theory of climate change, particularly of middle- and short-term changes.

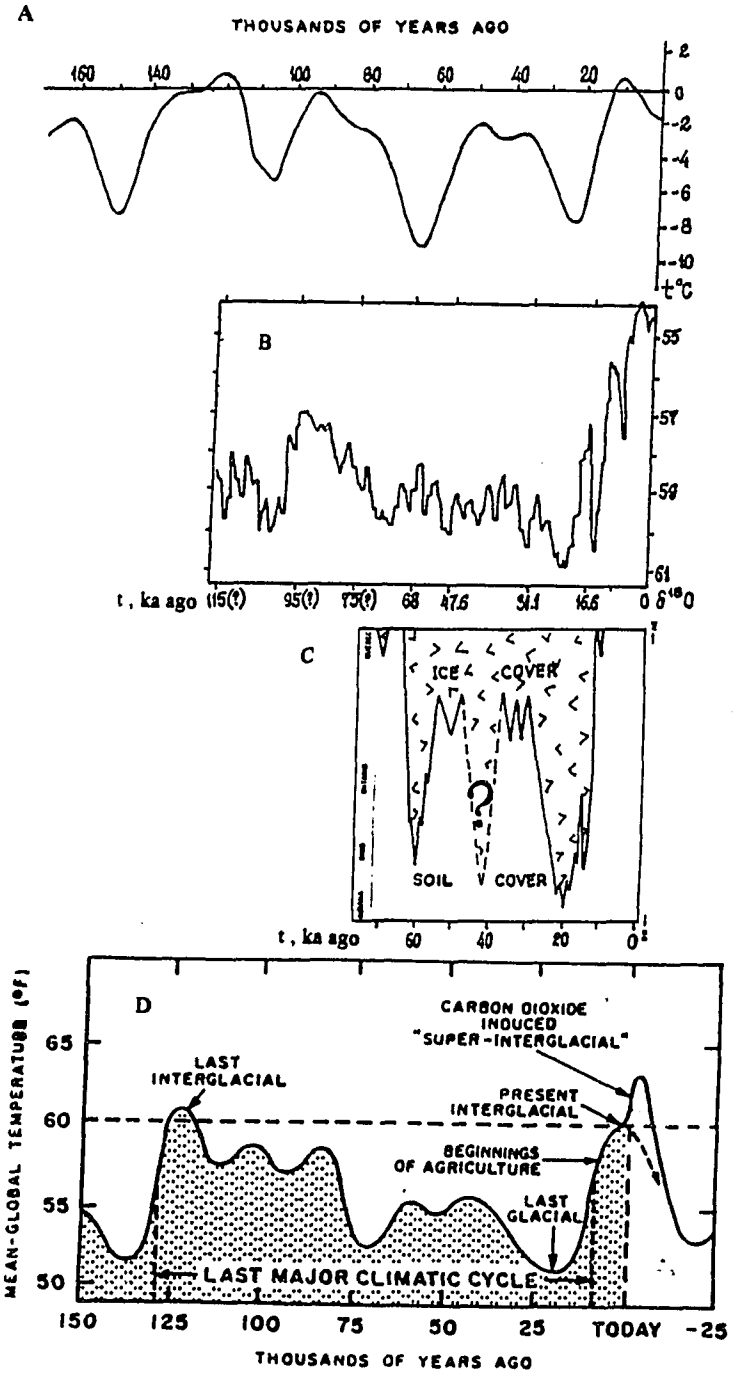

Figure 2.1 Principal climatic events of the late Pleistocene-Holocene: comparison of the theoretical paleotemperature curve for southern East Siberia (A) with isotopic oxygen profile of ice from boreholes at the Vostok station in the Antarctica (B), with fluctuations of the ice-sheet margin between Indiana and Quebec during the last major climatic cycle (adapted from Imbrie and Imbrie, 1986) (C), and with general mean-global temperature curve according to Imbrie and Imbrie (1986) (D).

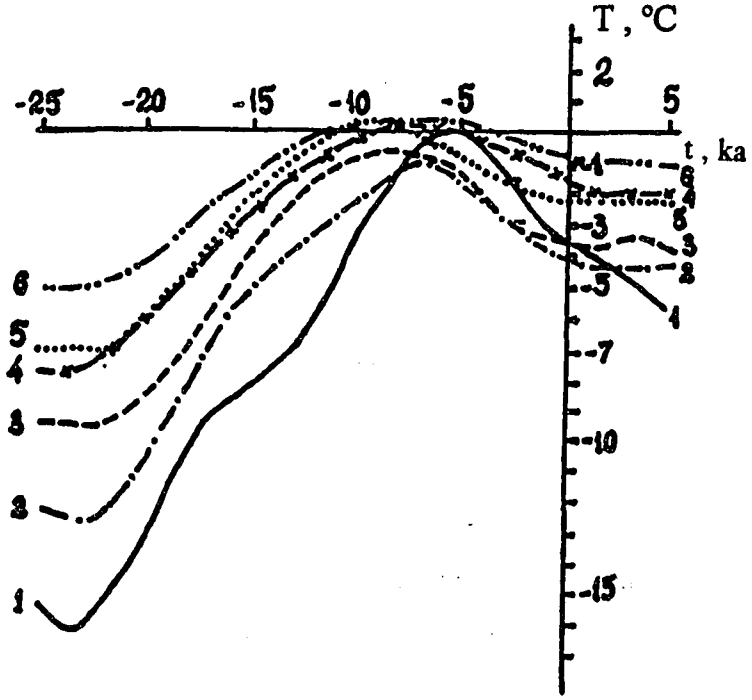

Figure 2.2 Relative changes of summary ground surface temperatures with time in different regions of the permafrost zone: 1, 2 - West Siberia (1 - Ob' River region; 2 - Yenisei River region); 3, 4 - East Siberia (3 - north of 65°N; 4 - south of 65°N); 5 - Transbaikal region; 6 - Far East.

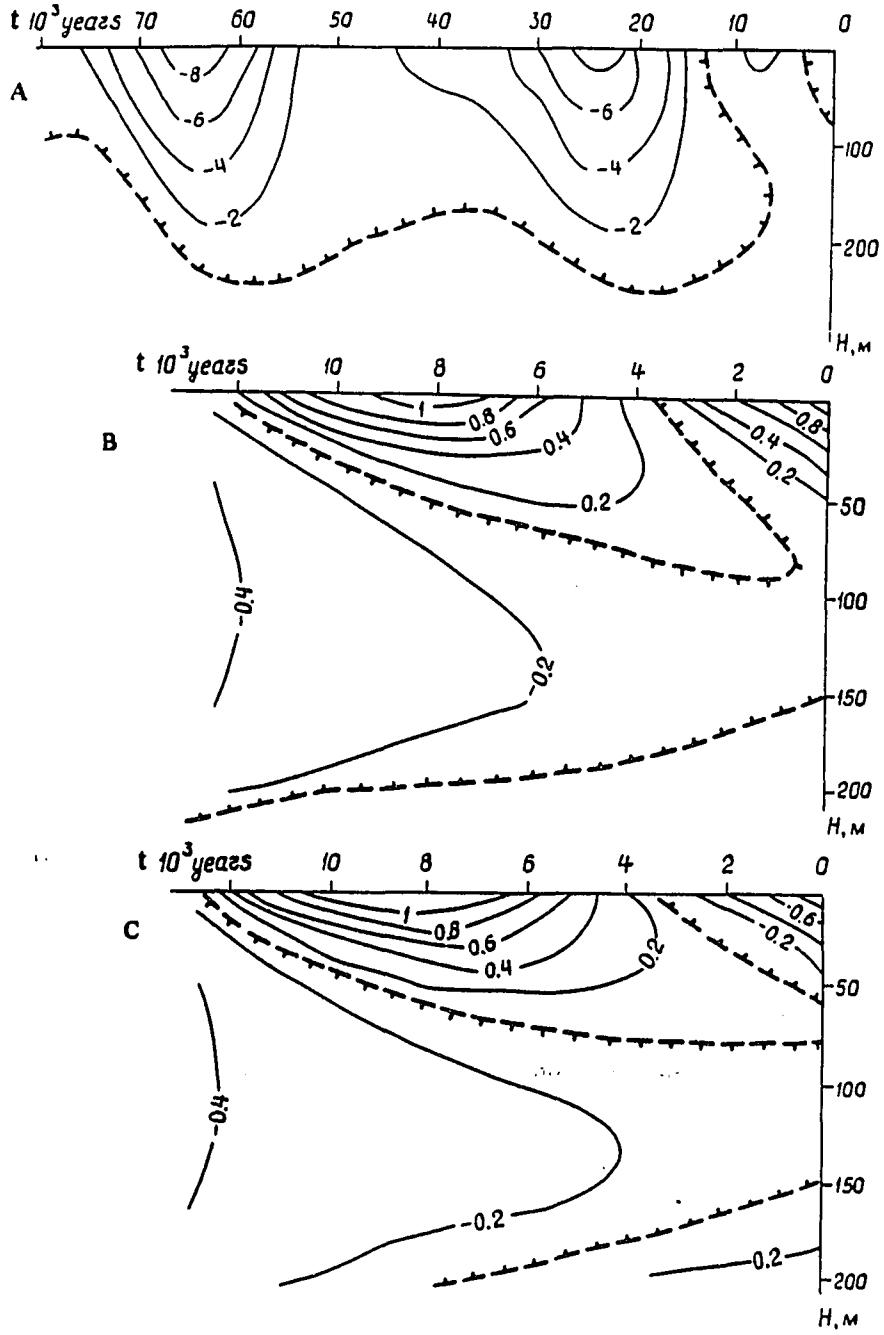

Figure 2.3 Variation of perennial thawing and freezing of rudaceous deposits in the mountain depressions of the Transbaikal region in the late Pleistocene and Holocene: (A) complete thawing of the Pleistocene frozen ground strata; in the section: perennially frozen grounds of the Holocenic age; (B) merging of partially thawed Pleistocene and formation of Holocene perennially frozen grounds into a single frozen strata; and (C) a two-stage section permafrost strata with the Pleistocene and Holocene horizons.

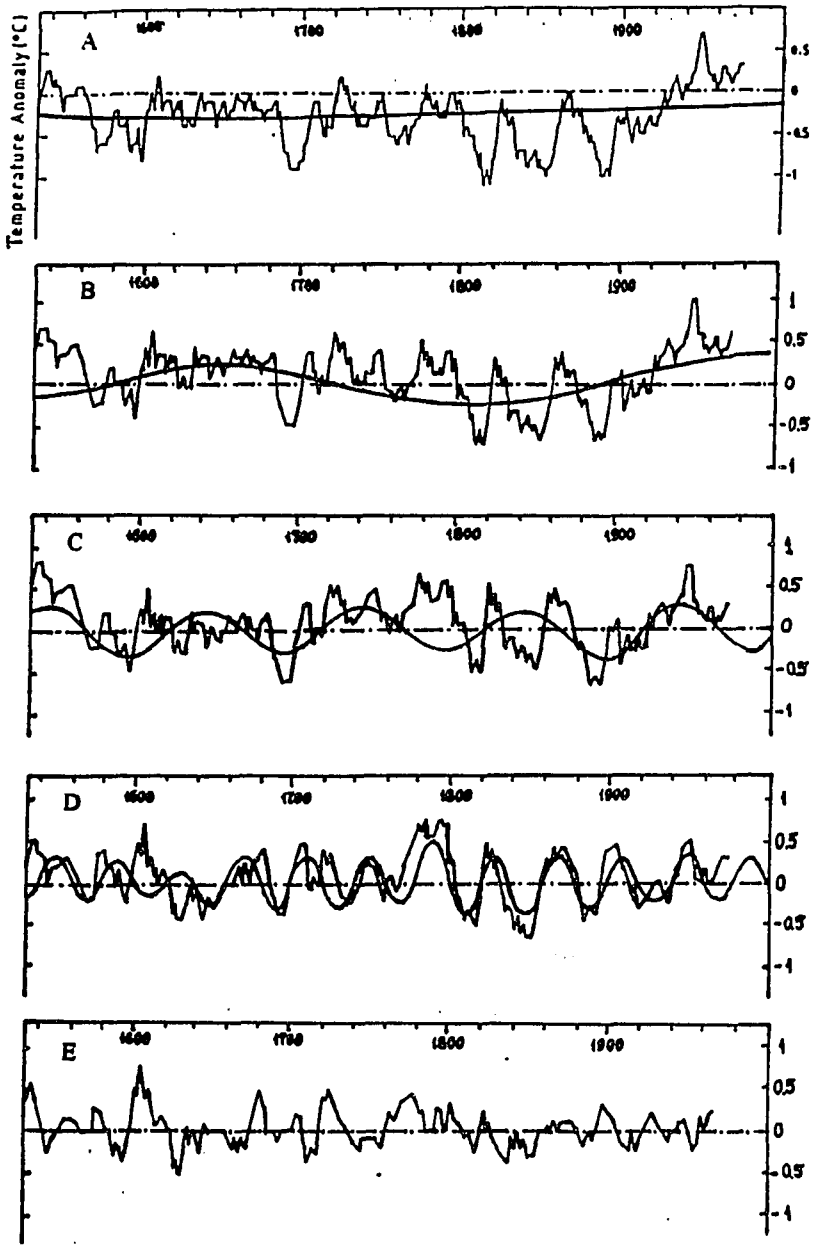

Figure 2.4 Temperature data dating back to 1530 for the north face of the Alps are given as 10-year running means and expressed as anomalies with respect to the 1901-1960 mean for Basel (from Huybrechts et al., 1989) and 1500-year cycle (A); temperature anomaly data except 1500-year rhythm and 300-year cycle (B); temperature anomaly without 1500-year and 300-year rhythms and 100-year cycle (C); temperature anomaly without 1500-, 300- and 100-year rhythms and 40-year cycle (D); temperature anomaly without 1500-, 300-, 100-, and 40-year rhythms; perhaps it includes 22-year cycle (E).

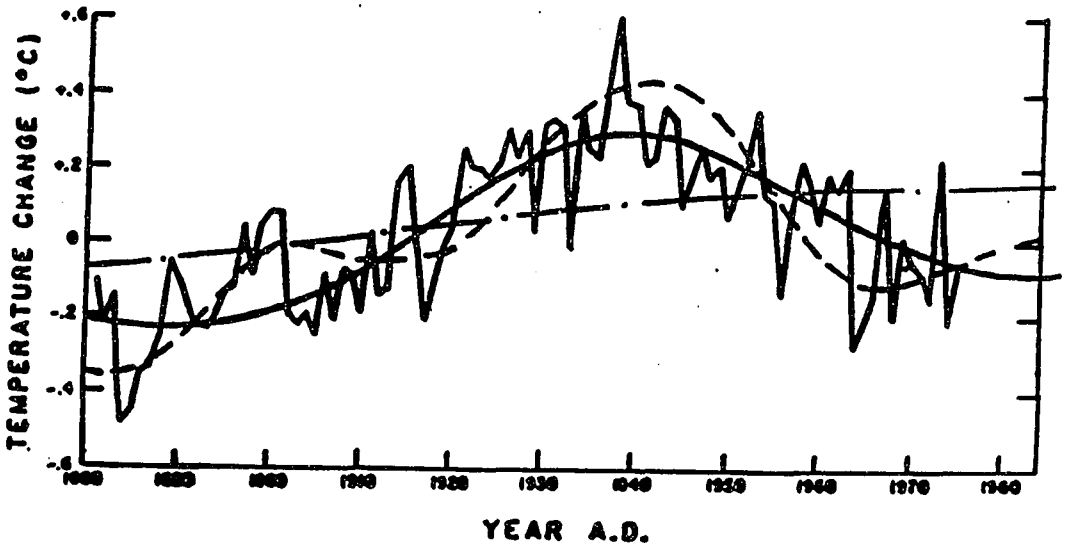

Figure 2.5 Climate of the past 100 years. This graph shows changes in the average annual temperature of the northern hemisphere. Since 1939, average temperatures have declined about 0.6°C (adapted from Imbrie and Imbrie, 1986).

CHAPTER 3

An Evaluation of Three Numerical Models Used in Simulations of the Active Layer and Near-Surface Permafrost Temperature Regimes

V. E. Romanovsky and T. E. Osterkamp, 1996. Numerical Models in Simulations of the Active Layer and Near-Surface Permafrost Temperature regime. *Cold Regions Science and Technology* (prepared for publication)

3.1 Abstract

Three numerical models (designated the Goodrich, Guymon/Hromadka, and Seregina models) used for calculations of the ground thermal regime which are based on different numerical methods and employ different treatments of freezing and thawing were compared with each other, with analytical solutions, and with measured temperature data. Comparisons of the models with the Neumann solution when no unfrozen water was present in the soils show differences generally less than 0.2°C between calculated temperatures using different models and a wide range of the time and space steps. However, in comparisons with data for the case of rapidly changing temperatures at the ground surface, the models with large time and depth steps could not reproduce the temperature field dynamics in the active layer and near-surface permafrost. Therefore, agreement with the Neumann solution is necessary but not sufficient to qualify the models for calculations of real temperature fields.

The Goodrich model requires a time step not longer than 1 hour and depth step in the upper 1 m not larger than 0.02 m to reproduce the temperature regime with

reasonable accuracy. Using the Guymon/Hromadka model, similar accuracy can be obtained with a 1 hour time step and 0.1 m space step within the upper 1 m depth or a 1 day time step and 0.01 m space step. However, the use of larger steps does not necessarily decrease the calculational time compared to the Goodrich model.

For the case with unfrozen water present in the soil, the results of calculations using the numerical models were compared with an analytical solution and were found to agree within 0.02°C.

3.2 Introduction

Predicted climatic changes can significantly alter the Arctic environment during the next half of century but the amplitude of these changes and their impact on the quality of human life in the Arctic are unknown. Numerical modeling is one of the few methods which can provide information on the direction and consequences of global changes. Most of the current GCM's are unable to reliably predict regional climatic changes resulting from a global-scale change (Hewitson and Crane, 1992; Hewitson, 1994). One of the reasons given for this is an insufficient consideration of land-atmosphere interactions. While in "classic" GCM's only snow albedo has been included, recent models take into account more complete information about surface conditions (snow cover characteristics, ground temperature, active layer thickness and characteristics, surface and ground hydrology) (Cohen and Rind, 1991; Verseghy, 1991; Giorgi et al., 1993; Marshal and Oglesby, 1994; Marshall et al., 1994; Giorgi, 1995; Lynch et al., 1995). For this reason, the accuracy of calculations of the active layer thicknesses and characteristics and the temperature regime of the active layer and near-surface permafrost become important.

Numerical modeling of the active layer and near-surface permafrost temperature field dynamics is also an important component of engineering design in Northern regions. Industrial activities in these regions occur in close relationship with

permafrost and periglacial processes. The significant role of permafrost relates to the dependence of its mechanical and physical properties on the temperature (especially if the temperature is close to 0°C). These properties change dramatically if permafrost becomes unstable and starts to thaw (Osterkamp, 1982; Osterkamp and Lachenbruch, 1990). All kinds of engineering construction in Arctic regions are affected by cold climate and permafrost. The permafrost conditions determine the principles of design, construction and utilization of the engineering works.

There are generally two approaches when using models of the active layer and near-surface permafrost temperature regime. In the first, the thermal model operates as a component of complex models of land-atmosphere interactions. Those models include also such components as energy and mass balance at the ground surface, moisture regime in the ground surface, vegetation cover and its effects on the energy and mass balance near the ground, and some of them take into account the effects of snow cover (Dickinson et al., 1986; Bonan, 1989; Bonan et al., 1993; Verseghy, 1991; Verseghy et al., 1993; Giorgi et al., 1993; Pollard and Thompson, 1995). Usually, with a few exceptions (e.g. Bonan, 1991) these models do not include detailed schemes for thermal processes in the soil and simplified solutions are often used to calculate the temperature regime and thickness of the active layer.

Second approach emphasizes in great detail the solution to the thermal problem of the temperature field dynamics and freezing-thawing processes in the active layer and near-surface permafrost (Nakano and Brown, 1971, 1972; Goodrich, 1976, 1978a, 1982a; Guymon and Hromadka, 1977; Guymon et al, 1980, 1984; Melamed, 1980; Gosink et al. 1988; Gosink and Osterkamp, 1990; Braley and Zarling, 1990; Osterkamp and Gosink, 1991; Romanovsky et al., 1991b; Waelbroeck, 1993). In this paper, three of these models will be considered; a finite difference model (Goodrich, 1976, 1978a, 1978b), designated as the Goodrich model, a finite element model (Gosink and Osterkamp, 1990; Osterkamp and Gosink, 1991; Osterkamp and Romanovsky, 1996), which is a modified version of the Guymon and Hromadka

(1977) and Guymon et al. (1984) model designated as the Guymon/Hromadka model, and a finite difference model (Seregina, 1989; Romanovsky et al., 1991b; Garagulya et al., 1995), designated as the Seregina model.

A comprehensive analysis of the numerical methods for ground thermal regime calculations was made by Goodrich (1982b). This analysis included a theoretical comparison of finite element and finite difference methods and the relative merits and disadvantages of different types of numerical treatments of freezing and thawing of the soil water (the latent heat as a distributed heat source (sink), an apparent heat capacity and enthalpy methods, explicit determination of the freezing (thawing) front position) and different types of surface boundary conditions. More recent publications on this topic also available (e.g. Alexiades and Solomon, 1993).

Application of any numerical methods for investigation of natural processes has to be justified by some kind of verification. Usually these verifications for thermal models are confined to comparison with analytical solutions for some simple cases with constant initial and boundary conditions (e.g. Neumann solution). Computer models are not often verified using measured temperature data, and seldom are models compared to each other running with the same set of input data. In this paper, three models which employ different numerical methods and different treatments of freezing and thawing will be compared with each other, with analytical solutions, and with measured temperature data.

3.3 Brief Models Description

All three models have been discussed in previous publications so only a brief description of the major characteristics of these models are reported in this paper. The formulation of the Stefan problem in two-dimensions is (Moiseenko and Samarsky, 1965)

[3.1] $$C(T,x,y)\frac{\partial T}{\partial t} = div(K(T,x,y)\nabla T)\ ,\ (x,y,t) \in D\ ,\ T \equiv T(x,y,t) \neq T_e$$

where $T(x, y, t)$ is the temperature field in the time-space domain $D=\{0<x<l_1;\ 0<y<l_2;\ 0<t<t_1\}$, T_e is the temperature of the phase transition, C is the volumetric heat capacity, and K is the thermal conductivity. The initial and boundary conditions are

[3.2a] $$T(x,y,0) = T_0(x,y)$$

[3.2b] $$\left.\frac{\partial T}{\partial n}\right|_{x=0} = \left.\frac{\partial T}{\partial n}\right|_{x=l_1} = 0,\quad \left.\frac{\partial T}{\partial n}\right|_{y=l_2} = g$$

[3.2c] $$T(x,0,t) = \psi(x,t)$$

where $\frac{\partial}{\partial n}$ is a normal derivative, g is the temperature gradient at the lower boundary of the domain D and $\psi(x, t)$ is the temperature changes at the ground surface. The Stefan conditions at the phase boundary are

[3.3] $$T(x,y,t) = T_e$$

[3.4] $$Q(x,y)\frac{\partial \Phi}{\partial t} = (((K\nabla T)|_{P+0} - (K\nabla T)|_{P-0}), \nabla\Phi)$$

with $P \in \Phi(x,y,t) = 0$, where $P \equiv P(x,y,t)$ is a point in an area D with coordinates x, y, t and $\Phi(x, y, t) = 0$ is the phase boundary equation in implicit form. $Q(x, y)$ is the latent heat of phase transitions, P+0 is an index that denotes the limiting value for a process that starts in a region with a higher enthalpy and proceeds towards

a point on the phase front, P-0 is an index denoting a similar value but for a process starting in a region with lower enthalpy.

The Goodrich model is a one-dimensional finite difference numerical model of heat flow in soils with phase changes, which includes the thermal effect of the snow cover with changing thicknesses and characteristics during the winter (Goodrich, 1976, 1978a, 1978b, 1982a). In this model, the one dimensional heat conduction equation is approximated by the central time finite difference equation for layered systems. The freezing and thawing interface is treated by a front tracking method which is capable of good accuracy for problems with all phase change at a fixed temperature. In case of the presence of two phase boundaries (during the freeze-up period), the heat flux between boundaries is assumed to be zero. This is justified by the fact that at a phase interface the heat flux from within the region bounded by two phase planes diminished rapidly (in a few days) and the temperatures in this zone quickly approach the freezing point (Osterkamp and Romanovsky, submitted).

The model was modified to include the possibility for the presence of unfrozen water and temperature-dependent thermal soil properties using an apparent heat capacity method. This method uses the same procedure as in the Guymon/Hromadka model for apparent heat capacity and temperature-dependent thermal conductivity calculations.

The temperature at the surface of the ground during the summer and at the surface of snow during the winter as a function of time must be defined for the upper boundary conditions. Input data also include the temperature or heat flux at the lower boundary as a function of time. The option to use linearized heat balance boundary conditions (Goodrich, 1982b) was also included. The snow cover thickness and density have to be described. There is an option in the program which allows density to be determined from the snow cover thickness. Thermal properties of snow can be defined in the input data or calculated in the program. Calculational outputs are the dynamics of the ground and snow temperature fields.

The Guymon/Hromadka model is a two-dimensional finite element model for simulation of heat and moisture flow in unsaturated soils with phase change (Gosink et al., 1988; Gosink and Osterkamp, 1990; Osterkamp and Gosink, 1991), which is a modified version of the Guymon and Hromadka (1977) and Guymon et al. (1984) model. In the full formulation, this model simulates the simultaneous fluxes of water and heat in freezing and thawing soils but only the thermal part of this model which incorporates heat flow alone, will be considered in this paper. This version include two possibilities for calculating the freeze front position. One is a delta function formulation where latent heat releases or absorbs completely at a specific freezing point temperature with step function changes at the freeze front for the thermal properties. The second formulation provides the possibility to simulate the thermal processes in the ground with significant amounts of unfrozen water based on an apparent heat capacity approach with temperature-dependent thermal properties of soils (Guymon and Hromadka, 1977; Guymon et al., 1980; Hromadka et al., 1981; Guymon et al., 1984; Gosink et al., 1988; Gosink and Osterkamp, 1990; Osterkamp and Gosink, 1991). This computer model was tested and identified as being physically realistic and appropriate for freezing soil conditions in Interior Alaska (Kawasaki et al., 1982; Gosink et al., 1988). Temperature-dependent thermal properties were calculated using equations from Osterkamp (1987).

The Seregina model is a two-dimensional finite difference formulation of the equations for heat flow in nonhomogeneous soils with phase changes (Seregina, 1989; Romanovsky et al., 1991a, 1991b; Garagulya et al., 1995). This model employs the enthalpy method where the heat capacity term in (3.1) is replaced by the time derivative of the enthalpy

$$[3.5] \qquad C_a(T, x, y)\frac{\partial T}{\partial t} = \frac{\partial H}{\partial t}$$

where C_a is an apparent heat capacity and H is enthalpy (Moiseenko and Samarsky, 1965; Alexiades and Solomon, 1993). The enthalpy and thermal conductivities were smoothed by polynomials of the first order. A completely implicit locally one-dimensional scheme was used to obtain a numerical solution to this problem with smoothed coefficients. Simple iterations were used to solve a discrete system of nonlinear grid equations at each time step. The solution from the previous time step was considered to be the initial approximation of the iterative process. The program bisects the time step in the case of iterative divergence at each half of the time step.

3.4 Evaluation of Models With no Unfrozen Water

All three models were compared first with each other and with the Neumann solution to the case when the initial and boundary conditions were constant. Initial conditions were -5°C and at the time of the beginning of calculations, the surface temperature jumped to 10°C and did not change for one year (period of calculations). Thermal conductivities in the frozen and thawed states were 1.97 $Wm^{-1}K^{-1}$ and 3.39 $Wm^{-1}K^{-1}$, and heat capacities were 2.9 $MJm^{-3}K^{-1}$ and 2.1 $MJm^{-3}K^{-1}$ respectively. Volumetric moisture content was 0.4. The thermal properties and water content were the same for entire space domain.

A sensitivity analysis of the models to the size of depth and time steps used two different sets of depth steps. One set consisted of 200 depth intervals from the surface to the 100 m depth with the smallest step of 0.1 m between 0 and 10 m depth, and the largest step was 2 m (between 60 and 100 m). Another set consisted of the same amount of depth intervals (200), but the smallest one was 0.01 m (between 0 and 1 m depth) and the largest step was 1.0 m (between 12 and 16 m). Total depth in this case was 16 m. Time steps were one day, one hour and 7.2 min. Seven simulations were conducted (simulations I through VII in Table 3.1) and the results were compared with each other and with the analytical Neumann solution. Results of simulations were the

daily mean temperatures during one year of simulation (365 rows) at 16 different depths (within the upper 1 m, output data interval was 0.1 m, between 1 m and 2 m this interval was 0.2 m, and the last depth in the output file was 2.5 m). Results of comparison in terms of root mean square (RMS) deviations between each pair of calculated daily mean temperatures during the whole year in the depth interval between 0 and 2.5 m are shown in the Table 3.2 (the RMS deviations between each pair of output data matrices were calculated).

Data from Table 3.2 showed differences less than 0.13°C between calculated temperatures using different models, time and space steps except for the results of simulation III. Moreover, the largest parts of deviations in simulations I through IV and especially simulation VII occurred during the first ten days of calculations. These results would appear to justify the use of the models for calculating the thermal regime of soils during freezing and thawing. However, the following will show that this conclusion may be premature in some cases.

The next series of calculations were made with rapidly changing temperatures at the ground surface for the upper boundary conditions. Measured daily mean ground surface temperatures (Romanovsky and Osterkamp, 1995a) during 1989 near Franklin Bluffs in the Prudhoe Bay region, Alaska, were used in these calculations. Thermal properties and moisture contents of soils were the same as in the first series. Seven simulations (from simulation VIII through XIV) were run using different models and different time and depth steps (Table 3.1). The values of RMS deviations between the results of these simulations were calculated as for the first series. Results are shown in Table 3.3. Calculated RMS deviations were significantly larger than those shown in Table 3.2. These values for simulation VIII and for XII are unacceptably large (more than 1°C). This means that calculations with such large time and space steps using these models cannot accurately reproduce the temperature field dynamics in the active layer and near-surface permafrost. Moreover, the behavior of the calculated values in these two simulated temperature fields show unrealistic features where, after freeze-up,

a "thaw bulb" appeared at the permafrost surface and continued downward during the following two months. Simulation V in the first series, which was the analogy for XII (Table 3.1), showed the best agreement with the Neumann solution. Thus, agreement with the Neumann solution is a necessary condition but not a sufficient one to justify the use of the models for calculating real temperature fields, especially in case of rapid temperature changes at the ground surface.

The differences between the Guymon/Hromadka and Goodrich models for small time and space steps (XI and XIII) appeared only after the start of active layer freezing from the ground surface downwards. RMS deviation between these two runs during the first 260 days is only 0.03°C with the maximum difference of 0.15°C for all depths. Additional calculations using the Goodrich model (results were not included in the Table 3.3) with different time and space steps showed, that to predict the thermal regime of the active layer and near-surface permafrost in real situations with reasonable accuracy (within 0.3-0.4°C), the time step should not be longer than 1 hour and depth step in the upper 1 m not larger than 0.02 m. Using the Guymon/Hromadka model, this accuracy can be reached with 1 hour time steps and 0.1 m space steps within the upper 1 m depth or 1 day time steps and 0.01 m space steps. However, the possibility of using larger steps does not necessarily decrease the time of calculations compared to the Goodrich model. Computational time is approximately equal in these two cases, because the two-dimensional Guymon/Hromadka model generally is more time consuming than the one-dimensional Goodrich model (for the same time and space steps).

Results of calculations using the Guymon/Hromadka and Goodrich models were compared with each other and also with the measured temperature data for the real situation of temperature field dynamics in the active layer and near-surface permafrost at the West Dock site in the Prudhoe Bay region, Alaska in 1987 (Romanovsky and Osterkamp, 1996). It was found that, for the case of small time and space steps (the same as in XI and XIII), the results of calculations of the daily

temperatures using both models differed by only 0.02°C for the whole year (1987) for 18 depths from 0.02 to 0.87 m, except for one day just after freeze-up, when the difference reached 0.35°C at the depth of 0.17 m. The RMS deviations between the results of these two models for a whole year and for all depths was 0.012°C. Figure 3.1 shows an example of a comparison between calculated, using the Guymon/Hromadka model (dashed lines and open symbols), and measured (solid lines and filled symbols) temperatures at three depths (0.12, 0.42 and 0.72 m) during 1987-1988 at the Deadhorse site in the Prudhoe Bay region, Alaska. This comparison shows differences between calculated and measured data of 0.1 to 0.2°C during the whole year, except for 30 to 40 days in the Spring (differences up to 0.5°C) and during freeze-up and the following cooling period, when deviations could reach 1 to 2°C and more. These large errors appear to be associated with the presence of a significant amount of unfrozen water in the cooling active layer after freeze-up (Osterkamp and Romanovsky, submitted). Additional examples of the comparison between calculated and measured temperature data can be found in Romanovsky and Osterkamp (1996).

3.5 Comparison of the Models With Unfrozen Water

The Guymon/Hromadka and modified Goodrich models were compared with an analytical solution to the problem of freezing and thawing of soils containing unfrozen water or brine (Osterkamp, 1987). The equations for calculations of the temperature-dependent thermal conductivity $K(T)$, apparent heat capacity $C_a(T)$ and other thermal properties and parameters were imported from Osterkamp (1987). The weighted geometric mean equation (e.g., Lachenbruch et al., 1982)

$$K(T) = K_s^{1-\theta_f} K_i^{\theta_f} \left(\frac{K_u}{K_i} \right)^{\theta_u} \qquad [3.6]$$

where K_s , K_i , and K_u are the thermal conductivities ($Wm^{-1}K^{-1}$) of the soil, ice and unfrozen water components was used to calculate thermal conductivities of soils. The porosity in the frozen state

[3.7] $$\theta_f = \theta_i + \theta_u \approx \theta_t$$

where θ_t is the thawed porosity, and θ_i and θ_u are the temperature-dependent volume fractions of ice and unfrozen water,

[3.8] $$\theta_i = \frac{\rho_b}{\rho_i} w_i,$$

and

[3.9] $$\theta_u = \frac{\rho_b}{\rho_u} w_u,$$

where w_i and w_u are the temperature-dependent mass fractions of ice and unfrozen water; ρ_b is the dry bulk density (kg m^{-3}) of the frozen soil; and ρ_i and ρ_u are the densities of the ice and unfrozen water, respectively. The mass fraction of unfrozen water was calculated using (Osterkamp and Romanovsky, unpublished)

[3.10] $$w_u(T) = A \left| T - E \right|^B + F$$

where T is temperature in degrees Celsius and A, B, E and F are empirical constants ($A = 0.3795$, $B = -0.7790$, $E = 0$, and $F = 0$).

Apparent heat capacity was calculated according to

[3.11] $$C_a(T) = C_v(T) + L \frac{\partial \theta_u}{\partial T}$$

with

[3.12] $$C_v(T) = (1-\theta_f)C_s + \theta_i C_i + \theta_u C_u$$

where C_s , C_i , and C_u , are the volumetric heat capacities of the soil, ice, and unfrozen water, and L is the volumetric latent heat of fusion of ice. Substitution of (3.9) and (3.10) into the second term on the right-hand side of (3.11) yields

[3.13] $$L\frac{\partial \theta_u}{\partial T} = -\frac{\rho_b}{\rho_u} LAB|T - E|^{B-1}$$

The initial temperature was assumed to be -1.0°C, equilibrium temperature of the phase transitions was -1.6°C, and a constant surface temperature of -12.1°C was maintained over the whole period of calculations.

Results of these calculations for each model and the analytical solution are shown in Figure 3.2 after 10 years of freezing which shows that all three temperature profiles are within 0.02°C of each other. More examples of comparisons of the calculated and measured temperature data can be found in (Osterkamp and Romanovsky, unpublished).

3.6 Conclusions

Three numerical models for ground thermal regime calculations based on different numerical methods and different treatments of freezing and thawing were compared with each other, with analytical solutions, and with measured temperature data. Comparisons with the Neumann solution for the case where no unfrozen water was present in frozen soils shows differences of typically less than 0.13°C between calculated temperatures using different models and a wide range of the time and space steps. However, in case of rapidly changing temperatures at the ground surface, the models using large time and space steps could not accurately reproduce the temperature field dynamics in the active layer and near-surface permafrost. Thus,

agreement with the Neumann solution is a necessary condition, but not a sufficient one to justify the use of the models in calculations of real temperature fields.

With the Goodrich model, time steps not longer than 1 hour and depth steps in the upper 1 m not larger than 0.02 m have to be used to reproduce the thermal regime with reasonable accuracy. Using the Guymon/Hromadka model, the same accuracy can be obtained with 1 hour time steps and 0.1 m space steps within the upper 1 m depth or a 1 day time steps and 0.01 m space steps. However, the use of larger steps does not necessarily decrease the time of calculations compared to the Goodrich model.

For the case with unfrozen water in the frozen soils, the results of calculations using a modified Goodrich and the Guymon/Hromadka models were compared with an analytical solution and found to agree within 0.02°C.

3.7 Acknowledgments

This research was funded by the Polar Earth Sciences Program, Office of Polar Programs, National Science Foundation and by the State of Alaska. We would like to thank Dr. L. Goodrich, Dr. G. Guymon, Dr. J. Gosink, and Dr. N. Seregina for providing their original models which were used in these studies with modifications.

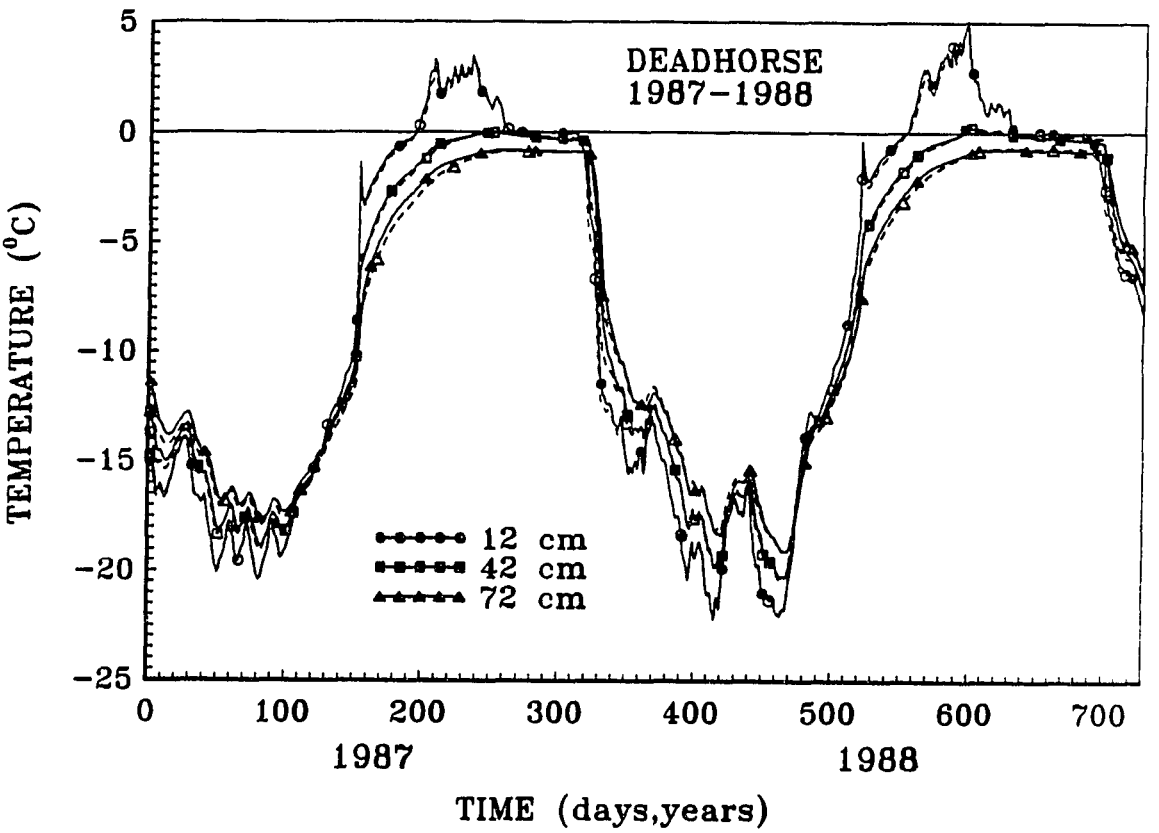

Figure 3.1 Comparison between calculated (dashed lines and open symbols) and measured (solid lines and filled symbols) temperatures at three depths (0.12, 0.42 and 0.72 m) during 1987-1988 at the Deadhorse site in the Prudhoe Bay region, Alaska.

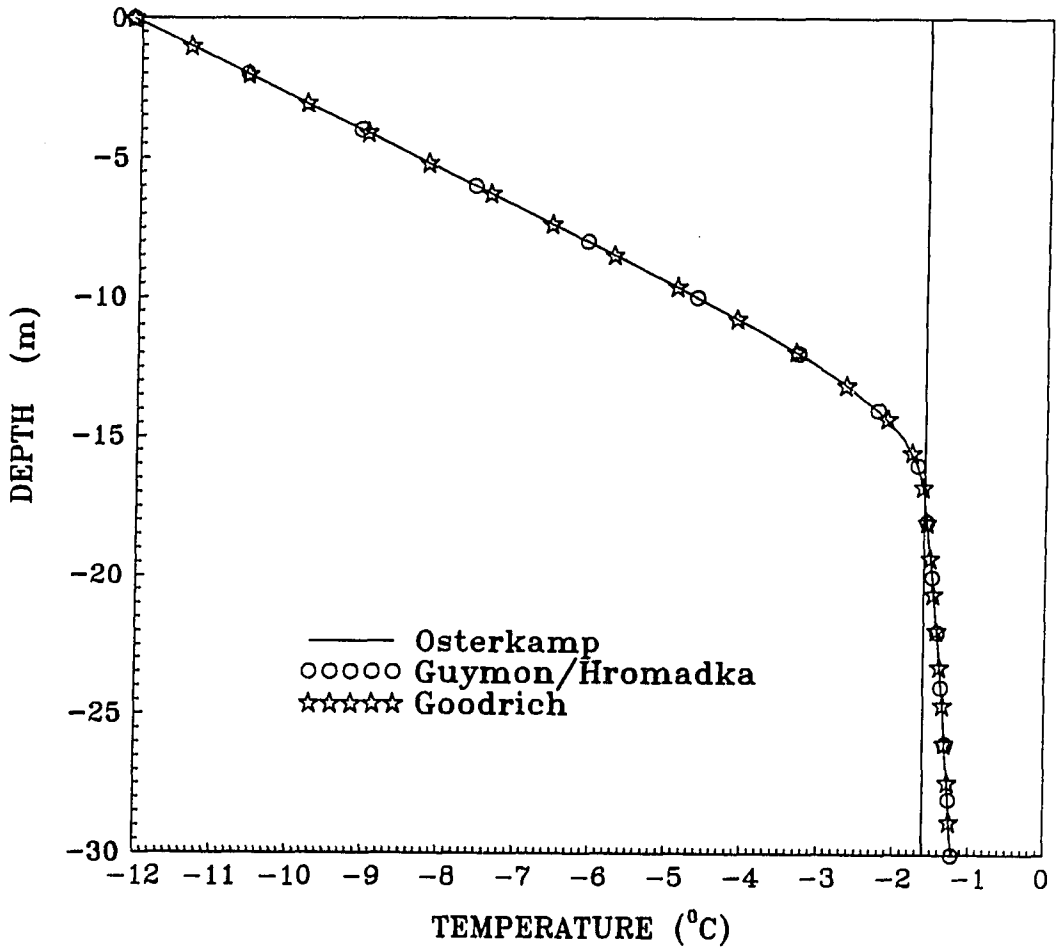

Figure 3.2 Comparison between the temperature profiles calculated using the Guymon/Hromadka and Goodrich models (open symbols) and an analytical solution from Osterkamp (1987) (solid line) when unfrozen water was present in the frozen soil.

Table 3.1 Models, time steps and minimal depth steps used in each of fourteen simulations.

Simulations	Model	Time step	Minimal depth step
I and VIII	Guymon/Hromadka	1 day	0.1 m
II and IX	Guymon/Hromadka	1 hour	0.1 m
III and X	Guymon/Hromadka	1 day	0.01 m
IV and XI	Guymon/Hromadka	1 hour	0.01 m
V and XII	Goodrich	1 hour	0.1 m
VI and XIII	Goodrich	7.2 minutes	0.01 m
VII and XIV	Seregina	1 hour	0.01 m

Table 3.2 Root mean square deviations between of each pair of calculated daily mean temperatures (in °C) in simulations I through VII and using the Neumann solution

Simulations	I	II	III	IV	V	VI	VII	Neumann
I		0.12	0.21	0.12	0.10	0.11	0.12	0.10
II			0.28	0.03	0.04	0.04	0.04	0.04
III				0.29	0.26	0.27	0.28	0.26
IV					0.03	0.02	0.03	0.03
V						0.01	0.03	0.01
VI							0.02	0.01
VII								0.03
Neumann								

Table 3.3 Root mean square deviations between of each pair of calculated daily mean temperatures (in °C) in simulations VIII through XIV

Simulations	VIII	IX	X	XI	XII	XIII	XIV
VIII		1.41	1.32	1.26	0.62	1.17	1.23
IX			0.42	0.34	1.33	0.79	0.36
X				0.21	1.42	0.48	0.25
XI					1.34	0.33	0.22
XII						1.23	1.37
XIII							0.35
XIV							

CHAPTER 4

Interannual Variations of the Thermal Regime of the Active Layer and Near-Surface Permafrost in Northern Alaska

V. E. Romanovsky and T. E. Osterkamp, 1995. Interannual Variations of the Thermal Regime of the Active Layer and Near-Surface Permafrost in Northern Alaska. *Permafrost and Periglacial Processes*, 6(4), 313-335.

4.1 Abstract

Air, ground surface, active layer and permafrost temperature measurements were made every four hours from 1986 through 1992 near Prudhoe Bay West Dock (WD), Deadhorse Airport (DH) and Franklin Bluffs (FB). Mean annual air temperatures (MAAT) were nearly identical (-12.6°C at WD, -12.9°C at DH, -12.5°C at FB) while the amplitudes increased from the coast inland (17.2°C at WD, 18.4°C at DH, 20.8°C at FB). Interannual variations were similar (3.2°C at WD, 2.9°C at DH and FB). Mean annual ground surface temperatures (MAGST) were similar at FB (-5.8°C) and DH (-6.2°C) and much colder at WD (-8.8°C) with amplitudes of 14.5°C at WD, 13.5°C at DH, and 15.2°C at FB. Interannual variations were about the same at WD (3.8°C) and DH (3.9°C) and much smaller at FB (1.4°C). Differences between MAGST and MAAT were about the same at FB (6.8°C) and DH (6.7°C) and much smaller at WD (3.9°C). The results suggest that the snow cover was thinner at WD and/or its properties were significantly different compared to the inland sites. Mean annual permafrost surface temperatures (MAPST) were the same at FB and DH (-6.8°C) and much colder at WD (-9.1°C) with interannual variations of 2.7°C at WD, 3.0°C at DH, and 1.8°C at FB. Thermal offset (MAPST - MAGST) was about the

same at WD (-0.7°C) and DH (-0.67°C) and larger at FB (-1.03°C). Generally, thawing at the ground surface began earlier at FB than at DH and WD. Average duration of thawing (99 days at WD, 104 days at DH, 107 days at FB) and dates of the start of ground freezing (September 16th at WD, September 18th at DH, September 17th at FB) were similar at all three sites. Average durations for freezing the active layer were similar at FB (62.5 days) and DH (68 days) and much less at WD (42 days). Active layer thicknesses increased from the coast inland (range of 0.21 m to 0.46 m at WD, 0.42 m to 0.69 m at DH, 0.57 m to 0.72 m at FB) and showed systematic temporal variations. These variations in active layer thicknesses may have a significant temporal and spatial effects on the carbon balance of the tundra.

4.2 Introduction

Developing an understanding of land-atmosphere interactions in arctic ecosystems requires information on the response of the thermal regime of the active layer and near-surface permafrost to seasonal and climatic changes. For example, climatic warming may be expected to increase the thickness of the active layer in the short term. The increased depth of thaw and lowering of the water table could accelerate the rate of carbon loss in arctic ecosystems providing a strong positive feedback for carbon dioxide and methane in the atmosphere (Oechel et al., 1993). This information is also useful for investigating surface geological processes related to permafrost (thermokarst development, frost heaving, ice wedge formation, mass wasting) (Washburn, 1980), for the design and construction of engineering works in permafrost regions (Esch and Osterkamp, 1990; Osterkamp and Lachenbruch, 1990), and for extracting information on past climate from permafrost temperature profiles (Lachenbruch and Marshall, 1986). On a regional scale, changes in the active layer and near-surface permafrost can be used as an indicator of global change (Nelson et al., 1993). Permafrost is linked to the atmosphere by the intervening active layer,

vegetation, and snow cover which vary strongly with time and location. Consequently, it is important to develop a better understanding of the spatial and temporal behavior of the active layer and upper permafrost to seasonal, annual, and multi-year changes in climate.

Active layer measurements in northern Alaska, Canada and Russia have a long history. Thaw depth dynamics have been measured sporadically under natural conditions near Barrow from the early 1950s to the present (McGaw et al., 1978; Brown et al., 1994) and since 1971 in an area disturbed by human activity at Prudhoe Bay (Everett, 1994). Continuous ground temperature measurements using automatic data acquisition systems were started in the middle 1980's at several sites in Northern Alaska including Toolik Lake (Nelson et al., 1988; Kane et al., 1991), West Dock, Deadhorse and Franklin Bluffs (Osterkamp et al., 1990; Zhang and Osterkamp, 1993a, 1993b; Romanovsky and Osterkamp, 1994). During the last few years, several new stations were established at West Fish Creek (Clow and Saltus, 1994), Barrow, Prudhoe Bay and Happy Valley (Everett and Nelson, 1994).

Data from these measurements were used to predict the thermal response of the active layer to climatic warming (Kane et al., 1991), to investigate the possibility of heat transfer in the active layer due to moisture migration (Nelson et al., 1988; Hinkel et al., 1990) and to investigate the relationships between climate and the thermal regime of the permafrost (Zhang and Osterkamp, 1993b). Comprehensive investigations of active layer hydrology at the Toolik Lake site were carried out by Hinzman et al., (1991) and Hinzman et al., (1993).

Canadian research on permafrost accelerated in the 1960s and 1970s in response to petroleum resource development in the Canadian Arctic and the prospect of global warming has provided new stimulus for permafrost investigations through concern for the effect of widespread permafrost degradation on terrain stability (Burn and Smith, 1993). The effects of snow and vegetation on permafrost and active layer temperatures have been investigated for many years (Gold, 1967; Nicholson and

Granberg, 1973; Judge, 1975; Nicholson, 1978; Smith, 1975 and 1976; Brown, 1978; Goodrich, 1978a and 1982a; Smith and Riseborough, 1983; Rouse, 1984; Desrochers and Granberg, 1988; Burn and Smith, 1988; Harris, 1990). Russian research has been summarized by Kudryavtsev, 1981; Kudryavtsev et al., 1978; Balobaev, 1991; Pavlov, 1980; Shur, 1988. Some of these books are available in English (Kudryavtsev et al., 1974; Pavlov, 1976).

However, there is little information about the temperature regime and long-term variations in active layer thickness. Evidence for a cyclic variation of the upper permafrost temperatures with a period of 10-11 years was obtained from temperature measurements in shallow (60 m) drill holes in the Prudhoe Bay region (Osterkamp et al., 1994). The existence of the rhythmic variability of the mean annual permafrost temperatures with periods of 9-13 and about 40 years was also reported by Kazantsev (1994) for the Russian Far East and North-East of Russia.

This paper presents the results of the field temperature measurements, including air and surface temperatures, as well as ground temperatures down to about the 1 m depth. The measurements were made every four hours for six years (1986-1992) in the Prudhoe Bay, Alaska region. The main purpose of these measurements was to develop a long-term continuous data base for investigating the thermal response of the active layer and near-surface permafrost to changes in climate. Analyses of these data can provide an understanding of the importance of the air temperature and surface conditions on the active layer and permafrost temperatures. Since the permafrost can usually be treated as a conductive medium, a determination of the surface temperature history is a key element in predicting it's future thermal regime.

4.3 Site conditions and Methods

The results of measurements made from 1986 through 1992 at three sites, West Dock (WD), Deadhorse (DH), and Franklin Bluffs (FB), are discussed in this paper.

These sites are located in Northern Alaska on the coastal plain adjacent to the Beaufort Sea and extend southward from Prudhoe Bay along the trans-Alaska oil pipeline and road. The WD site is located on the northwest corner of Prudhoe Bay at a distance of about 0.3-0.4 km from the beach. It is situated on a slightly raised ridge (3 m elevation above the sea level). Sea water came to within 0.1 km of the site during late 1991 or early summer 1992, probably as a result of a storm tide. The site surface is flat with low-centered polygonal ground microrelief (Everett et al., 1980). Vegetation consists of a continuous cover of low grasses (typically less than 0.1 m) and is classified as Wet Tundra (Selkregg, 1975; Brown and Kreig, 1983).

The DH site is located 2.5 km south of the Deadhorse airport at an elevation of about 17 m above sea level. It is about 23 km SSE from the WD site and 16 km from the ocean (Prudhoe Bay). The FB site is located 3 km south of Franklin Bluffs camp on a low terrace of the Sagavanirktok River. It is about 47 km SSW from the DH site and about 63 km from the ocean at an elevation of 88 m. Both the DH and FB sites can be described as Moist Tundra (Selkregg, 1975; Brown and Kreig, 1983). The continuous vegetation cover consists mostly of grasses, includes more species than at WD, and is generally much higher at the DH and FB sites. Dwarf shrubs are sparse at the DH site but common at the FB site. The ground surface at these sites is flat with small surface irregularities (0.1 m scale) and with occasional small frost boils.

Measurements made at each site include air temperatures in a radiation shield 1.5 m above the ground surface, ground surface temperatures, and active layer and permafrost temperatures at nine different depths, three within the active layer, three at the permafrost table, and three in the permafrost to the 0.8 m depth. Temperature measurements were made every four hours from the fall of 1986 until present using an automatic data acquisition system (Omnidata, Inc. Model El-824). The ground surface temperature was measured by a probe type thermistor placed in organic material about 0.02 m under the surface. Active layer and permafrost temperatures were measured using thermistors which were sealed in a plastic rod. The thermistor sensors were

calibrated in an ice bath to an accuracy of about 0.05°C. Air and ground surface temperatures include daily minimum, maximum, and mean temperatures. Data were collected annually at the time that batteries were replaced. During the period of measurements, three sensors out of thirty three failed. All calculations of mean annual values were made for calendar years. At the DH site, 38 days of data in 1989 (from June 7 till July 15) were lost, because of flooding. These data for air temperatures were reconstructed using WD and FB air temperature records and to fill these gaps in the ground temperatures interpolation was used.

Two methods were used to correct the measurements. The first method used the fact that, once the ground surface freezes, temperatures in the remaining thawed active layer are constrained at the phase equilibrium temperature because of the presence of two nearby phase boundaries. This phase equilibrium temperature was always between 0°C and -0.1°C so that the method is essentially an absolute calibration of each thermistor each year during freeze-up. In the second method, vertical temperature profiles were constructed every fifteen to twenty five days. Significant deviations (> 0.1°C) from smooth profiles were used to determine the corrections. Using these methods, sixteen thermistors required little or no correction. Nine thermistors required typical corrections of about 0.5°C and values for the rest of the thermistors were generally less than 0.3°C. Most of the thermistors did not require corrections until the last two or three years. Air temperatures and ground surface temperatures were not corrected. Except for a few unexplained excursions, typical accuracy of the measurements appears to be about 0.1 - 0.2°C with a resolution of 0.01°C over the full time period.

4.4 Results and discussion

4.4.1 Air Temperatures

The coastal plain has a modified arctic coastal maritime climate (Rawlinson, 1983). An important feature of this type of climate is the strong influence of the ocean on the surface air temperatures. Air temperatures were colder during the summer and warmer during the winter at WD compared to the inland sites (Figures 4.1 and 4.2). Mean summer (June, July, and August) air temperatures increased strongly with distance from the ocean (4.0, 5.2, and 8.3°C for WD, DH, and FB respectively). During October through December, the effect of the ocean was to reverse this trend with air temperatures of -19.2°C, -20.4°C, and -22.1°C at WD, DH, and FB respectively. Later in the winter (January through March), the ocean's influence was hardly noticeable (Figures 4.1 and 4.2) so that the difference between winter air temperatures at coastal sites and inland ones was not as large as for summer temperatures (Figures 4.1 and 4.2A). Annual amplitudes of the air temperatures were 17.2°C at WD, 18.4°C at DH, and 20.8°C at FB, which are typical of a continental climate (Kudryavtsev et al., 1978) and the region is designated as an inland coastal climate (Brown, 1975). This is typical of the warming that occurred since 1977 throughout Alaska (Hoffman and Osterkamp, 1986; Osterkamp and Lachenbruch, 1990).

Mean annual air temperatures (MAAT), averaged over the period of measurements were practically the same for all three sites (WD $\cong$-12.6°C, DH $\cong$12.8°C, and FB $\cong$-12.5°C). Mean monthly air temperatures (MMAT) changed at all sites simultaneously (Figure 4.1). The only difference was the amplitude of annual temperature changes which was noticed by other investigators (Brown, 1975; Haugen, 1982). Figure 4.2A shows that the average ranges of annual air temperature variations (difference between MMAT of the warmest and the coldest months) were 34.5°C for

WD, 36.7°C for DH, and 41.5°C for FB. Annual amplitude of the air temperature increased inland by 3.6°C from WD to FB.

Nineteen hundred and eighty nine was an unusually warm year for all the sites (Figure 4.3A) with MAAT -10.2°C at WD, -10.5°C at DH, and -10.4°C at FB. For the coldest year, MAAT were -13.3°C at WD in 1992, -13.4°C at DH in 1990, and -13.3°C at FB in 1988. Ranges of interannual variations in MAAT were similar for all sites, 3.1°C at WD and 2.9°C at DH and FB. The coldest MAAT (-13.4°C) at DH in 1990 was 1.5°C warmer than the value reported for 1971 at a site near Deadhorse airport (Brown, 1975). This is typical of the warming that occurred since 1977 throughout Alaska (Hoffman and Osterkamp, 1986; Osterkamp and Lachenbruch, 1990).

Measurements of air temperatures at the Prudhoe Bay/ARCO meteorological station are in agreement with those shown in Figure 4.1. The MAAT at the station (averaged over the period of 1987 - 1992) was -12.3°C and the range of annual temperature variations was 37.6°C (amplitude 18.8°C).

4.4.2 Ground Surface Temperatures

In addition to climate, the primary natural factors which influence heat and mass exchange on the ground surface and the ground surface temperature regime are the vegetation, snow cover, hydrologic regime of the surface during the thaw season, composition, and water/ice content of the active layer (Kudryavtsev et al., 1974, 1978; Luthin and Guymon, 1974). From November through April, ground surface temperatures were similar at FB and DH and significantly warmer than WD (Figure 4.2B). However, air temperatures at WD were warmer or about the same as DH and FB during this period so that other factors must be responsible for this effect. All three sites differ in the summer. The average values of mean annual ground surface temperature (MAGST) for the period of measurements were -5.8°C at FB, -6.2°C at

DH, and -8.8°C at WD which was warmer than FB by 3°C and DH by 2.6°C. Amplitudes of the mean monthly ground surface temperatures were 14.5°C at WD, 13.5°C at DH, and 15.2°C at FB.

The difference between mean monthly ground surface temperature (MMGST) and MMAT (at Franklin Bluffs for example) is

$$\Delta T_{sa}(FB) = MMGST(FB) - MMAT(FB) \qquad (4.1)$$

which is a quantitative indicator of the influence of natural factors. Mean annual values of ΔT_{sa} are

$$\overline{\Delta T_{sa}}(FB) = MAGST(FB) - MAAT(FB) \qquad (4.2)$$

Values of ΔT_{sa} averaged over the period of measurements for all sites are shown in the first three lines of Table 4.1. All values were positive (ground warmer than air) except for the month of May, which was probably due to the influence of the snow cover while air temperatures warmed strongly, and for WD in August. Table 4.1 shows that ΔT_{sa} for FB and DH were very similar and much larger than for WD except during May through September. The difference ΔT_{sa} *(FB)* - ΔT_{sa} *(DH)* is shown in the fourth row of the table and it was less than 1°C for most months, while the temperature varies over a range of more than 40°C and ΔT_{sa} can be as large as 20°C (Table 4.1). The range for this difference is from -0.8°C to +1.6°C and the annual effect differs by only 0.06°C (i.e. $\overline{\Delta T_{sa}}(FB) - \overline{\Delta T_{sa}}(DH) = 0.06^{o}C$).This coincidence means that natural factors, which determine the difference between ground surface and air temperatures, provided the same total effect for the two sites.

At WD, the ground surface temperature regime differed significantly from that at DH and FB, except during May, September, and October (Figure 4.2B and Table 4.1). Values of ΔT_{sa} for WD were substantially different than those for DH and FB (Table 4.1). The difference $\Delta T_{sa}(DH)$ - $\Delta T_{sa}(WD)$ reached 50% of the $\Delta T_{sa}(DH)$

value and almost 100% of the $\Delta T_{sa}(WD)$ value during the winter. The difference in mean annual values, $\overline{\Delta T_{sa}}(DH) - \overline{\Delta T_{sa}}(WD) = 2.8^{0}C$, was also large.

To explain these differences it is necessary to examine the factors which cause spatial variations in the ground surface temperatures. Most of these factors, such as hydrology of the surface, the character of heat and moisture exchange between surface and atmosphere are important only during the summer time (Kudryavtsev et al., 1978). The vegetative cover acts as an insulator mostly during the summer (Rouse, 1984). During the winter, grass cover can influence ΔT_{sa} only through modifications to the snow cover (Smith, 1975; Rouse, 1984; Sturm and Holmgren, 1994). Table 4.1 shows, that the values of ΔT_{sa} for the snow free months at all three sites were very close to each other. This means that the above factors had approximately the same total influence on ΔT_{sa} at these sites and didn't contribute significantly to the spatial variability of the MAGST. Moreover, the values of ΔT_{sa} for the summer months were very small, compared to the winter (Figure 4.4). The mean values for June to August were 0.6°C at WD, 1.1°C at DH, and 0.5°C at FB. These differences were nearly compensated in the annual means by negative values of ΔT_{sa} in May, which were probably the result of the cooling effect of the snow during the snowmelt. The mean values of ΔT_{sa} for four months (May - August) were -0.15°C at WD, 0.4°C at DH, and -0.1°C at FB.

Significant differences between MMGST for WD and DH (Figure 4.2B) existed during the winter indicating the warming effect of snow cover as the main cause of the spatial variations of MAGST. Comparison of the mean monthly ground temperatures at the depth of 0.02 m between DH and WD shows that in May, June and July these temperatures differed less than 0.3°C (Figure 4.5). Differences appeared in August and September, but remained small (less than 1°C). In October these started to increase (1.25°C) and reached their maximum values in November (6.1°C) and December (6.7°C). During the rest of the winter the differences remained large (4.75°C in

January, 4.25°C in February, and 3.1°C in March). The contribution of the four "summer" months (May - August) to the total 2.6°C MAGST difference was less than 0.1°C or 3.3% and can be explained by slightly warmer summer temperatures at the DH site (Figure 4.2A). Temperatures at the 0.02 m depth for DH, during these four months, averaged 0.3°C warmer than for WD, while average air temperatures during the same period were 0.7°C warmer.

The difference in the warming effect of the snow cover between DH and WD can also be shown by comparing of records of MMGST variations during 1987 - 1992 at DH and WD and snow cover variations at the Prudhoe Bay/ARCO meteorological station (Figure 4.6). During winters with deep snow (1988-1989 and 1990-1991) the differences between MMGST at DH and WD were the most significant while the anomalous snowless winter of 1989-1990 shows the smallest difference in MMGST.

Data for the winter of 1987 - 1988 show something different. The snow cover during that winter at the Prudhoe Bay/ARCO station was thick (compared to other winters), but the difference between MMGST at WD and DH sites was very small (Figure 4.6B). This could be a result of local snow variability, but other explanations are possible, such as variations in thermal properties of the upper part of active layer due to differences in water content during the summer and fall of 1987 compared to other years. Thermal properties and active layer water content can have a significant influence on the warming effect of the snow cover (Lachenbruch, 1959; Romanovsky, 1987). It is interesting to note that, in 1987, there was no thermal offset in the mean annual ground temperature profile at the DH site (Figure 4.7B). Variations in snow cover thickness, density and depth hoar fraction (Zhang et al., submitted) can influence the temporal variations of MAGST. Hence, any scenarios of global warming should include forecasts of snow cover to realistically estimate ground temperatures.

The ground surface freezing index was generally larger at the WD site (Figure 4.12A) presumably because of the snow cover thickness (thinner at WD) and/or its characteristics compared to DH and FB. Franklin Bluffs was always larger than DH

because of the colder winters inland (Figures 4.1 and 4.2A) and apparently similar snow cover. For the winter of 1989-1990 when the snow cover was extremely thin (Figure 4.6C), the ground surface freezing index at WD was less than at FB.

As a result of interannual MAAT and snow cover changes, the MAGST had significant temporal variations (Figure 4.3B). The range of MAGST variations for the two sites nearest the coast (3.8°C for WD and 3.9°C for DH with a maximum in 1989) were slightly larger than ranges of MMAT variations. For the FB, site the range of MAGST variations were almost one third that for DH and WD and equaled 1.4°C.

This analysis provides strong evidence that, in the Prudhoe Bay region, the warming effect of the snow cover was the most significant natural factor which determined the temperature difference between the air and ground surface and played the most important role in spatial variations of MAGST.

4.4.3 Active Layer and Permafrost Table

The thermal properties of the active layer do not remain constant during the year because of thawing and freezing and the difference in thermal conductivity between thawed and frozen ground causes a "negative thermal offset" defined as the difference between the MAPST and MAGST (Kudryavtzev et al., 1974; Goodrich, 1978a; Burn and Smith, 1988). As a result, the mean annual ground temperature usually decreases with depth in the active layer. Thermal offset depends on soil thermal properties and it is usually largest within a peat layer. Summer temperature conditions on the ground surface also have significant influence on the thermal offset value (Romanovsky, 1989).

The active layer at all three sites typically has a two-layer structure with the upper part (0.1 to 0.2 m and sometimes deeper) consisting of a peat or peaty silt overlying silt with a few organic inclusions. Some of the physical properties of peat and silt for the sites are shown in Table 4.2, adopted with modifications from Zhang

(1993). The thermal properties of peat samples, both in the frozen and thawed states were measured in the laboratory. Thawed values of the thermal properties at all three sites were measured in the field.

Laboratory measurements showed that the thermal conductivity values of the peat using the needle probe method were nearly constant over a range of temperatures (from -0.5°C to -14°C) with no evidence for significant unfrozen water as suggested by Hinzman et al. (1991). The mean value for the thermal conductivity of thawed peat was $K_t = 0.6$ $Wm^{-1}K^{-1}$, and for frozen peat $K_f = 1.2$ $Wm^{-1}K^{-1}$ so that the ratio, $K_f / K_t = 2$, was large enough to produce a noticeable thermal offset. The measured conductivity values are similar to results of measurements carried out for samples from Toolik Lake (Hinzman et al., 1991). Laboratory measurements of these authors show that for saturated silt the ratio K_f/K_t does not exceed 1.3.

These differences in K_f and K_t should cause thermal offsets in the active layer and profiles of decreasing mean annual ground temperatures with depth confirm this hypothesis (Figure 4.7). For WD and DH, the thermal offset was generally larger when the active layer was deeper and the thawing index on the ground surface was higher (compare Figures 4.7 and 4.11). For FB, the thermal offset was significant but it did not depend on depth of the active layer. This effect can be explained by comparatively small variations in active layer thickness at FB (0.6 to 0.7 m), while at WD and DH the variations (Figure 4.11) are larger (0.21 m to 0.46 m at WD and 0.42 m to 0.69 m at DH).

The main feature of the curves in Figure 4.7 is that the most significant changes in MAGST took place within the upper part of the active layer. For FB, the main changes occurred in the depth interval 0 - 0.4 m and deeper than 0.5 - 0.6 m the temperature remained nearly constant (Figure 4.7A). For DH (Figure 4.7B), the changes took place within the upper 0.2 m and deeper than 0.3 - 0.4 m the changes were much smaller. The same is true for WD where the most significant changes occurred in the upper 0.2 m (Figure 4.7C).

For 1989, when the MAGST reached its maximum, and for the previous year, a significant decrease of the mean annual temperatures with depth was noted at all depths at the DH and WD sites (Figure 4.7B and 4.7C). This is probably related to the 10 - 11 year cycle of ground temperature variations observed by Osterkamp et al. (1994).

The average profiles (1987-1992, Figure 4.8) show the same basic features of the thermal offset (the main changes of mean annual ground temperatures occur within the upper 0.3 m). Temperatures remained practically constant at depths of 0.5 - 0.6 m or more for DH and FB. However, for WD the temperatures continued to decrease slightly at all depths (down to 0.72 m). The largest thermal offset was found at FB (1.03°C), and it was significantly smaller at DH (0.67°C) and WD (0.7°C). The mean annual permafrost surface temperatures were the same at DH and FB (-6.8°C) and much colder at WD (-9.1°C). Interannual variations in MAPST were similar at WD (2.7°C) and DH (3.0°C) and much smaller at FB (1.8°C). These values are in agreement with estimations of the range of the ground surface temperature variations (4°C for WD and DH and 1.2°C for FB) obtained from analysis of the temperature profiles from shallow boreholes (60 m) which were located at the same sites (Osterkamp et al., 1994).

An approximate solution which was used to estimate the value of the thermal offset is derived below using the following assumptions: 1) thermal conductivity, K, and heat capacity, C, vary with the temperature (as a step function at T_e , the equilibrium temperature) but are independent of position; 2) $T_e = 0$°C, this assumption is not restrictive, because if $T_e \neq 0$°C a change of variable $T \rightarrow \Theta = (T - T_e)$ can be made; 3) the ground temperature regime is in a periodic steady state with period, P, equal to one year so that $T(x, y, z, t + P) = T(x, y, z, t)$, where x, y, z are spatial coordinates, and t is time.

The one-dimensional diffusion equation for heat

$$C(T)\frac{\partial T}{\partial t} = \frac{\partial}{\partial x}(K(T)\cdot\frac{\partial T}{\partial x}) \tag{4.3}$$

can be modified by introducing a new variable T'(Carslaw and Jaeger, 1959) which is (for the case of a seasonally thawed active layer)

$$T' = \begin{cases} T \quad , \text{ if } T \le 0^0 C, \\ \dfrac{K_t}{K_f}\cdot T, \text{ if } T > 0^0 C. \end{cases} \tag{4.4}$$

The usual Stefan thawing problem is transformed into (in T'space)

$$\begin{cases} K_f \cdot \dfrac{\partial^2 T'}{\partial x^2} = (C_t \cdot \dfrac{K_f}{K_t}) \cdot \dfrac{\partial T'}{\partial t} \quad , \quad x < X, \\ K_f \cdot \dfrac{\partial^2 T'}{\partial x^2} = C_f \cdot \dfrac{\partial T'}{\partial t} \quad , \quad x \ge X, \\ T'(X-0,t) = T'(X+0,t) = 0 \ ^0C, \\ K_f \cdot \dfrac{\partial T'}{\partial x}\Big|_{X-0} - K_f \cdot \dfrac{\partial T'}{\partial x}\Big|_{X+0} = -\rho \cdot L \cdot \dfrac{dX}{dt}. \end{cases} \tag{4.5}$$

where C_t and C_f are the thawed and frozen volumetric heat capacities, X is the position of the phase boundary, ρ is the density, and L is the latent heat. The quantity $X-0$ refers to the upper side and $X+0$ the lower side of the phase boundary.

The set of equations (4.5) shows that the transformation (4.4) has the effect of creating a homogeneous half space with thermal conductivity, K_f, in both the thawed and frozen states and heat capacity, $C_t \cdot \dfrac{K_f}{K_t}$, in the thawed state and C_f in the frozen state.

The thermal offset is defined as the difference between the MAPST and the MAGST,

$$\Delta T_k = \overline{T_{ps}} - \overline{T_{gs}} \tag{4.6}$$

and is a result of different thermal conductivities in the frozen and thawed states. It is not necessary to obtain a detailed solution of (4.5) to determine ΔT_k since ΔT_k is given in terms of mean annual values. In the case of a periodic steady state regime with the same thermal conductivity in both the frozen and thawed states (4.5) there will be no thermal offset in the active layer. This means that the mean annual temperature of the ground $\overline{T'}(x)$ will be constant in the active layer and

$$\overline{T'_{ps}} = \overline{T'_{gs}}\ , \tag{4.7}$$

where $\overline{T'_{ps}}$ is the mean annual value of T' at the permafrost surface ($x = X$), and $\overline{T'_{gs}}$ is the mean annual value of T' at the ground surface ($x = 0$).

This fact can be used to calculate the value of ΔT_k. By definition

$$\overline{T_{gs}}' = \frac{I_t' - I_f'}{P}\ , \tag{4.8}$$

where I_t' and I_f' are the thawing and freezing indices for T' at the ground surface. The thawing index is the sum of all positive (above 0°C) mean daily ground surface temperatures during the calendar year and the freezing index is the absolute value of the sum of all negative (below 0°C) mean daily ground surface temperatures during the calendar year ($I_f' > 0$). Because $T' = T$, when $T \le 0$°C, $I_f' = I_f$. Here, I_f is the freezing index at the ground surface for temperature T.

Recalling the definition of T' (4.4), I_t' can be expressed in terms of the thawing index I_t so that

$$I_t' = \frac{K_t}{K_f} \cdot I_t \ , \tag{4.9}$$

and, consequently, combining (4.8) and (4.9)

$$\overline{T_{gs}'} = \frac{\frac{K_t}{K_f} \cdot I_t - I_f}{P} \ . \tag{4.10}$$

Then, according to (4.7) and (4.10)

$$\overline{T_{ps}'} = \frac{\frac{K_t}{K_f} \cdot I_t - I_f}{P} \ . \tag{4.11}$$

At the permafrost surface where $T \leq 0°C$, (4) implies $\overline{T_{ps}'} = \overline{T_{ps}}$.

In analogy to (4.8), $\overline{T_{gs}} = \frac{I_t - I_f}{P}$, and using (4.6) and (4.11)

$$\Delta T_k = \frac{I_t}{P} \cdot \left(\frac{K_t}{K_f} - 1 \right) \tag{4.12}$$

Equation (4.12) was derived for a seasonally thawed active layer (i.e. MAPST $\leq 0°C$). Using (4.11)

$$\overline{T_{ps}} = \frac{K_t \cdot I_t - K_f \cdot I_f}{K_f \cdot P} \leq 0 \quad , \tag{4.13}$$

or $K_t I_t \leq K_f I_f$.

When a seasonally frozen layer exists with a thawed layer under it $K_t I_t > K_f I_f$ The same derivation can be used to obtain expressions for the thermal offset value in this case, except that a "homogeneous thawed half-space" instead of the "homogeneous frozen half-space" should be used. The final results are

$$\Delta T_k = \begin{cases} \frac{I_t}{P} \cdot \left(\frac{K_t}{K_f} - 1 \right), & \text{if } K_t \cdot I_t \leq K_f \cdot I_f \ , \\ \frac{I_f}{P} \cdot \left(1 - \frac{K_f}{K_t} \right), & \text{if } K_t \cdot I_t > K_f \cdot I_f \ . \end{cases} \tag{4.14}$$

Equations (4.14) were stated by (Kudryavtsev, 1981), but no derivation of them was ever published.

Equation (4.14) was compared to the predictions of a numerical method (Goodrich, 1976; 1982). The calculations were made for two soil types (clay and sand) and for both permafrost and seasonally frozen cases. Soil thermal properties were K_f = 2.21 $Wm^{-1}K^{-1}$ and K_t = 1.13 $Wm^{-1}K^{-1}$ for clay, and K_f = 3.01 $Wm^{-1}K^{-1}$ and K_t = 2.19 $Wm^{-1}K^{-1}$ for sand. The MAGST = -10°C for permafrost with no snow cover and the amplitude of the annual sinusoidal variations was 20 K. For the seasonally frozen layer case, the MAGST = 5°C, and the amplitude was 15 K. Data from Table 4.3 shows excellent agreement between these two methods.

Using (4.14), the thermal offset values were calculated for all sites and for each year (Table 4.4) using the thermal conductivities of the peat. The agreement between calculated and measured values may be somewhat fortunate because in (4.14) the active layer is treated as homogeneous.

4.4.4 Thawing and Freeze-up of the Active Layer

These ground temperature measurements allow estimates of the dates of the beginning of thawing, freezing, and freeze-up dates. Dates for the beginning of thawing were taken to be the dates when ground surface temperatures became stable positive (above 0°C). These dates were consistent with the snowmelt dates obtained from the Prudhoe Bay/ARCO meteorological station. Dates for the beginning of freezing were taken to be the dates when ground surface temperatures became stable negative (below 0°C). Generally, thawing began earlier at FB than at DH and WD. Thawing started (Figure 4.9A) very uniformly at all sites between June 4th and June 16 during the first three years of measurements (except at FB in 1987). Average dates for the beginning of thawing were June 9th at WD, June 6th at DH, and June 1st at FB. Thawing started significantly earlier in 1990 (May 25th for WD, May 30th for DH, and May 17th for FB), because of an extremely shallow snow cover during the 1989 - 1990 winter and an anomalously early snowmelt. At the Prudhoe Bay/ARCO meteorological station, there was no snow during May 1990 and the maximum depth of snow during April was only 0.05 m (Figure 4.6C). After 1990, the thawing dates were still earlier than 1987 - 1989 for DH and FB (between May 29th and June 1st) and approximately the same for WD (June 12th in 1991 and June 11th in 1992). These data indicate that the beginning of thawing of the active layer depends primarily on air temperatures and the timing of snowmelt.

Duration of thawing (difference between the dates for the start of freezing and thawing at the ground surface) was longest for the FB site and reached its maximum (128 days) in 1990 (Figure 4.10A). Except for this year, the duration was almost identical for DH and FB during 1987 -1992 (the maximum difference is 5 days). After 1990, the duration of thawing returned to 1988, 1989 values. Comparing Figures 4.9A and 4.10A shows that, in addition to Fall air temperatures, the timing of the start of thawing was important in determining the duration of thawing. Comparison of annual

variations of thawing duration shows poor agreement with MAGST variations (Figure 4.3B) and with thaw index variations (Figure 4.12B). The latter were influenced more by summer temperatures rather than summer duration. Average duration of thawing were 99 days for WD, 104 days for DH, and 107 days for FB. Average dates for the start of freezing (Figure 4.9B) were very uniform; September 16th for WD, September 18th for DH, and September 17th for FB.

Freeze-up dates for the active layer were determined using mean daily ground temperature records, one example of such records is shown in Figure 4.11. These dates were taken to be the dates when the temperatures at all depths began to decrease sharply after the "zero curtain" disappeared (Figure 4.11). Freeze-up dates (Figure 4.9C) depend on air temperatures, active layer thickness (a deeper active layer takes longer to freeze), soil water content, thermal properties of the soil, the date for the start of freezing at the ground surface, and especially the timing of the snow cover and its variation with time. The deepest active layer for all sites occurred in 1989 (Figure 4.12C) when the snow on the ground appeared in October and was very shallow (0.025 m maximum snow depth for October and November). As a result, the freeze-up took place earlier in 1989 than in 1988 and 1990 for the FB and DH sites. For WD, freeze-up was 8 days earlier in 1988 and 20 days earlier in 1990 than in 1989. Variations of the freeze-up date show poor agreement with thaw index variations and better agreement with the MAGST variations (especially for WD and FB). For 1987 to 1990, freeze-up occurred significantly earlier at the FB site than at DH despite the deeper active layer at FB. This may have been a result of the slightly colder surface temperatures at FB.

Variations in the duration of the freeze-up period (difference between the start of freezing and freeze-up date) are shown in Figure 4.10B. The longest duration was measured at the DH site. It increased slightly from 1987 to 1991 and then decreased in 1992 to the 1988 value. At the FB site, freeze-up duration was almost constant during 1987 to 1990 and then increased in 1991 and 1992. The freeze-up duration generally

decreased at the WD site during the period of measurements with some local maximum in 1989 and minimum in 1990. Average duration of freeze-up period for DH was 68 days. This is similar to FB (62.5 days) and much longer than WD (42 days).

Normally, freezing occurs both from the top and bottom (upward freezing) of the active layer. The most favorable conditions for freezing from the bottom are cold MAPST (which results in a large thermal gradient and high heat flux into the permafrost) and early snow cover appearance. The most common case for all three sites was when about two thirds of the active layer froze from the top and one third from the bottom, though this proportion had significant interannual variations.

4.4.5 Active Layer Thickness

Values of MAGST and the range of annual ground surface temperature variations together determine the value of the ground surface thawing index which influences the thickness of the active layer (defined as the maximum thaw depth) (Lachenbruch, 1959; Kudryavtsev et al., 1974). The most important soil properties are the ice content within the active layer which determines the value of latent heat and influences other thermal properties of the ground, and the thermal conductivity and heat capacity of the active layer both in the frozen and thawed states (Kudryavtsev et al., 1974; Pavlov, 1980; Balobaev, 1991). The value of the MAPST also has some influence on active layer thickness (Kudryavtsev et al., 1974). In some cases (sand and gravel with high hydraulic conductivity and a good drainage conditions), infiltration of summer precipitation can play a significant role in determining thickness of the active layer (Kudryavtsev et al., 1974). For the area of investigations, this process probably did not have a noticeable effect on active layer thickness because of the low water permeability of the soils and their saturated conditions.

Active layer thickness increases from the coast inland with the increasing thawing index and MAGST (Figures 4.12B and 4.12C). The mean for measurements of the active layer thicknesses was 0.36 m at WD, 0.53 m at DH, and 0.62 m at FB.

Interannual changes of the active layer thickness were large ranging from 0.57 m to 0.72 m at FB, 0.42 m to 0.69 m at DH, and 0.21 m to 0.46 m at WD (Figure 4.12C). In general, variations in active layer thickness coincided with MAGST and MAPST changes (Figures 4.3B and 4.3C), reaching a maximum in the warmest year (1989). However, the active layer thickness is much more sensitive to summer temperature (thawing index) changes (Figure 4.12B) than to MAGST changes. Comparing 1990 and 1991 for FB and DH it is clear that the relative increase in MAGST in 1991 was due to a significantly warmer winter, compared to the winter of 1990 (Figure 4.12A). The summer of 1991 was colder than 1990 and the thawing index in 1991 was 41% less for FB and 35% less for DH than in 1990 (Figure 4.12B). As a result, the active layer thickness in 1991 was 15% less for FB and 20% less for DH than in 1990 (Figure 4.12C). At FB, in spite of a decrease of MAGST from 1991 to 1992 (Figure 4.3B), the summer of 1992 was warmer and thawing index was higher in 1992 by 16% (Figure 4.12B). As a result, the active layer was slightly thicker by 2% (Figure 4.12C).

When the thawing index remained approximately constant, the MAGST and MAPST became major factors in the active layer thickness variations. The most typical years are 1987, 1988, 1991, and 1992 at DH and WD. While the thawing index remained almost constant (Figure 4.12B), the MAGST increased substantially from 1987 to 1988 (more than 1°C) and decreased approximately by the same value from 1991 to 1992 (Figure 4.3B). As a result, the active layer thickness increased from 1987 to 1988 (by 7% for DH and 28% for WD) and decreased from 1991 to 1992 (by 14% for DH and 30% for WD) (Figure 4.12C).

Figure 4.12C shows that the active layer thicknesses were generally shallower at the beginning of the measurement period, thickest in 1989, and thinner in the early 1990's. In general, the significant interannual variations of active layer thickness make a comparative analysis of the spatial behavior of the active layer difficult. The large observed variations of the active layer thicknesses, especially at WD and DH, may be expected to influence the carbon balance of the active layer (Oechel et al., 1993). These results suggest that the carbon balance in the active layer near the coast may have significant spatial variations and may be time-dependent with large variability over times of a few years.

4.5 Conclusions

Temperature measurements made in the air, active layer and permafrost (to the 1 m depth) on a transect southward from Prudhoe Bay, Alaska are reported for the period from 1987 to 1992. The sites included one near the coast (WD), one 16 km inland (DH), and one 63 km inland (FB). Mean annual air temperatures (MAAT) were similar for all three sites (-12.6°C at WD, -12.8°C at DH, -12.5°C at FB) while the annual amplitude of the mean monthly temperatures increased with distance inland (17.2°C at WD, 18.4°C at DH, 20.8°C at FB). Interannual variations in MAAT were similar at all three sites; 3.1°C at WD and 2.9°C at DH and FB. The WD site was typical for its coastal setting with warmer winters and colder summers compared to the inland sites.

While MAAT were similar at all three sites, the mean annual ground surface temperatures (MAGST) for the period of measurements were similar at FB (-5.8°C) and DH (-6.2°C) and much colder at WD (-8.8°C). Amplitudes of the mean monthly ground surface temperatures were 14.5°C at WD, 13.5°C at DH, and 15.2°C at FB. Interannual variations in MAGST were about the same at WD (3.8°C) and DH (3.9°C) and much smaller (1.4°C) at FB. Although mean monthly air temperatures at the

coastal site (WD) were warmer in winter and colder in summer compared to the inland sites (DH and FB), the mean monthly ground surface temperatures at WD were always colder than DH and FB. Generally, mean monthly ground surface temperatures were always warmer than the air temperatures except for the month of May which was due to the cooling effect of the snow cover while air temperatures warmed. The differences between the MAGST and MAAT were about the same at FB (6.8°C) and DH (6.7°C) and much smaller at WD (3.9°C). Mean monthly air temperatures for winter (November through April) were similar for all sites but the ground surface temperatures were similar for FB and DH which differ significantly from those at WD. These results suggest that snow cover was the major factor in determining ground surface temperatures and that there were significant differences in snow cover thicknesses (thinner at WD) and/or properties at the WD site.

The mean annual permafrost surface temperatures (MAPST) were the same at DH and FB (-6.8°C) and much colder at WD (-9.1°C). Interannual variations in MAPST were similar at WD (2.7°C) and DH (3.0°C) and much smaller at FB (1.8°C). These values for the 1987 to 1992 period are similar to those obtained by analyses of the temperature profiles (to 60 m) which produced a cycling of permafrost temperatures for the 1983 to 1993 period (Osterkamp et al., 1994).

Thermal offset in the active layer (ΔT_k = MAPST - MAGST) was about the same at WD (-0.7°C) and DH (-0.67°C) and larger at FB (-1.03°C). Calculated values of ΔT_k using an analytical and a numerical method were similar and the analytical method yielded values in good agreement with measured values.

Generally, thawing at the ground surface began earlier at FB than at DH and WD. The average date for all sites was June 5th (June 9th at WD, June 6th at DH, and June 1st at FB). Average duration of thawing was 99 days for WD, 104 days for DH, and 107 days for FB. There was no spatial pattern to the dates for the beginning of freezing but, in 1991 and 1992, the ground began freezing earlier than in previous

years. The average dates for the start of ground freezing were September 16th at WD, September 18th at DH, and September 17th at FB. Active layer freeze-up always occurred earlier at WD generally followed by FB and then DH. Average durations for freezing the active layer were similar at FB (62.5 days) and DH (68 days) and much less for WD (42 days). Freeze-up at WD was much earlier in 1990, 1991, and 1992, compared to the three previous years. A thin snow cover during October and November resulted in an earlier date for active layer freeze-up.

Active layer thicknesses (maximum thaw depth) increased from the coast inland with an increasing thaw index and MAGST. Interannual changes in the thicknesses of the active layer were 0.15 m at FB (0.57 m to 0.72 m), 0.27 m at DH (0.42 m to 0.69 m), and 0.25 m at WD (0.21 m to 0.46 m). These changes were more sensitive to the thaw index than to MAGST. Active layer thicknesses generally increased from 1987 through 1989 and then decreased through 1992. At WD, the thicknesses varied by more than a factor of two over this period. These large variations in thickness may have a significant temporal and spatial effect on the carbon balance of the tundra.

4.6 Acknowledgments

This research was funded by the Polar Earth Sciences Program, Office of Polar Programs, National Science Foundation and by the State of Alaska. The data reported herein will be available in 1996 from the WDC-A/NSIDC, NOAA, Boulder, CO.

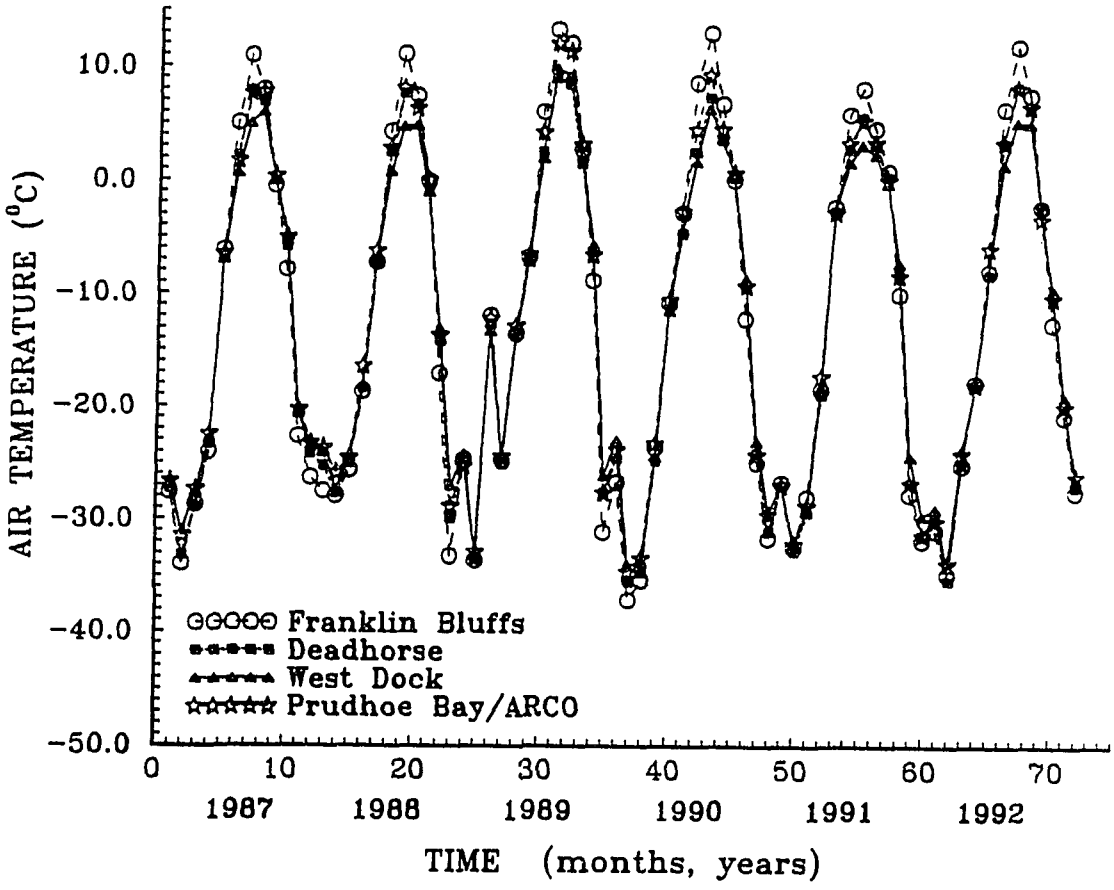

Figure 4.1 Mean monthly air temperature measurements for the period from January, 1987 through December, 1992) at West Dock, Deadhorse, and Franklin Bluffs. Measurements made at the Prudhoe Bay/ARCO station are shown for comparison.

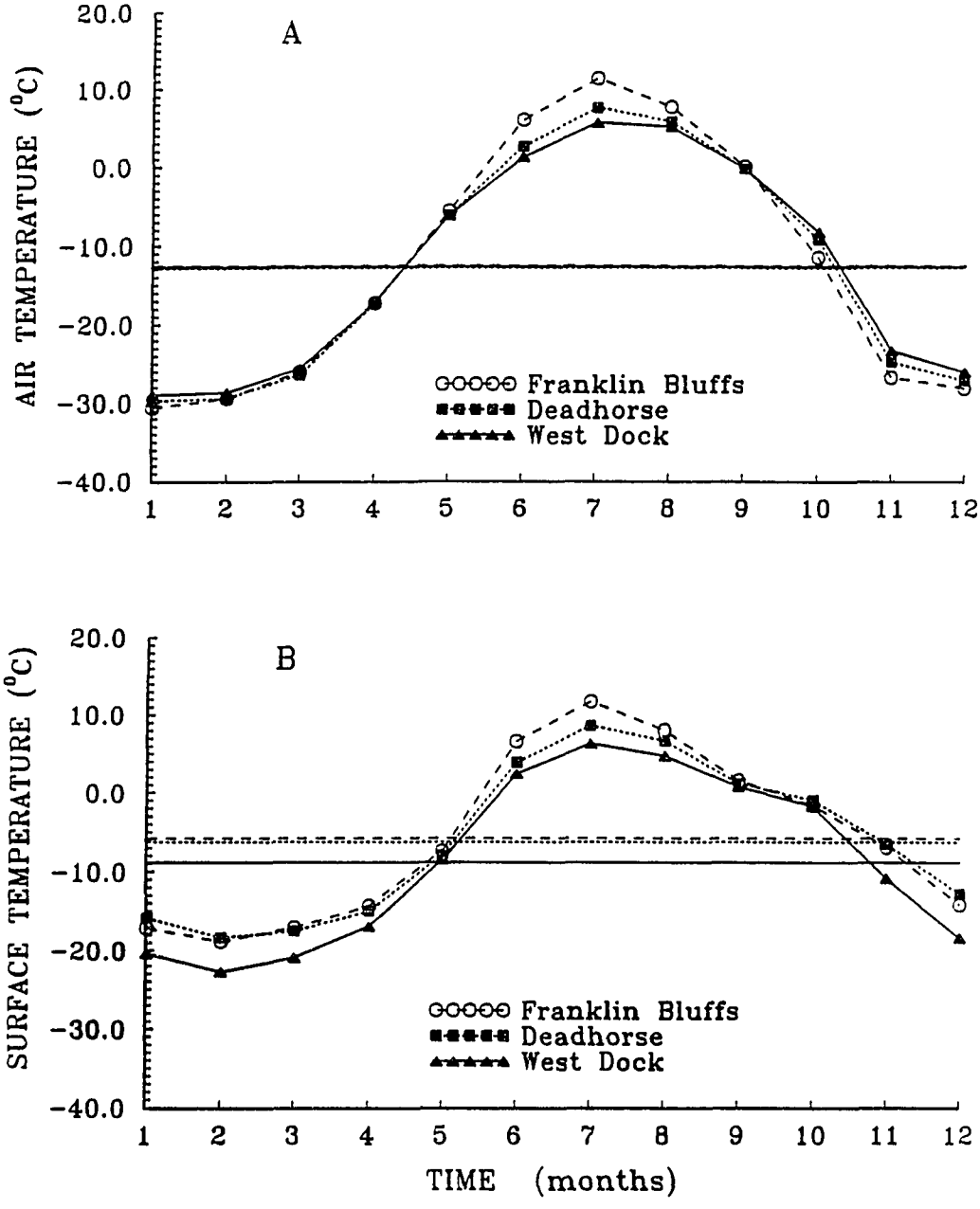

Figure 4.2 The averaged mean monthly temperatures at all sites for the period of measurements (1987 - 1992): A - air temperature, B - ground surface temperatures.

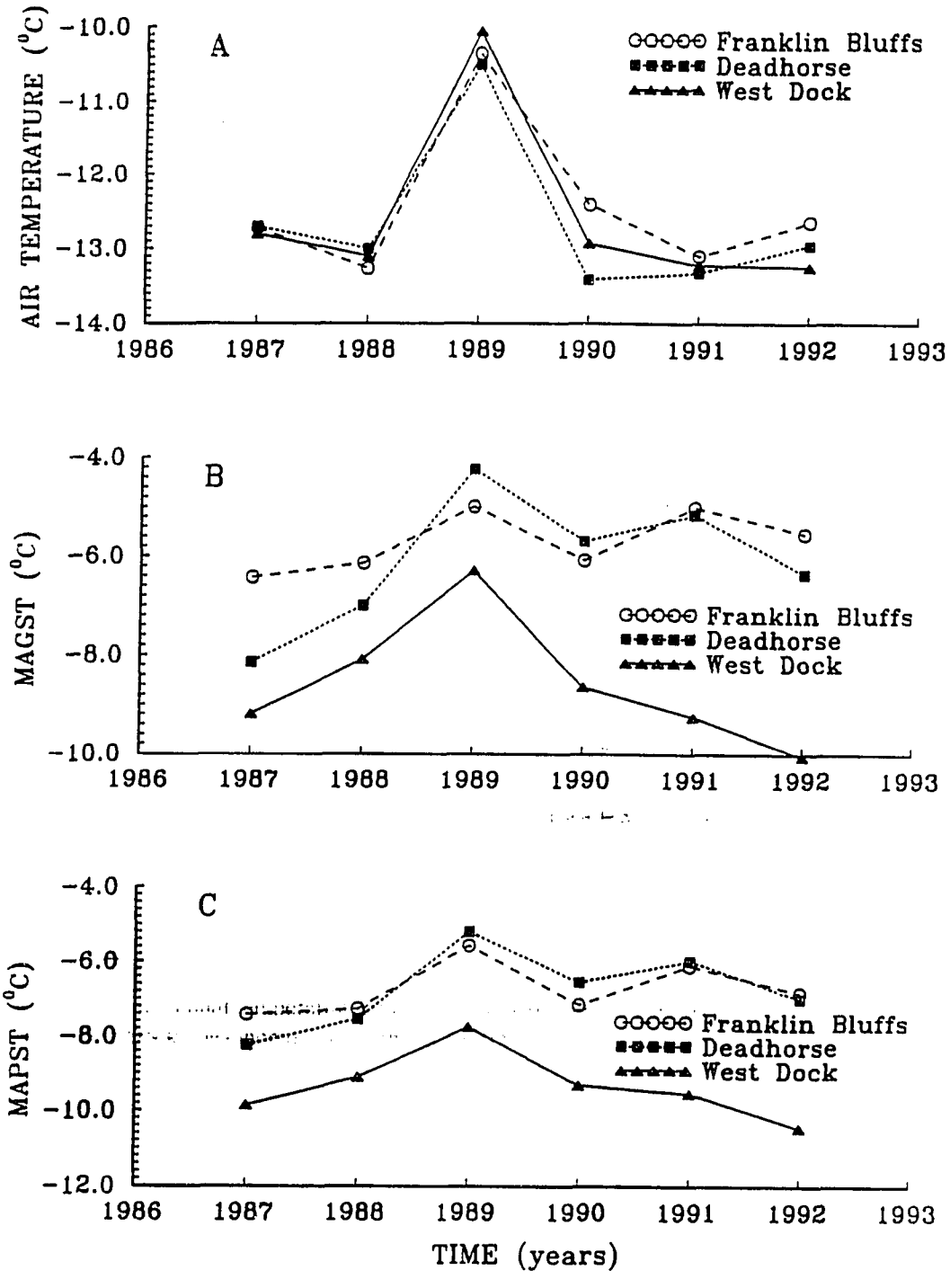

Figure 4.3 Mean annual temperatures (calendar year) at all sites: A - mean annual air temperature (MAAT); B - mean annual ground surface temperature (MAGST); C - mean annual temperature at the permafrost table (MAPST).

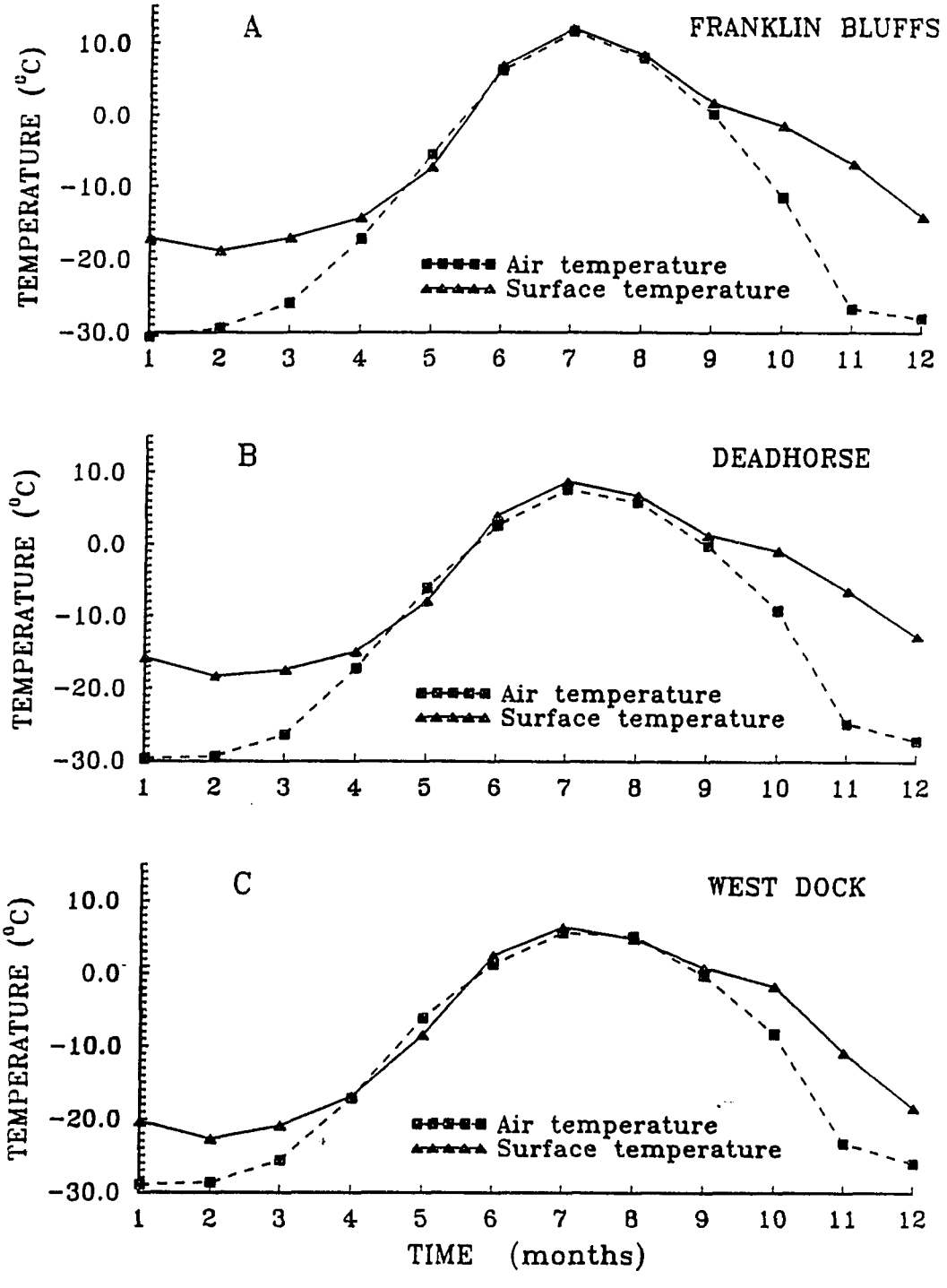

Figure 4.4 Mean monthly air and ground surface temperatures, averaged over the period of measurements (1987-1992): A - at the FB site, B - at the DH site, C - at the WD site.

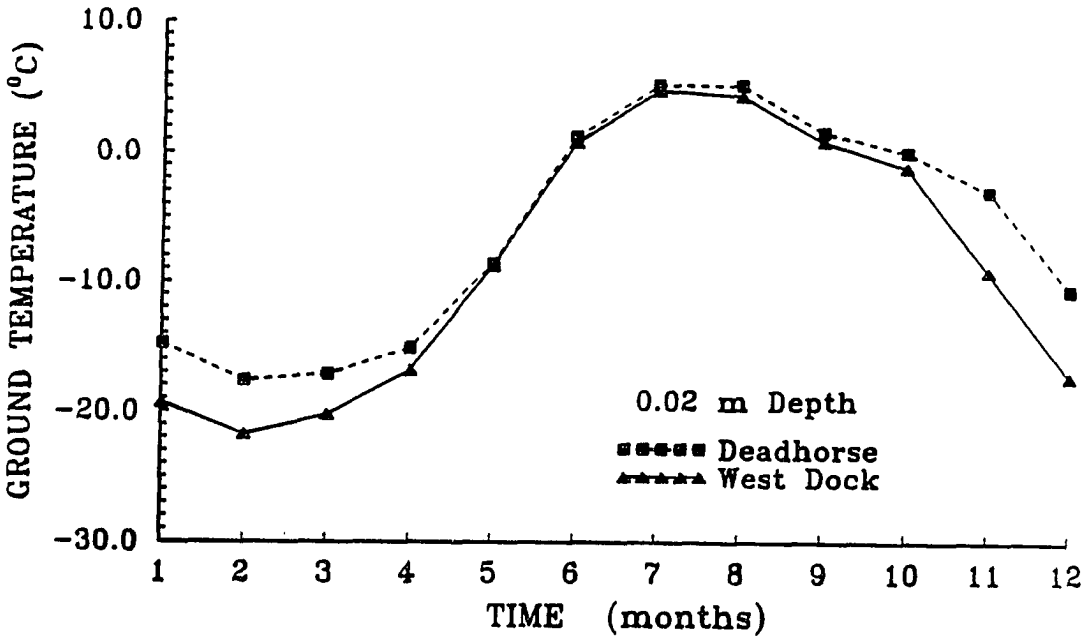

Figure 4.5 Mean monthly ground temperatures at the 0.02 m depth, averaged over the period of measurements (1987-1992) at the DH and WD sites.

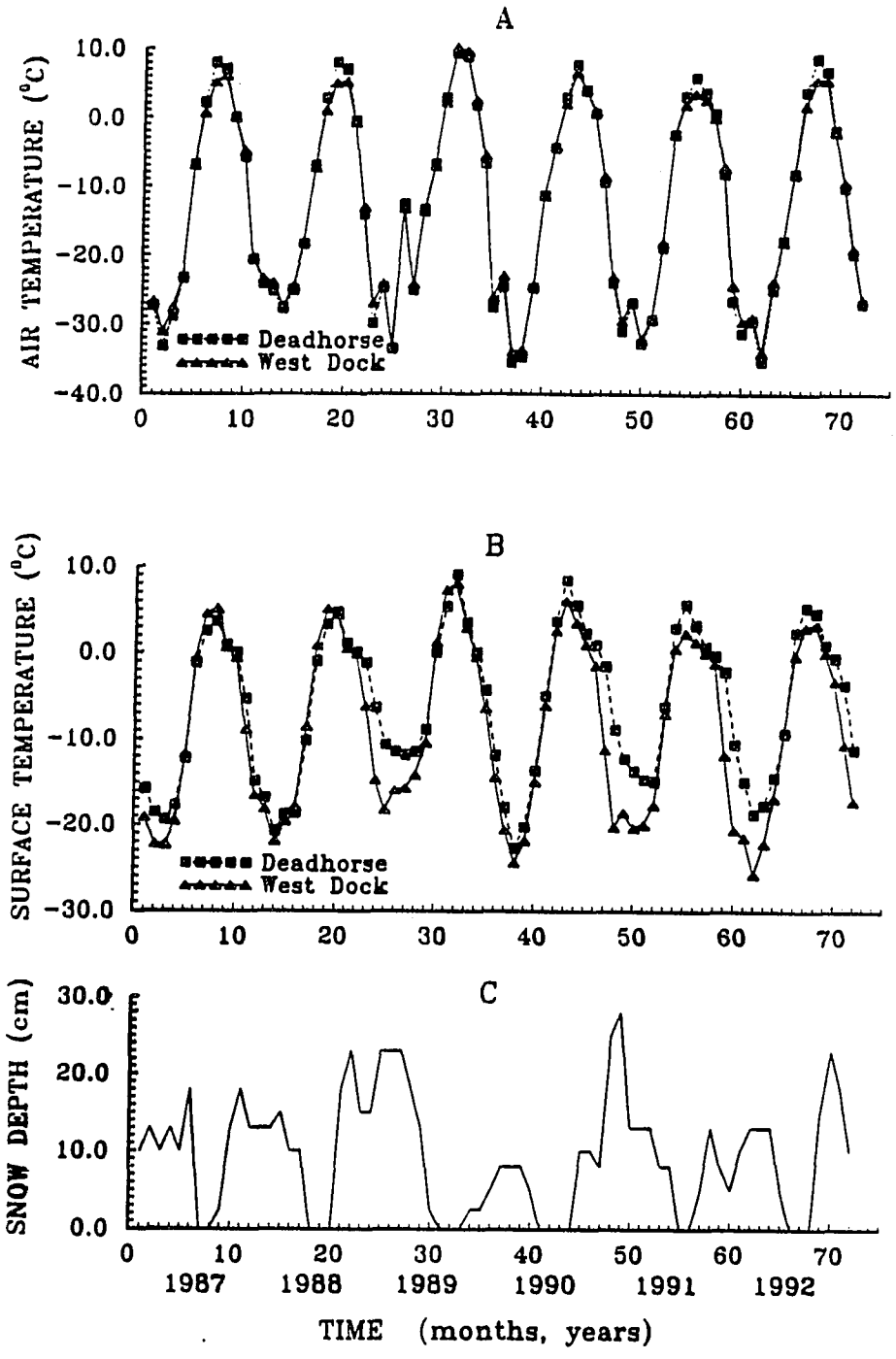

Figure 4.6 Mean monthly air temperatures (A) and ground surface temperatures (B) over the period of measurements at the DH and WD sites, and the maximum monthly snow cover depth at the Deadhorse airport (C).

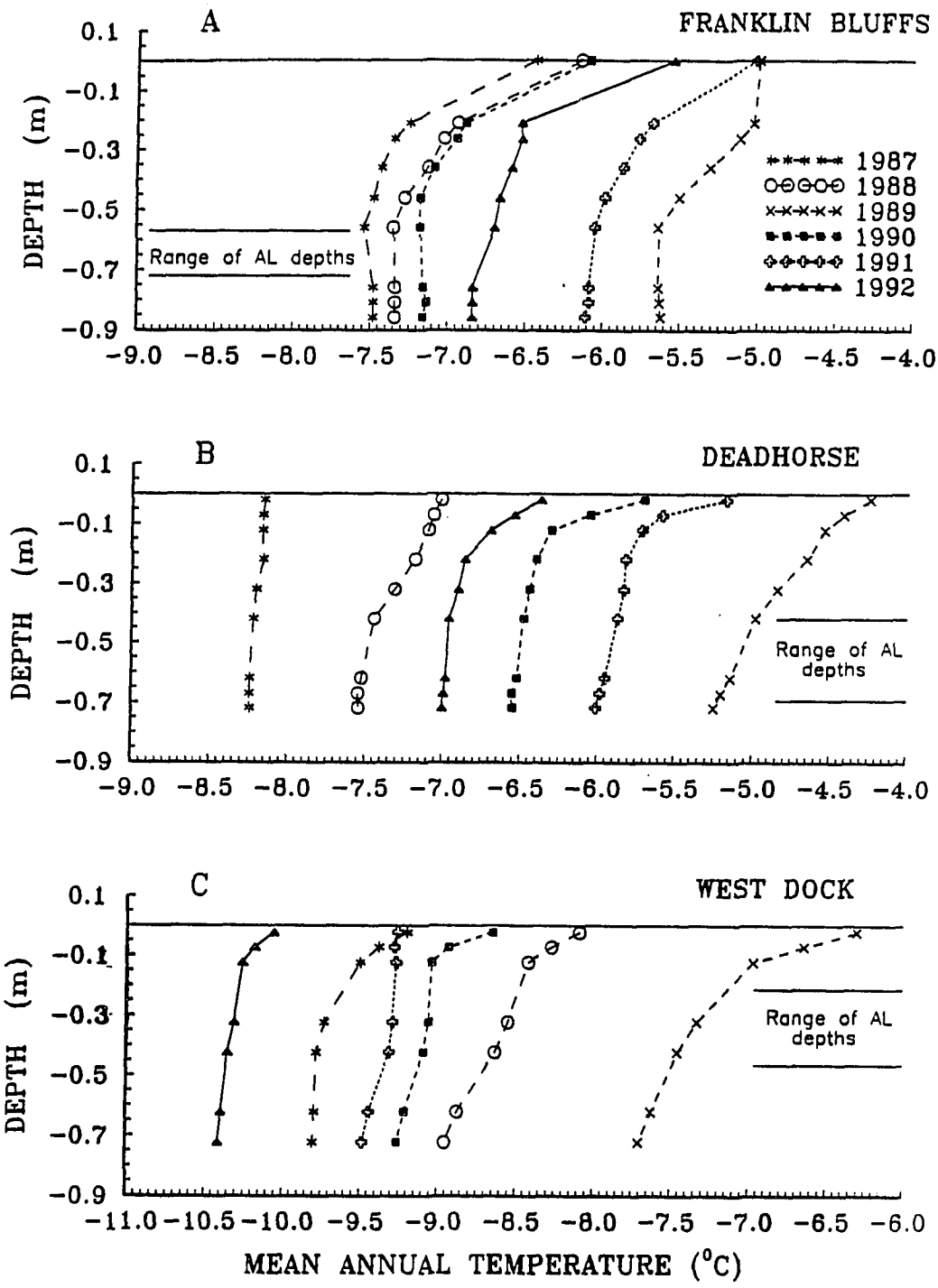

Figure 4.7 Mean annual (calendar year) temperature profiles for each year of measurements at FB (A), DH (B), and WD (C). The range of the active layer (AL) thickness variations is shown.

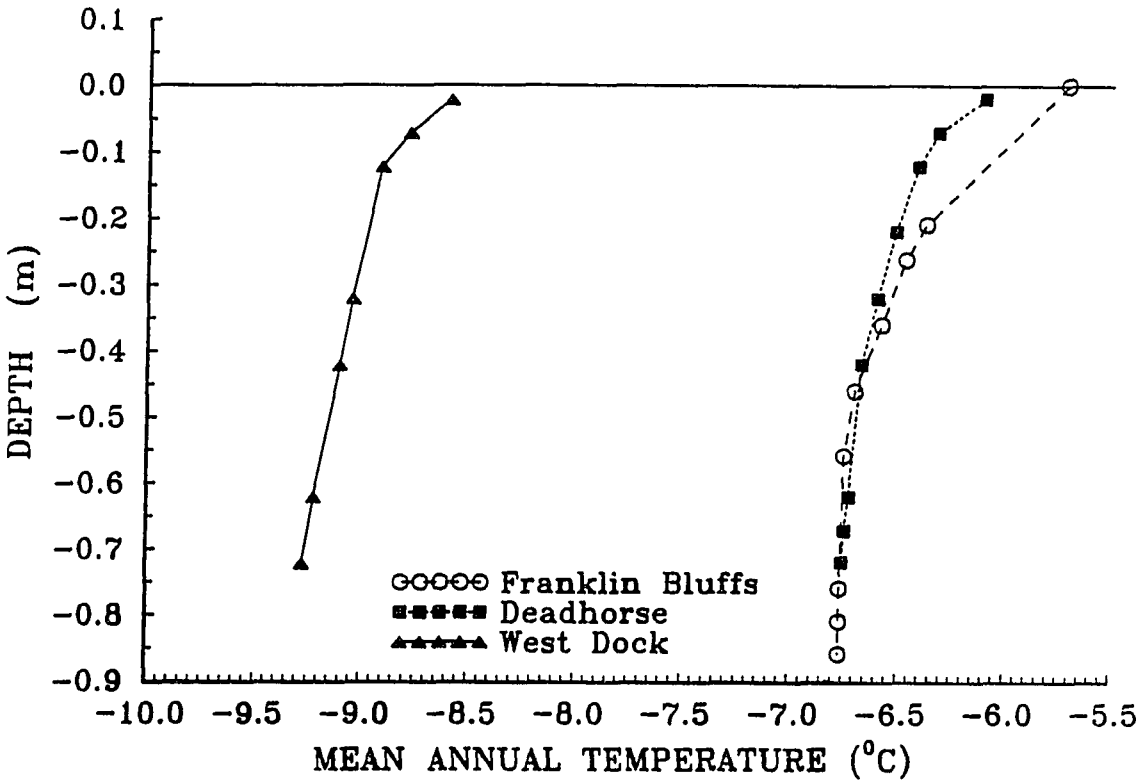

Figure 4.8 Mean annual temperature profiles, averaged over the period of measurements (1987 - 1992) at West Dock, Deadhorse, and Franklin Bluffs.

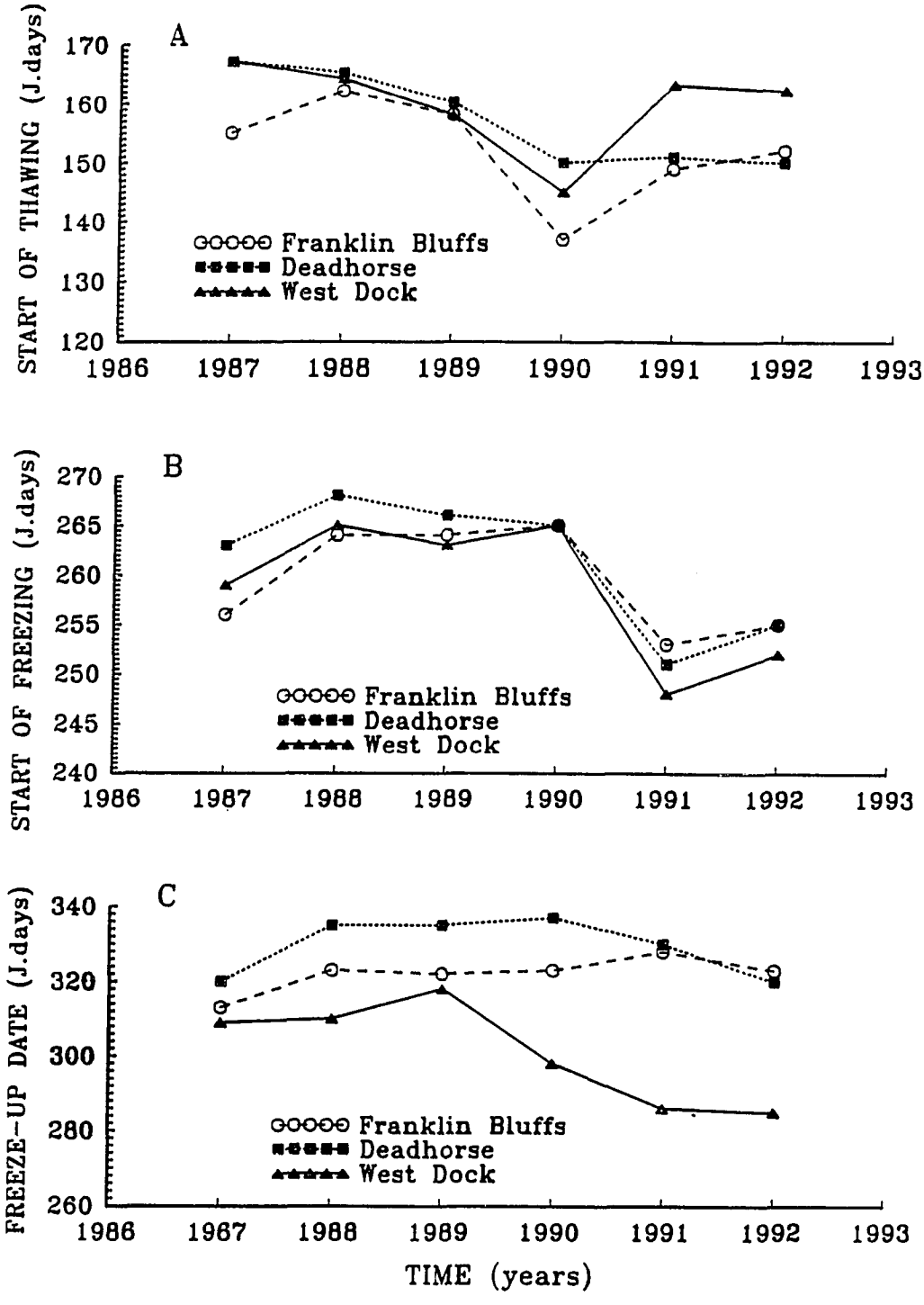

Figure 4.9 Times for the beginning of thawing of the active layer (A), beginning of freezing from the surface (B), and final freeze-up dates (C) for West Dock, Deadhorse, and Franklin Bluffs.

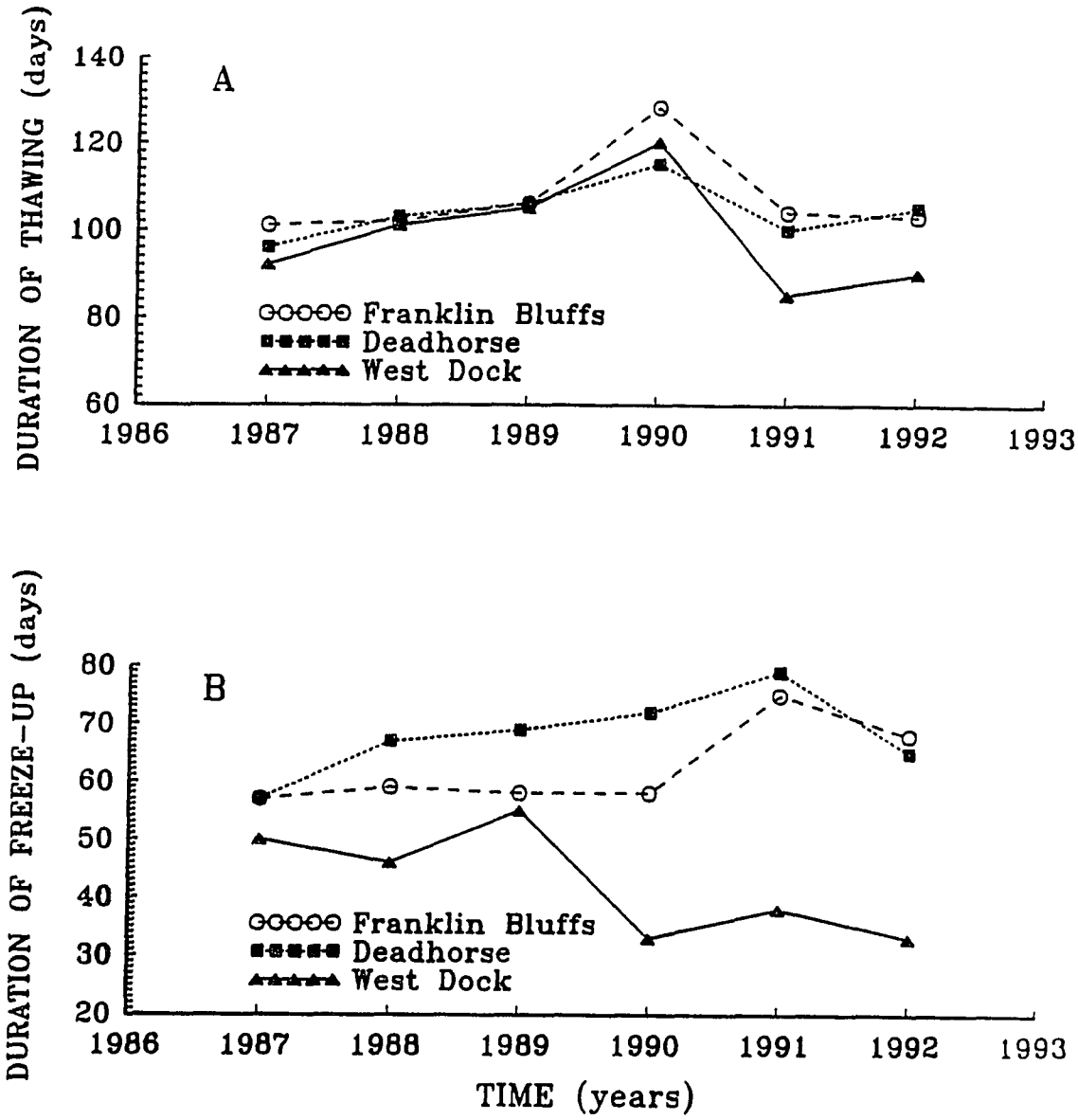

Figure 4.10 Durations of thawing (difference between the dates for the start of freezing and thawing at the ground surface) (A) and durations of the freeze-up period (the difference between start of freezing and freeze-up date) (B) for West Dock, Deadhorse, and Franklin Bluffs.

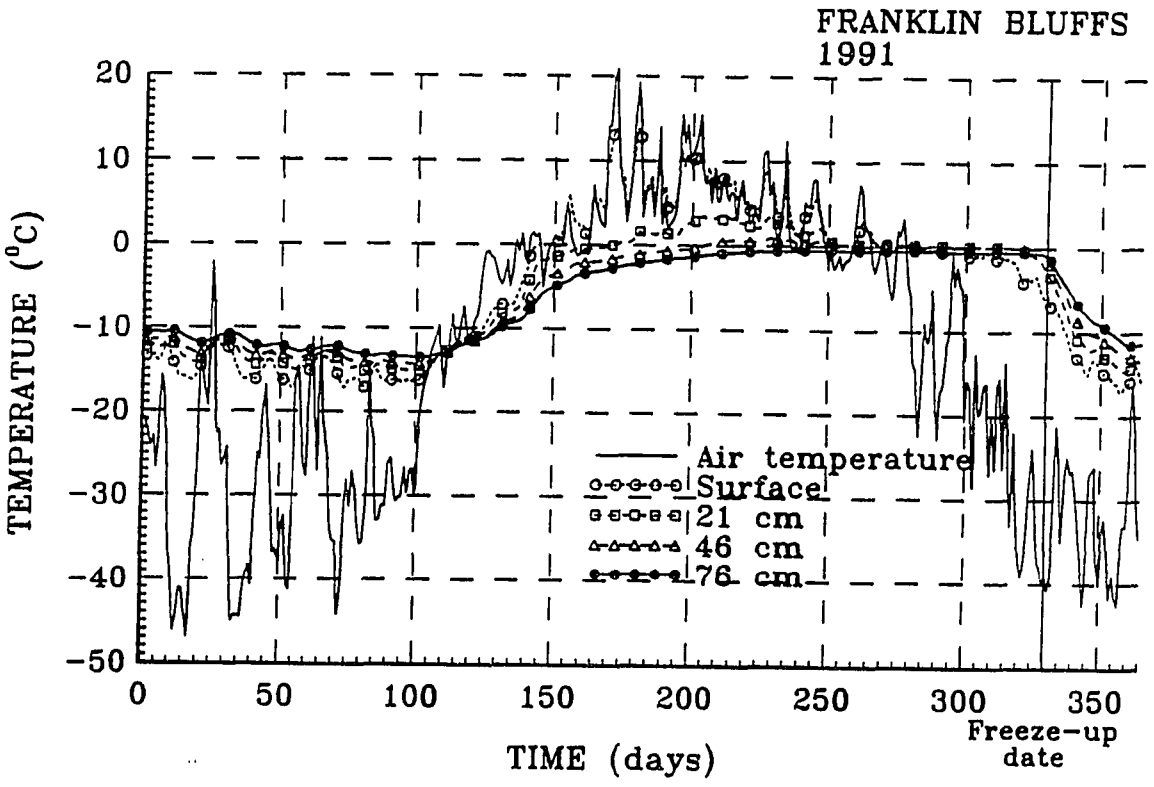

Figure 4.11 Daily mean air, ground surface and ground temperature variations at Franklin Bluffs during 1991.

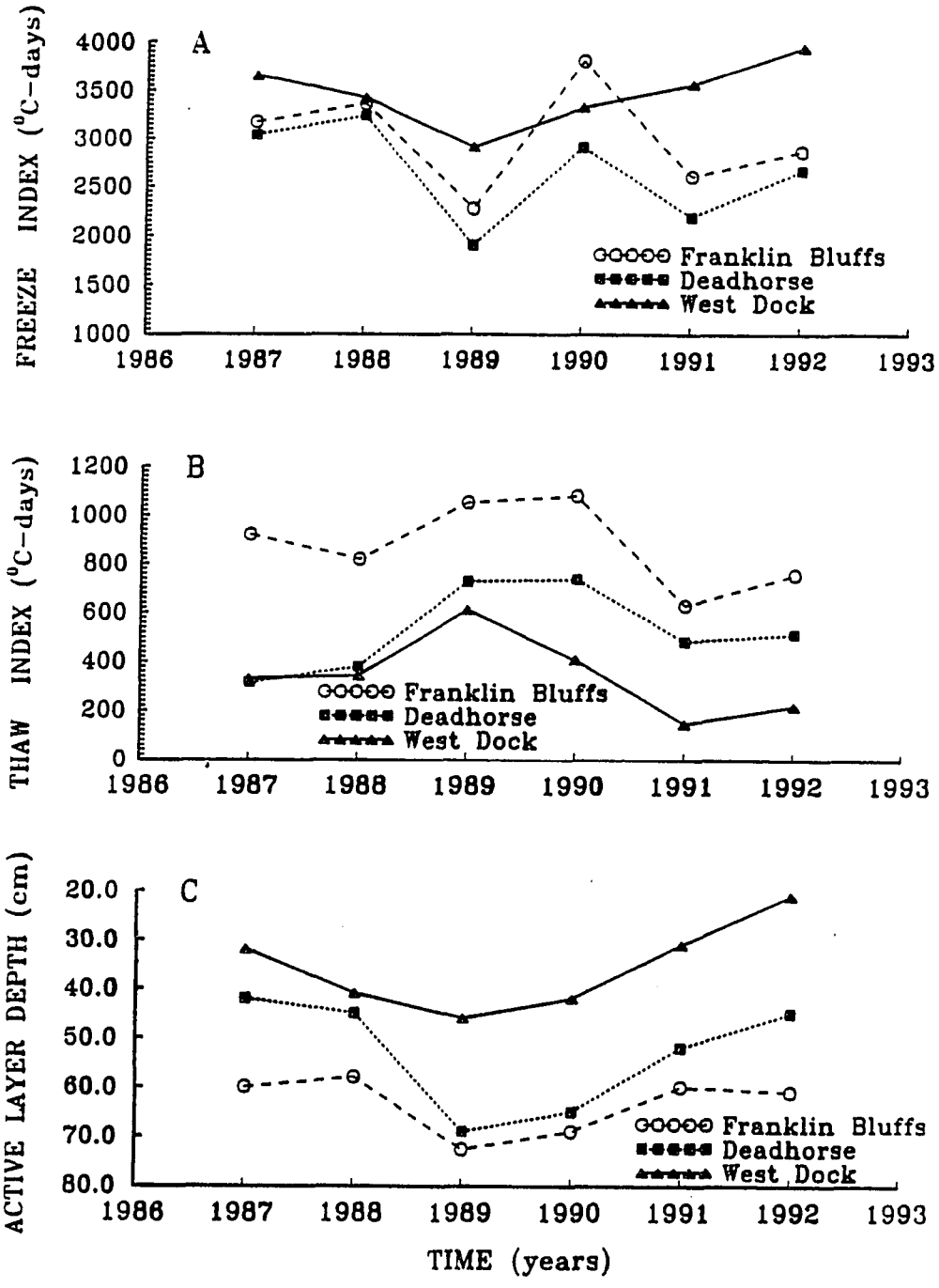

Figure 4.12 Temporal variations of the ground surface freeze index (A) and thaw index (B) and the active layer depth (C) for all sites. The freeze index was calculated for July 1st of the previous year through June 30th of the present year.

Table 4.1 The difference between mean monthly ground surface temperature and mean monthly air temperature for all sites and its difference between sites. Positive values indicate the ground was warmer than the air.

Sites	Jan	Feb	Mar	Apr	May	Jun	Jul	Aug	Sep	Oct	Nov	Dec	Ann
Franklin Bluffs ΔT_{sa} (FB)	13.5	10.6	9.0	3.0	-1.8	0.6	0.4	0.4	1.6	9.9	19.9	14.0	6.76
Deadhorse ΔT_{sa} (DH)	13.9	11.0	9.0	2.4	-1.8	1.4	1.1	1.0	1.4	8.3	18.3	14.4	6.70
West Dock ΔT_{sa} (WD)	8.6	5.9	4.9	0.2	-2.4	1.4	0.8	-0.4	1.0	6.6	12.5	7.7	3.90
ΔT_{sa}(FB)- ΔT_{sa} (DH)	-0.4	-0.4	0.0	0.6	0.0	-0.8	-0.7	-0.6	0.2	1.6	1.6	-0.4	0.06
ΔT_{sa}(DH)- ΔT_{sa}(WD)	5.3	5.1	4.1	2.2	0.6	0.0	0.3	1.4	0.4	1.7	5.8	6.7	2.80

Table 4.2 Soil type, dry bulk density and water content of the soils at the investigation sites.

Depth (m)	Soil type	ρ_b (kg/m^3)	Gravimetric water content (%)	Volumetric water content (%)
West Dock				
0.0 - 0.10	peat	---	319.3	---
0.10 -0.20	peat	455	150.0	68.2
0.20 - 0.31	peat	371	207.1	76.8
Deadhorse				
0.0 - 0.12	peat	---	119.0	---
0.12 - 0.23	peat	531	113.0	60.0
0.23 - 0.40	silt	1377	32.5	44.8
0.40 - 0.60	silt	1250	36.0	45.0
Franklin Bluffs				
0.0 - 0.08	peat	---	247.3	---
0.08 - 0.20	peat	502	163.9	82.3
0.20 - 0.40	silt	1466	34.0	49.8

Table 4.3 Comparison of calculations for ΔT_k obtained using a numerical method (Goodrich, 1976; 1982) and (4.14)

Methods of ΔT_k estimation	Permafrost		Seasonally frozen ground	
	sand	clay	sand	clay
Goodrich model	-0.58	-1.10	-0.95	-2.40
Equation (10)	-0.59	-1.07	-0.95	-2.43

Table 4.4 Calculated and measured values of the thermal offset

Year	Calculated thermal offset			Measured thermal offset		
	WD	DH	FB	WD	DH	FB
1987	-0.65	-0.40	-1.25	-0.66	-0.10	-1.00
1988	-0.61	-0.50	-1.12	-1.00	-0.55	-1.10
1989	-1.08	-1.10	-1.44	-1.45	-1.08	-0.60
1990	-0.85	-0.85	-1.48	-0.67	-0.90	-1.10
1991	-0.26	-0.68	-0.86	-0.28	-0.84	-1.10
1992	-0.42	-0.78	-1.04	-0.40	-0.63	-1.30
Mean	-0.65	-0.72	-1.20	-0.74	-0.68	-1.03

CHAPTER 5

Thawing of the Active Layer on the Coastal Plain of the Alaskan Arctic

V. E. Romanovsky and T. E. Osterkamp, 1996. Thawing of the Active Layer on the Coastal Plain of the Alaskan Arctic. *Permafrost and Periglacial Processes* (prepared for publication)

5.1 Abstract

Air, surface, active layer and near-surface permafrost (to 0.7-0.9 m) high frequency (every four hours) temperature measurements were made in 1986 through 1993 on a transect southward from Prudhoe Bay, Alaska together with annually temperature measurements in the deeper boreholes (down to 60-70 m). Using these data for analytical models validation it was shown that modified Kudryavtsev's equation has several advantages and can be effectively used for estimation of the maximum depth of the seasonal thaw in the Prudhoe Bay region. The onset of thawing of the ground surface is closely related to snowmelt. Although a convenient approximation of the duration of the thaw season is the number days with positive (above 0°C) ground surface temperatures, the actual time of downward movement of the lower boundary of the active layer is somewhat shorter. The simple analytical model provides an estimation of the temperature at the ground surface which indicate the time of cessation of the downward movement of the thawing front.

Active layer thicknesses increase from the coast inland, the mean for measurements of the active layer thicknesses was 0.36 m at WD, 0.53 m at DH, and 0.62 m at FB. Active layer thicknesses have changed systematically from 1986 to present. At WD, they changed by a factor of two (from 0.22 m to 0.45 m). Maximum thicknesses occurred at all sites in 1989 and our recent data indicate a broad minimum from 1992 until 1994. These significant interannual variations of active layer

thicknesses make a comparative analysis of the spatial behavior of the active layer difficult.

The available data were used to calibrate a finite element thermal model which was then applied to simulate process of seasonal thawing and temperature field dynamics in the active layer and near-surface permafrost. Comparison of the results of these simulations for WD in 1987 with temperatures calculated using another numerical (finite difference) model showed a perfect agreement with 0.012 K of the RMS deviation for the whole year and all depth. The deviations (RMS) between calculated and measured temperatures were in the range 0.2-0.3 K. The calculations were used to estimate the interannual variability of the thermal properties of soils. The nature of temporal variations in the thermal conductivities are thought to be a result of interannual variations of the average water content during the summer in the upper part of the active layer.

The joint interpretation of daily temperature measurements in the active layer and near-surface permafrost and annually measured permafrost temperatures in deeper boreholes significantly increases the usefulness of these data. Numerical modeling based on the pure conductive heat exchange scheme can be effectively used to investigate the processes of thawing in the active layer. However, more efforts need to be done to collect data on the thermal properties of soils and their temporal variations.

5.2 Introduction

Air and ground temperature conditions, snow cover, and the active layer are important components for land-atmosphere interactions in the Arctic, and their investigation is one of the primary thrusts of arctic system research. Permafrost occupies extensive areas in the Arctic. Northern ecological systems depend on permafrost conditions and permafrost directly influences human activities. At the same time, permafrost is extremely sensitive to climatic change. Therefore, studies of the

interactions between permafrost and climate, especially during the period of possible climatic warming, is an important aspect of arctic system research.

Permafrost is linked to the atmosphere by the intervening active layer, vegetation, and snow cover which vary strongly with time and location. Consequently, it is important to develop a better understanding of the spatial and temporal behavior of the active layer and upper permafrost to seasonal, annual, and multi-year changes in climate. Dynamics of the permafrost distribution and of the active layer significantly influence the hydrology and hydrogeology of the land as well as its geomorphology. Together these conditions influence the biota and landscape so that permafrost dynamics determines changes in the ecosystem as a whole.

Another very important application for results discussed in this paper is the interaction between the carbon cycle and permafrost and active layer variations. This interaction is an essential element in the positive feedback mechanism in the natural global system "Terrestrial Permafrost - Land - Atmosphere." Large amounts of carbon and methane are stored in permafrost below the annually thawed active layer and are not presently involved in the carbon cycle. Climatic warming may accelerate the rate of decomposition, which is limited now by low temperatures, and thaw deeper layers of formerly frozen organic soils making them available for decomposition. Some experimental evidence exists indicating that arctic tundra and boreal forests are changing from a carbon dioxide sink to a source (Kolchugina and Vinson, 1993; Oechel et al., 1993; Oechel and Vourlitis, 1994). In the case of the strong temporal variations in active layer thicknesses the results of measurements of greenhouse gas fluxes may be time dependent.

Monitoring ground temperatures and active layer thicknesses and characteristics is also necessary for assessing changes in the environment (Barry et al., 1994), which directly influence the conditions and quality of human life and activity in the circumpolar north. Active layer thicknesses are particularly important because of their direct effects on human activities, especially engineering features.

Seasonal thawing of the ground as a thermodynamic process is determined by certain thermal parameters. These include the temperature regime at the ground surface (especially during the summer), thermal properties of the ground to the depth of 15 to 20 m (thermal conductivity and heat capacity), and water and ice content within the active layer. Natural factors which determine the values of these parameters are the air temperatures (mean annual and the range of seasonal variations), precipitation, snow cover characteristics (snow depth and thermal conductivity), type of vegetation and its thermal characteristics, soil composition, drainage conditions and others (Kudryavtsev et al., 1974).

This paper will concentrate on thermal processes in the active layer and near-surface permafrost during seasonal thawing using measured temperatures at the ground surface as input data. These data were obtained from 1986 to 1993 from high frequency (every four hours) air, surface, active layer and permafrost (down to 0.7-0.9 m) temperature measurements at three sites on the Coastal Plain of the Alaskan Arctic adjacent to the Beaufort Sea. The sites are along the Dalton Highway south from Prudhoe Bay and include West Dock (WD), Deadhorse (DH), and Franklin Bluffs (FB) (Figure 5.1). The data also include annually measured temperatures in the deeper boreholes (nominally 60 m) located at the same sites. Detailed descriptions of site conditions and methods of measurements and data processing were published in (Osterkamp, 1985; Osterkamp et al., 1994; Romanovsky and Osterkamp, 1995a; Osterkamp and Romanovsky, 1996).

In previous publications (Romanovsky and Osterkamp, 1994; Romanovsky and Osterkamp, 1995a; Osterkamp and Romanovsky, 1996), we considered the interannual variability of the active layer thickness and the thermal regime of the active layer and near-surface permafrost. This paper is concerned with the thawing portion of the annual cycle, specifically how seasonal thawing progresses and methods for determining the maximum depth of the active layer.

5.3 Interpretation and Theory. Approximate Analytical Solutions for the Thickness of the Active Layer

Many methods have been proposed to calculate approximate active layer thicknesses using simplified analytical solutions (Lukyanov and Golovko, 1957; Porkhaev, 1970; Kudryavtsev et al., 1974; Pavlov, 1980; Zarling, 1987; Balobaev, 1991; Aziz and Lunardini, 1992, 1993). The simple Stefan equation

[5.1] $$X = \sqrt{\frac{2K_t I_t}{\rho L}}$$

where X is the maximum thaw depth, K_t is the value of the soil thermal conductivity in the thawed state, I_t is the thawing index at the ground surface, ρ is the density, and L is the latent heat is one of the simplest. Kudryavtsev's equation (Kudryavtsev et al., 1974)

[5.2] $$X = \frac{2(A_{gs} - |\overline{T_{ps}}|)\sqrt{\frac{K_t C_t P}{\pi}} + \frac{(2\overline{A}C_t X_{2C} + \rho L X)\rho L\sqrt{\frac{K_t P}{\pi C_t}}}{2\overline{A}C_t X_{2C} + \rho L X + (2\overline{A}C_t + \rho L)\sqrt{\frac{K_t P}{\pi C_t}}}}{2\overline{A}C_t + \rho L}$$

where

[5.3] $$\overline{A} = \frac{A_{gs} - |\overline{T}_{ps}|}{\ln \frac{A_{gs} + \frac{\rho L}{2C_t}}{|\overline{T}_{ps}| + \frac{\rho L}{2C_t}}} - \frac{\rho L}{2C_t} \quad ,$$

and

$$X_{2C} = \frac{2(A_{gs} - |\overline{T}_{ps}|)\sqrt{\frac{K_t C_t P}{\pi}}}{2\overline{A}C_t + \rho L} \quad , \qquad [5.4]$$

were C_t is the thawed volumetric heat capacity, P is the period (one year), A_{gs} is the amplitude of annual periodic temperature variations at the ground surface and $\overline{T_{ps}}$ is the mean annual permafrost surface temperature (MAPST) is much more complex. The necessary input data for this quadratic equation in X includes averaged thermal properties of the active layer and climatic parameters, $\overline{T_{ps}}$ and A_{gs}. Equation (5.2) was derived for a homogeneous active layer but for the area of investigations a two-layered or even three-layered structure is typical (Tables 5.1 and 5.5).

Most simple approximate equations for determining active layer thicknesses were derived with the assumption that the amount of heat, necessary for phase changes in the active layer is much larger than the sensible heat. Consequently, these equations become invalid as the latent heat approaches zero ($L \rightarrow 0$); however, Kudryavtsev's equation behaves differently. Substitution of $L = 0$ in (5.2), (5.3) and (5.4) yields

$$X = \sqrt{\frac{K_t P}{\pi C_t}} \ln \frac{|\overline{T}_{ps}|}{A_{gs}} \qquad [5.5]$$

which is the equation for the maximum penetration depth of the 0°C isotherm in case of a periodic steady state temperature regime in material without phase changes ($L = 0$) with harmonic temperature oscillations at the surface (where $\overline{T}_{ps}$ is mean annual temperature at the maximum depth of the 0°C isotherm which is the amplitude at this depth, A_{gs} is the amplitude of oscillation, and P is the period).

Kudryavtsev's equation is a result of the application of the Fourier temperature wave propagation theory (see e.g. Tikhonov and Samarsky, 1966), to materials with phase changes ($L > 0$). It was derived with the assumption of a periodic steady state temperature regime (Kudryavtsev et al., 1974). The equation can be simplified by introducing the new dimensionless variables $\alpha = \frac{2C_t A_{gs}}{\rho L}$ and $\beta = \frac{2C_t |\overline{T}_{ps}|}{\rho L}$. These variables are analogous to the "Stefan number" (the ratio of sensible and latent heats) in the Neumann equation (e.g. Zarling, 1987). After some algebraic transformations, (5.2) becomes

[5.6] $$X = X^* \sqrt{\frac{K_t P}{\pi C_t}} \quad ,$$

where X^* is a solution to the quadratic equation

[5.7] $$X^* \frac{\alpha - \beta}{\ln \frac{\alpha + 1}{\beta + 1}} = \alpha - \beta + \frac{X^* + \alpha - \beta - \ln \frac{\alpha + 1}{\beta + 1}}{X^* + \alpha - \beta - \ln \frac{\alpha + 1}{\beta + 1} + \frac{\alpha - \beta}{\ln \frac{\alpha + 1}{\beta + 1}}}$$

The variables α and β do not depend on K_t making X^* independent of K_t also. Hence, (5.6) shows that the thickness of the active layer for the case of an harmonic temperature oscillation at the ground surface is proportional to the square root of the thermal conductivity. The same is true for cases with step temperature changes at the ground surface (Stefan's equation and the Neumann's solution).

A further advantage of (5.6) and (5.7) is that in (5.7) the solution for X^* depends only on two variables. This makes it possible to establish a simple nomogram

(Figure 5.2) to estimate the value of X^*. The value of X^* can be also calculated from the solution to the quadratic equation (5.7)

$$X^* = B + \sqrt{B^2 + D},$$

[5.8] where $B = \delta + \frac{\delta}{2\gamma} - \frac{\gamma}{2\delta} - \frac{\gamma}{2}$ and $D = \delta + \delta\gamma + \gamma - \delta^2 - \frac{\delta^2}{\gamma}$

where $\gamma = \alpha + \beta$ and $\delta = \ln\frac{\alpha + 1}{\beta + 1}$.

Equations (5.6) and (5.7) can be used to show another feature of the Kudryavtsev equation. Under the conditions which were used to derive (5.1) ($\overline{T_{ps}}$ is equal to 0 and $L \to \infty$ with C_t constant), Kudryavtsev's equation converts to Stefan's equation (5.1). Indeed, if $L \to \infty$, then $\alpha \to 0$, $\beta \to 0$, $ln(\alpha+1) \to \alpha$, and $ln(\beta+1) \to \beta = 0$, since $\overline{T_{ps}} = 0$. Substituting these values in (5.7), solving the quadratic equation, and taking only the lowest order of α (because $\alpha \to 0$), yields $X^* \cong \alpha^{1/2}$. Substitution of this result in (5.6) yields

[5.9] $$X = \sqrt{\frac{2K_t A_{gs} P}{\rho L \pi}}$$

For harmonic oscillations with period P, mean temperature 0°C and amplitude A_{gs}, the thaw index $I_t = (A_t P)/\pi$ which makes equations (5.9) and (5.1) identical.

The simplicity of the Stefan equation (5.1) is attractive and it has been recently used in a modified form (Hinkel and Nicholas, 1995)

[5.10] $$X = b\sqrt{I_t} + a$$

where b is obvious from (5.9) and the intercept, a, was introduced to account for a non-zero intercept indicated by their data. Hinkel and Nicholas (1995) obtained (5.10) by fitting two years of data on the partial thaw depths of an active layer with a very thick organic mat in a boreal forest setting underlain by discontinuous permafrost. These authors claim that the empirically estimated coefficient of proportionality between thaw depth and square root of thawing index (using two years of data for one site) can be used to calculate the thaw depth for similar sites, although it does not appear to have been tested at other sites.

Several problems appear because restrictive assumptions were used in deriving the Stefan equation. The most important simplification is the assumption that the temperature in the frozen ground is equal to 0°C, hence significant errors can be expected in applications of this equation in the more northern regions of the permafrost zone. The assumption of a small Stefan number $(C_f T)/(\rho L)$ can also be restrictive in some cases (T is the constant temperature at the ground surface during the thawing period). Temperature, T, was supposed to be a constant (it is not) during the period of thawing. This problem is treated by using mean temperature(s) during thawing. However, it has been shown (Tipenko, 1987) that the function $X(t)$ depends not only on the integral, $\int_{t_0}^{t} T(t)dt$, where t_0 is the time at the start of thawing, but also on the form of the surface temperature history, $T(t)$. The spatial and temporal variations of the thermal properties of soils in the active layer also aggravate the problem of predicting active layer depths for all models.

5.4 Analysis and Discussion

5.4.1 Onset and Duration of Active Layer Thawing

The onset of thawing of the ground surface is closely related to snowmelt. Daily mean air temperatures during snowmelt typically vary around 0°C, but the

ground surface temperatures must remain at or below 0°C until the snow on the surface melts completely. This is because the presence of both snow (ice) and water constrain the maximum surface temperature to the ice-point. Once the snow melts, the ground surface can warm above the ice-point and thawing of the active layer can begin. Dates for the beginning of thawing were taken to be the dates when the daily mean ground surface temperatures exceeded 0°C, which were typically very distinct times in the surface temperature history (Figures 5.3, 5.4 and 5.5). However, these are point measurements and cannot represent even the local tundra as a whole. The dates of snow disappearance, which are areal observations, at the Prudhoe Bay/ARCO station for 1987-92 are shown in Figure 5.6 together with dates for the beginning of the active layer thawing at WD, DH and FB sites (see also Figures 5.3, 5.4 and 5.5). Given the limitations of the data, it is not possible to draw firm conclusions although some general trends seem evident.

At FB, ground thawing began about the same time or earlier than at WD and DH and usually preceded snowmelt at the ARCO station. This may be related to the typical pattern of snowmelt which begins earlier in the Foothills compared to the Coastal Plain. Thawing started (Figure 5.6) very uniformly at all sites between June 4th and June 16 during the first three years of measurements (except at FB in 1987). Average dates for the beginning of thawing were June 9th at WD, June 6th at DH, and June 1st at FB. Thawing started significantly earlier in 1990 (May 25th for WD, May 30th for DH, and May 17th for FB), because of an extremely shallow snow cover during the 1989 - 1990 winter and an anomalously early snowmelt. At the Prudhoe Bay/ARCO meteorological station, there was no snow during May 1990 and the maximum depth of snow during April was only 0.05 m. After 1990, the thawing dates were still earlier than 1987 - 1989 for DH and FB (between May 29th and June 1st) and approximately the same for WD (June 12th in 1991 and June 11th in 1992). There is a trend in Figure 5.6 toward earlier dates for the beginning of active layer thawing but the time series is relatively short. These data indicate, as expected, that the

beginning of thawing of the active layer depends primarily on factors that control the timing of snowmelt.

As air and ground surface temperatures increased, the active layer deepened progressively (Figures 5.3, 5.4 and 5.5). The rate of thawing was not uniform but increased during periods of warmer air and ground surface temperatures and decreased during stable and cooler periods. Some of these changes could be associated with changes in the active layer lithology and/or ice content in soils.

Decreases in the thawing rate were measured, typically, within the lower 0.1 - 0.15 m of the active layer (Figures 5.3, 5.4 and 5.5) and are probably a result of changes in surface temperatures (which normally decrease in August) and decreases with depth in the thawing rate even if surface temperature remains constant (Carslaw and Jaeger, 1959). However, it could also result from an increase in ice content near the active layer base due to freeze up from the bottom in the previous year (Shur, 1988).

A convenient approximation of the duration of the thaw season is the number of days with positive (above 0°C) ground surface temperatures (Romanovsky and Osterkamp, 1995a). However, the actual time of downward movement of the lower boundary of the active layer is somewhat shorter. This can be seen from the requirement for energy conservation at the phase boundary

[5.11] $$K_f G_f - K_t G_t = \rho L \frac{dX}{dt}$$

where K_f is the frozen thermal conductivity of the soil, and G_f and G_t are the frozen and thawed temperature gradients. The phase boundary velocity, dX/dt, becomes zero when

[5.12] $$G_t = G_f K_f / K_t .$$

For a linear temperature gradient in the thawed portion of the active layer, (5.12) is satisfied when the surface temperature is

[5.13] $$T_s = G_f X K_f / K_t .$$

Using the measured temperatures and estimated thermal conductivities for silt (Table 5.7), the values of T_s were calculated for each year for all three sites. Averaged over six years, the values were very similar for all sites, 1.75°C for WD and DH and 1.9°C for FB. The ranges of changes were also very similar; from 1.25°C to 2.8°C at WD, from 1.4°C to 2.2°C at DH, and from 1.6°C to 2.3°C at FB. Thus, when ground surface temperatures become colder than 2°C, typically, the thawing season ends and the active layer begins freezing from the bottom up.

At the WD, DH, and FB sites the active layer reached its maximum thickness and began freezing from the bottom upward about one to two weeks earlier than the beginning of freezing from the surface (Figures 5.3, 5.4 and 5.5). Figure 5.7 shows the comparison of these dates for all sites and for each year. While average dates for the start of freezing from the surface were 16 September for WD, 18 September for DH and 17 September for FB, average dates for maximum active layer thicknesses were 5 September for WD, 3 September for DH and 4 September for FB.

5.4.2 Active Layer Thickness

Values of the mean annual ground surface temperature (MAGST) and A_{gs} together determine the value of I_t which influences the thickness (maximum thaw depth) of the active layer (Lachenbruch, 1959; Kudryavtsev et al., 1974). The most important soil properties are the ice content within the active layer which determines the value of latent heat, and the thermal conductivity and heat capacity of the active layer both in the frozen and thawed states (Kudryavtsev et al., 1974; Pavlov, 1980; Balobaev, 1991). The value of $\overline{T_{ps}}$ also influences active layer thickness (Kudryavtsev

et al., 1974). In some cases (highly permeable soils), infiltration of summer precipitation can play a significant role in determining thickness of the active layer (Kudryavtsev et al., 1974). For the area of investigations, this process probably did not have a noticeable effect on active layer thickness because of the low water permeability of the soils and their saturated condition.

Active layer thicknesses increase from the coast inland with the increasing I_t and MAGST (Figure 5.8). The mean for measurements of the active layer thicknesses was 0.36 m at WD, 0.53 m at DH, and 0.62 m at FB.

In general, variations in active layer thickness coincided with changes in MAGST and $\overline{T_{ps}}$, reaching a maximum in the warmest year (1989). However, the active layer thickness was much more sensitive to summer temperature (thawing index) changes (Figure 5.8B) than to MAGST changes (Figure 5.8A). Comparing 1990 and 1991 for FB and DH it is clear that the relative increase in MAGST in 1991 was due to a significantly warmer winter. The summer of 1991 was colder than 1990 and the thawing index in 1991 was 41% less for FB and 35% less for DH than in 1990 (Figure 5.8B). As a result, the active layer thickness in 1991 was 15% less for FB and 20% less for DH than in 1990 (Figure 5.8C). At FB, in spite of a decrease of MAGST from 1991 to 1992 (Figure 5.8A), the summer of 1992 was warmer and thawing index was higher by 16% (Figure 5.8B). As a result, the active layer was slightly thicker by 2% (Figure 5.8C).

When the thawing index remained approximately constant, the MAGST and $\overline{T_{ps}}$ became more important for the active layer thickness variations. The most typical years were 1987 and 1988, and 1991 and 1992 at DH and WD. While the thawing index remained almost constant (Figure 5.8B), the MAGST increased substantially from 1987 to 1988 (more than 1°C) and decreased approximately by the same value from 1991 to 1992 (Figure 5.8A). As a result, the active layer thickness increased from

1987 to 1988 (by 7% for DH and 28% for WD) and decreased from 1991 to 1992 (by 14% for DH and 30% for WD) (Figure 5.8C).

Active layer thicknesses have changed systematically from 1986 to present (Figure 5.8C). At WD, they changed by a factor of two (from 0.21 m to 0.46 m). At DH, the range of interannual variations in the maximum active layer thicknesses was very similar (from 0.42 m to 0.69 m), while at FB it was twice smaller (from 0.57 m to 0.71 m). Maximum thicknesses occurred at all sites in 1989 and our recent data indicate a broad minimum from 1992 until 1994. Unfortunately, the data time series are not yet long enough to determine if these changes are part of natural variability, a cycle or a trend. These significant interannual variations of active layer thicknesses make a comparative analysis of the spatial behavior of the active layer difficult.

Since trace gas emissions from the tundra depend on temperatures, active layer thicknesses and water table levels among other factors, then these results suggest systematic changes in the emissions. Indeed the tundra appears to have recently changed from a sink to a source of CO_2 (Oechel et al., 1993; Oechel and Vourlitis, 1994). If the observed changes in active layer thicknesses are part of a cycle then this would imply a reversal of their result in the near future. Thus, it is important to have a long-term record of ground temperatures and active layer thicknesses.

Figures 5.9, 5.10 and 5.11 show how the measured changes in thaw depth relate to the increasing thaw index over the summer thawing period for WD, DH, and FB. These data show that the functional dependence of thaw depth changes not only from site to site, but also from year to year for each site. Some years show somewhat similar curves (1987 and 1988 for DH, 1988, 1989 and 1991 for FB) but significant differences are more common (all four curves for WD, 1992 and all other curves for DH, 1990 and all other curves for FB). Moreover, these curves change their form during a single year. This could be a result of changes in thermal properties of the soils with depth and/or time during the year (due variations in lithology and/or water content).

Figures 5.12, 5.13, and 5.14 show the thaw depth of the active layer vs the square root of I_t for WD, DH, and FB. The solid lines are a fit of (5.10) to the data for each thaw season. At FB (Figure 5.12), the value for the slope, b, in (5.10) remains practically constant (2.12 to 2.34). However, differences in the intercept, a, exceed 0.1 m. At DH (Figure 5.13), values of the slope, b, vary from 2.28 to 2.92 and, at WD (Figure 5.14), b varies from 1.37 to 2.45. These variations in the parameters of (5.10) lead to maximum errors of 14%, 37%, and 51% at FB, DH, and WD, respectively. Consequently, it appears that (5.10) can be used with confidence only at FB and would lead to relatively large errors at the other sites.

The maximum active layer thicknesses were calculated using the Stefan equation (5.1) and modified Kudryavtsevs' equation (5.6 - 5.8) and the results compared. For the calculations, the values of active layer thermal properties in Table 5.2 were used. All properties were averaged over the full thickness of the active layer using a series heat conduction model. To calculate C_t the estimations of the active layer thermal diffusivity (Zhang, 1993) were used.

The results of these calculations (Table 5.3) show that Stefan's equation overestimates the active layer depth because it does not take into account the heat flux in the permafrost at the permafrost table (in the case of cold permafrost this overestimation is significant). Kudryavtsev's equation provides more realistic results.

To further examine the modified Kudryavtsev's equation (5.6-5.8), the results were compared to numerical calculations of the active layer thicknesses using a hypothetical periodic steady state surface temperature (Goodrich, 1976). The values of $\overline{T_{ps}}$ and A_{gs} which were used in these calculations are shown in the first two columns of Table 5.4. The thermal properties used in these calculations were $K_t = 1.13$ $Wm^{-1}K^{-1}$, $C_t = 3.15$ $MJm^{-3}K^{-1}$, and $\rho L = 151.97$ MJm^{-3}. Comparison of these results for different temperature conditions at the ground and permafrost surface with results provided by equations (5.6) and (5.8) shows a maximum percent difference of 9%.

5.4.3 Numerical Modeling of the Active Layer and Near-Surface Permafrost Temperature Regime During the Seasonal Thawing

Figures 5.9 through 5.14 indicate that significant interannual changes may have occurred in the thermal properties of soils (primarily in the thermal conductivities) especially at WD and DH. To examine this possibility, simulations of the active layer and near-surface permafrost temperature regime were performed for sites. These simulations also allowed an examination of the use of a purely conductive heat flow model with moving phase boundary to describe the temperature field dynamics for the case of seasonal thawing.

A finite element model (Gosink and Osterkamp, 1990; Osterkamp and Gosink, 1991; Osterkamp and Romanovsky, 1996), which is a modified version of the Guymon and Hromadka (1977) and Guymon et al. (1984) model, was used to reconstruct the one-dimensional temperature field in the active layer and near-surface permafrost. Daily mean ground temperatures measured from 1986 to 1992 at the ground surface (0.02 m at WD and DH, and 0.0 m at FB) were used for the upper boundary conditions. The lower boundary was placed at the 16 m depth. Daily temperatures at this depth were calculated for all sites for the period of measurements (1987 through 1992) in the process of reconstructing the daily permafrost temperatures to the 60 m depth (Romanovsky and Osterkamp, 1995b; Osterkamp and Romanovsky, 1996). A combination of the daily temperature profiles measured to the depth of 0.7 - 0.8 m and calculated to the depth of 55 m from (Osterkamp and Romanovsky, 1996) were used for the initial conditions.

Drilling records were used to determine the lithology and results of previous investigations (Lachenbruch et al., 1982; Lachenbruch and Marshall, 1986; Hinzman et al., 1991; Zhang, 1993; Romanovsky and Osterkamp, 1995a; Osterkamp and Romanovsky, 1996) were used to determine the initial approximate thermal properties of the soils in the thawed and frozen states (Table 5.5). The time step in these

calculations was 1 hour, while the space steps (200) were changed from 0.01 within the upper 1 m of soils to 1 m at the lower boundary of the space domain (16 m).

The results of calculations for the WD site in 1987 using the finite element model were compared with a simulation using a one-dimensional finite difference model (Goodrich, 1976, 1978a) with exactly the same input parameters. It was found that, for the case of these small time steps, the results of calculations of the daily temperatures using both models differed by only 0.02°C for the whole year (1987) for 18 depths from 0.02 to 0.87 m, except for one day just after freeze-up, when the difference reached 0.35°C at the depth of 0.17 m. The RMS deviations between the results of these two models for the whole year and for all depths was 0.012°C.

Starting with the initial approximations for the thermal properties of the soils (Table 5.5) those values were adjusted, where necessary, by trial and error to produce the smallest differences between calculated and measured temperature profiles (Figures 5.15, 5.16 and 5.17). Only values of the thermal conductivity of soils in thawed and frozen states were changed, while heat capacity and latent heat were kept the same.

It was impossible (for the WD and DH sites) to produce reasonably small deviations (less than 0.5 - 0.6°C) running the model with the same parameters for each year during the period from 1987 to 1992. For these sites, the values of the thermal conductivity were held constant during the year and were allowed to change from year to year. In this case, the deviations (RMS) between calculated and measured temperatures were in the range 0.2 - 0.3°C, except for an unexplained increase in 1990 at WD and in 1989 at FB (Table 5.6). Large value of the RMS deviations in 1989 at DH can be explained by the short interruption in data continuity (Romanovsky and Osterkamp, 1995a) due to flooding of the site. A comparison between calculated and measured temperatures at several depths during 1987 and 1988 for the DH site is shown in Figure 5.18 which illustrates the agreement between calculated values and measured data. Deviations during the period of warming and especially during the

period of cooling after freeze-up can be explained by the influence of unfrozen water in the partially frozen soils (Osterkamp and Romanovsky, unpublished).

Examples of measured and calculated temperature profiles are shown in Figures 5.15, 5.16 and 5.17. The values of the thermal conductivities which provided the best fit of the numerical model to the data are shown in Table 5.7.

The most pronounced adjustments in the thermal conductivity were made in thawed peat for the WD and DH sites, where its values varied in the range of 40-48 % of the mean values, and for FB with variations of 20-27 % of the mean values (Table 5.7). Much smaller variations were observed in the frozen peat (about 10 % from the averages), and minimal variations were typical for the thawed and frozen mineral soils, (about 6 % for WD, no variations at DH, and about 10 % for FB).

The necessity for these adjustments in the thermal conductivities are thought to be a result of interannual variations of the average water content during the summer in the upper part of the active layer. McGaw et al. (1978) have shown that the thermal conductivity of the active layer depends strongly on the water content using thermal conductivity measurements both in-situ and in the laboratory. Other investigations have confirmed these results (Smirnova and Artushina, 1984; Roman and Konovalov, 1984; Hinzman et al., 1991). Investigations of active layer hydrology at the Toolik Lake site carried out by Hinzman et al., (1991) and Hinzman et al., (1993) show significant variations from summer to summer in the moisture content of the organic layer, while the mineral soil (silt) remained saturated with little interannual variations and "shows little response to precipitation events." These results obtained from the numerical modeling (Table 5.7) are consistent with the data.

The adjusted values of the thermal conductivities of the active layer (Table 5.7) were used to recalculate maximum active layer thicknesses using the modified Kudryavtsev's equation (5.6-5.8) (Table 5.8). Comparison with previous data (Table 5.3) shows better agreement between calculated and measured active layer thicknesses.

The adjusted values of the thermal conductivities can also be used to interpret the anomalous values of the thermal offset found at these sites in some years and which remained unexplained in a previous paper (Romanovsky and Osterkamp, 1995a). Figure 5.19 shows the correlation between interannual variations in the thermal offset and in the ratio K_f/K_t. It is important to remember that the value of thaw index also has a strong influence on the thermal offset which makes the relationship between thermal offset and ratio K_f/K_t not so pronounced.

5.5 Conclusions

High frequency (every four hours) air, ground surface, active layer and near-surface permafrost (to 0.7-0.9 m) temperature measurements were made from 1986 through 1993 on a transect southward from Prudhoe Bay, Alaska together with annual temperature measurements in deeper boreholes (nominally 60 m). Using these data for validating analytical models it was shown that the modified Kudryavtsev's equation (5.6-5.8) has several advantages compared to the classical Stefan's equation (5.1) and the recent modification (5.10) introduced by Hinkel and Nicholas (1995) and can be effectively used for estimation of the maximum depth of the seasonal thaw in the Prudhoe Bay region.

The onset of thawing of the ground surface is closely related to snowmelt. At FB, ground thawing began about the same time or earlier than at WD and DH and usually preceded snowmelt at the ARCO station. For 1987-1989, thawing started very uniformly at all sites between June 4 and June 16. Thawing started significantly earlier in 1990. After 1990, the thawing dates were still earlier than 1987 - 1989 for DH and FB (between May 29th and June 1st) and approximately the same for WD (June 12th in 1991 and June 11th in 1992).

Although a convenient approximation of the duration of the thaw season is the number of days with positive (above 0°C) ground surface temperatures (Romanovsky

and Osterkamp, 1995a), the actual time of downward movement of the lower boundary of the active layer is somewhat shorter. A simple analytical model (5.13) provides an estimate of the temperature at the ground when the downward movement of the thawing front ceases. These temperatures vary in the range between 1.25°C and 2.8°C for WD, between 1.4°C and 2.2°C for DH, and between 1.6°C and 2.3°C for FB with averages of 1.75°C for WD and DH and 1.9°C for FB. At all sites, the active layer typically reached its maximum thickness and began freezing upward from the bottom one to two weeks earlier than the beginning of freezing from the surface.

Active layer thicknesses increase from the coast inland, the mean for measurements of the maximum active layer thicknesses was 0.36 m at WD, 0.53 m at DH, and 0.62 m at FB. In general, variations in active layer thicknesses coincided with changes in MAGST and $\overline{T_{ps}}$. However, active layer thicknesses are much more sensitive to summer temperature (thawing index) than to MAGST. Active layer thicknesses have changed systematically from 1986 to present. At WD, they changed by a factor of two (from 0.22 m to 0.45 m). Maximum thicknesses occurred at all sites in 1989 and our recent data indicate a broad minimum from 1992 until 1994. These significant interannual variations of active layer thicknesses make a comparative analysis of the spatial behavior of the active layer difficult.

The available data were used to calibrate a finite element thermal model which was then applied to simulate seasonal thawing and temperature field dynamics in the active layer and near-surface permafrost. Comparison of the results of these simulations for WD in 1987 with temperatures calculated using another numerical (finite difference) model showed 0.012 K of RMS deviation for the whole year and all depths. The deviations (RMS) between calculated and measured temperatures were usually in the range 0.2-0.3 K. Adjusting the thermal conductivities of the active layer to produce the smallest deviations between measured and calculated temperatures allowed estimates of the interannual variability of the thermal properties of soils. The

most pronounced changes in the thermal conductivity occurred in thawed peat for the WD and DH sites, where its values varied in the range of 40-48 % of the mean values, and for FB with variations of 20-27 % of the mean values. Much smaller variations were observed in the frozen peat (about 10 % from the averages), and minimal variations were typical for the thawed and frozen mineral soils, (about 6 % for WD, no variations at DH, and about 10 % for FB). The nature of these temporal variations in the thermal conductivities are thought to be a result of interannual variations of the average water content during the summer in the upper part of the active layer.

The joint interpretation of daily temperature measurements in the active layer and near-surface permafrost and annually measured permafrost temperatures in deeper boreholes significantly increased the usefulness of these data. Numerical modeling based on conductive heat flow only can be effectively used to investigate the processes of thawing in the active layer.

5.6 Acknowledgments

This research was funded by the Polar Earth Sciences Program, Office of Polar Programs, National Science Foundation and by the State of Alaska. We would like to thank Dr. G.Guymon, Dr. L. Goodrich and Dr. J. Gosink for providing the models which were used in these studies with minor modifications. We also thank numerous colleagues, graduate students and family members who helped obtain this long time series of data.

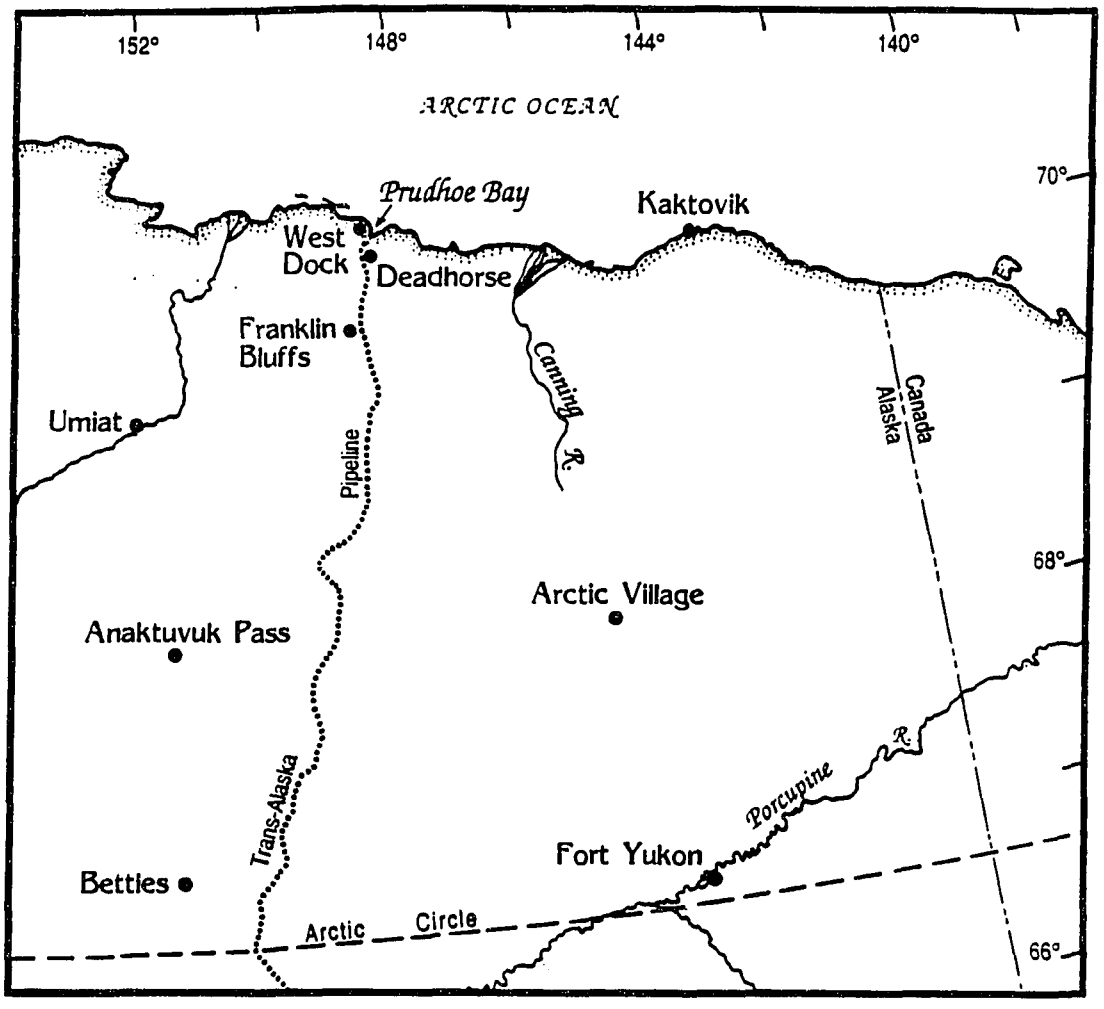

Figure 5.1 Map showing the sites of the investigations.

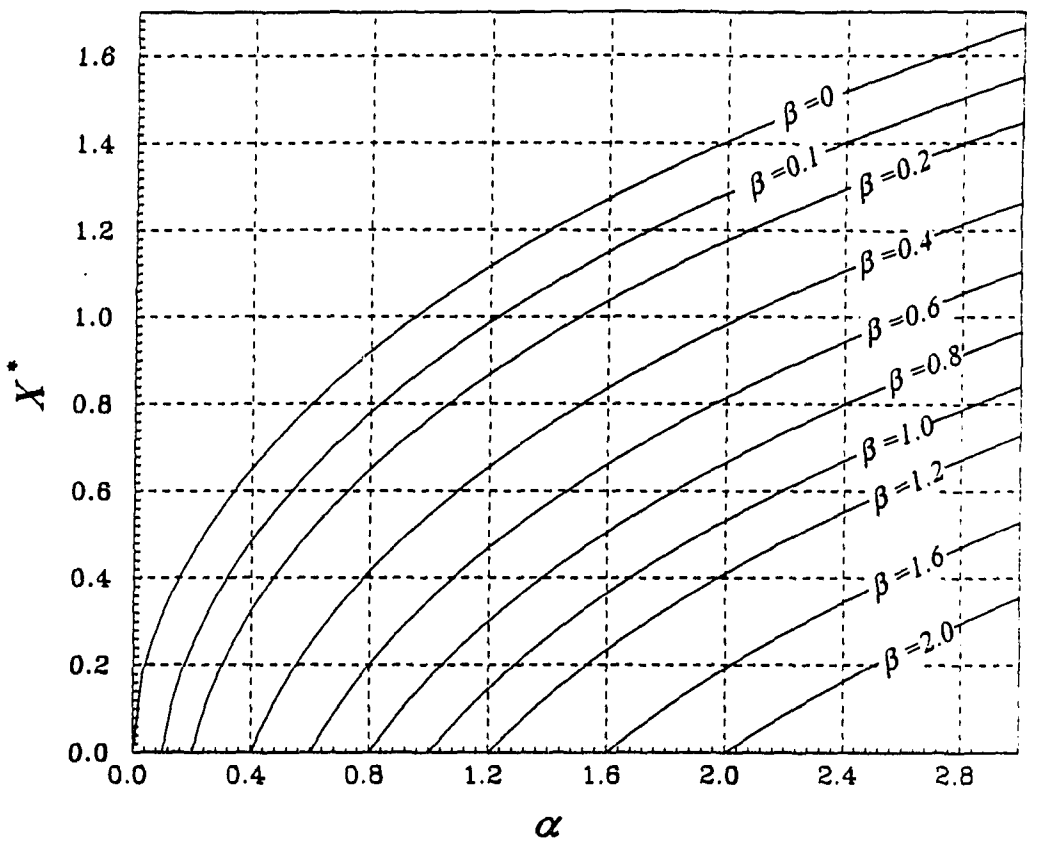

Figure 5.2 Nomogram for calculations of the maximum thaw depth X. The dimensionless parameters $\alpha = \frac{2C_t A_{gs}}{\rho L}$ and $\beta = \frac{2C_t |\overline{T}_{ps}|}{\rho L}$. X should be calculated using the value of X^* from the nomogram and $X = X^* \sqrt{\frac{D_t}{\pi}}$, where D_t is the thermal diffusivity of the thawed soil ($m^2\ yr^{-1}$).

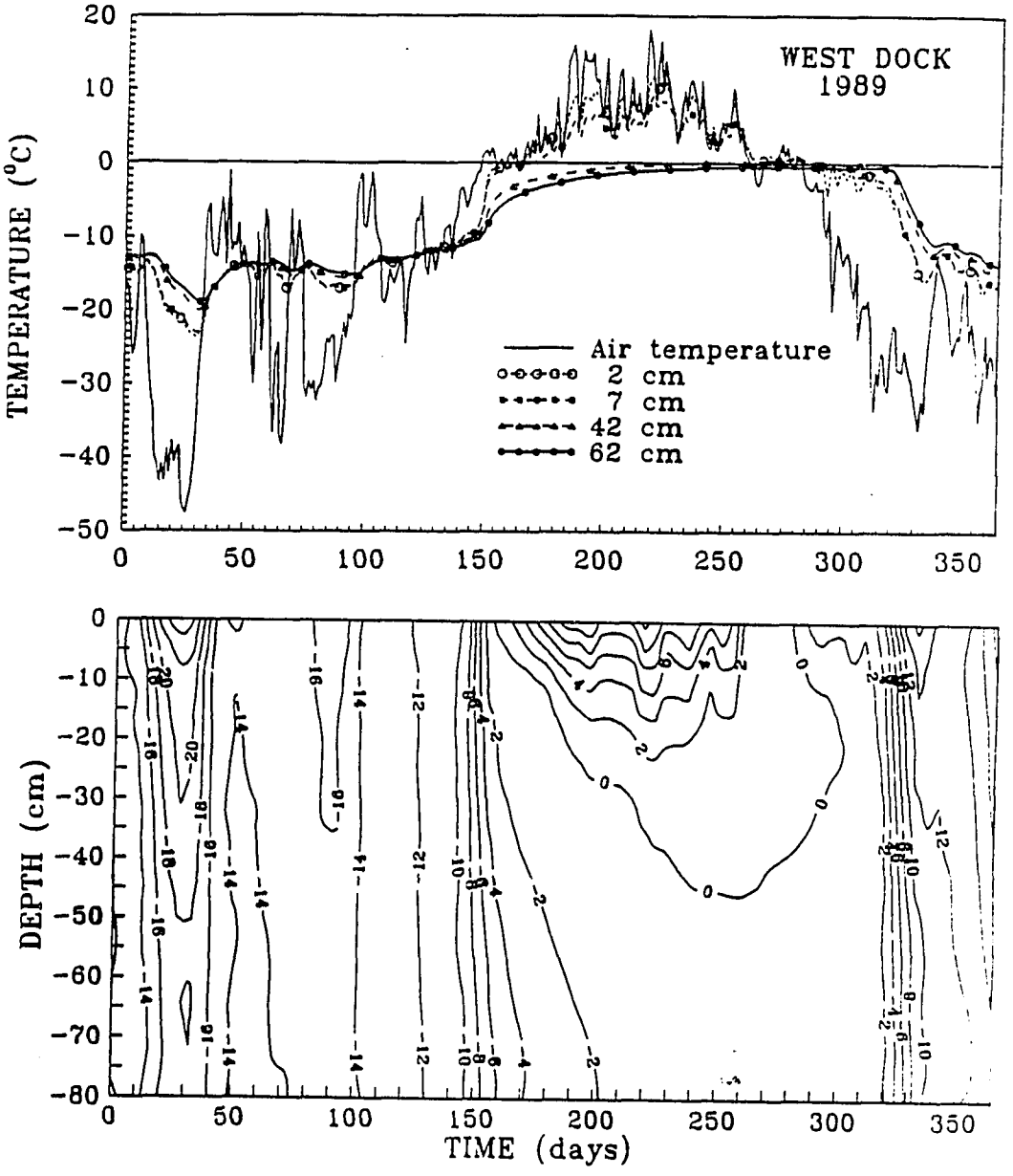

Figure 5.3 Temperature-time series for the different depths (upper part of the Figure) and temperature field dynamics within the active layer and near-surface permafrost (lower part) at West Dock, Alaska, in 1989.

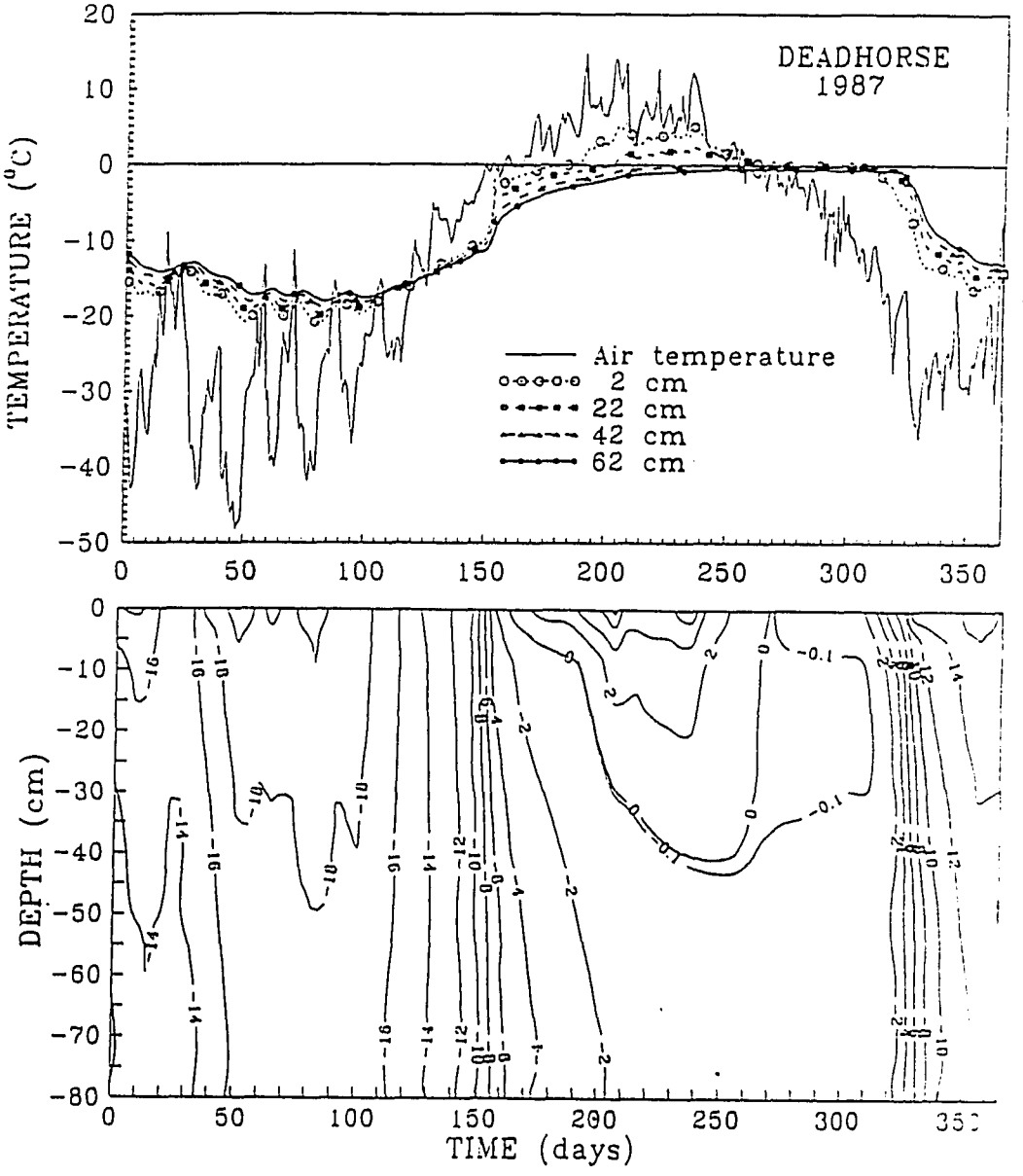

Figure 5.4 Temperature-time series for the different depths (upper part of the Figure) and temperature field dynamics within the active layer and near-surface permafrost (lower part) at Deadhorse, Alaska, in 1987.

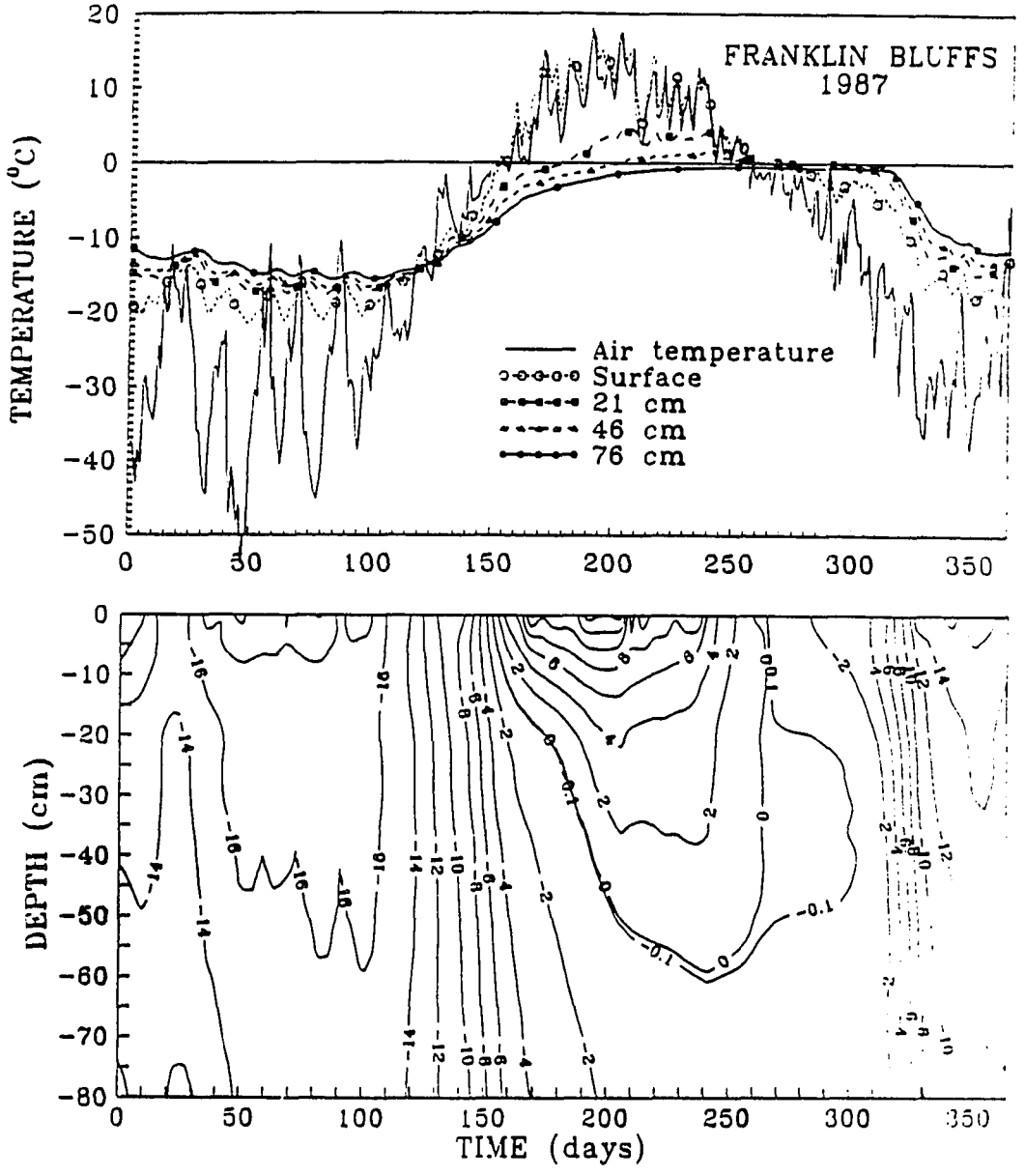

Figure 5.5 Temperature-time series for the different depths (upper part of the Figure) and temperature field dynamics within the active layer and near-surface permafrost (lower part) at Franklin Bluffs, Alaska, in 1987.

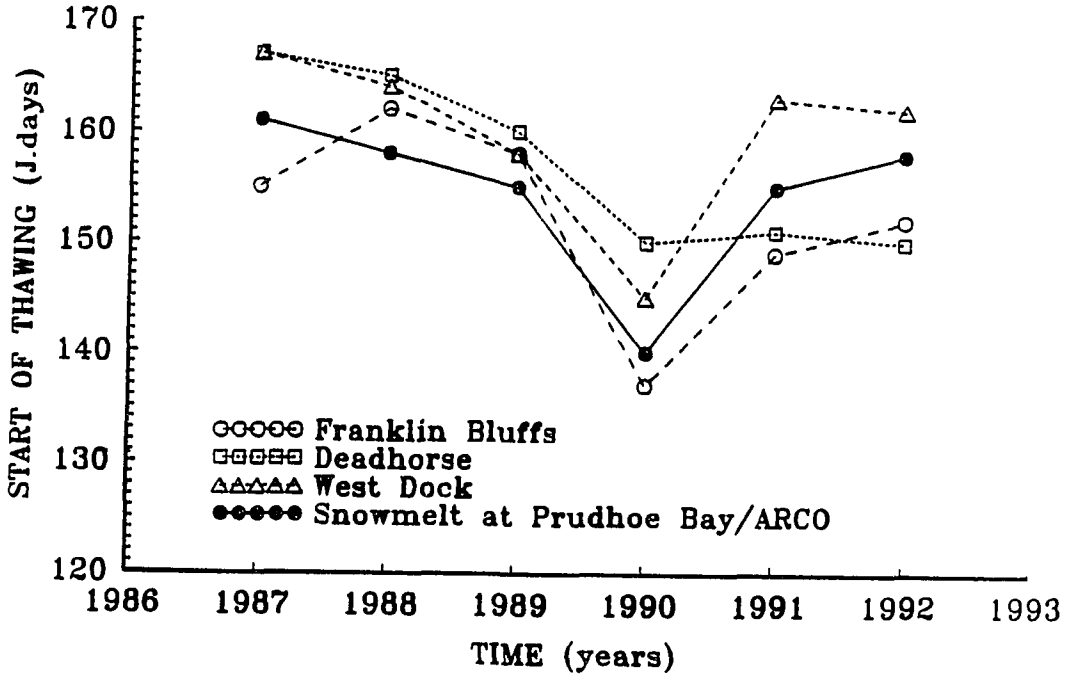

Figure 5.6 Interannual variations of the dates of snow disappearance at the Prudhoe Bay/ARCO station together with dates for the beginning of the active layer thawing at West Dock, Deadhorse and Franklin Bluffs.

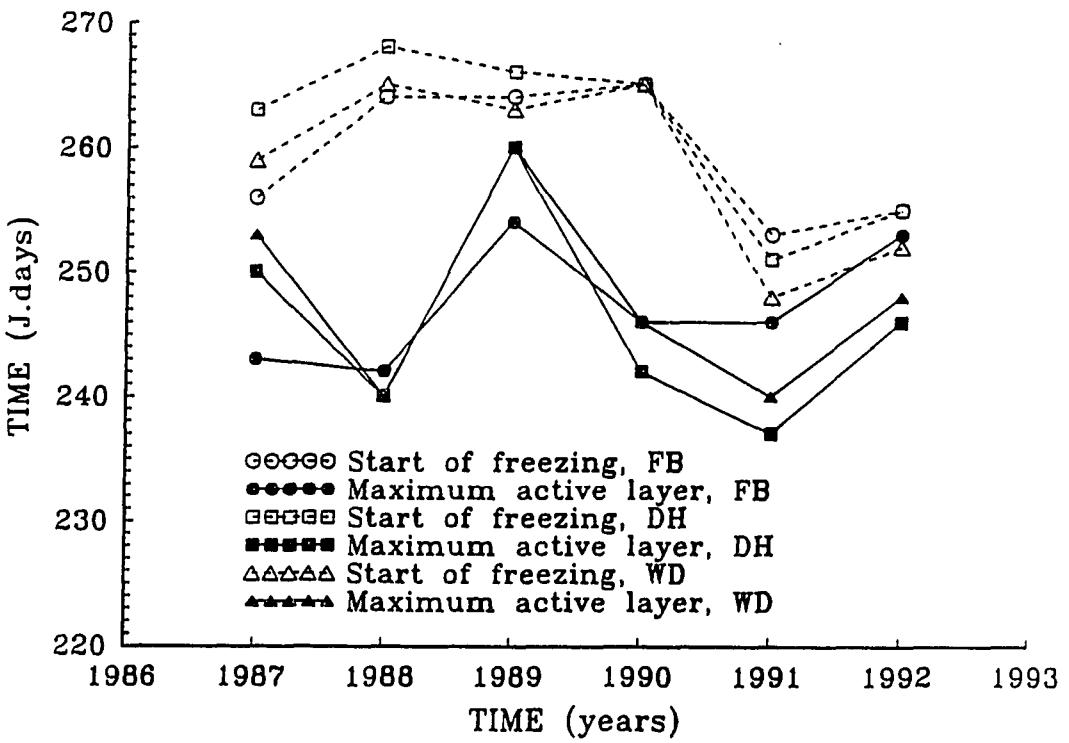

Figure 5.7 Interannual variations of the dates when the active layer reached its maximum thickness and dates for the start of the active layer refreezing from the ground surface downwards at West Dock, Deadhorse and Franklin Bluffs.

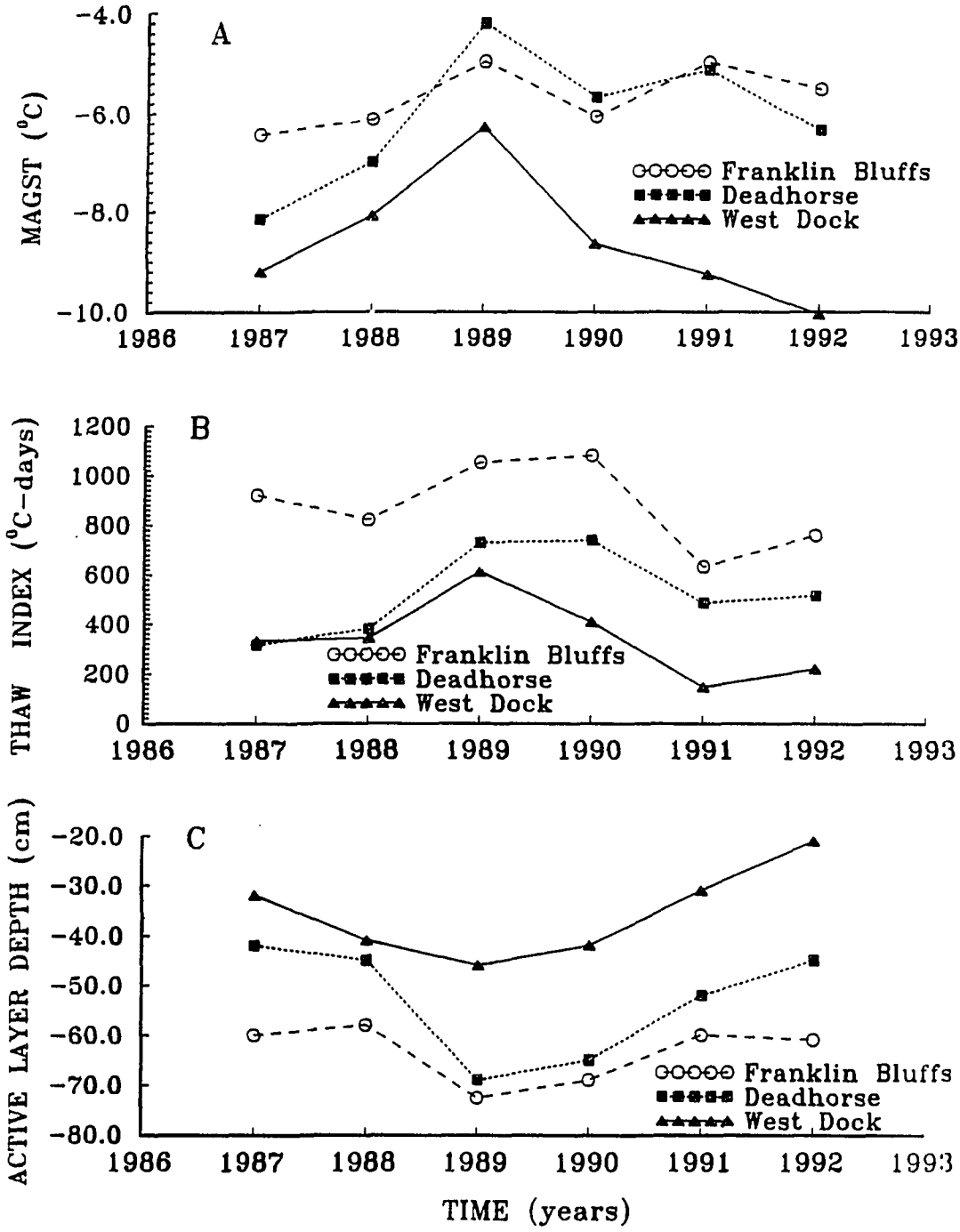

Figure 5.8 Temporal variations of the mean annual ground surface temperatures (A), ground surface thaw index (B) and the active layer depth (C) for West Dock, Deadhorse and Franklin Bluffs.

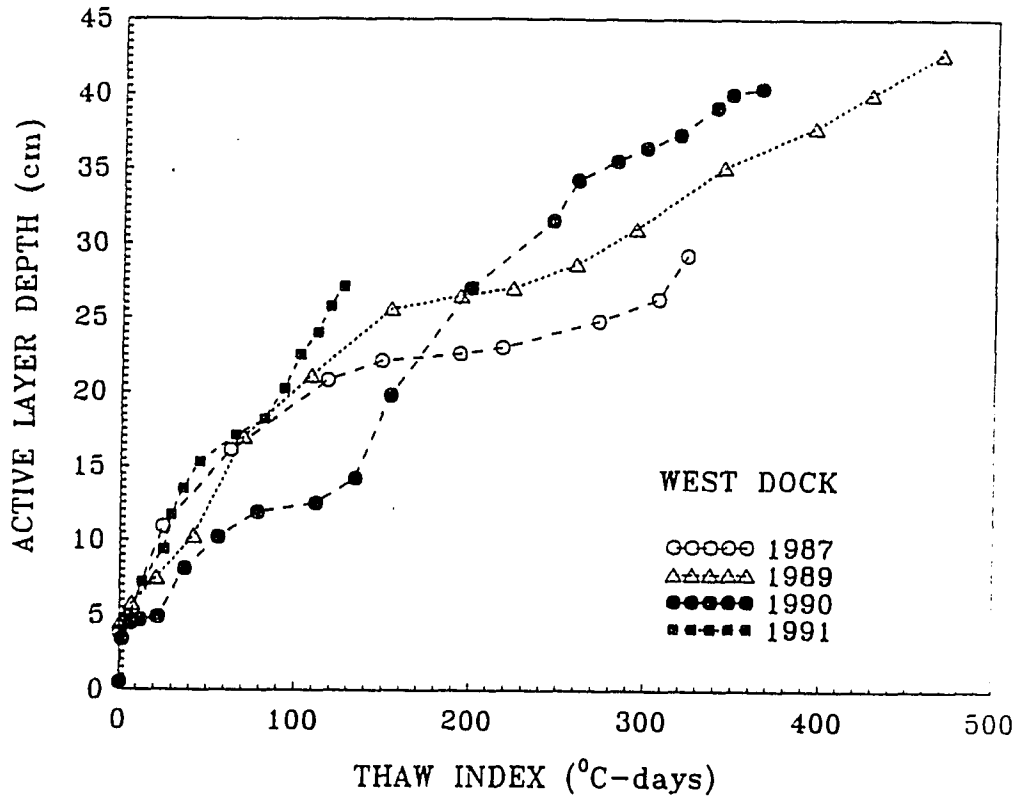

Figure 5.9 Relationship between the measured thaw depth and the thaw index at the ground surface for different years at West Dock.

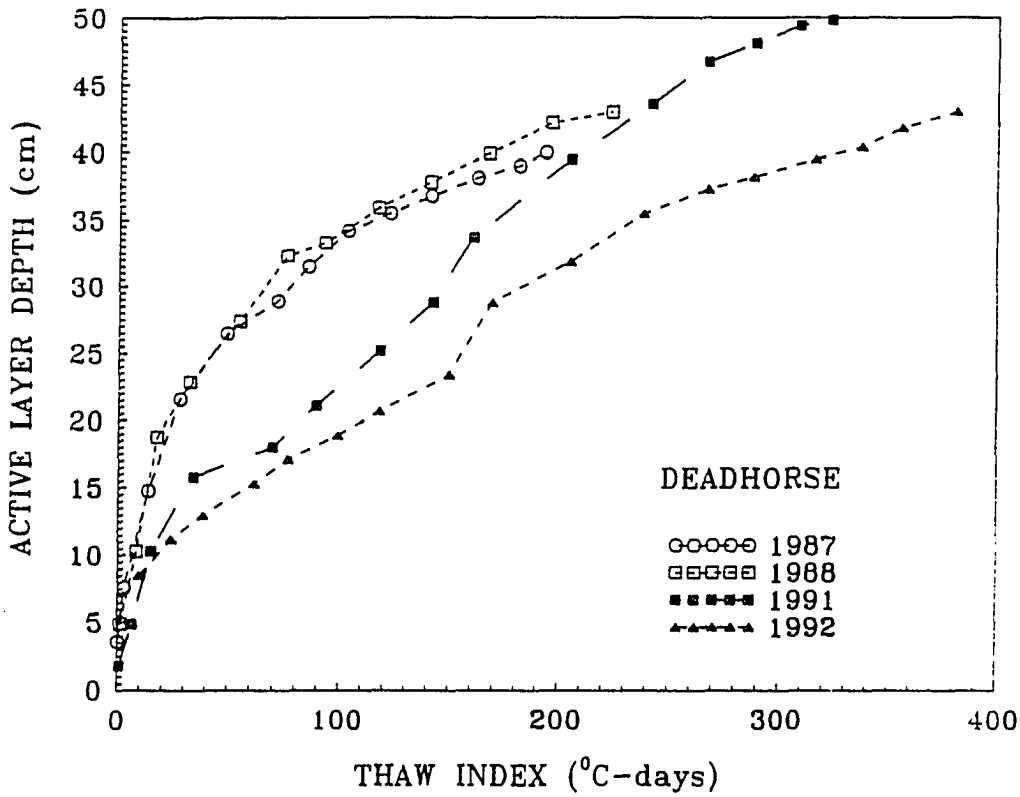

Figure 5.10 Relationship between the measured thaw depth and the thaw index at the ground surface for different years at Deadhorse.

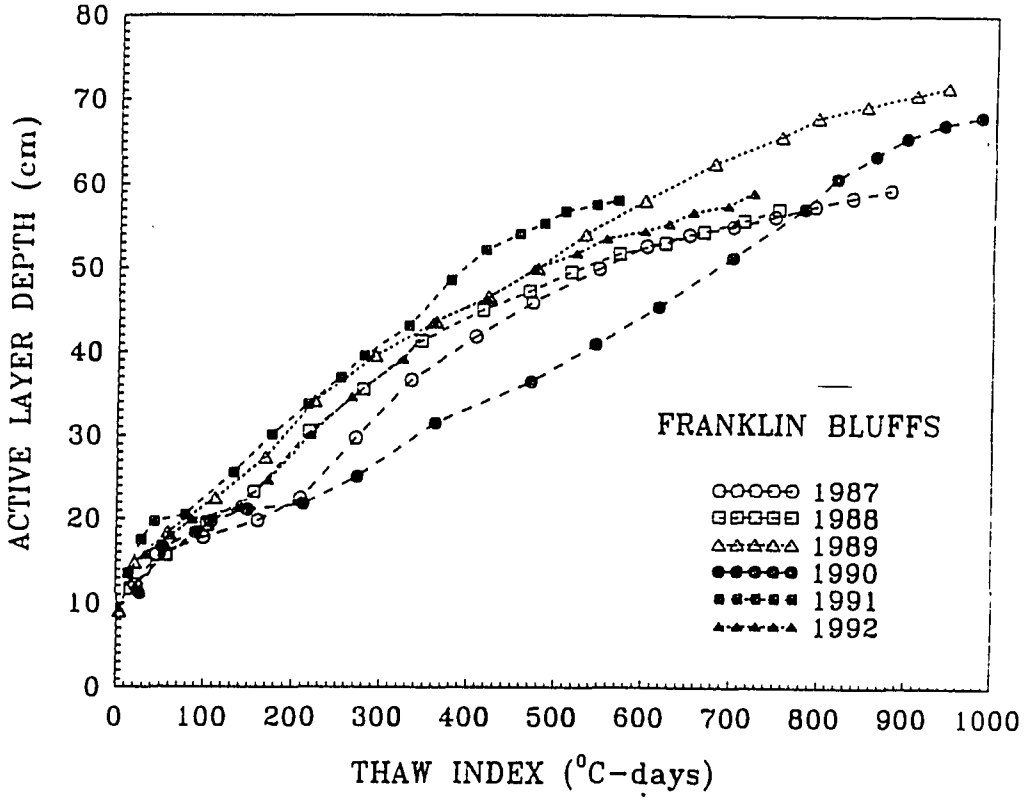

Figure 5.11 Relationship between the measured thaw depth and the thaw index at the ground surface for different years at Franklin Bluffs.

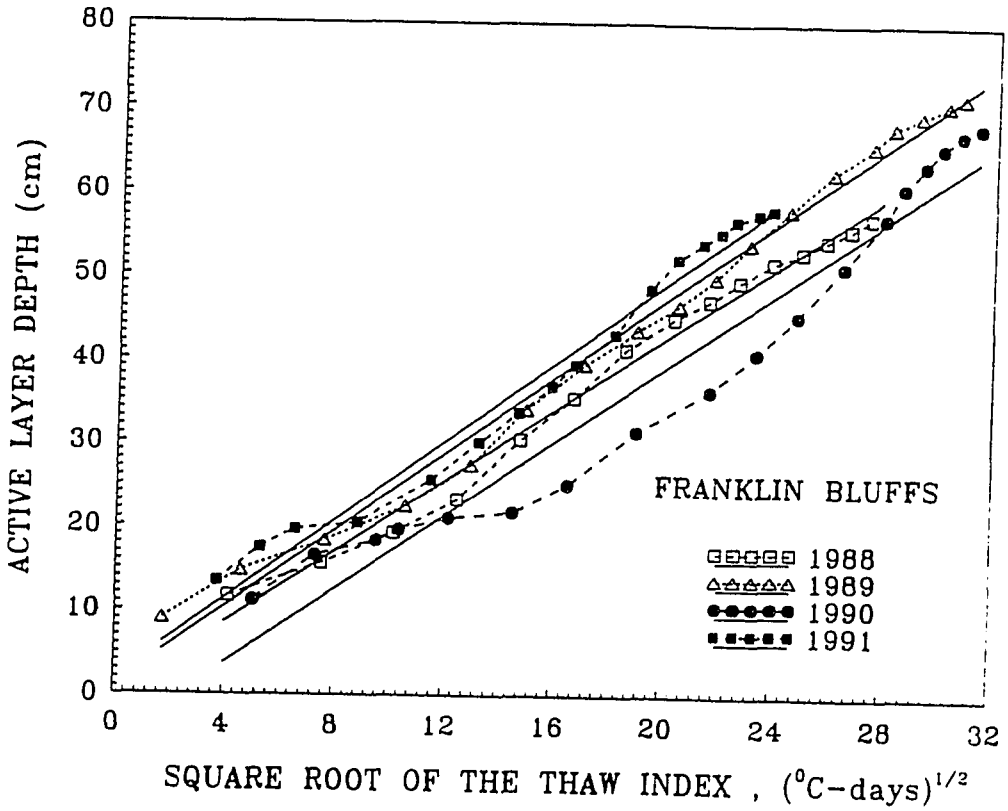

Figure 5.12 Relationship between the measured thaw depth and square root of thaw index at the ground surface for different years at Franklin Bluffs.

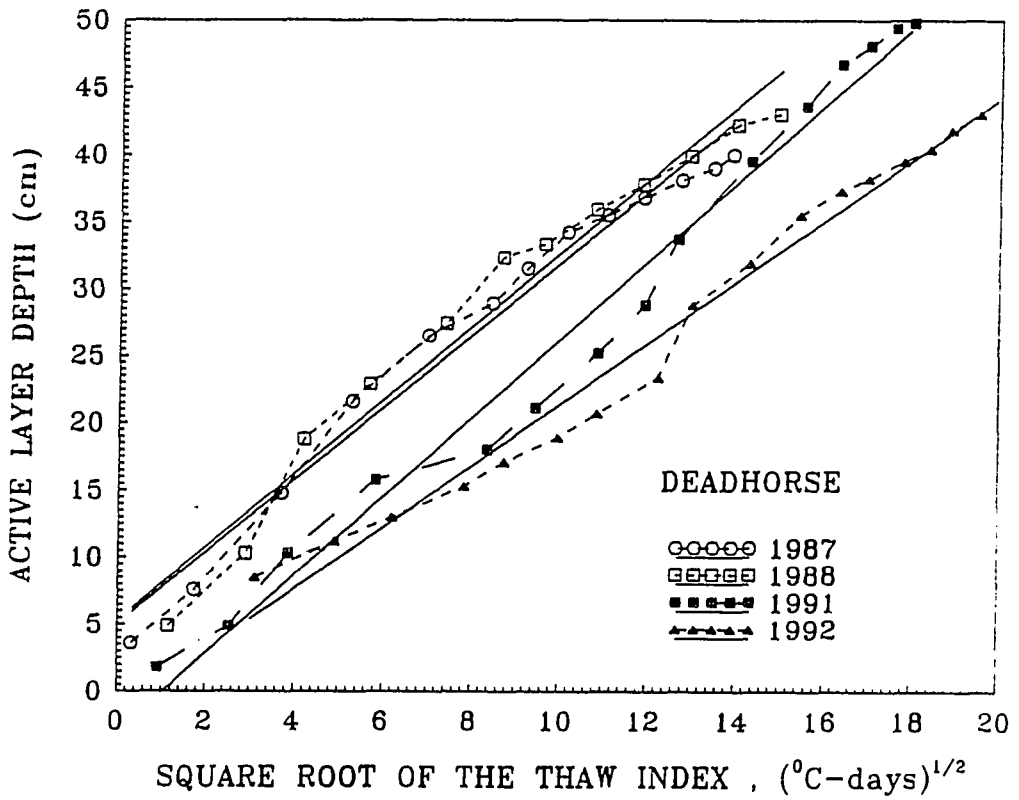

Figure 5.13 Relationship between the measured thaw depth and square root of thaw index at the ground surface for different years at Deadhorse.

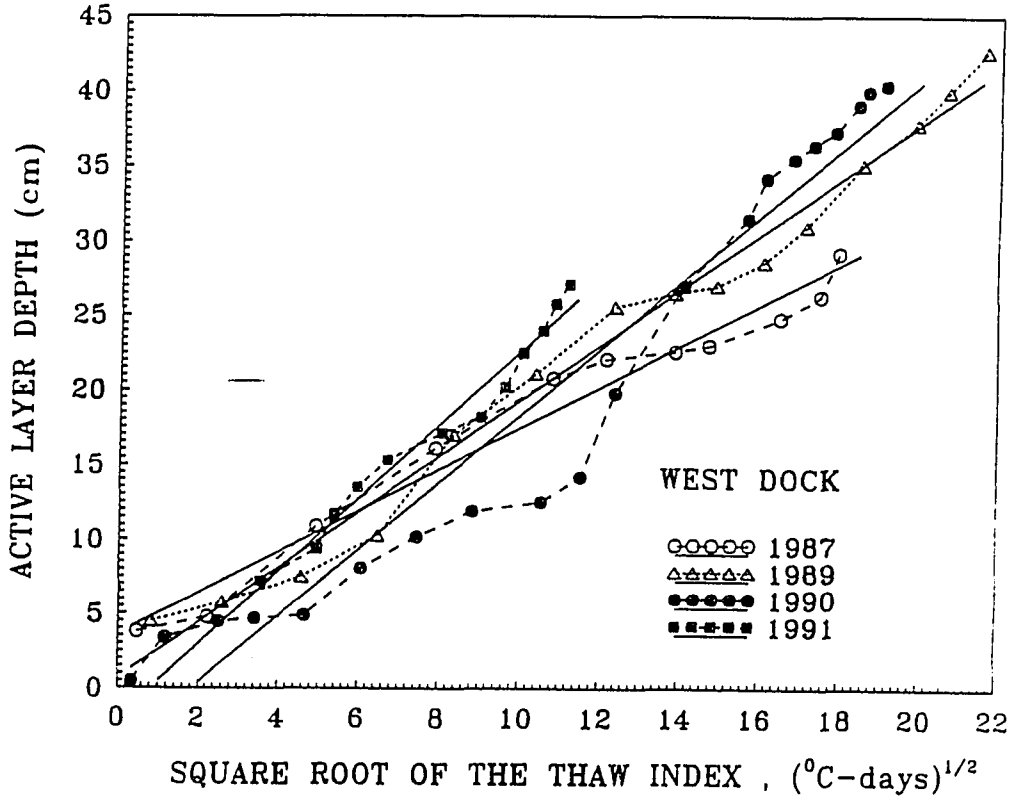

Figure 5.14 Relationship between the measured thaw depth and square root of thaw index at the ground surface for different years at West Dock.

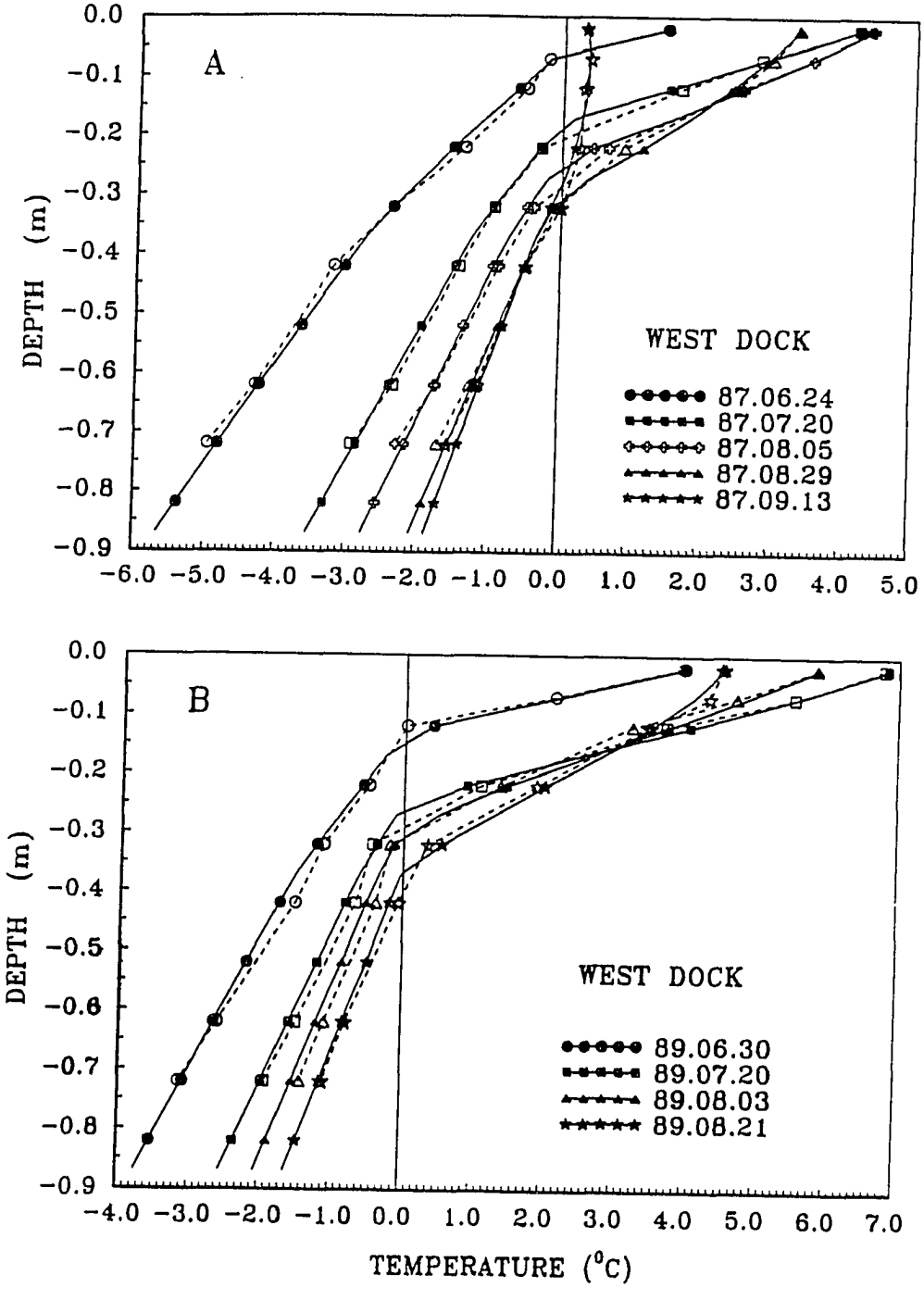

Figure 5.15 Measured (dashed lines and open symbols) and calculated (solid lines and filled symbols) temperature profiles at West Dock during the thawing period of 1987 and 1989.

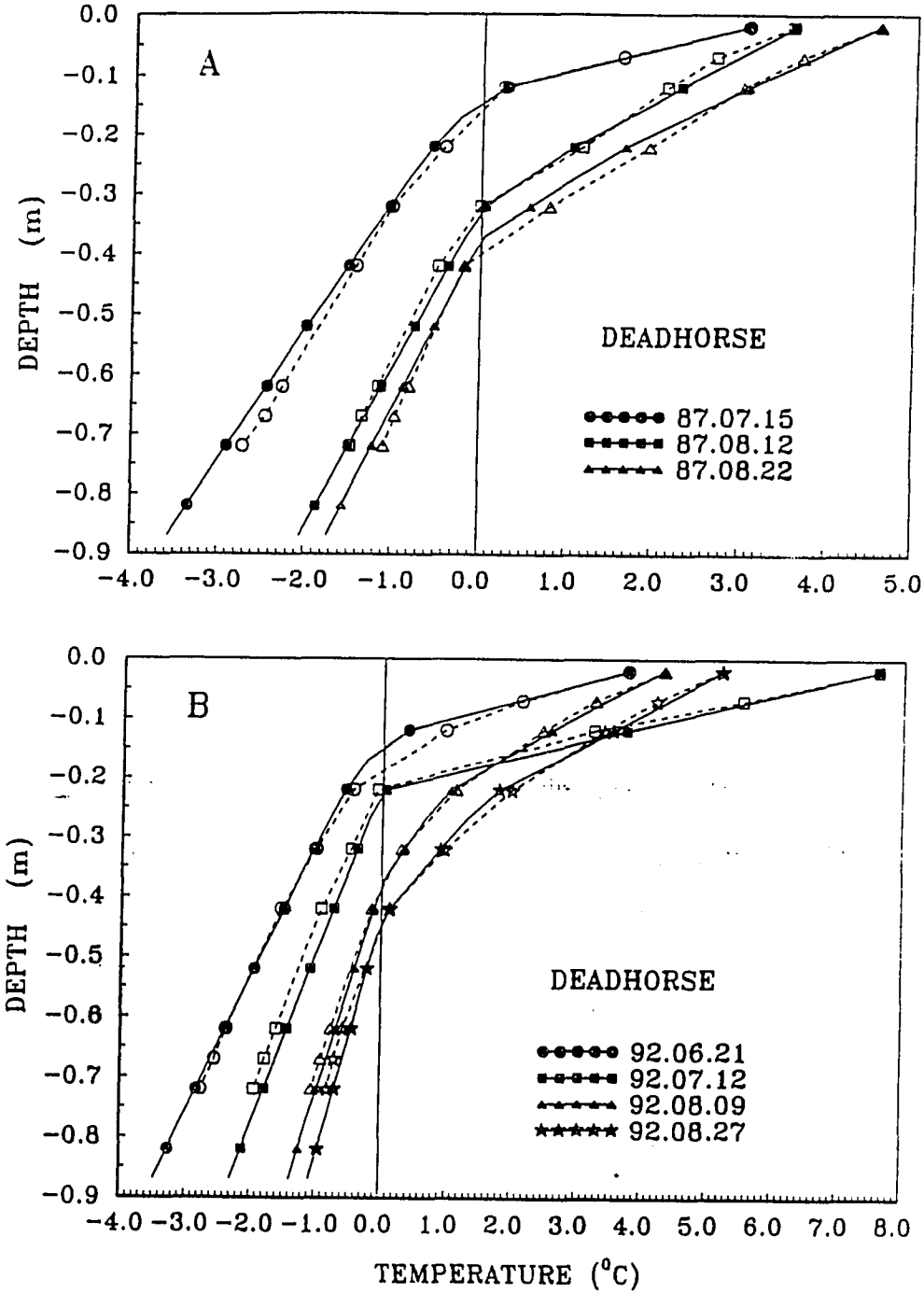

Figure 5.16 Measured (dashed lines and open symbols) and calculated (solid lines and filled symbols) temperature profiles at Deadhorse during the thawing period of 1987 and 1992.

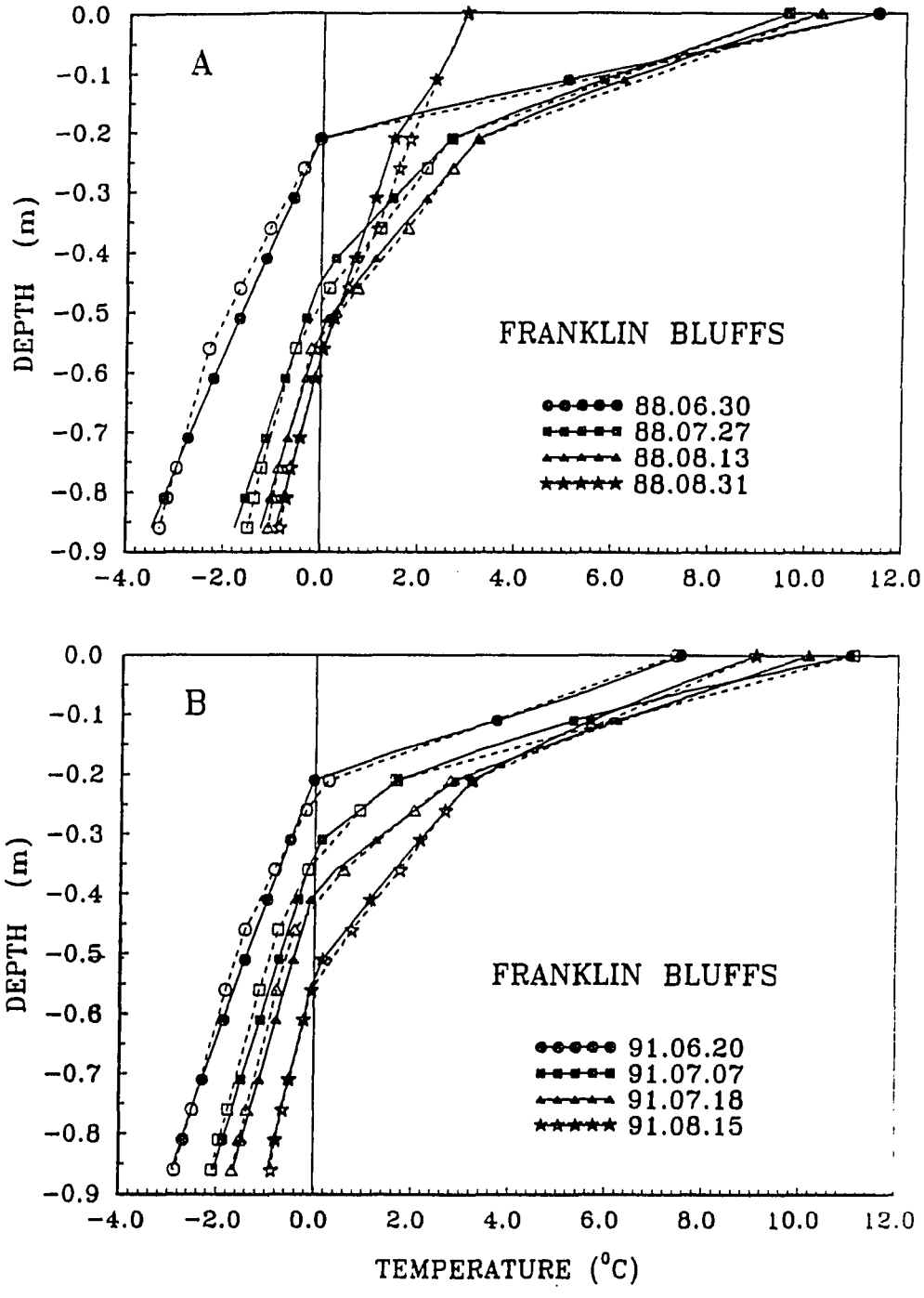

Figure 5.17 Measured (dashed lines and open symbols) and calculated (solid lines and filled symbols) temperature profiles at Franklin Bluffs during the thawing period of 1988 and 1991.

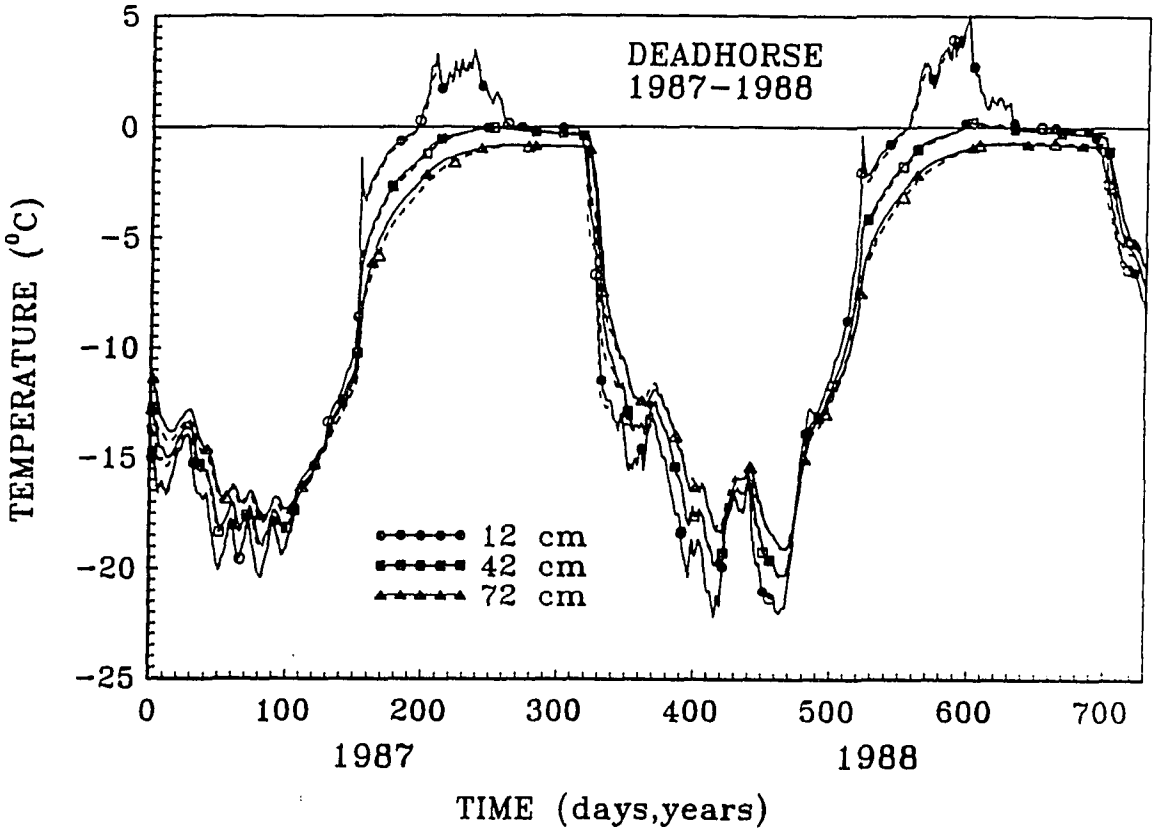

Figure 5.18 Comparison between calculated (dashed lines and open symbols) and measured (solid lines and filled symbols) temperatures at three depths (0.12, 0.42 and 0.72 m) during 1987-1988 at the Deadhorse site.

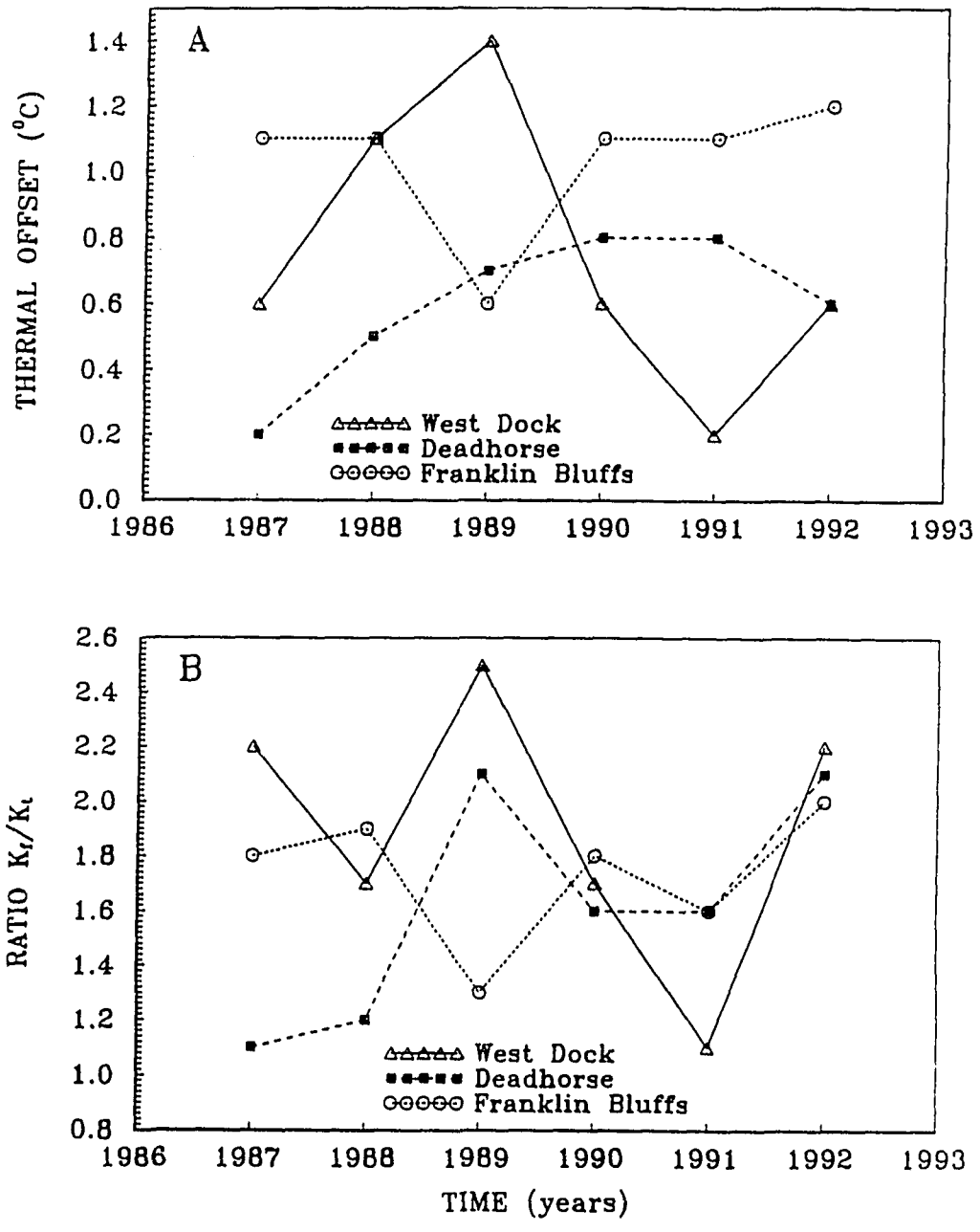

Figure 5.19 Interannual variability of the measured thermal offset (A) and the ratio of the estimated thermal conductivities in frozen and thawed states (see Table 5.7) (B) for the West Dock, Deadhorse and Franklin Bluffs sites.

Table 5.1 Soil type, dry bulk density and water content of the soils at the investigation sites (Romanovsky and Osterkamp, 1995).

Depth (m)	Soil type	ρ_b (kg/m^3)	Gravimetric water content (%)	Volumetric water content (%)
West Dock				
0.0 - 0.10	peat	---	319.3	---
0.10 -0.20	peat	455	150.0	68.2
0.20 - 0.31	peat	371	207.1	76.8
Deadhorse				
0.0 - 0.12	peat	---	119.0	---
0.12 - 0.23	peat	531	113.0	60.0
0.23 - 0.40	silt	1377	32.5	44.8
0.40 - 0.60	silt	1250	36.0	45.0
Franklin Bluffs				
0.0 - 0.08	peat	---	247.3	---
0.08 - 0.20	peat	502	163.9	82.3
0.20 - 0.40	silt	1466	34.0	49.8

Table 5.2 Thermal properties of the active layer, used in the calculations with equation (5.6).

Site	Average volum. water content, θ, %	Average latent heat, ρL, MJm^{-3}	Thermal conductivity, K_t, $Wm^{-1}K^{-1}$	Heat capacity, C_t, $MJm^{-3}K^{-1}$
West Dock	72.5	242	0.60	2.70
Deadhorse	51.5	172	0.77	2.36
Franklin Bluffs	58.3	195	0.82	2.30

Table 5.3 Thickness of the active layer (m) calculated using the Stefan equation (Stef), modified Kudryavtsev's equation (Kud) and measured (Meas) values.

Year	West Dock			Deadhorse			Franklin Bluffs		
	Stef	Kud	Meas	Stef	Kud	Meas	Stef	Kud	Meas
1987	0.46	0.34	0.32	0.49	0.36	0.42	0.82	0.63	0.59
1988	0.44	0.36	0.41	0.53	0.44	0.45	0.77	0.67	0.57
1989	0.59	0.49	0.46	0.79	0.74	0.69	0.87	0.75	0.71
1990	0.52	0.38	0.42	0.70	0.68	0.65	0.88	0.86	0.68
1991	0.30	0.19	0.31	0.62	0.54	0.52	0.68	0.53	0.58
1992	0.36	0.25	0.21	0.66	0.49	0.45	0.74	0.64	0.59
Mean	0.44	0.32	0.35	0.63	0.50	0.53	0.79	0.65	0.62

Table 5.4 Comparison of calculations for the active layer thickness obtained using a numerical method (Goodrich, 1976) and equations (5.6) and (5.8).

$\overline{T_{ps}}$ (°C)	A_{gs} (K)	Active layer thickness (m)	
		Goodrich model	Equations (5.6) and (5.8)
2.67	15.00	1.40	1.29
-11.10	20.00	0.74	0.70
-4.50	11.10	0.84	0.77
-4.24	12.25	0.85	0.89
-8.14	14.85	0.76	0.69

Table 5.5 Thermal properties of the active layer and near-surface permafrost estimated from the results of previous investigations.

Depth (m)	Soil type	Volum. water content, θ (%)	Volumetric heat capacity, C_t/C_f ($MJm^{-3}K^{-1}$)	Thermal conductivity, K_t/K_f ($Wm^{-1}K^{-1}$)
WD				
0.0 - 0.2	peat I	68.2	2.7 / 1.26	0.6 / 1.2
0.2 - 0.35	peat II	76.8	2.7 / 1.26	0.6 / 1.2
0.35 - 0.9	silt	44.4	2.1 / 1.54	1.2 / 1.56
0.9 - 8.5	silt & sand	43.4	2.9 / 2.34	2.0 / 3.39
8.5 - 16	sand & gravel	38.9	2.9 / 2.04	2.0 / 3.39
DH				
0.0 - 0.12	peat I	.....	2.7/ 1.26	0.6 / 1.2
0.12 - 0.23	peat II	60.0	2.7/ 1.26	0.6 / 1.2
0.23 - 0.92	silt	45.0	2.1/ 1.54	1.35 / 1.76
0.92 - 2.7	sand & silt	--	-- / 2.14	-- / 3.39
2.7 - 16	gravel	--	-- / 1.94	-- / 3.59
FB				
0.0 - 0.08	peat I	70.0	2.7 / 1.26	0.6 / 1.2
0.08 - 0.2	peat II	80.3	2.7 / 1.26	0.6 / 1.2
0.2 - 1.2	silt	48.0	2.1 / 1.54	1.35 / 1.76
1.2 - 14	gravel	--	-- / 1.94	-- / 3.59
14 - 16	silt	--	-- / 1.54	-- / 1.76

Table 5.6 Values of the root mean square deviations (RMS) of calculated daily mean temperatures from the measured ones.

Site	1987	1988	1989	1990	1991	1992	Average
WD	0.14	0.22	0.25	0.63	0.34	0.35	0.33
DH	0.24	0.21	0.68	0.31	0.32	0.25	0.34
FB	0.31	0.20	0.59	0.24	0.17	0.22	0.29

Table 5.7 Thermal conductivities ($Wm^{-1}K^{-1}$) of the active layer in the thawed and frozen states with the ratio K_t/K_f estimated from the best fit of the numerical model to the data.

Soil type	1987	1988	1989	1990	1991	1992	Average
WD							
peat I	0.7 /1.4	1.0 /1.7	0.6 /1.5	1.0 / 1.7	1.3 / 1.4	0.7 / 1.4	0.88 / 1.52
peat II	0.6 /1.5	1.0 /1.7	0.75/1.5	1.0 / 1.7	1.3 / 1.5	0.6 / 1.5	0.88 / 1.57
silt	1.6 /2.1	1.4/1.85	1.6 /2.1	1.4/1.85	1.4/1.85	1.6 / 2.1	1.5 / 1.98
DH							
peat I	1.3 /1.5	1.2 /1.3	0.8 /1.5	0.8 / 1.3	0.8 / 1.3	0.7 / 1.5	0.93 / 1.4
peat II	1.3 /1.5	1.1 /1.5	0.6 /1.5	0.8 / 1.3	0.8 / 1.3	0.7 / 1.5	0.88 / 1.43
silt	1.6 /2.1	1.6 /2.1	1.6 /2.1	1.6 / 2.1	1.6 / 2.1	1.6 / 2.1	1.6 / 2.1
FB							
peat I	0.4 /0.8	0.5 /0.9	0.7 /0.9	0.5 / 0.8	0.6/0.95	0.55/1.2	0.55 / 0.92
peat II	0.5/0.9	0.5 /1.0	0.5 /0.9	0.5 / 0.9	0.6/0.95	0.6 / 1.2	0.54 / 0.98
silt	1.15/1.5	1.35/1.7	1.15/1.5	1.15/1.5	1.4 / 1.7	1.3 / 1.8	1.25 / 1.62

Table 5.8. Comparison of the thicknesses of the active layer (m) calculated using thermal conductivities from Table 5.7 in the modified Kudryavtsev's equations (5.6-5.8) and measured values. Averaged depths (bottom row) were calculated using input data, averaged over the whole period of measurements (1987-1992).

Year	West Dock		Deadhorse		Franklin Bluffs	
	Eq (5.8)	Measured	Eq (5.8)	Measured	Eq (5.8)	Measured
1987	0.32	0.32	0.44	0.42	0.56	0.59
1988	0.42	0.41	0.52	0.45	0.60	0.57
1989	0.48	0.46	0.70	0.69	0.72	0.715
1990	0.46	0.42	0.68	0.65	0.77	0.68
1991	0.27	0.31	0.53	0.52	0.53	0.58
1992	0.23	0.21	0.46	0.45	0.60	0.59
Mean	0.36	0.355	0.555	0.53	0.63	0.62
Averaged	0.36	0.355	0.53	0.53	0.60	0.62

CHAPTER 6

Freeze-up of the Active Layer on the Coastal Plain of the Alaskan Arctic.

T. E. Osterkamp and V. E. Romanovsky, 1996. Freeze-up of the Active Layer on the Coastal Plain of the Alaskan Arctic. *Permafrost and Periglacial Processes* (prepared for publication)

6.1 Abstract

Results of analyses and interpretation of daily temperature data, particularly during freezing and cooling, in the upper 1 m of soils from 1986 through 1993 at three sites West Dock, Deadhorse Airport, and Franklin Bluffs in Prudhoe Bay region and in 1993 and 1994 at Barrow are presented in this paper. Annual temperature measurements in deeper boreholes (nominally 60 m) from 1986 to 1993 at the same sites were used as well.

This paper concentrates on thermal processes and unfrozen water behavior in the ground during freezing and continued cooling of the active layer. Freezing begins in the upward direction from the top of the permafrost. The ground surface temperature becomes negative one or two weeks later. In a few days, temperatures between the two freezing fronts become very close to the equilibrium freezing temperature establishing a so called "zero curtain" which exists until the time of freeze-up and protects underlying permafrost from significant cooling. On the average, 34% of the active layer froze upwards at West Dock, 36% at Deadhorse and Franklin Bluffs.

The dynamics of the temperature field within the active layer and near-surface permafrost was very peculiar during the freeze-up and following cooling period. Measured temperature profiles show very slow temperature decreases after freeze-up occurred. Temperature profiles had a parabolic form with temperature maximum near the base of the active layer. This behavior appears to be associated with unfrozen water

in the frozen soils. Precise temperature data together with computer modeling of the temperature field dynamics provide essential new information on the dynamics of the unfrozen water content in the ground in natural undisturbed conditions during freezing and continued cooling of the active layer.

The most appropriate unfrozen water content curves (i.e. produced the smallest differences between calculated and measured temperature profiles) for each site and for different depths were determined by trial and error.

Results of modeling for all four sites show that a layer with high unfrozen water content existed during the freeze-up of the active layer at the depth where final freeze-up occurred. For the Deadhorse site, this layer continued from the ground surface to the depth of 0.3 m in 1987 and 0.36 m in 1991. For Franklin Bluffs in 1987, for West Dock in 1988, and for Barrow in 1993 the thickness of this layer was 0.1 m and it was located in the depth intervals between 0.2 and 0.3 m at Franklin Bluffs, between 0.15 and 0.25 m at West Dock, and between 0.21 and 0.31 m at Barrow. Reconstructed curves of unfrozen water content as a function of temperature for these layers show unexpectedly large values at low temperatures.

6.2 Introduction

General circulation models project global mean equilibrium temperature increases of between 1.8°C and 5.2°C for a doubling of preindustrial CO_2 concentrations. The temperature rise in Arctic regions may be 2 to 3 times greater than the global average. Climatic warming will significantly influence permafrost conditions and, as a result, stability of roads, buildings and pipelines. Virtually all surface activities associated with the development of natural resources will be effected.

The fate of permafrost (whether it degrades or aggrades) is controlled by climatologic, biologic, hydrologic, geologic, and oceanographic factors through their influence on the transfer of heat and mass (moisture and solutes) to and from the permafrost table. Consequently, there is a need for developing a better understanding

of how the climate, biota (primarily vegetation), hydrology, geology, and the ocean influence heat and mass transfer processes at the ground surface, within the active layer, and at the permafrost table. Warming air temperatures would generate a somewhat different change at the surface of the permafrost because of the effects on heat balance of the material between the permafrost and the atmosphere. In the continuous permafrost zone, the effect on the permafrost would be to warm it and, possibly, to change the depth of the active layer (Osterkamp and Lachenbruch, 1990; Nelson et al., 1993).

To predict the behavior of the active layer in connection with the predicted climatic warming it is necessary to understand active layer thawing and freezing under natural conditions which vary significantly from year to year. It has been found (Osterkamp et al., 1994; Romanovsky and Osterkamp, 1995a; Osterkamp and Romanovsky, 1996) that the interannual variability in active layer temperatures over the last decade has the same order of magnitude as the predicted long-term warming (i.e. about 4°C). In addition, the measured long-term changes in the active layer and permafrost can be sensitive indicators of global change in the Arctic.

The dynamics of active layer freezing are also important for the cryogenic structure of the frozen active layer and near-surface permafrost because the rate and proportion of freezing from the top and from the bottom of the active layer determine the characteristics of the ice lenses. This is true especially for the case of progressive formation of syngenetic permafrost (Shur, 1988). For this reason, it is necessary to know which part of the active layer froze downward from the ground surface and which part froze upward from the permafrost table.

The physical and mechanical properties of soils become strongly temperature dependent when unfrozen water is present in frozen ground. Problems related to the presence of unfrozen water in frozen soils have been investigated in laboratory experiments (Nersesova and Tutunov, 1957; Lovell, 1957; Tsytovich, 1973; Anderson et al., 1973; Anderson and Tice, 1973; Tice et al., 1978; Ershov et al., 1979; Black and

Tice, 1988; Tice et al., 1988). At the present time, precise high frequency temperature measurements in the active layer and near-surface permafrost have been collected. These data, when used with numerical models of the freezing and thawing processes, provide new opportunities to study *in situ* the unfrozen water contents in soils and their dynamics during the year.

This paper continues the discussion of the processes related to seasonal thawing and freezing of the active layer in the Alaskan Arctic (Romanovsky and Osterkamp, 1995a; Romanovsky and Osterkamp, 1996). It will concentrate on the thermal processes and unfrozen water behavior in the ground during freezing of the active layer. The data used in these studies were obtained from 1986 to 1993 from high frequency (every four hours) temperature measurements in the air, ground surface, active layer and near-surface permafrost (down to 0.7-0.9 m) at three sites on the Coastal Plain of the Alaskan Arctic adjacent to the Beaufort Sea. The sites are along the Dalton Highway south from Prudhoe Bay and include West Dock (WD), Deadhorse (DH), and Franklin Bluffs (FB). The data also include annually measured permafrost temperatures in deeper boreholes (nominally 60 m) located at the same sites. Detailed descriptions of site conditions, methods of measurements and data processing have been published (Osterkamp, 1985; Osterkamp et al., 1994; Romanovsky and Osterkamp, 1995a; Osterkamp and Romanovsky, 1996). In addition, hourly measured temperatures in the active layer and near-surface permafrost (to the 1 m depth) at Barrow from August 1993 through August 1994 (Hinkel, unpublished data) were used in these studies.

6.3 Analysis and Interpretation

6.3.1 General Features of the Freezing Process in the Active Layer

Freezing of the active layer at the study sites usually started at the end of August or beginning of September while the ground surface temperature remained

above 0°C. Initially, freezing proceeded upward from the permafrost table (Figures 6.1, 6.2, Table 6.1). The ground surface temperature became negative one or two weeks later, typically, and a second freezing front formed at the top of the active layer. In a few days, the temperature between the two freezing fronts became very close to the equilibrium freezing temperature establishing a so called "zero curtain". The length of the time required for this "zero curtain" to form can be estimated using the time constant (τ) for the response of a slab (the active layer) to a step change in surface boundary conditions which is

$$\tau = \frac{X^2}{4D} \qquad [6.1]$$

where X is in this case an average active layer thickness (about 0.5 m), and D is the average thermal diffusivity of thawed soils (about 0.8×10^{-6} $m^2 s^{-1}$). For these values, (6.1) yields $\tau \cong 1$ day. Since τ is small and since ground surface temperatures typically decrease slowly, the assumption, that the thawed active layer goes to zero instantaneously, used in some models (Goodrich, 1978b), is a realistic one.

The zero curtain existed until the date of freeze-up and protected the underlying permafrost from cooling (Sumgin et al., 1940; Muller, 1947). Some investigators relate the presence of the zero curtain with mass and nonconductive heat transfer processes (Outcalt et al., 1990; Hinkel et al., 1990; Hinkel and Outcalt, 1994). The equilibrium temperature for all sites and all years was slightly lower than 0°C, varying in the interval between -0.05°C and -0.12°C (Figures 6.1, 6.2, 6.4, and 6.5) although these values are not significantly larger than the accuracy of the measurements.

The main characteristics of freezing downwards from the ground surface and upwards from the permafrost table are shown in Table 6.1. Ground temperature measurements were used to estimate dates for the beginning of downward freezing

from the ground surface which were taken to be the dates when ground surface temperatures became stable below 0 ^{0}C. Dates for the beginning of freezing upwards from the permafrost table were taken from the graphs of the temperature field dynamics (e.g. Figures 6.1 and 6.2). Average dates for the start of freezing both from the bottom and from the top were about the same for all sites; 5 and 16 September for WD, 3 and 18 September for DH and 4 and 17 September for FB while the interannual variations of these dates ranged up to three weeks (Table 6.1).

Freeze-up dates for the active layer were taken to be the dates when the temperatures at all depths began to decrease sharply after the zero curtain disappeared. In general, freeze-up dates (Table 6.1) depend on air temperatures, active layer thickness (a deeper active layer takes longer to freeze), soil water content, thermal properties of the soil, mean annual permafrost surface temperature, the dates for the start of freezing at the ground surface, and especially the timing of the snow cover and its rate of accumulation. The deepest active layer for all sites occurred in 1989 (Table 6.1). Snow on the ground at the Prudhoe Bay/ARCO meteorological station appeared in October of that year and was very shallow (0.025 m maximum snow depth for October and November). As a result, the freeze-up took place slightly earlier in 1989 than in 1988 and 1990 for the FB and DH sites. For WD, freeze-up was 8 days earlier in 1988 and 20 days earlier in 1990 than in 1989. Variations of the freeze-up date show poor agreement with thaw index variations and better agreement with the permafrost temperature variations (especially for WD and FB). For 1988 to 1990, freeze-up occurred significantly earlier at the FB site than at DH despite the deeper active layer at FB. This may have been a result of the slightly colder ground surface and permafrost temperatures during freeze-up at the FB site.

The longest duration of the freeze-up period (difference between the start of freezing from the ground surface and freeze-up date), 79 days, was measured at the DH site in 1991. It increased slightly from 57 days in 1987 to 79 days in 1991 and then decreased in 1992 to the 1988 value. At the FB site, freeze-up duration was almost

constant (about 58 days) from 1987 through 1990 and then increased in 1991 and 1992. The freeze-up duration generally decreased at the WD site during the period of measurements from 50 days in 1987 to 33 days in 1992 with some local maximum in 1989 and minimum in 1990. Average duration of freeze-up period for DH was 69 days. This is similar to FB (63 days) and much longer than WD (42 days).

The relative amount of the active layer frozen from the top downwards (ΔX_{top}) and from the bottom upwards (ΔX_{bot}) determines the cryogenic structure of the frozen active layer and near-surface permafrost (Shur, 1988). Favorable conditions for maximum freezing from the bottom are a cold temperature at the permafrost table during the freeze-up period and cold mean annual permafrost temperatures (which results in a large thermal gradient and high heat flux into the permafrost) and an early and thick snow cover which retards freezing from the top extending the time for freezing from the bottom up. The average ratio between ΔX_{bot} and maximum depth of the active layer X_{max} was very similar for all three sites (Figure 6.3, Table 6.1): 34% for WD, 36% for DH and FB, although this proportion varied by as much as 26% (at WD).

Figure 6.3 illustrates the dependence of the ratio $\Delta X_{bot}/X_{max}$ on interannual variations of the air and temperatures at the permafrost table and snow cover thicknesses averaged over the period of freeze-up (September through October for WD and September through November for DH and FB. Values of $\Delta X_{bot}/X_{max}$ vary in a small range at DH. For the WD site, the ratio followed in general the air temperature changes, except 1991 when the ratio was unexpectedly low. The most influential factor at the FB site was the average snow depth and to a lesser extent the averaged permafrost temperature at the depth of 0.76 m (Figure 6.3).

Some examples (typical for all three sites and for all years of measurements) of the daily changes in the active layer and near-surface permafrost temperature profiles for two sites are shown in Figures 6.4 and 6.5. The temperature profiles on these

figures look somewhat strange because of linear interpolation between measurement points, but are clear enough to provide information on the freezing process in the active layer.

Generally, temperatures decreased slowly after freeze-up occurred (when temperature within the entire active layer becomes negative) staying above -1°C at the maximum depth of the active layer even 20 days after the freeze-up date. This conflicts with an estimate of the time constant τ for conductive heat flow with constant thermal properties which in this case will be about 2 days (X about 1 m and D about 1.5×10^{-6} $m^2 s^{-1}$). Measured temperature profiles kept a parabolic form with maximum temperatures occurring near the base of the active layer. The temperatures in the active layer changed slowly in the range from 0°C to -0.4°C for WD, to -0.25°C for DH (Figures 6.4 and 6.5) and to -0.15°C or -0.2°C for FB. Similar ranges of the phase change temperatures of the ground water (-0.05°C to -0.2°C for Barrow and -0.5°C for the Lena River Delta in Russia) were reported by (Shur et al., 1995). One possible explanation of such behavior of the temperatures in those ranges is that the equilibrium temperatures for soils in the active layer fall within these ranges. However, even after the temperatures decrease further, the thermal response is still very slow suggesting that this hypothesis may not be correct.

Another explanation of the slow temperature changes noted above and in wider ranges (to -1°C and colder) is the possible presence of significant amounts of unfrozen water in the frozen soil. The temperature regime in the ground is extremely sensitive to the unfrozen water content and to changes in its amount during the freeze-up period. This hypothesis will be explored below using data from the active layer and near-surface permafrost and numerical simulations of the temperature field dynamics.

6.3.2 Results of Modeling With no Unfrozen Water

A finite element model (Gosink and Osterkamp, 1990; Osterkamp and Gosink, 1991; Osterkamp and Romanovsky, 1996), which is a modified version of the Guymon and Hromadka (1977) and Guymon et al. (1984) model, was used to reconstruct the one-dimensional temperature field in the active layer and near-surface permafrost. Daily mean ground surface temperatures (0.02 m at WD, 0.02 m at DH; and 0.0 m at FB) measured from 1986 to 1993 (Romanovsky and Osterkamp, 1995a) were used for the upper boundary conditions. The lower boundary was placed at the 30 m depth. Daily temperatures at this depth were calculated for all sites and for the full period of measurements (1986 through 1993) using a combination of the daily permafrost surface measurements and annual measurements of the permafrost temperatures to the 60 m depth (Osterkamp and Romanovsky, 1996). Combined daily temperature profiles measured to the depth of 0.7 - 0.8 m and calculated to the depth of 55 m (Osterkamp and Romanovsky, 1996) were used for the initial conditions. Drilling records and results of previous investigations were used to determine the lithology and the initial thermal properties of the soils in the thawed and frozen states (Romanovsky and Osterkamp, 1995a; Osterkamp and Romanovsky, 1996; Romanovsky and Osterkamp, 1996). The time step in these calculations was 1 hour, while the space steps (200) were changed from 0.01 m within the upper 1 m to 1 m at the lower boundary of the space domain (30 m).

The effectiveness of this approach for calculating active layer and near-surface permafrost temperature field dynamics throughout the year, except for the freeze-up period was shown in earlier publications (Romanovsky and Osterkamp, 1995b; Osterkamp and Romanovsky, 1996; Romanovsky and Osterkamp, 1996). Figures 6.6 and 6.7 show comparisons between calculated (dashed lines) and measured (solid lines) temperature profiles in the active layer and near-surface permafrost. In the model, temperatures sharply decreased a few days after freeze-up and temperature profiles

became almost linear within the upper 1 m. However, the measured temperatures decreased much more slowly (Figures 6.6 and 6.7). Deviations of the modeling results from the measurements during the cooling period following freeze-up of 2 K and more were found. Similar results were obtained for all three sites and for each freeze-up period from 1986 through 1992.

To investigate the range of temperatures deviations were found in the temperature field dynamics, a series of calculations were made with initial conditions well below the freezing point of the ground (with temperatures at the bottom of the active layer around -13°C for WD, -11°C for DH and -8°C for FB). The measured temperature profiles for the active layer and near-surface permafrost (down to 0.72-0.86 m) and calculated profiles for the deeper part of permafrost (to 30 m depth) (Osterkamp and Romanovsky, 1996; Romanovsky and Osterkamp, 1996) were used as initial conditions. Measured temperatures at 0.02 m for WD and DH and at the ground surface for FB were used as the upper boundary conditions. Calculated daily temperatures at the depth of 30 m were used as the lower boundary conditions. For subsequent calculations, the time of the initial conditions was shifted backwards to higher temperatures.

Figure 6.8 shows the results of some of these calculations. For each site, three sets of three profiles each are presented. In each set, the right-hand profile represents the initial temperature profile on the dates indicated in the figures, the other two are measured (solid lines) and calculated (dashed lines) the day after the indicated dates. For all three sites the "coldest" set of profiles (-13°C at the depth of the active layer base for WD, -11°C for DH and -8°C for FB) show very good agreement between calculated and measured temperatures. Differences became noticeable when initial temperatures at the active layer base were around -9°C for the WD and DH sites and -3°C for FB. The difference at the FB site was 0.6 K when the initial temperature at the active layer base was -1.7°C (Figure 6.8C), while at WD and DH these differences were 1 K and 1.4 K with initial temperatures about -4°C and -5°C respectively (Figures

6.8A and 6.8B). The largest differences between calculated and measured temperatures were reached when initial temperatures were warmer than -1°C (Figures 6.8A and 6.8C).

The results of these calculations show that exactly the same model with the same values of the thermal parameters which provided very good agreement (within 0.1 - 0.2 K) between calculated and measured temperatures during the winter period with the temperatures at the permafrost surface around -9°C and colder, failed to produce reasonable results for the cooling period following freeze-up. The range of temperatures where this model did not work properly was unexpectedly large for WD and DH (from 0°C to -8°C or -8.5°C) and much smaller for the FB site (from 0°C to -2°C or -2.5°C).

The most likely explanation is that this behavior of the temperature field was due to the presence of unfrozen water in the frozen soils with temperature-dependent thermal properties of the soils and the latent heat release over a range of temperatures with changing in the unfrozen water contents.

6.3.3 Modeling Freezing of the Active Layer With Unfrozen Water

A finite element model which uses an apparent heat capacity approach (Guymon and Hromadka, 1977; Guymon et al., 1980; Hromadka et al., 1981; Guymon et al., 1984; Gosink et al., 1988; Gosink and Osterkamp, 1990; Osterkamp and Gosink, 1991) was used to investigate this hypothesis. The model has been tested and identified as being physically realistic and appropriate for freezing soil conditions in Interior Alaska (Kawasaki et al., 1982; Gosink et al., 1988). Temperature-dependent thermal properties were calculated according to the methods given in Osterkamp (1987).

Unfrozen water contents were related to temperature by a simple power law (Lovell, 1957)

[6.2] $$w_u = A|T|^B$$

where w_u is the gravimetric unfrozen water content (kg of H_2O/kg of dry soil), T is the temperature (°C), and A and B are empirical constants. Measurements exist for Fairbanks silt (Tice et al., 1988) and for Barrow silt (Nakano and Brown, 1971; 1972; McGaw et al., 1978) and Nakano and Brown (1971) introduced an exponential law for the phase composition curve (unfrozen water content as a function of temperature). Both curves are shown in Figure 6.9 with the Fairbanks silt curve designated as CRREL-1 (power law) and the Barrow curve as CRREL-2 (exponential law).

These curves were used in the calculations as an initial approximation for the unfrozen water contents curves. Thermal conductivity and heat capacity values for completely frozen soils (when temperatures at the permafrost surface were lower than -10°C for WD and DH and lower than -4°C for FB) were the same as in previous modeling (Figure 6.8). The measured temperature profiles in the active layer and near-surface permafrost on the dates of freeze-up were used for initial conditions. Deeper parts of the initial temperature profiles (down to 30 m) and the lower boundary conditions were taken from results of the previous modeling (Osterkamp and Romanovsky, 1996). Measured daily temperatures at 0.02 m for WD and DH and at the ground surface for FB were used for the upper boundary conditions. Calculations started about the time of freeze-up and continued for 20 to 27 days until temperatures in the active layer and near-surface permafrost dropped to about -12°C and lower. The most appropriate unfrozen water contents curves (those that produced the smallest differences between calculated and measured temperature profiles) for each site and for different depths were found by trial and error. Results of the calculations of the temperature profiles for all three sites are shown in Figures 6.10 and 6.11.

For the FB, site it was possible to construct one set of unfrozen water content curves (which are different for different depths) for the whole range of temperatures starting with the freeze-up date until there was essentially no more phase change (when the temperature at the permafrost surface at FB decreased to about -3°C as was

described in the previous section) (Figure 6.10C). These unfrozen water contents curves for the FB site are described in Table 6.2 and in Figures 6.9 and 6.12. The curve for the depth interval from 0.2 m to 0.3 m indicated in Table 6.2 as Model-1 is very similar to the CRREL-2 curve for Barrow silt (compare Figures 6.9 and 6.12).

For the other sites (WD and DH), the agreement between calculated and measured values lasted only for one or two weeks and then the calculated temperatures became too cold compared to the measurements (Figures 6.10A and 6.10B). To re-establish agreement (Figures 6.11A and 6.11B), it was necessary to correct the form of the unfrozen water content curves. Two formal stages in the process of the active layer and near-surface permafrost cooling after freeze-up at WD and DH were introduced (formal, because in reality the unfrozen water content curves probably change their form continuously with temperature). The form of these curves changes from one stage to another (Table 6.2 and Figures 6.9 and 6.12). The expressions which were used for approximating the curves in soils in the Prudhoe Bay region are shown in Table 6.3.

Additional calculations were made for DH for the 1991 freeze-up period to confirm the results of 1987 calculations. The results obtained were essentially the same as for 1987, but the depth of the layer with an increased amount of unfrozen water was larger for 1991 by 0.07 m (Table 6.2) which is in a good agreement with the deeper active layer in 1991 compared to 1987 (Table 6.1).

Results of modeling for all three sites show that a layer with large unfrozen water content existed during cooling of the active layer following freeze-up at the depth where freeze-up (i.e. closure by freezing from the top down and from the bottom up) occurred. For the DH site this layer continued from the ground surface to the depth of 0.3 m in 1987 and 0.36 m in 1991. For FB in 1987 and for WD in 1988 the thickness of this layer was 0.1 m and it was located in the depth intervals between 0.2 and 0.3 m at FB and between 0.15 and 0.25 m at WD. These unfrozen water contents (Figure 6.12) show unexpectedly large values at low temperatures. For FB, the curve (Model-1) is similar to the measured CRREL-2 curve (Barrow silt). Model-2 and

especially Model-3 curves are well above the CRREL-2 curve (compare Figures 6.9 and 6.12) and show a slow reduction of the unfrozen water contents over wide negative temperature intervals (at least between 0°C and -8°C for WD and DH, and between 0°C and -3°C for FB).

Such behavior of the unfrozen water content curves and the generally large amount of unfrozen water could be associated with increased salt concentrations in the pore water in those layers, especially at the WD and DH sites. Unfortunately, there are no data available about soil salinity at these sites. Changes in unfrozen water content curves at WD and DH could also be associated with freeze concentration of the pore solutes due to expulsion of the impurities from the growing ice lenses to the soil between lenses. This process under specific conditions can produce a significant shift in the freezing point (Banin and Anderson, 1974). The process also leads to drying of soils between the ice lenses due to water migration to the lenses. However, at the present time there is not enough information to choose between these hypotheses.

6.3.4 Modeling of the Active Layer and Near-Surface Permafrost Temperature Regime During the Freeze-up Period at Barrow

A high quality data set for Barrow which includes hourly ground temperature measurements from August 1993 through August 1994 (from 0.02 m to 1 m depth) (Hinkel et al., unpublished data) was used to confirm results obtained in the Prudhoe Bay region. These data were analyzed in the same way as for Prudhoe Bay. The difference was that, at Barrow, the deep borehole temperature data were not available. Therefore, the lower boundary was placed at the 1 m depth and measured temperatures at this depth were used as the lower boundary condition. The model with no unfrozen water was used to estimate thermal properties of the soils in the thawed and completely frozen states. Data on lithology and total water content were obtained from (Brown and Johnson, 1965; Brown, 1969) and (Hinkel, unpublished data). The maximum

active layer thickness in 1993 was around 0.32 m and freeze-up occurred at the depth of 0.2 m. Throughout the year there was agreement between calculated and measured data, except for the cooling period following freeze-up (from the beginning of November through the beginning of December). At this time, calculated temperatures were colder than measured values by more than 1 K (Figure 6.13A).

Using the model with unfrozen water content and a trial and error approach as before, the unfrozen water contents curves were determined. As for the Prudhoe Bay area, the effect of shifting unfrozen water content curves when temperature decreased was necessary for Barrow as well. At the first stage, when temperatures at the permafrost surface were not colder than -5°C the curve (Model-4, Figure 6.14) provided very good agreement between calculated and measured temperature profiles (Figure 6.13B). However, for lower temperatures it was found that a new unfrozen water curve (Model-5, Figure 6.14) improved the agreement (Figure 6.13C).

Results of this reconstruction of the unfrozen water content curves for Barrow are shown in Tables 6.4 and 6.5 and Figure 6.14. The thickness of the layer with increased unfrozen water content at the Barrow site in 1993 was 0.1 m (0.21 m to 0.31 m), the same as at FB and WD sites. Freeze-up (closure) occurred at the 0.2 m depth therefore the layer with large unfrozen water content again corresponds to the layer which was frozen upwards from the bottom of the active layer.

6.3.5 Apparent Thermal Diffusivity

The unfrozen water content curves allowed the apparent thermal diffusivity of the soils as a function of temperature to be calculated for each depth interval during the freeze-up period of 1993. For these calculations the values of the temperature-dependent thermal conductivity $K(T)$ and apparent volumetric heat capacity $C_a(T)$ were used with

[6.3] $$D_a(T) = K(T)/C_a(T).$$

These values were calculated in the course of modeling of the temperature field dynamics using the model with unfrozen water. The equations for these calculations were from Osterkamp (1987), where the weighted geometric mean equation (e.g., Lachenbruch et al., 1982)

[6.4] $$K(T) = K_s^{1-\theta_f} K_i^{\theta_f} \left(\frac{K_u}{K_i} \right)^{\theta_u}$$

where K_s , K_i , and K_u are the thermal conductivities of the soil, ice and unfrozen water components, was used to calculate the thermal conductivities of the soils. The porosity in the frozen state

[6.5] $$\theta_f = \theta_i + \theta_u \approx \theta_t$$

where θ_t is the thawed porosity, and θ_i and θ_u are the temperature-dependent volume fractions of ice and unfrozen water by

[6.6] $$\theta_i = \left(\frac{\rho_b}{\rho_i} \right) w_i$$

[6.7] $$\theta_u = \left(\frac{\rho_b}{\rho_u} \right) w_u$$

where w_i and w_u are the temperature-dependent mass fractions of ice and unfrozen water; ρ_b is the dry bulk density of the frozen soil; and ρ_i and ρ_u are the densities of the ice and unfrozen water, respectively. The mass fraction of unfrozen water was calculated using the equations in Tables 6.3 or 6.5.

Apparent heat capacity was calculated using

[6.8] $$C_a(T) = C_v(T) + L \frac{\partial \theta_u}{\partial T}$$

with

[6.9] $$C_v(T) = (1-\theta_f)C_s + \theta_i C_i + \theta_u C_u$$

where C_s , C_i , and C_u , are the volumetric heat capacities of the soil, ice, and unfrozen water, and L is the volumetric latent heat of fusion of ice. Expanding the second term on the right-hand side of (6.8) yields

[6.10] $$L\frac{\partial \theta_u}{\partial T} = -\frac{\rho_b}{\rho_u} LAB|T - E|^{B-1}$$

for the power law form of w_u (Tables 6.3 or 6.5) and

[6.11] $$L\frac{\partial \theta_u}{\partial T} = 0.17\frac{\rho_b}{\rho_u} Le^{0.17(T-7)}$$

for the exponential law form of w_u (Model-5, Table 6.5)

Results of these calculations for each model of the unfrozen water curves are shown in Figure 6.15. Significant changes of the apparent thermal diffusivity values are still noticeable for Model-5 within the entire range of temperatures to -12°C. For Model-4, the main changes occurred in the range from 0°C to -8°C, and for the CRREL-1 curve from 0°C to -5°C. These curves are similar to the results of calculations of the apparent thermal diffusivities based on the temperature measurements in Barrow during the thawing season in the Summer of 1971 (Figures 7 and 8 in McGaw et al., 1978). The apparent diffusivity curve for the depths of 0.6 m and 0.8 m (Figure 7 in McGaw et al., 1978) looks very similar to the curve for the Model-4 (Figure 6.15 and Table 6.4), the curve for 0.2 m depth (Figure 8 in McGaw et al., 1978) coincides almost exactly with the curve for CRREL-1 (Figure 6.15 and Table 6.3), and curves for 0.25 m and 0.3 m depth (Figure 8 in McGaw et al., 1978) are between the Model-4 and Model-5 curves (Figure 6.15 and Table 6.3). The layer with

anomalously low apparent thermal diffusivity, which was discovered by these authors (Figure 10 in McGow et al., 1978) was located at exactly the same depth as we obtained independently in the above described calculations (i.e. 0.23 m to 0.32 m).

6.4 Conclusions

Results of analyses and interpretation of daily temperature data, particularly during freezing, in the upper 1 m of soils from 1986 through 1993 at three sites West Dock, Deadhorse Airport, and Franklin Bluffs in the Prudhoe Bay region and for August, 1993 to August, 1994 at Barrow are presented in this paper. Annual temperature measurements in deeper boreholes (nominally 60 m) during 1986-1993 at the same sites at the Prudhoe Bay region were used as well.

This paper concentrates on the thermal processes and unfrozen water behavior in the ground during freezing of the active layer. Upward freezing from the bottom of the active layer in the Alaskan Arctic usually started at the end of August or beginning of September when the ground surface temperature still remained above 0°C. The ground surface temperature became negative one to two weeks later. Average dates for the start of freezing both from the bottom and from the top were very uniform: 5 and 16 September for WD, 3 and 18 September for DH and 4 and 17 September for FB, although the interannual variations of these dates were significant. In a few days, temperatures between the two freezing fronts approached the equilibrium freezing temperature establishing a so called "zero curtain" which existed until the time of freeze-up and protected the underlying permafrost from cooling until it disappeared.

The longest duration of the freeze-up period (difference between the start of freezing and freeze-up date) was 79 days at the DH site, where the average was 69 days. This average was similar to FB (63 days) and much longer than WD (42 days). The ratio of the active layer thickness frozen from the bottom to the total thickness of the active layer averaged, 34% at WD and 36% at DH and FB.

Measured temperature profiles decreased slowly after freeze-up occurred (the time when temperatures within the entire active layer became negative). Temperatures remained warmer than -1°C at the maximum depth of the active layer 20 days after the freeze-up date. Temperature profiles had a parabolic form with a temperature maximum near the base of the active layer. One hypothesis is that significant amounts of unfrozen water were present in the freezing active layer. Precise temperature data together with computer modeling of the temperature field dynamics verified this hypothesis and provided essential new information on the dynamics of the unfrozen water content in the ground (under undisturbed conditions) during cooling of the active layer following freeze-up.

A finite element model with no unfrozen water content failed to produce agreement between measured and calculated temperatures for the cooling period. To estimate the temperatures when unfrozen water becomes an important factor in the temperature field dynamics, a series of calculations were made for all sites using a model with no unfrozen water. The differences between calculated and measured temperatures became noticeable when initial temperatures at the active layer base were around -9°C for the WD and DH sites and -3°C for FB. Thus, the range of the temperatures where this model did not work properly was unexpectedly wide for WD and DH and much smaller for the FB site.

A finite element model which included the unfrozen water content was used to investigate its influence on the ground temperature regime and to determine the temperature field and unfrozen water content changes during the freeze-up and following cooling period in the Prudhoe Bay region and at Barrow. The most appropriate unfrozen water contents curves for each site and for different depths were found by trial and error (i.e. those curves that produced the smallest differences between calculated and measured temperature profiles). For the FB site only, it was possible to construct one set of unfrozen water content curves (which were different for different depths) for the whole range of temperatures during the cooling process,

starting on the freeze-up date until there was practically no more phase changes of the unfrozen water. For the two other sites in the Prudhoe Bay region (WD and DH) and for Barrow, agreement between calculated and measured data lasted only for one or two weeks and then the calculated temperatures again became too cold compared to measurements. To re-establish agreement, it was necessary to modify the form of the unfrozen water content curves when temperatures at the permafrost surface became colder than -6°C (WD and Barrow) to -7°C (DH).

Results of modeling for all four sites show that a layer with large unfrozen water content existed during the freeze-up of the active layer near the depth where freeze-up occurred. For the DH site, this layer continued from the ground surface to the depth of 0.3 m in 1987 and 0.36 m in 1991. For FB (1987), for WD (1988), and for Barrow (1993) the thickness of this layer was 0.1 m and it was located in the depth intervals between 0.2 and 0.3 m at FB, between 0.15 and 0.25 m at WD, and between 0.21 and 0.31 m at Barrow. Unfrozen water content curves as a function of temperature for these layers show unexpectedly large values at low temperatures.

6.5 Acknowledgments

This research was funded by the Polar Earth Sciences Program, Office of Polar Programs, National Science Foundation and by the State of Alaska. We would like to thank Dr. G. Guymon, Dr. L. Goodrich and Prof. J. Gosink for providing the models which were used in these studies with minor modifications. We would like also to thank Dr. K. Hinkel for permission to use his precision temperature data from Barrow.

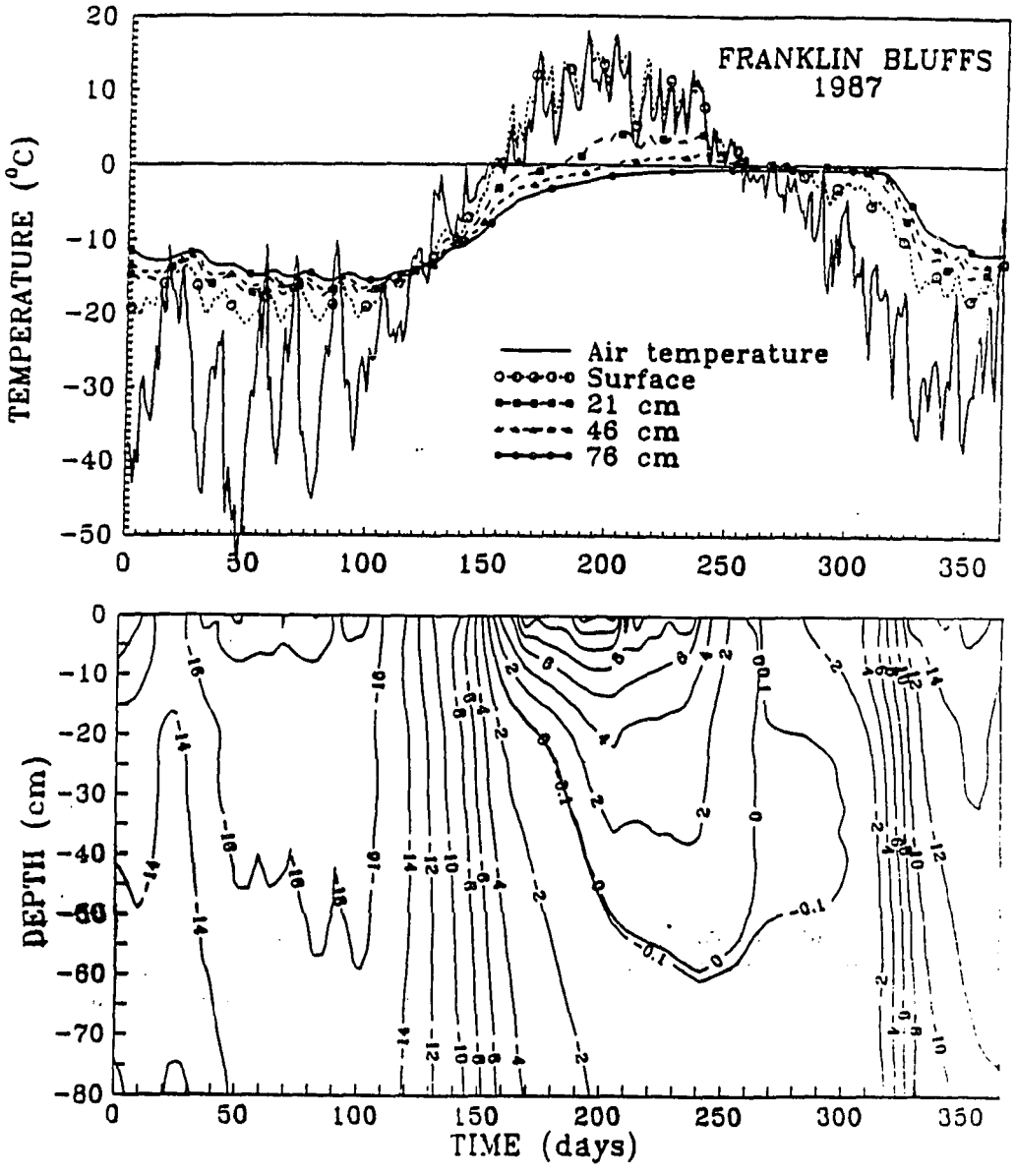

Figure 6.1 Temperature-time series for different depths (top) and temperature field dynamics within the active layer and near-surface permafrost (bottom) at Franklin Bluffs, Alaska, in 1987

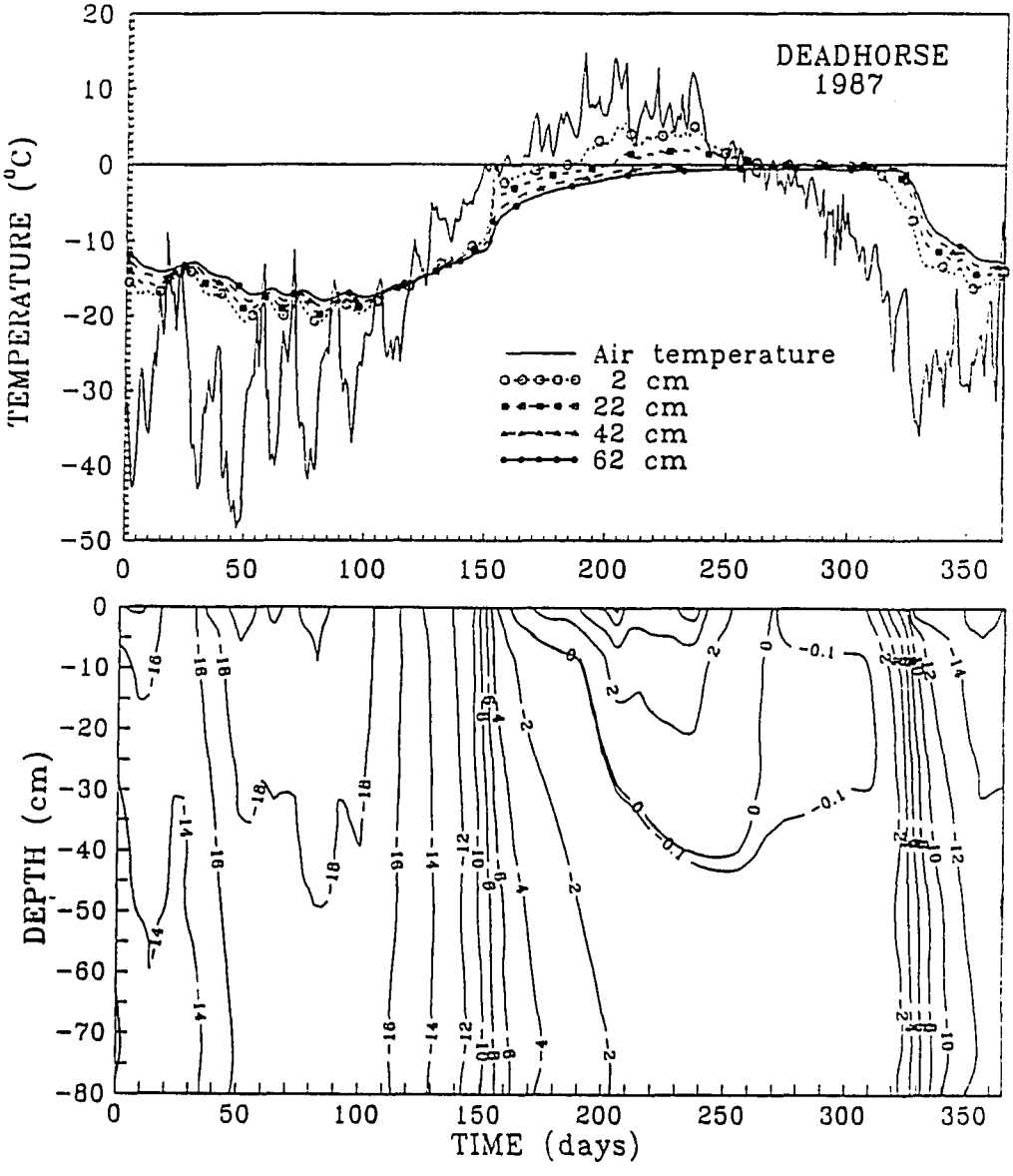

Figure 6.2 Temperature-time series for different depths (top) and temperature field dynamics within the active layer and near-surface permafrost (bottom) at Deadhorse, Alaska, in 1987.

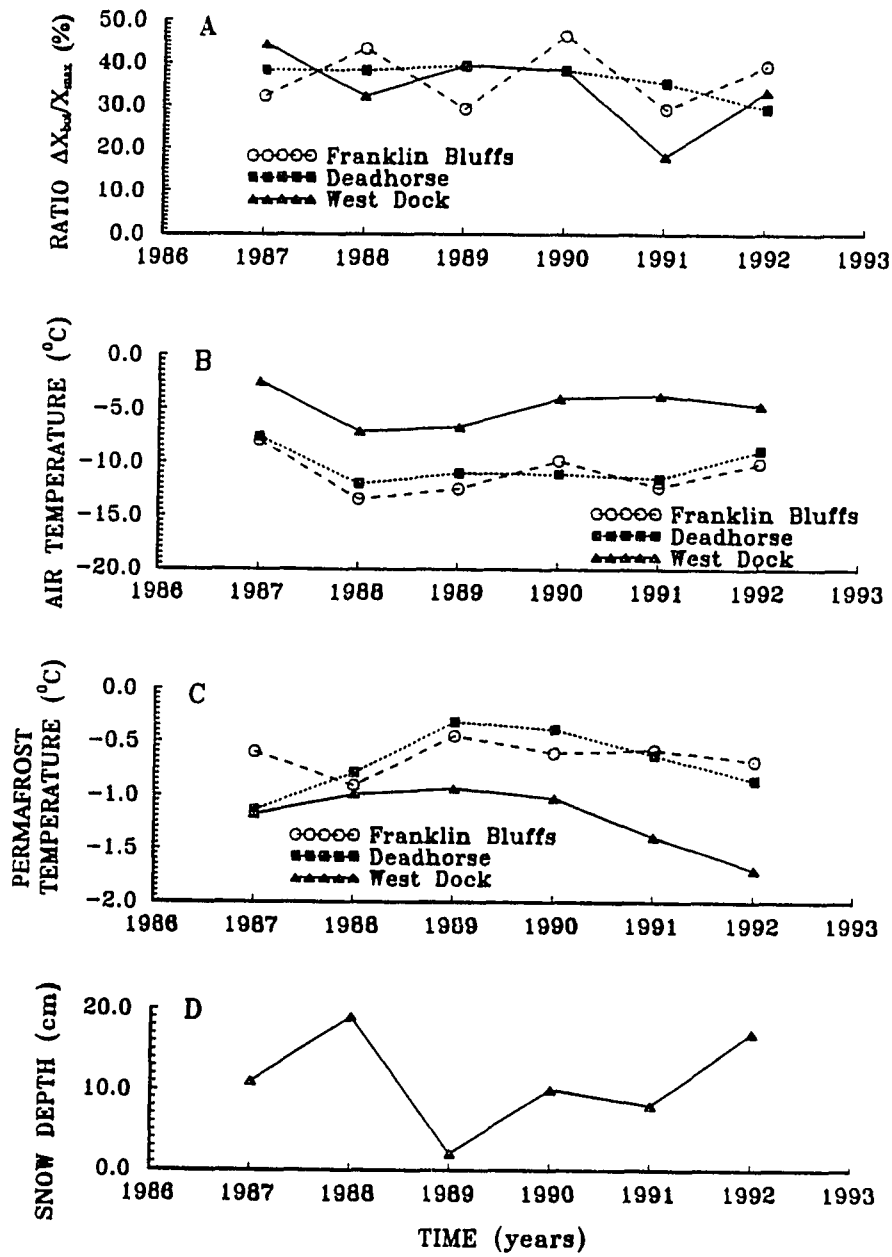

Figure 6.3 Interannual variations of the ratio between the part of the active layer which was frozen from the bottom (ΔX_{bot}) and maximum of the active layer thickness (X_{max}) (A), and air (B) and permafrost table (C) temperatures and snow cover thicknesses at the Prudhoe Bay/ARCO meteorological station (D), all averaged over the period of freeze-up at Franklin Bluffs, Deadhorse and West Dock.

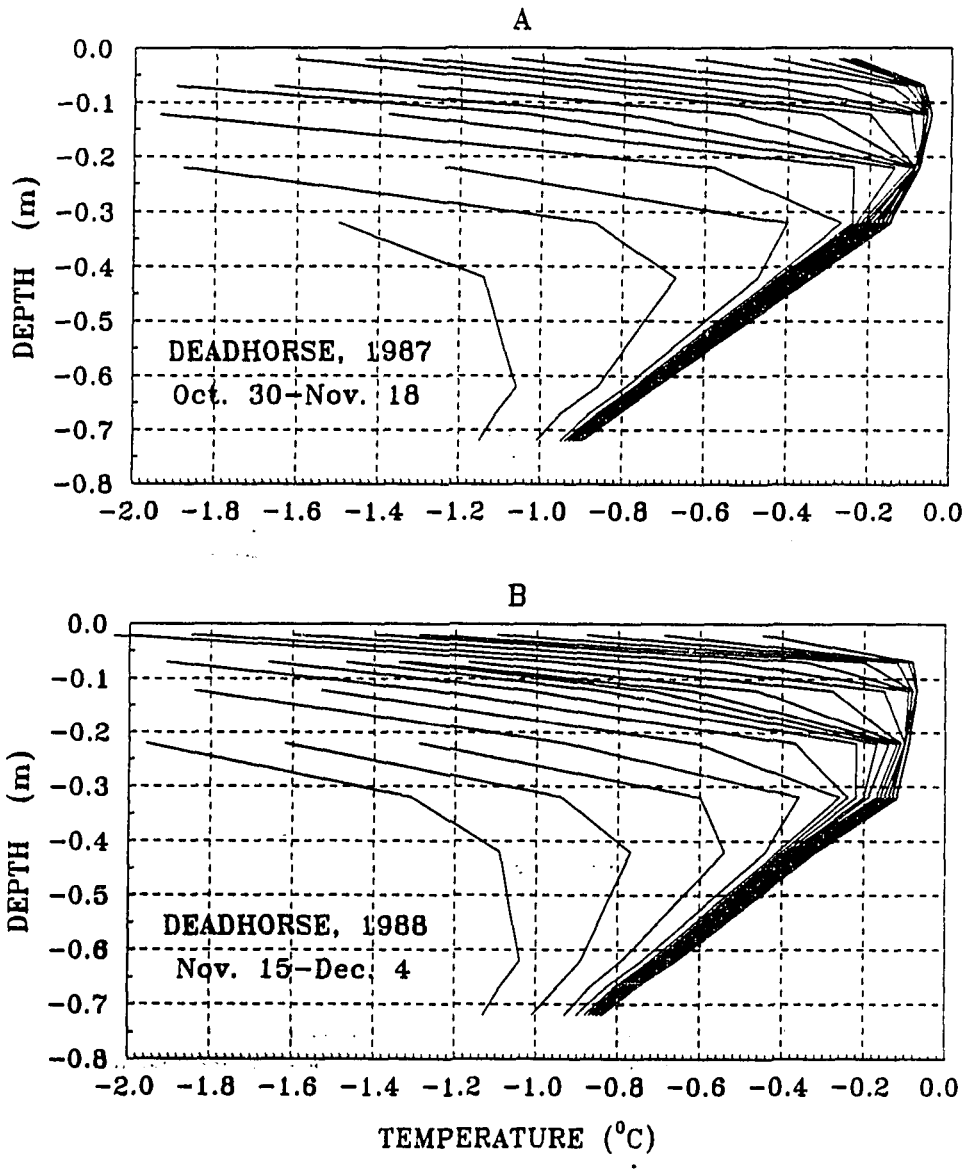

Figure 6.4 Daily means of the measured temperature profiles at the Deadhorse site during the period of freeze-up between October 30 and November 18, 1987 (A), and between November 15 and December 4, 1988 (B).

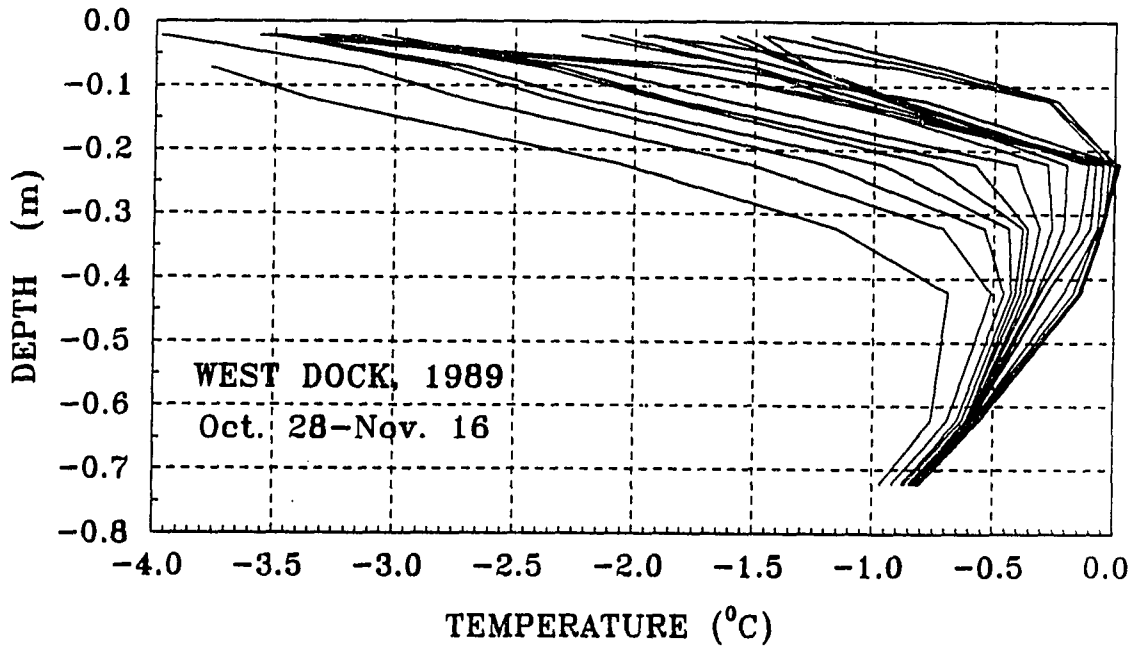

Figure 6.5 Daily means of the measured temperature profiles at the West Dock site during the period of freeze-up between October 28 and November 16, 1989.

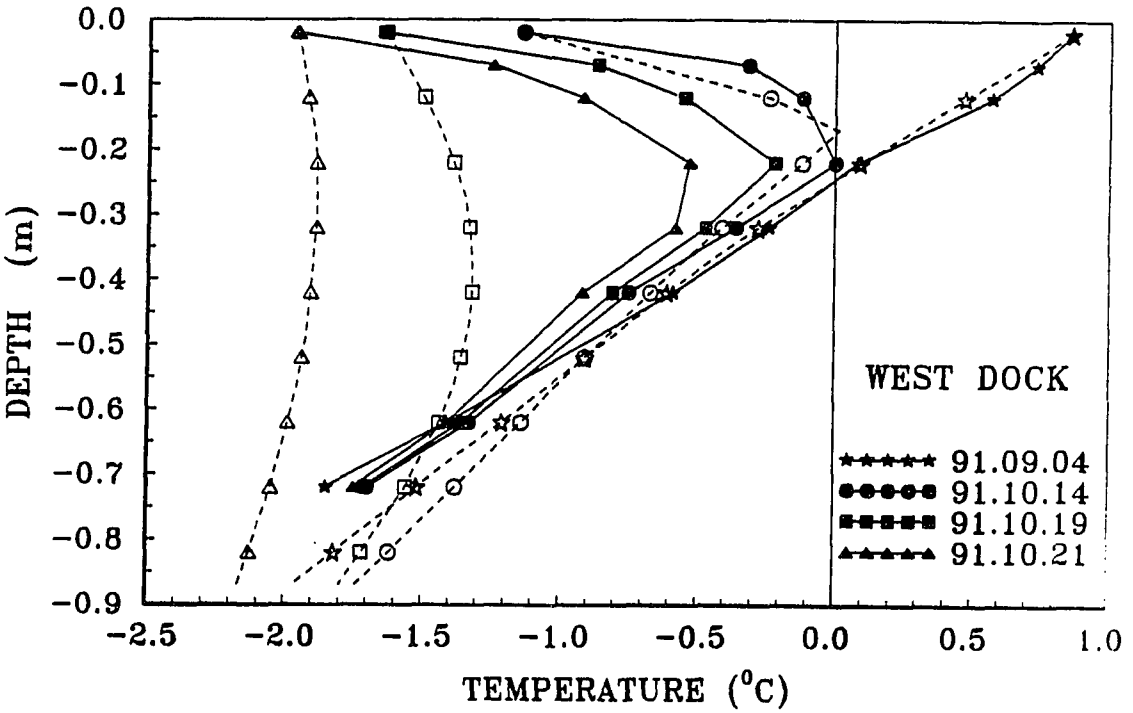

Figure 6.6 Calculated (dashed lines and open symbols for the model with no unfrozen water content) and measured (solid lines and filled symbols) temperature profiles during the freeze-up and following cooling period at West Dock in 1991.

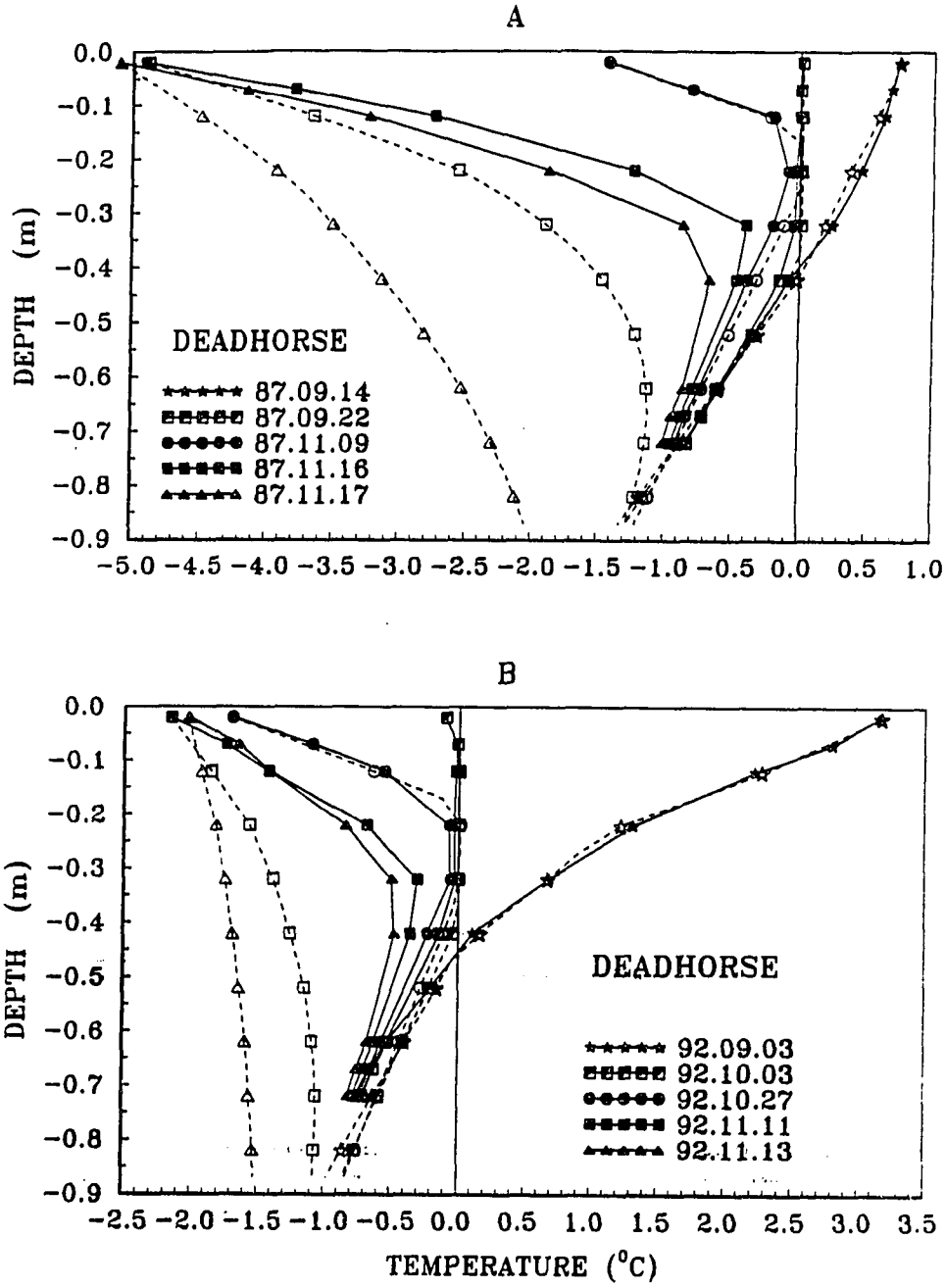

Figure 6.7 Calculated (dashed lines and open symbols for the model with no unfrozen water content) and measured (solid lines and filled symbols) temperature profiles during the freeze-up and following cooling period at Deadhorse in 1987 (A) and 1992 (B).

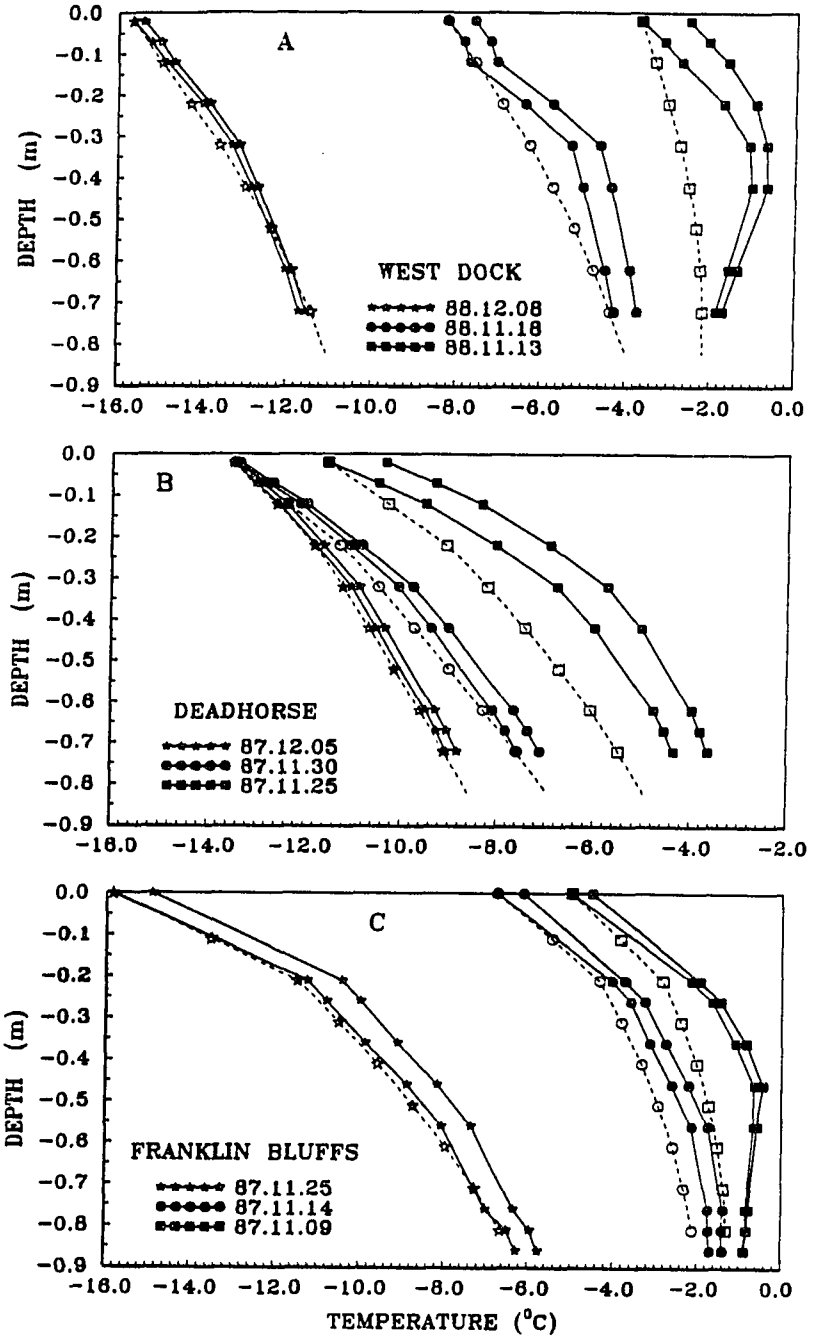

Figure 6.8 Sets of calculated (dashed lines and open symbols for the model with no unfrozen water content) and measured (solid lines and filled symbols) temperature profiles at West Dock in 1988 (A), at Deadhorse in 1987 (B), and at Franklin Bluffs in 1987 (C). Each set contents three profiles: the right-hand profile represents initial conditions, the other two are calculated and measured profiles on the next day.

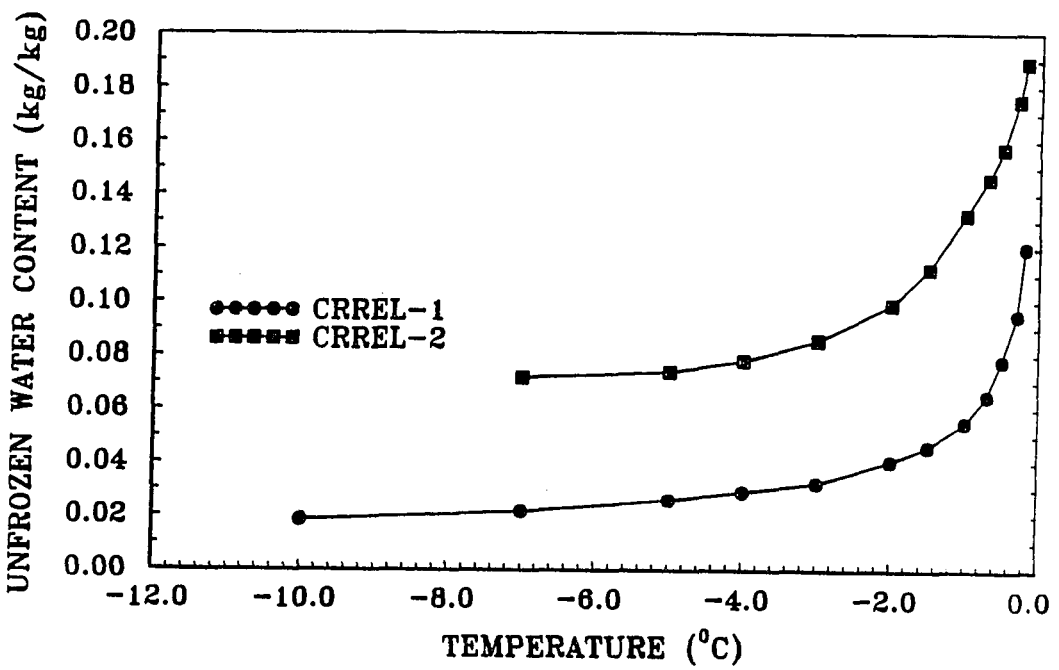

Figure 6.9 Unfrozen water content curves for Fairbanks silt (CRREL-1) and Barrow silt (CRREL-2) adapted from (Tice et al., 1988) and (Nakano and Brown, 1971).

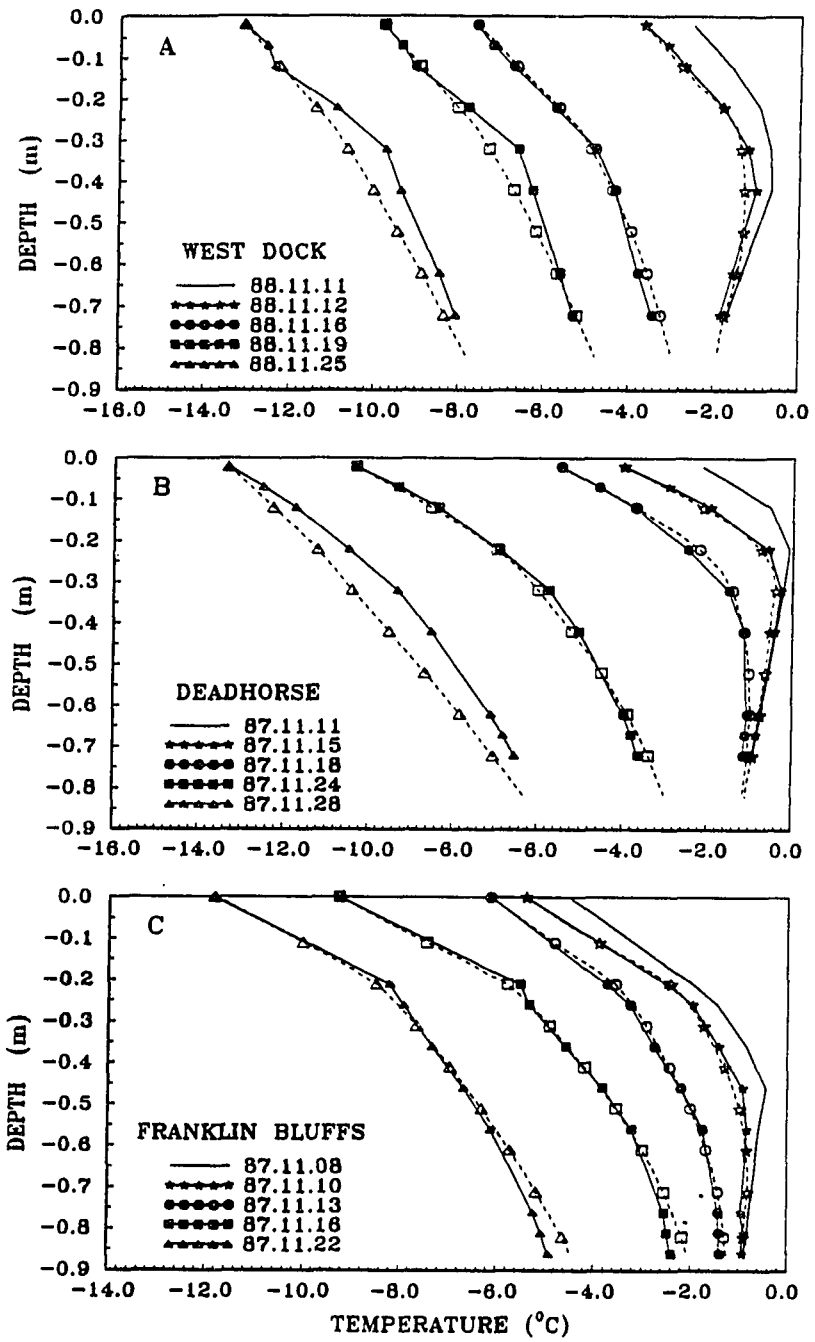

Figure 6.10 Stage I. Calculated (dashed lines and open symbols for the model with unfrozen water content) and measured (solid lines and filled symbols) temperature profiles during the cooling period following freeze-up at West Dock in 1988 (A), at Deadhorse in 1987 (B), and at Franklin Bluffs in 1987 (C). The right-hand curves (solid lines and no symbols) represent initial conditions.

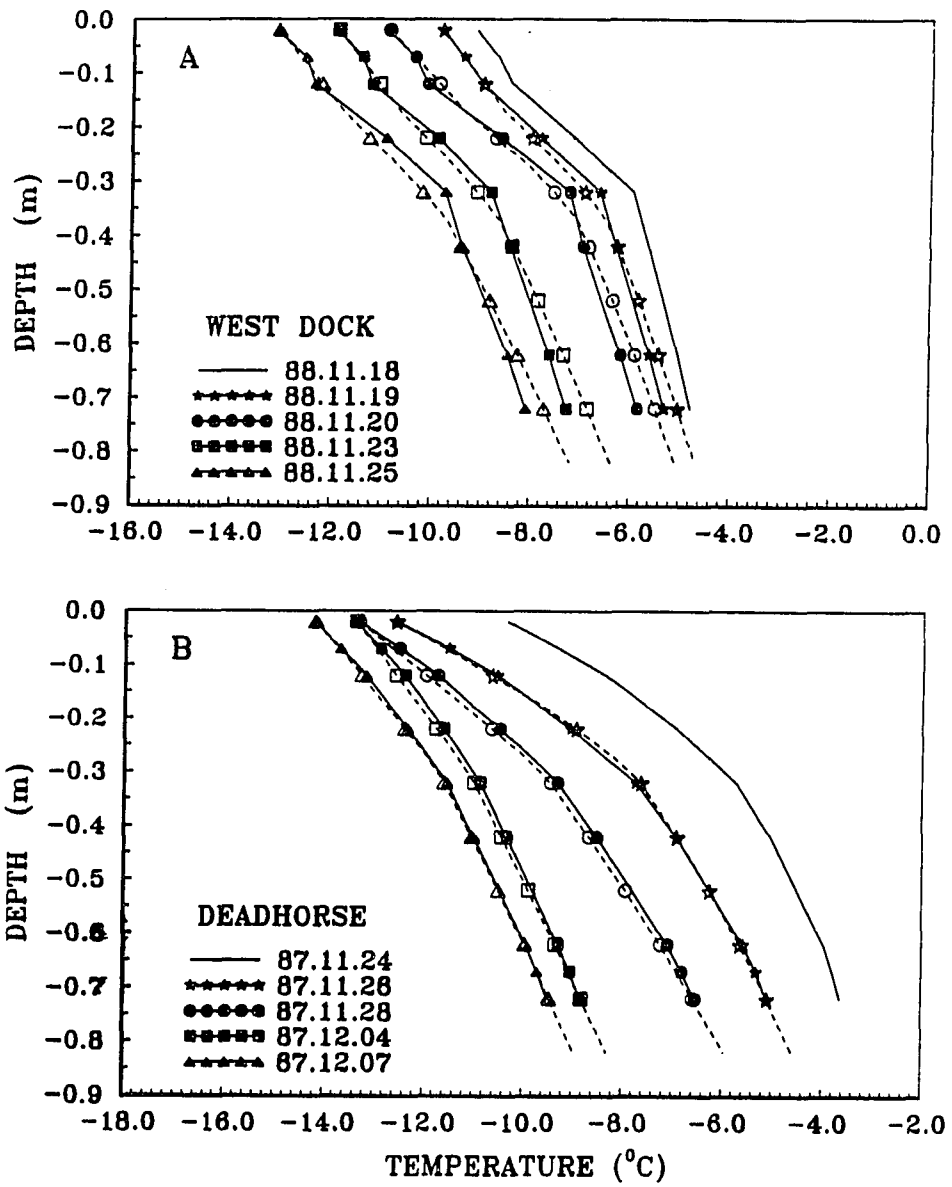

Figure 6.11 Stage II. Calculated (dashed lines and open symbols for the model with unfrozen water content) and measured (solid lines and filled symbols) temperature profiles at West Dock in 1988 (A) and at Deadhorse in 1987 (B). The right-hand curves (solid lines and no symbols) represent initial conditions.

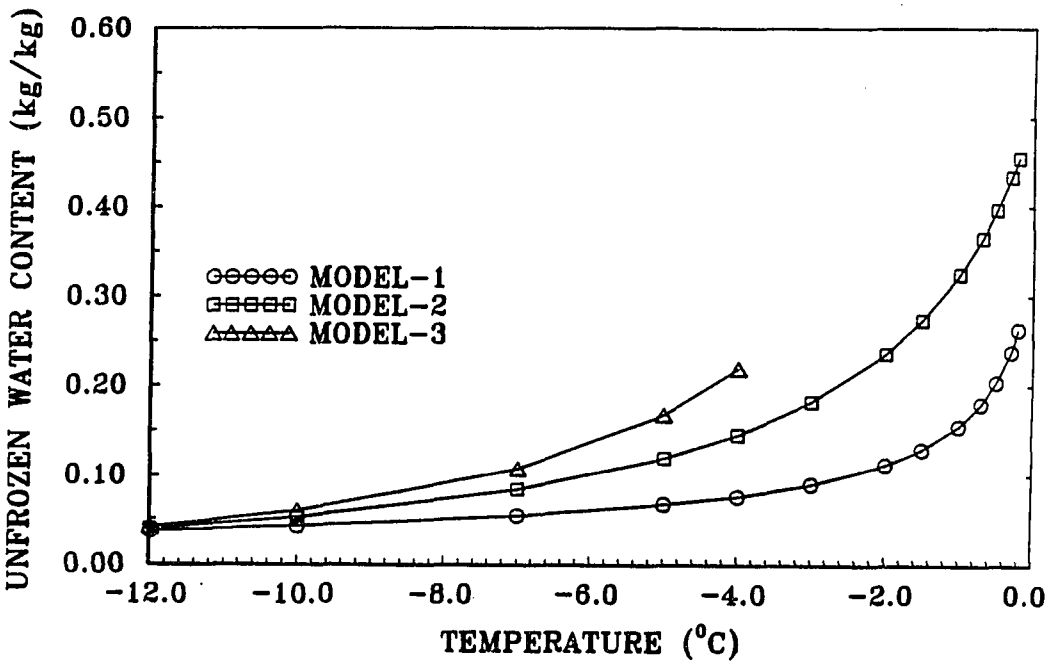

Figure 6.12 Unfrozen water content curves for West Dock, Deadhorse and Franklin Bluffs (see also Table 6.2) which were determined by trial and error to minimize the differences between measured and calculated temperatures.

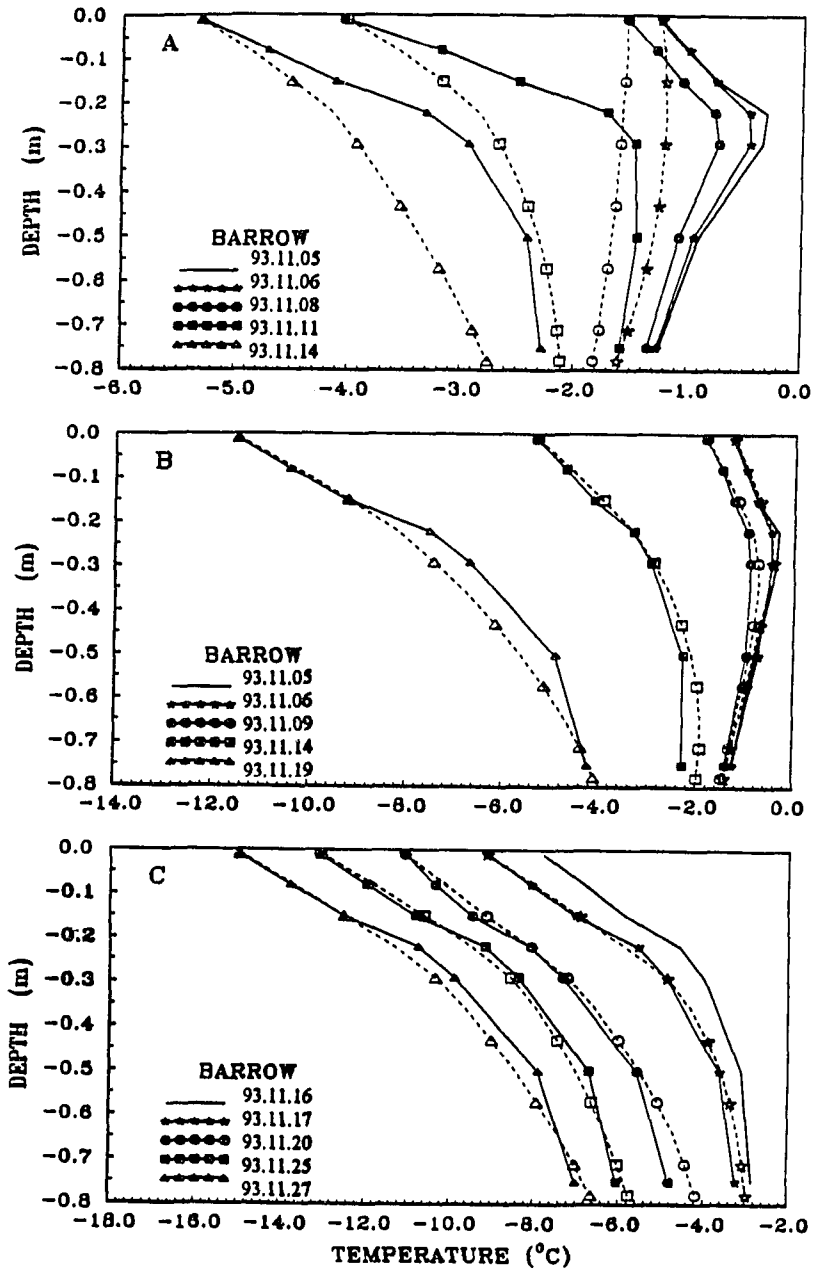

Figure 6.13 Calculated (dashed lines and open symbols) and measured (solid lines and filled symbols) temperature profiles at Barrow during the cooling period following freeze-up in 1993, using the model with no unfrozen water (A), with unfrozen water, stage I (B), and with unfrozen water, stage II (C). Solid lines and no symbols represent initial conditions.

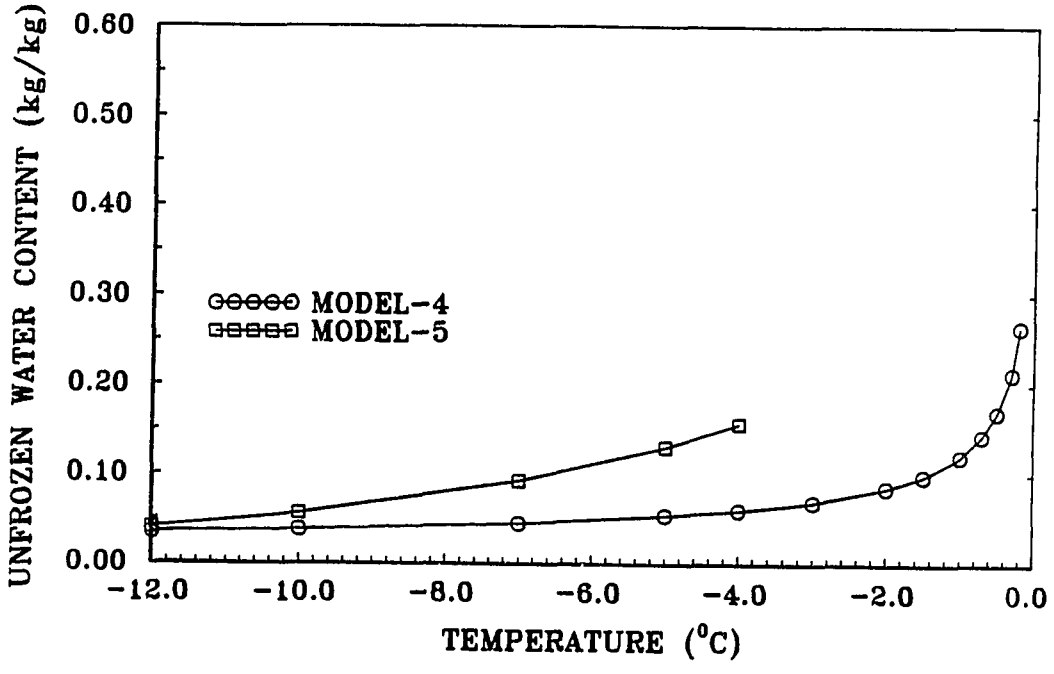

Figure 6.14 Unfrozen water contents curves for Barrow (see also Table 6.3) which were determined by trial and error to minimize the differences between measured and calculated temperatures.

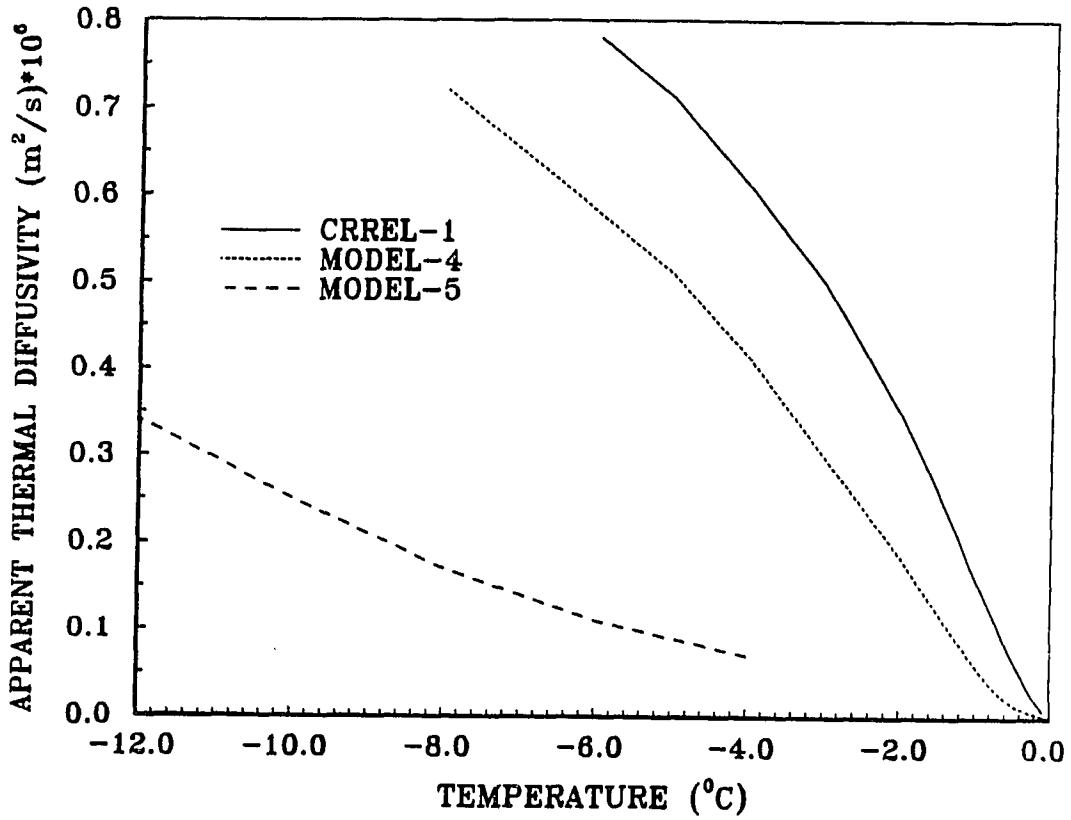

Figure 6.15 Apparent thermal diffusivity values calculated for Model-4 and Model-5 and the adapted (CRREL) unfrozen water curves using the temperature-dependent thermal properties of the soils.

Table 6.1 Dates of the most important freeze-up events, depth where freeze-up occurred, and maximum active layer thicknesses and percent of upward freezing.

	1987	1988	1989	1990	1991	1992	Average
WD							
Beginning of freeze-up:							
- from the bottom	Sept. 10	Aug. 28	Sept. 17	Sept. 3	Aug. 28	Sept. 5	Sept. 5
- from the top	Sept. 16	Sept. 14	Sept. 20	Sept. 22	Sept. 5	Sept. 9	Sept. 16
Date of freeze-up	Nov. 5	Nov. 6	Nov. 14	Oct. 25	Oct. 13	Oct. 12	Oct. 28
Duration of freeze-up (days)	50	53	55	33	38	33	42
Depth of freeze-up, ΔX_{top} (m)	0.18	0.28	0.28	0.26	0.255	0.14	0.23
Maximum active layer, X_{max} (m)	0.32	0.41	0.46	0.42	0.31	0.21	0.355
Ratio $\Delta X_{bot} / X_{max}$ (%)	44	32	39	38	18	33	34
DH							
Beginning of freeze-up:							
- from the bottom	Sept. 7	Aug. 28	Sept. 17	Aug. 30	Aug. 25	Sept. 3	Sept. 3
- from the top	Sept. 20	Sept. 25	Sept. 23	Sept. 22	Sept. 8	Sept. 12	Sept. 18
Date of freeze-up	Nov. 16	Dec. 1	Dec. 1	Dec. 3	Nov. 26	Nov. 16	Nov. 26
Duration of freeze-up (days)	57	67	69	72	79	65	69
Depth of freeze-up, ΔX_{top} (m)	0.26	0.28	0.42	0.40	0.34	0.32	0.34
Maximum active layer, X_{max} (m)	0.42	0.45	0.69	0.65	0.52	0.45	0.53
Ratio $\Delta X_{bot} / X_{max}$ (%)	38	38	39	38	35	29	36
FB							
Beginning of freeze-up:							
- from the bottom	Aug. 31	Aug. 30	Sept. 11	Sept. 3	Sept. 3	Sept. 10	Sept. 4
- from the top	Sept. 13	Sept. 21	Sept. 21	Sept. 22	Sept. 10	Sept. 12	Sept. 16
Date of freeze-up	Nov. 9	Nov. 19	Nov. 18	Nov. 19	Nov. 24	Nov. 19	Nov. 18
Duration of freeze-up (days)	57	59	58	58	75	68	63
Depth of freeze-up, ΔX_{top} (m)	0.40	0.31	0.51	0.36	0.41	0.36	0.39
Maximum active layer, X_{max} (m)	0.59	0.57	0.72	0.68	0.58	0.59	0.62
Ratio $\Delta X_{bot} / X_{max}$ (%)	32	43	29	46	29	39	36

Table 6.2. Unfrozen water content curves for different depths at the FB, DH, and WD sites which were found to minimize differences between calculated and measured temperatures. The curves are shown in Figures 6.9 and 6.12.

Stage I	Stage II
Franklin Bluffs, 1987 0 - 0.20 m : CRREL-1 0.20 - 0.30 m : Model-1 0.30 - 1.18 m : CRREL-1	None
Deadhorse, 1987 0 - 0.30 m : Model-2 0.30 - 0.88 m : CRREL-1	 0 - 0.30 m : Model-3 0.30 - 0.88 m : CRREL-1
Deadhorse, 1991 0 - 0.36 m : Model-2 0.36 - 0.88 m : CRREL-1	 0 - 0.06 m : Model-1 0.06 - 0.36 m : Model-3 0.36 - 0.88 m : CRREL-1
West Dock, 1988 0 - 0.15 m : CRREL-1 0.15 - 0.25 m : Model-2 0.25 - 0.86 m : CRREL-1	 0 - 0.15 m : CRREL-1 0.15 - 0.30 m : Model-3 0.30 - 0.86 m : CRREL-1

Table 6.3. Approximation equations for the unfrozen water content curves mentioned in Table 6.2 which were used in calculations for the Prudhoe Bay region.

Model	Equation
CRREL -1	$0.053 \lvert T \rvert^{-0.383}$
Model -1	$0.2 \lvert T - 0.3 \rvert^{-0.5} - 0.02$
Model -2	$\lvert T - 1.9 \rvert^{-0.92} - 0.05$
Model -3	$\lvert T \rvert^{-0.92} - 0.06$

Table 6.4. Results of the determination of the unfrozen water content curves for different depths at the Barrow site. The curves are shown in Figures 6.9 and 6.14.

Stage I	Stage II
Barrow, 1994	
0 - 0.21 : CRREL-1	0 - 0.23 : CRREL-1
0.21 - 0.31 : Model-4	0.23 - 0.32 : Model-5
0.31 - 1.00 : CRREL-1	0.32 - 1.00 : Model-4

Table 6.5. Approximation equations for the unfrozen water content curves which were used in calculations for the Barrow site.

Model	Equation
CRREL -1	$0.053 \mid T \mid^{-0.383}$
Model -4	$0.12 \mid T \mid^{-0.5}$
Model -5	$e^{0.17 (T - 7)}$

CHAPTER 7

Characteristics of Changing Permafrost Temperatures in the Alaskan Arctic, U. S. A.

T. E. Osterkamp and V. E. Romanovsky, 1996. Characteristics of Changing Permafrost Temperatures in the Alaskan Arctic, U. S. A. *Arctic and Alpine Research* (in press).

7.1 Abstract

Temperatures in permafrost were measured annually from 1983 through 1993 in drill holes (nominally 60 m in depth) at three sites in Northern Alaska; West Dock, Deadhorse, and Franklin Bluffs. Active layer and near-surface permafrost temperatures (to 1 m) were measured every 4 h from 1986 through 1993. This paper combines two previously published data sets with numerical simulations to fill the data gap in daily permafrost temperatures from 1m to the depth of penetration of the annual temperature wave (about 20 m). These daily values were used to calculate mean temperature profiles for the annual period, a 10 to 11 yr cycle and for other periods. Calculated profiles were used to revise estimates of the surface amplitude of the 10 to 11 yr cycle at Franklin Bluffs from 0.6 K to about 1 K. The data show that, for the 10 to 11 yr cycle, cooling of the permafrost began prior to 1983 with the warming part of the cycle beginning in the late 1980's. This is consistent with the U.S. Geological Survey data suggesting that their reported cooling may have been part of a natural cycle and not an effect of the disturbance at the ground surface associated with drilling. The means of the measured temperature profiles below the 20 m depth show curvatures toward warmer temperatures. These curvatures may be associated with climatic fluctuations, a cycle or a longer-term warming trend. While these time series of permafrost temperatures are too short to distinguish between these alternatives, it is important to

do so because of their possible relationship with the predicted climatic warming.

7.2 Introduction

The predicted climatic warming associated with projected increases in greenhouse gas concentrations in the atmosphere will be most pronounced in the Arctic and should be detectable there first (Nelson et al., 1993). Changes in air temperatures may be expected to generate somewhat different changes at the surface of the permafrost because of the effects of the intervening snow cover, vegetation, and active layer and because of the effects of possible changes in other climatic variables, particularly precipitation, on these intervening materials. Permafrost is an exceedingly sensitive indicator of changes in heat balance at its surface. For example, precise measurements of temperatures in permafrost can be used to detect changes in its surface heat balance an order of magnitude smaller than can be determined by heat balance measurements (Lachenbruch and Marshall, 1986; Osterkamp et al., 1994). Thus, temperature variations in permafrost can be used as a sensitive indicator of changes in its surface boundary condition as a result of changes in climate (Lachenbruch and Marshall, 1986; Lachenbruch et al., 1988; Clow et al., 1991; Beltrami and Taylor, 1994; Majorowicz and Judge, 1994).

Lachenbruch and Marshall (1986) used temperature measurements in permafrost to show that there has been a general warming of the permafrost in the Alaskan Arctic of 2 to 4 K over the last century. Permafrost in many regions of the earth is currently warming (Gravis et al., 1988; Haeberli et al., 1993; Osterkamp, 1994; Pavlov, 1994; Wang and French, 1994). Recently, Osterkamp et al. (1994) reported an unexpected cycling of permafrost temperatures in the Alaskan Arctic from 1983 through 1993 with a period of about 10 to 11 yr. The amplitude of the cycle was about 2 K near the coast (West Dock and Deadhorse) and about 0.6 K at Franklin Bluffs and it was in phase with the solar sunspot cycle. The calculated mean energy flux required to produce the observed temperature changes in the permafrost (0.6 to 0.7 Wm^{-2}) was

about one-fourth the change in solar total irradiance during the cycle. Kazantsev (1994) has reported a similar effect in Eastern Siberia and the Russian Far East. It is important to understand any changes in the thermal regime of permafrost because of the importance of permafrost as an early indicator of climatic warming and also because degrading permafrost may enhance climatic warming by releasing additional greenhouse gases to the atmosphere (Nelson et al., 1993; Oechel et al., 1993).

This paper provides additional analyses and interpretation of two data sets previously reported by Osterkamp et al. (1994) and Romanovsky and Osterkamp (1995a). These data sets included precise temperature profiles (resolution 0.001°C and accuracy 0.01°C) obtained from 1983 to 1995 in drill holes (to the 60 m depth) at three sites along the Dalton Highway south from Prudhoe Bay; West Dock, Deadhorse, and Franklin Bluffs. In addition, high frequency (4 h time interval) measurements of temperatures (resolution 0.01°C and accuracy 0.1 to 0.2°C) in the air, at the ground surface, in the active layer and permafrost (down to 0.7-0.9 m) from 1986 to 1993 at the same sites are used in this paper. These sites are well suited to investigate long-term variations in active layer and permafrost conditions. Special care was taken to minimize the thermal disturbance in the drill holes and to the ground surface surrounding the sites. Detailed descriptions of site conditions and methods of measurements and data processing were published in Osterkamp (1985), Zhang and Osterkamp (1993b), Osterkamp et al. (1994), and Romanovsky and Osterkamp (1995a).

In the previous publications (Osterkamp et al., 1994; Romanovsky and Osterkamp, 1995a), these two sets of data were used separately. The primary problem in using the permafrost temperature profiles, which were measured only once per year, is the gap in information on annual and interannual permafrost temperature variations within the depth of annual temperature changes, typically 20 to 25 m. This lack of information makes it difficult to relate the deeper permafrost temperature changes with the temperature variations at the permafrost surface. The problem was resolved

through the use of computer simulations of the dynamics of the permafrost temperature field which allow reconstruction of the ground temperatures for all times from 1986 to 1993 and for all depths.

7.3 Reconstruction of the Daily Permafrost Temperature Profiles

A finite element heat conduction model (Gosink and Osterkamp, 1990; Osterkamp and Gosink, 1991), which is a modified version of the Guymon and Hromadka (1977) and Guymon et al. (1984) model, was used to reconstruct the one-dimensional temperature field in the permafrost. Daily mean ground temperatures measured from 1986 to 1993 at the permafrost surface (0.62 m at West Dock, 0.72 m at Deadhorse, and 0.76 m at Franklin Bluffs) were used for the upper boundary conditions. Temperatures remained below 0°C at these depths for the period of modeling (summer 1986 to summer 1993). The lower boundary was placed at the 55 m depth. According to the measurements in the drill holes, permafrost temperatures at this depth changed very slowly (from -9.51°C in 1986 to -9.54°C in 1990 and back to -9.51°C in 1993 for West Dock, from -8.24°C in 1986 to -8.25°C in 1990 and back to -8.19°C in 1993 for Deadhorse, and increased from -6.05°C in 1986 to -6.02°C in 1993 at Franklin Bluffs). The lower boundary temperature conditions were obtained by linear interpolation between annually measured values at the 55 m depth. Temperature profiles measured in 1987 were used for the initial conditions.

Drilling records were used to determine the lithology (Table 7.1) and results of previous investigations (Lachenbruch et al., 1982; Lachenbruch and Marshall, 1986; Zhang, 1993) were used to determine the initial approximate thermal properties of the permafrost. These values were adjusted, where necessary, by trial and error to produce the smallest differences between calculated and measured temperature profiles. The time step in these calculations was 1 h, while the space steps (200) were changed from 0.02 m at the upper boundary to 5 m at the lower boundary of the space

domain. The results of estimations of the thermal properties of the permafrost are shown in the Table 7.1.

Comparison of the calculated and measured permafrost temperatures provides information on the errors of this calibration of the numerical model. Figure 7.1 shows the calculated and measured temperature profiles for the simulation which began 25 June 1987 and ended 29 July 1993. The largest errors at this time are a few tenths of a degree (see also Figures 7.2, 7.3, 7.4). Deviations (RMS) of the calculated data from the measured temperatures were determined using all measurements and calculations from 1988 through 1993. Values of the deviations were 0.16 K for West Dock, 0.24 K for Deadhorse, and 0.14 K for Franklin Bluffs for an average of 0.18 K. When the estimated thermal conductivities (Table 7.1) were changed by 10% the deviations increased by a factor of two or more.

7.4 Seasonal Variations of the Permafrost Temperature

The seasonal cycle of the air and ground surface temperature variations causes periodic changes in temperatures with the same period in the upper 20 m or so of permafrost. Calculated temperature profiles of these seasonal variations for 1991 are shown in Figures 7.2, 7.3, and 7.4. Typically the range of the seasonal variations at the permafrost surface was much larger at West Dock (18 K in 1991), than at Deadhorse and Franklin Bluffs (15 K and 14 K, respectively). The much colder ground surface temperatures occurring during the winter at the coastal West Dock site compared to Deadhorse and Franklin Bluffs (Romanovsky and Osterkamp, 1995) caused this difference. Seasonal variations practically disappeared at the 20 m depth (the temperature changes at this depth for the year were 0.2 K for West Dock and Deadhorse and 0.15 K for Franklin Bluffs). The trumpet curves are asymmetric because the annual means changed with time which will be discussed below.

7.5 Cyclic Permafrost Temperature Variations with a Period of 10 to 11 yr

Calculated daily permafrost temperature profiles were used to determine the mean annual temperature profiles for each year from 1987 through 1992 and the mean profiles for the whole period. These mean annual profiles can be linked to the mean annual temperature profiles in the active layer calculated from measurements in the active layer (Romanovsky and Osterkamp, 1995a). The linked profiles are shown in Figures 7.5, 7.6 and 7.7. Strong changes in the gradient of the temperature profiles at the permafrost surface are caused by the effects of thermal offset. The mean annual profiles are free from the annual temperature variations but they still show significant systematic variations. These variations are the result of a 10 to 11 yr cycling of temperature changes within the upper 60 m of permafrost (Osterkamp et al., 1994).

Trumpet curves for all three sites have an asymmetric form (especially at Deadhorse) because these six profiles (1987-1992) represent data not for the whole period of variations (about 10 to 11 yr) but only for the warmer part of this period. This set of profiles does not include the coldest part of the cycle which occurred in the mid-1980s. Another reason for the asymmetry in the trumpet curves may be a long-term warming effect which is noticeable in the profiles.

Osterkamp et al. (1994) estimated the amplitudes of the 10 to 11 yr cycle to be about 2 K for West Dock and Deadhorse, and about 0.6 K for Franklin Bluffs. These values agree with estimates based on Figures 7.5 and 7.6 for West Dock and Deadhorse but not for Franklin Bluffs (Figure 7.7) where it is at least 1 K. Underestimation of the amplitude at Franklin Bluffs was a result of the difference in thermal diffusivity of the permafrost at the Franklin Bluffs site compared to the other two sites. The presence of the thick layer of silt (Table 7.1) with much smaller thermal diffusivity from the depth of 14 meters downward at Franklin Bluffs would cause a significantly larger amplitude decrease with depth (Figures 7.5, 7.6, 7.7).

The range of permafrost temperature variations caused by this 10 to 11 yr cycle (Figure 7.8) decreased exponentially with depth and was (20 m depth) 0.65 K at West Dock, 0.85 K at Deadhorse, and 0.4 K at Franklin Bluffs. At 30 m, it was 0.3 K at West Dock, 0.42 K at Deadhorse, and 0.16 K at Franklin Bluffs. Using the amplitude ratio method, the calculated diffusivities at these depths are 1.52, 1.82, and 1.08 (in units of 10^{-6} m^2 s^{-1}), respectively, in reasonable agreement with those obtained from modeling (Table 7.1).

Temperature profiles measured from 1983 to 1993 below the depth of annual variations (Figure 7.8) indicate that the cooling part of the cycle began prior to 1983 and had penetrated to more than 40 m by 1984. The U.S. Geological Survey data of Lachenbruch and Marshall (1986) for the region to the west of Prudhoe Bay, which was also obtained in 1984, indicate a similar cooling effect. Although they did not rule out "a general climatic cause" completely, they strongly believed that "modification of the surface for the drilling operation ... is responsible for the latest secular trend observed in permafrost surface temperature at these sites." Measured and calculated temperature data from the West Dock, Deadhorse and Franklin Bluffs sites show that the "cooling trend" in the upper part of permafrost reversed in the late 1980s being replaced by a pronounced "warming trend" in the upper 20 to 40 meters of permafrost (Figures 7.5, 7.6, 7.7, 7.8). In more recent publications (Nelson et al., 1993; Lachenbruch, 1994), the U.S. Geological Survey data also indicate a reversal of the cooling trend to a warming trend. It is difficult to explain how this trend could have reversed if it was caused entirely by surface modifications associated with drilling. This suggests that the observed cooling trend in the U.S.G.S. data and its recent reversal may be part of the same natural cycle observed at Prudhoe Bay by Osterkamp et al. (1994). However, longer time series of data and additional information on site conditions and thermal parameters will be required to verify this conclusion.

7.6 Mean Temperature Profiles for the Whole Period of Measurements

Mean temperature profiles over the period of measurements are shown in Figure 7.9. Values in the active layer and near-surface permafrost to 0.9 m represent measurements made from 1987 through 1992 and for greater depths (below 20 to 25 m) from 1983 through 1993. Permafrost temperature profiles calculated from the calibrated numerical model and linked to the near-surface profiles are also shown. Differences between the measured and calculated profiles in the deeper permafrost do not exceed 0.03 K for West Dock and Deadhorse and 0.05 K for Franklin Bluffs. The curvatures toward warmer permafrost temperatures in the calculated profiles (above 20 to 25 m) are caused by using only the warmer part of the cycle for the calculations.

All three measured mean profiles for the depths below 20 to 25 m are essentially unaffected by the 10 to 11 yr cycle and show definite curvatures toward warmer temperatures. The curvatures could be part of the warming portion of a cycle with a period longer than 10 to 11 yr. Indeed there is some evidence for longer cycles in geothermal data (Romanovsky et al., 1991a, 1991b; Pavlov, 1994; Safanda et al., 1994). Unfortunately the current time series of temperature data is not long enough to determine the present phase of this cycle and consequently to estimate its amplitude reliably. If this postulated cycle exists, then it is more noticeable at the Deadhorse site, where its amplitude would have to be at least 1 K, than at West Dock and Franklin Bluffs (amplitude about 1/2 K) as determined by upward continuation of the profiles, an uncertain procedure.

These curvatures may also represent changes in permafrost temperatures associated with climatic fluctuations. For example, air temperature and snowfall, which influence permafrost temperatures strongly, have fluctuated over decadal and longer time scales at Barrow (Zhang and Osterkamp, 1993b).

The curvatures could also be evidence for a warming trend in permafrost temperatures associated with climatic change. Global climate models have been

predicting such changes for two decades (Manabe and Wetherald, 1975). However, these time series of permafrost temperatures are too short to distinguish between the alternative interpretations. Nevertheless, it is important to do so because changes in the permafrost temperatures are related to climatic changes.

7.7 Summary

Temperatures in permafrost were measured annually from 1983 through 1993 in drill holes (nominally 60 m in depth) at three sites in Northern Alaska; West Dock, Deadhorse, and Franklin Bluffs (Osterkamp et al., 1994). Active layer and near-surface permafrost temperatures (to 1 m) were measured every 4 hr from 1986 through 1993 (Romanovsky and Osterkamp, 1995a). For these two data sets, there is a gap in the daily permafrost temperatures from 1m to the depth of penetration of the annual temperature wave (about 20 m). The available data were used to calibrate a finite element thermal model which was then applied to simulate the daily permafrost temperatures at the sites. These daily values were used to calculate mean profiles for the annual period, a 10 to 11 yr cycle, and for other periods.

The calculations were used to revise previous estimates of the amplitude of the 10 to 11 yr cycle at Franklin Bluffs from 0.6 K to about 1 K. The data show that, for the 10 to 11 yr cycle, cooling of the permafrost began prior to 1983 with the warming part of the cycle beginning in the late 1980s. This is consistent with the U.S.G.S. data (Lachenbruch and Marshall, 1986) indicating that their reported cooling was part of a natural cycle and not primarily associated with the disturbance at the ground surface associated with drilling.

The means of the measured temperature profiles below the 20 m depth show a curvature toward warmer temperatures suggesting climatic fluctuations, a cycle or a longer-term warming trend. While these time series of permafrost temperatures are too

short to distinguish between these alternatives, it is important to do so because of their possible relationship with the predicted climatic warming.

7.8 Acknowledgments

This research was supported by the National Science Foundation, Office of Polar Programs, Polar Earth Sciences Section and by the State of Alaska.

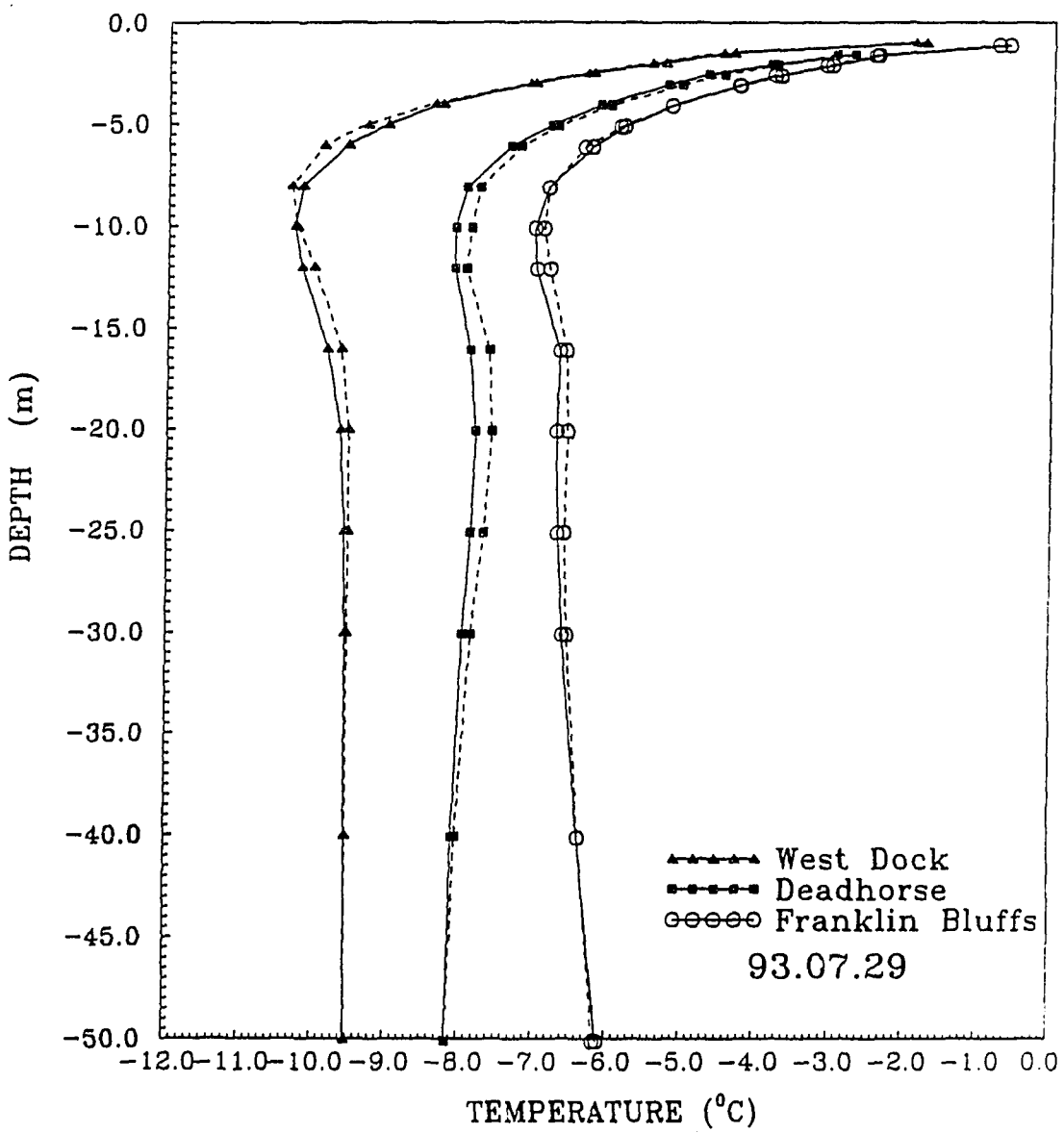

Figure 7.1 Measured (solid line) and calculated (dashed line) permafrost temperature profiles at three sites; West Dock, Deadhorse and Franklin Bluffs for the last day, 29 July 1993, of nearly 7 yr of simulation.

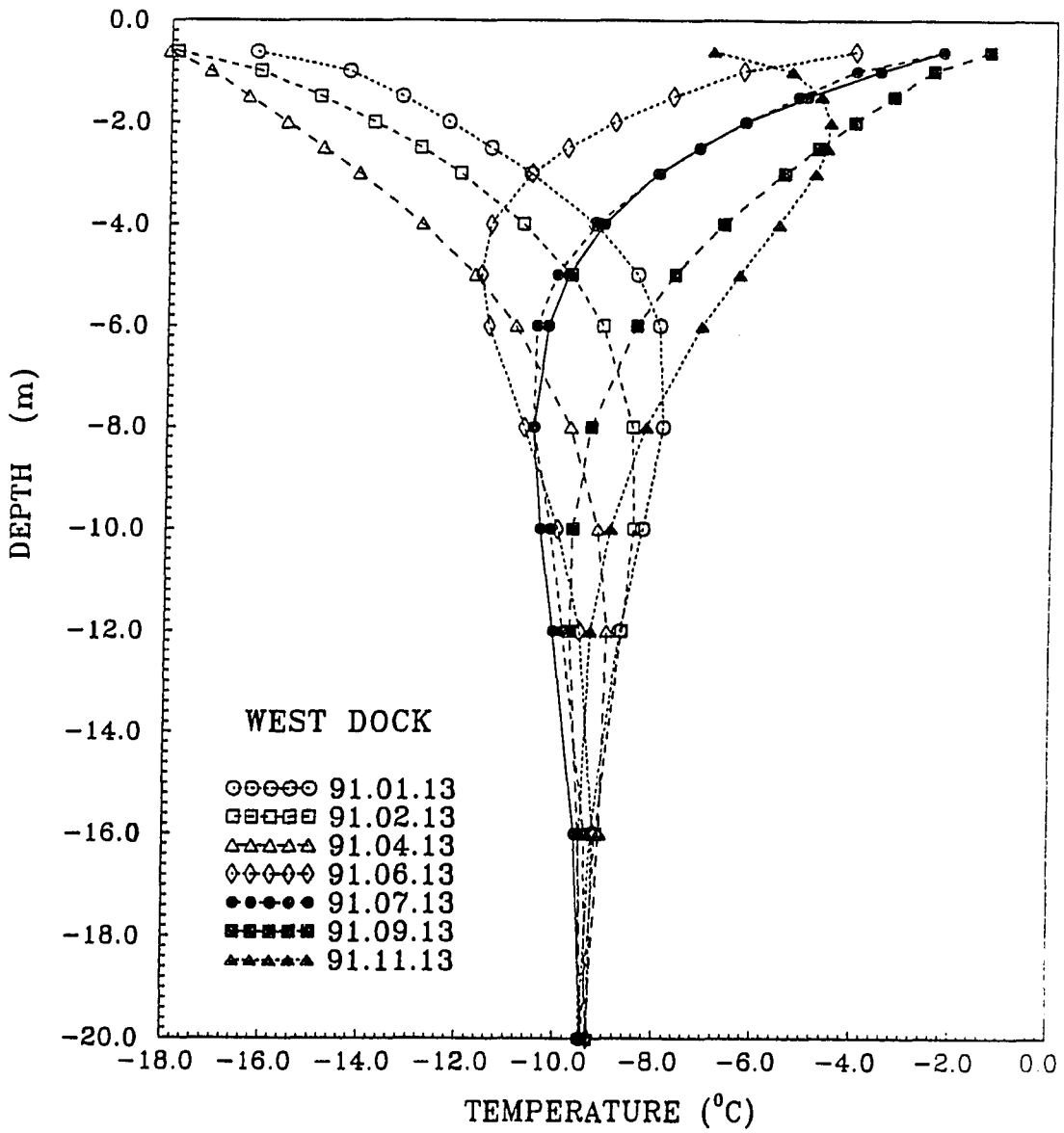

Figure 7.2 Calculated permafrost temperature profiles during 1991 at West Dock (dashed lines) and measured profile on 13 July 1991 (solid line) for comparison.

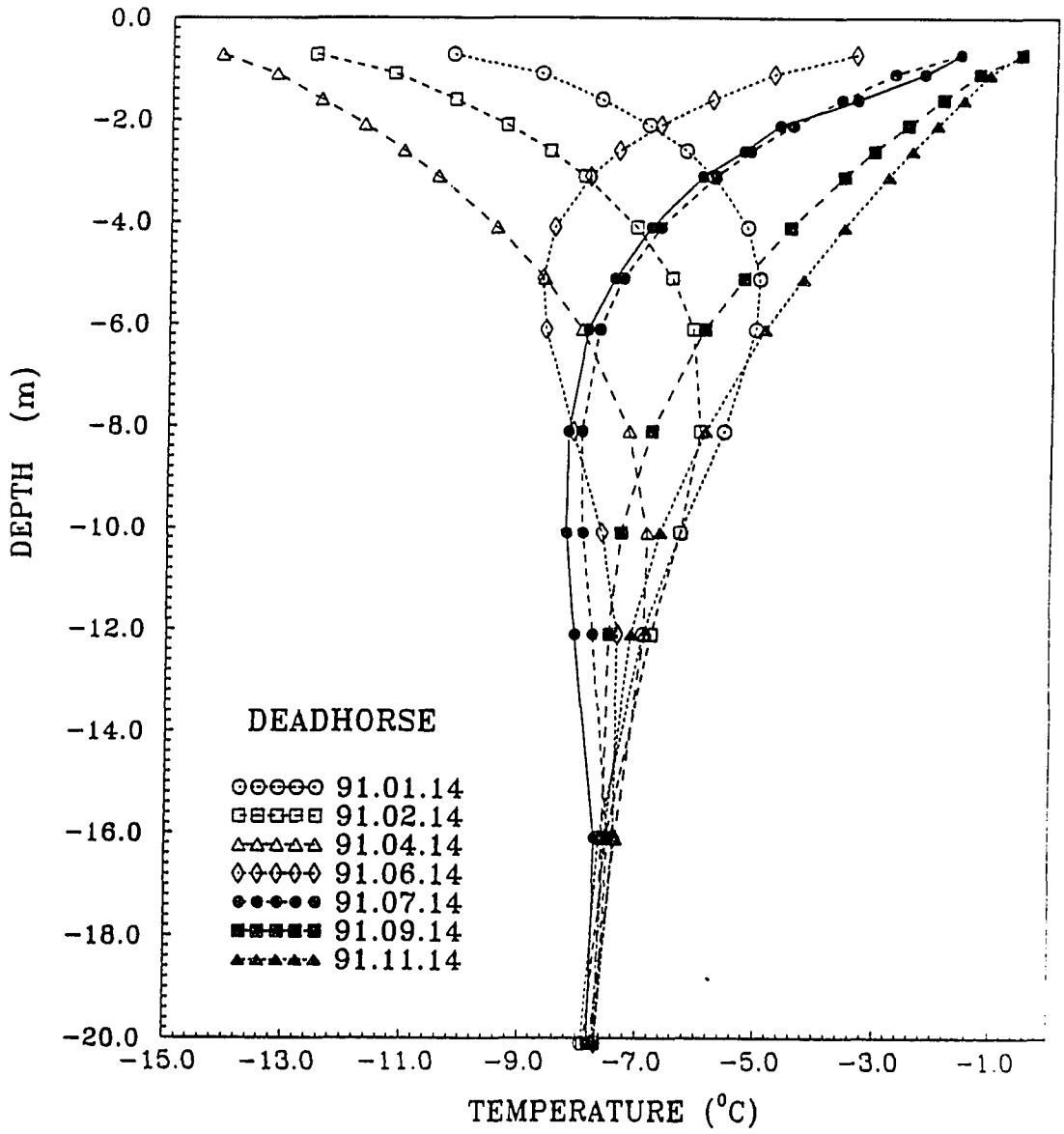

Figure 7.3 Calculated permafrost temperature profiles during 1991 at Deadhorse (dashed lines) and measured profile on 14 July 1991 (solid line) for comparison.

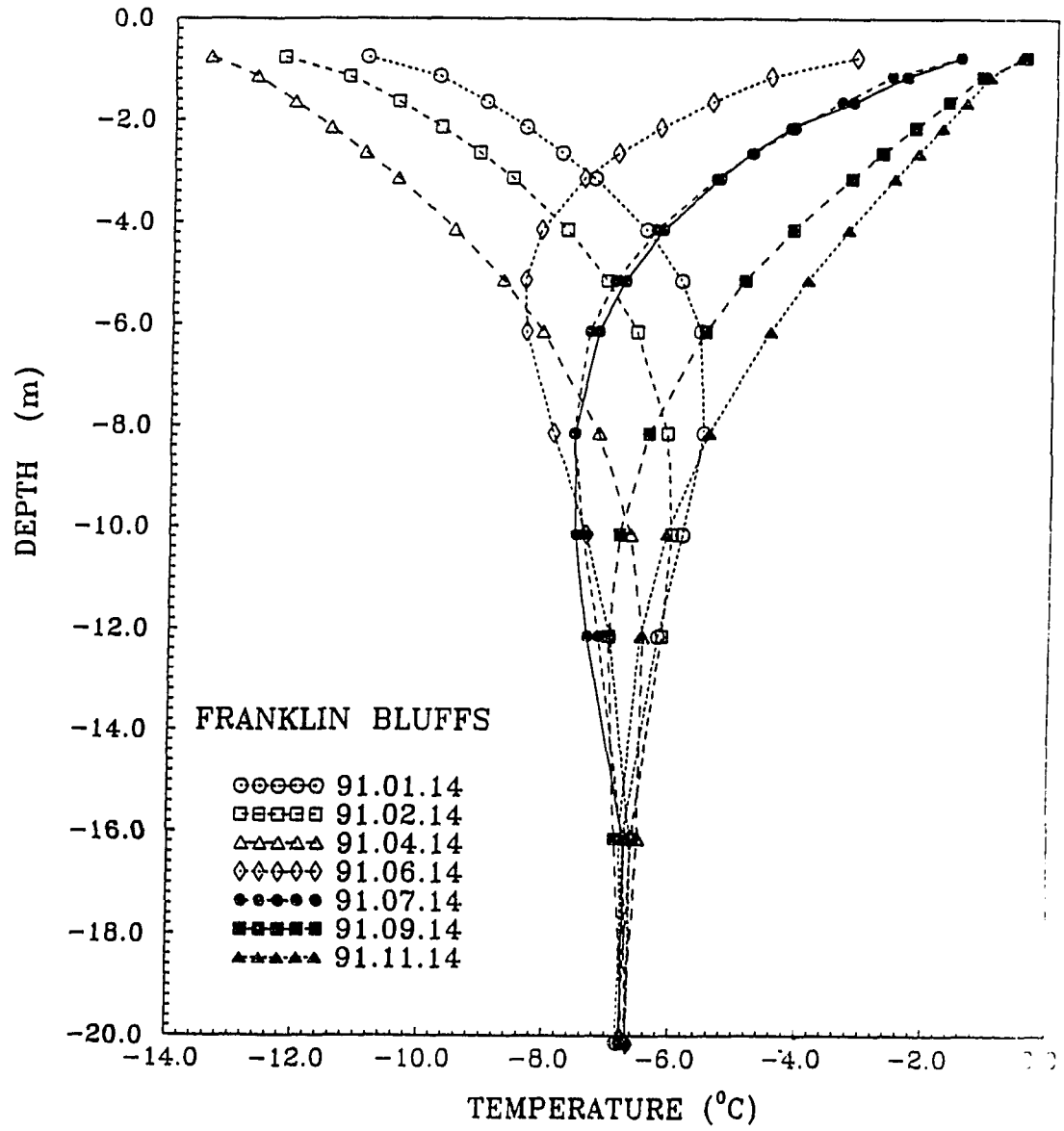

Figure 7.4 Calculated permafrost temperature profiles during 1991 at Franklin Bluffs (dashed lines) **and measured profile on 14 July 1991** (solid line) **for comparison.**

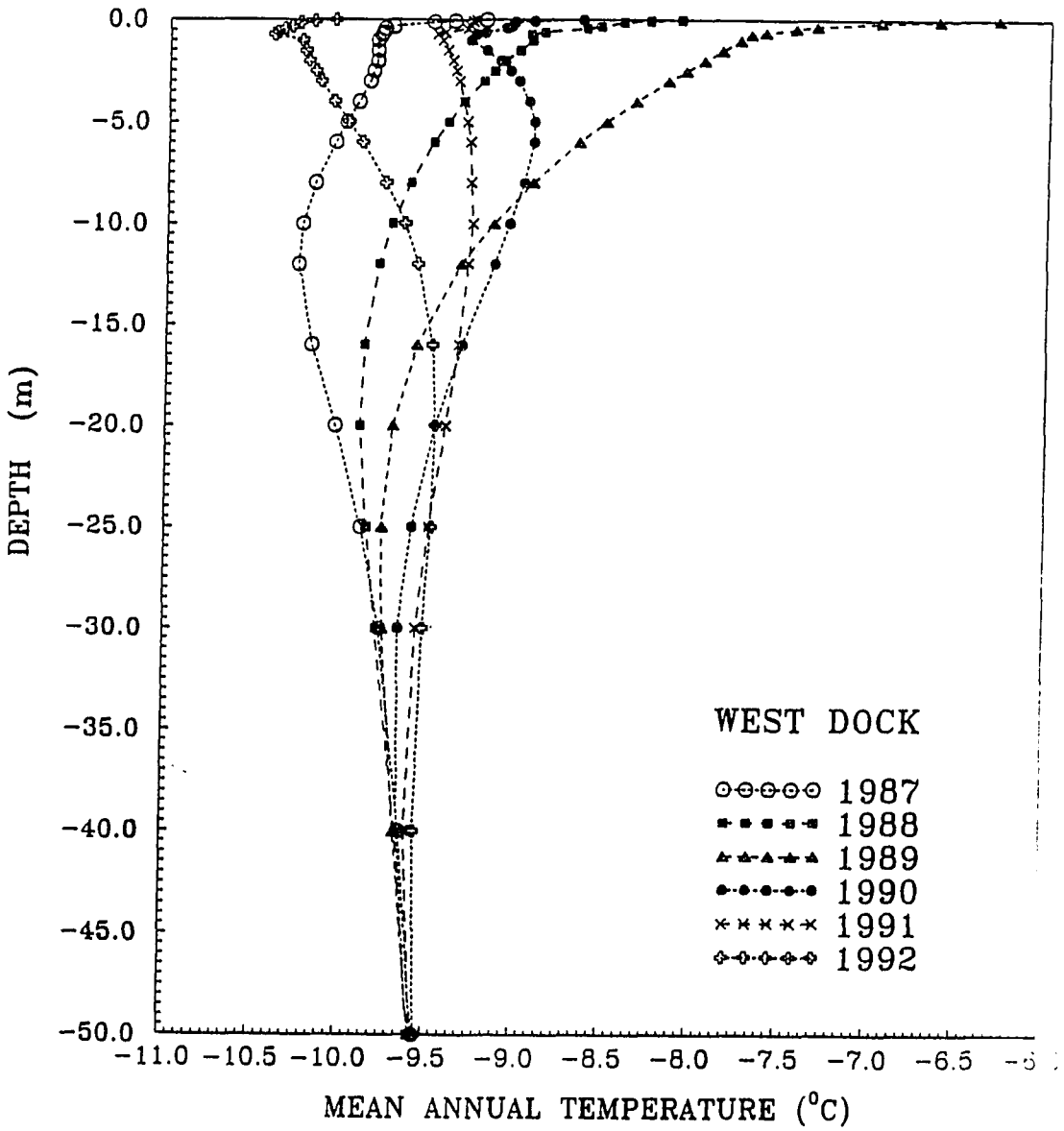

Figure 7.5 Measured mean annual active layer temperature profiles at West Dock for 1987 through 1992 linked to the calculated profiles for the same period.

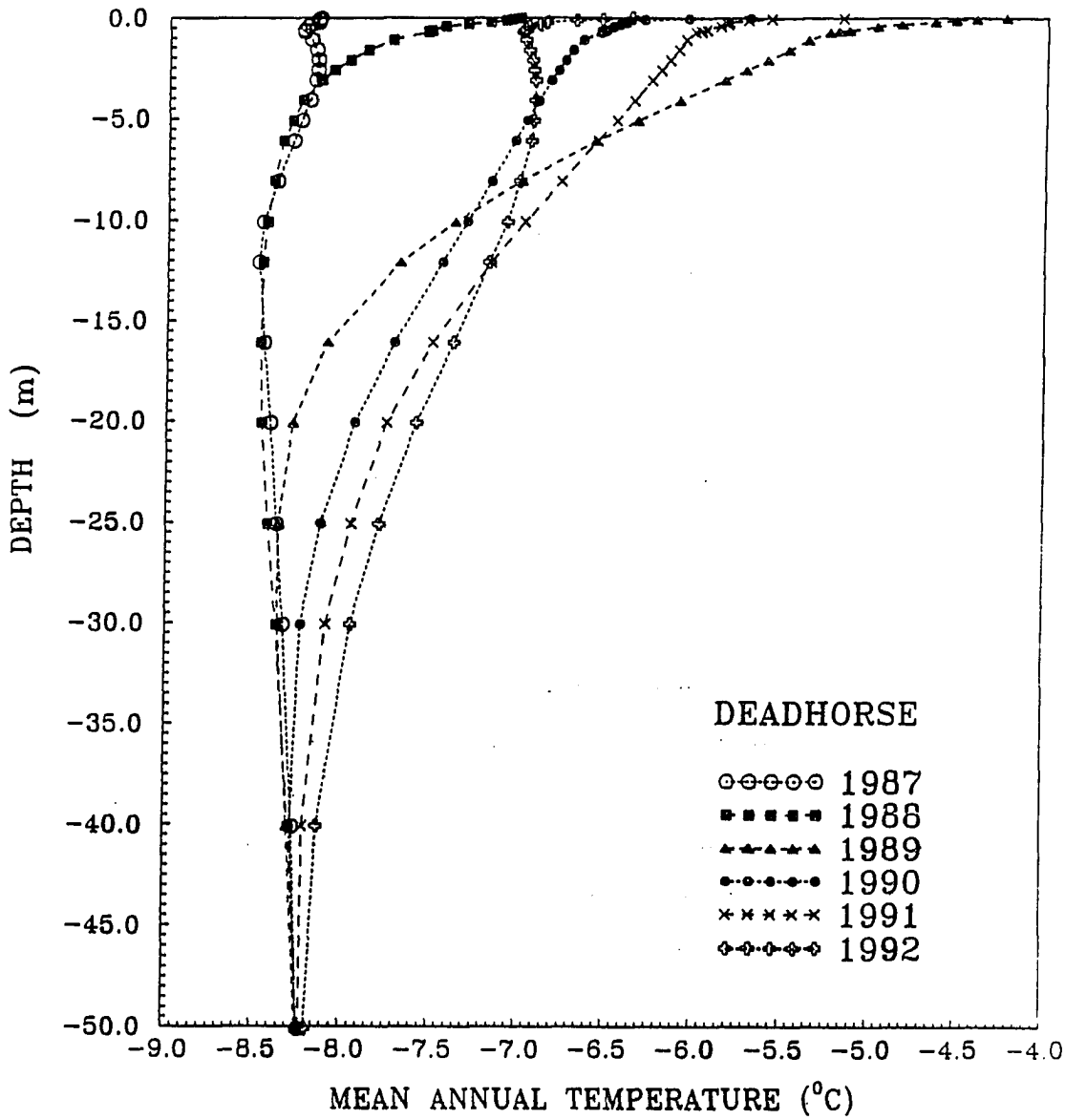

Figure 7.6 Measured mean annual active layer temperature profiles at Deadhorse for 1987 through 1992 linked to the calculated profiles for the same period.

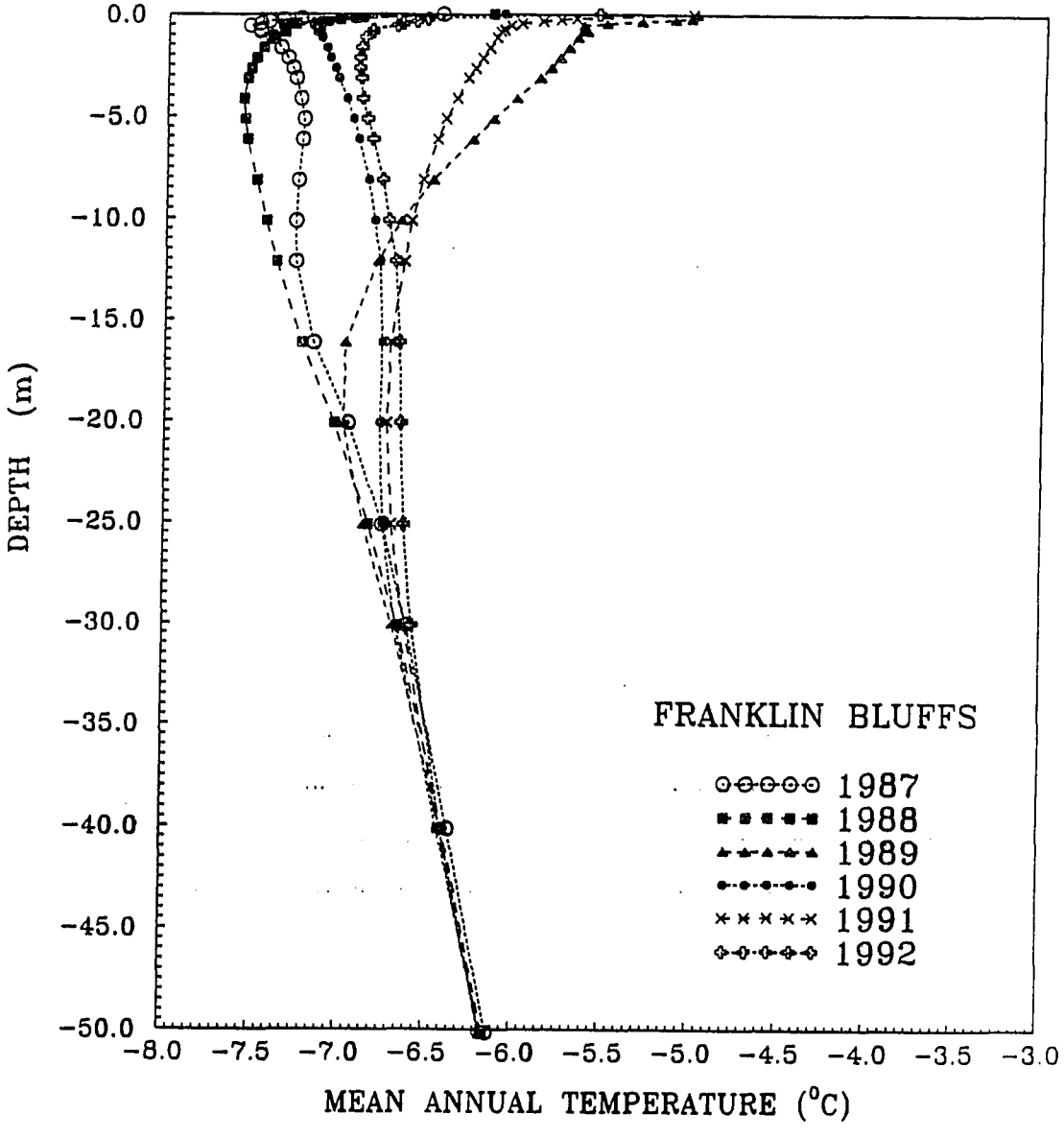

Figure 7.7. Measured mean annual active layer temperature profiles at Franklin Bluffs for 1987 through 1992 linked to the calculated profiles for the same period.

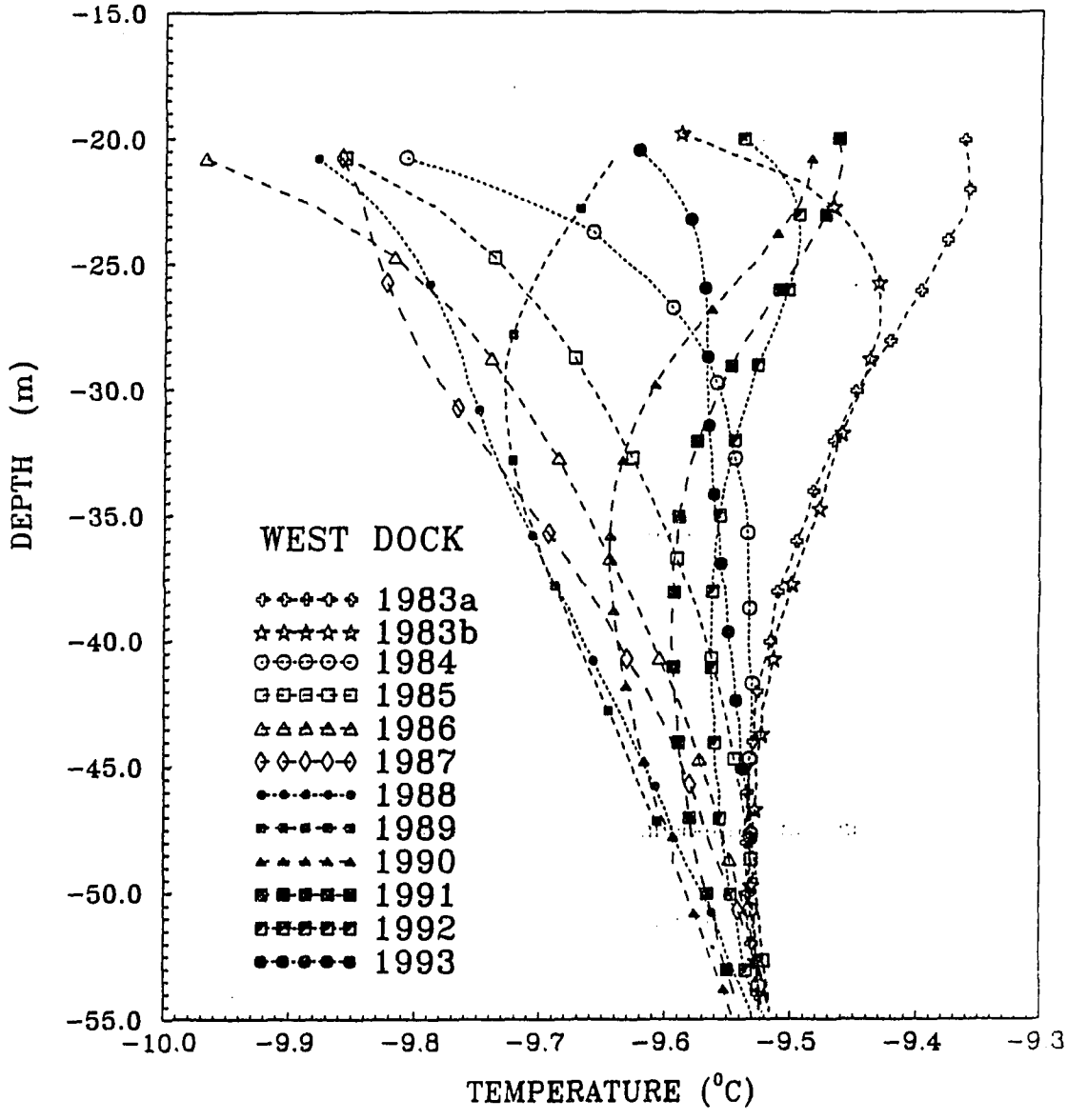

Figure 7.8 Measured permafrost temperature profiles at West Dock for 1983 through 1993.

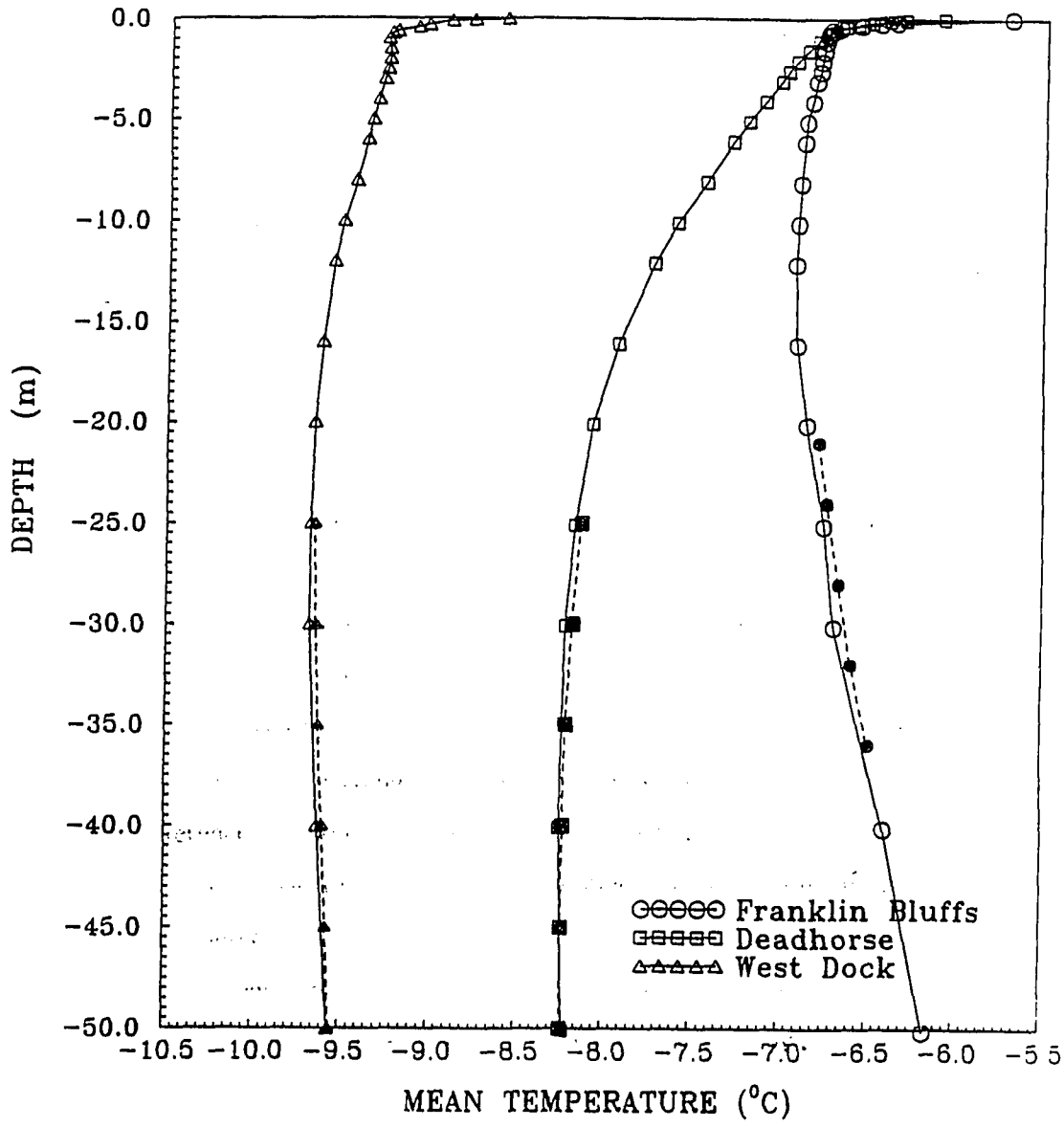

Figure 7.9. Measured mean temperature profiles in the active layer and near-surface permafrost (to 0.9 m) linked to the calculated temperature profiles in the permafrost for the period from 1987 through 1992 (solid lines). Measured mean temperature profiles in the permafrost below the depth of annual temperature variations (20 to 25 m) for the period from 1983 through 1993 (dashed lines).

Table 7.1 Thermal properties of the permafrost estimated from the best fit of the numerical model to the data.

Depth (m)	Soil type	Volumetric heat capacity, C_f ($MJm^{-3}K^{-1}$)	Thermal conductivity, K_f ($Wm^{-1}K^{-1}$)	Thermal diffusivity, D_f (10^{-6} m^2s^{-1})
West Dock				
0.62 - 1.0	silt	1.54	1.56	1.01
1.0 - 8.5	silt and sand	2.34	3.39	1.45
8.5 - 22	sand and gravel	2.04	3.39	1.66
22 - 55	gravel and sand	1.94	3.39	1.75
Deadhorse				
0.72 - 1.0	silt	1.54	1.76	1.14
1.0 - 2.7	sand and silt	2.14	3.39	1.58
2.7 - 27	gravel	1.94	3.59	1.85
27 - 55	sand,silt, gravel	2.04	3.49	1.70
Franklin Bluffs				
0.76 - 1.2	silt	1.54	1.76	1.14
1.2 - 14	gravel	1.94	3.59	1.85
14 - 23	silt	1.54	1.76	1.14
23 - 55	silt with shale	1.54	1.84	1.19

CHAPTER 8

Freezing and Thawing of Inhomogeneous Soils Under the Influence of 300- and 90-Year Periods of Temperature Fluctuation

V. E. Romanovsky, L. S. Garagulya and N. V. Seregina, 1991. Freezing and Thawing of Inhomogeneous Soils Under the Influence of 300- and 90-Year Periods of Temperature fluctuation. In *Proceedings of the International Conference on the Role of Polar Regions in Global Change*, University of Alaska, Fairbanks, vol. 2, pp. 543-548, and

L. S. Garagulya, V. E. Romanovsky and N. V. Seregina, 1995. Modeling Temperature Fields During Inhomogeneous Rocks Freezing and Thawing. In *Russian Geocryological Research*, Russian Academy of Science, Moscow, vol. 1, pp. 34-42.

8.1 Abstract

A numerical permafrost temperatures model was developed for the southern Siberia region to study the influence of short-term rhythmic climatic variations on the dynamics of permafrost. The mathematical model is represented as a two-dimensional heat conduction problem for a moist substrate with the latent heat effect for complex geological structures. This model takes into account a complex periodic temperature changes at the ground surface and a stable heat flow at the lower and lateral boundaries for a study domain. It has been realized as a fully implicit local one-dimensional finite difference scheme on an irregular grid.

The calculations of the dynamics of temperature fields and permafrost boundaries are discussed to evaluate this model for the southern permafrost region of Eastern Siberia. The results of modeling show that two-dimensional temperature field along some profiles (particularly at sites with complex geological structures) contain

much more information about past permafrost dynamics than temperature profiles from single boreholes. The joint use of both the field temperature data along profiles, and numerical modeling can provide a more reasonable explanation of present permafrost structure and more accurate forecast of permafrost changes in the future.

8.2 Introduction

Under natural conditions the formation and dynamics of permafrost takes place as the result of temperature changes at the Earth's surface caused by the superposition of climatic cycles with different periods (Kudryavtsev et al., 1978; Balobaev and Pavlov, 1983; Maximova and Romanovsky, 1986, 1988; Zubakov, 1986; Romanovsky et al., 1991a; Romanovsky and Maximova, 1991). The objective of discussed studies was to construct a mathematical model to simulate natural conditions and to compare the results of modeling with different types of inhomogeneities in geological structure and boundary conditions.

One-dimensional models of temperature fields are used most often when studying the effect of geological structure and climate on the formation and dynamics of permafrost and the temperature field in the ground. Numerous examples are known, however, when the measured temperatures cannot be explained by a one-dimensional conductive model. In this case the conclusion is often that the temperature field is not one-dimensional and its formation is affected by horizontal inhomogeneities. The latter are most frequently due to the geological structure of ground mass and temperature conditions on their surface. An attempt is made in this article to analyze the impact of such inhomogeneities on a temperature field. Such an analysis is most interesting for non-stationary temperature fields, i.e. when the natural climate dynamics is taken into consideration. The latter is expressed as the superposition of the different time scale temperature variations at the ground surface.

8.3 Numerical Model Formulation

The following problem was formulated while studying thermal processes in the ground: to determine the ground temperature field with horizontal inhomogeneities caused by geological structure and the spatial variability of the landscape. The dynamics of the temperature field is defined by the rhythmical structure of temperature variations on the surface. The problem can be described by the following mathematical model for a time-space domain $D=\{0<x<l_1;\ 0<y<l_2;\ 0<t<t_1\}$ in the space of variables (x, y, t) :

$$[8.1]\quad C(T,x,y)\frac{\partial T}{\partial t} = div(K(T,x,y)\nabla T)\ ,\ (x,y,t) \in D\ ,\ T \equiv T(x,y,t) \neq T_e$$

where T_e is the temperature of the phase transition, C is the volumetric heat capacity, and K is the thermal conductivity. The initial and boundary conditions are

$$[8.2]\quad \begin{aligned} & T(x,y,0) = T_0(x,y) \\ & \left.\frac{\partial T}{\partial n}\right|_{x=0} = \left.\frac{\partial T}{\partial n}\right|_{x=l_1} = 0, \quad \left.\frac{\partial T}{\partial n}\right|_{y=l_2} = g \\ & T(x,0,t) = \psi(x,t) \end{aligned}$$

where $\frac{\partial}{\partial n}$ is a normal derivative, g is the temperature gradient at the lower boundary of the domain D and $\psi(x, t)$ is the temperature changes at the ground surface. The Stefan conditions at the phase boundary are

$$[8.3]\quad \begin{aligned} & T(x,y,t) = T_e \\ & Q(x,y)\frac{\partial \Phi}{\partial t} = (((K\nabla T)|_{P+0} - (K\nabla T)|_{P-0}), \nabla\Phi) \end{aligned}$$

with $P \in \Phi(x,y,t) = 0$, where $P \equiv P(x,y,t)$ is a point in an area D with coordinates x, y, t and $\Phi(x, y, t) = 0$ is the phase boundary equation in implicit form. $Q(x, y)$ is the latent heat of phase transitions, P+0 is an index that denotes the limiting value for a process that starts in a region with a higher enthalpy and proceeds towards a point on the phase front, P-0 is an index denoting a similar value but for a process starting in a region with lower enthalpy.

The physical problem is periodic in time and the initial propagation of the temperature field in the problem (8.1-8.3) is unknown. However, the solution of the initial boundary value problem with $\psi(x, t)$ periodic with respect to t is known to reduce the solution of a periodic problem. This topic was considered by Meyermanov (1986).

An approach based on an enthalpy function and its subsequent smoothing with a first order polynomial was used to compile a difference scheme (Uspensky, 1975). The temperature field can thus be defined at each time step without determining the front position for the preceding time step, which is the way it must be done for a variation-difference method (Moiseyenko and Samarsky, 1965). This is the only possible method in case of a multi-frontal problem (three freezing fronts and over) which we considered.

A completely implicit locally one-dimensional scheme on irregular grids was used to solve a smoothed differential problem with an enthalpy formulation. Let us consider in terms of spatial variables an irregular grid with $h_{xi} = x_i - x_{i-1}$ steps along the x-axis and $h_{yj} = y_j - y_{j-1}$ steps along the y-axis. We introduce a grid in terms of the time axis t with $\Delta t_n = t_n - t_{n-1}$ steps, and set $t_{n+1/2} = t_n + \Delta t_n/2$. We write T^2_{ij} for the solution at the next time step $n + 1$; if T_{ij} is the value for time step n, let

T^1_{ij} be an intermediate value and let $\tilde{c}$, $\tilde{k}$ be the smoothed coefficients of heat capacity and thermal conductivity, respectively. Then the difference scheme will be:

$$\tilde{c}(x_i, y_j, T^1_{ij})(T^1_{ij} - T_{ij}) = \Delta t_{n+1} \Lambda_1 T^1_{ij}$$
$$\tilde{c}(x_i, y_j, T^2_{ij})(T^2_{ij} - T^1_{ij}) = \Delta t_{n+2} \Lambda_2 T^2_{ij} \quad [8.4]$$

where

$$\Lambda_1 T_{ij} = \frac{2}{h_{x,i} + h_{x,i+1}} \left(\tilde{k}(x_{i+1} - 0.5h_{x,i}, y_j, \frac{T_{i+1,j} + T_{ij}}{2}) \frac{T_{i+1,j} - T_{ij}}{h_{x,i+1}} - \tilde{k}(x_i - 0.5h_{x,i}, y_j, \frac{T_{i,j} + T_{i-1,j}}{2}) \frac{T_{i,j} - T_{i-1,j}}{h_{x,i}} \right) \quad [8.5]$$

$$\Lambda_2 T_{ij} = \frac{2}{h_{y,j} + h_{y,j+1}} \left(\tilde{k}(x_i, y_{j+1} - 0.5h_{y,j}, \frac{T_{i,j+1} + T_{ij}}{2}) \frac{T_{i,j+1} - T_{ij}}{h_{y,j+1}} - \tilde{k}(x_i, y_j - 0.5h_{y,j}, \frac{T_{i,j} + T_{i,j-1}}{2}) \frac{T_{i,j} - T_{i,j-1}}{h_{y,j}} \right)$$

The boundary conditions for the first equation in system (8.5) are given as $t = t_{n+1/2}$,and for the second equation as $t = t_{n+1}$. The boundary conditions of the second type for the scheme (8.2) are approximated with the second order of spatial steps h_x and h_y (Seregina, 1989) and with the first order of time step Δt . Then the approximation order of the scheme is $O(h_x^2 + h_y^2 + \Delta t)$.

Simple iterations were used to solve a discrete system of nonlinear grid equations at each time step. The solution from the previous time step was considered to be the initial approximation of the iterative process. The program bisects the time

step in the case of iterative divergence at each half of the time step. A three-point equation was solved by the sweep method at each iteration.

8.4 Initial Data

The permafrost dynamics was studied using this model for southern regions of East Siberia. Paleogeographers have established the climatic rhythms with periods close to 90 and 300 years and a fluctuation amplitude of about 2°C with the mean perennial value close to 0°C (Balobayev and Pavlov, 1983; Zubakov, 1986; Kovalenko et al., 1987; Rozanov, 1987). These variations in temperature were used as the upper boundary conditions. The lower boundary conditions were set by a geothermal gradient of 0.01°C m^{-1} at 200 m down. Part of the valley was considered, where the rock mass is of a block two-layered structure. A cross-section within one block contains alluvial, mainly sand deposits 10 m thick underlain by sandstone. In another tectonically moved block, the section contains the same rocks but the thickness of the dispersed deposits is 50 m.

The thermal properties of the rock are given in Table 8.1. K_t and K_f represent thermal conductivities in thawed and frozen states, and C_t and C_f represent thawed and frozen heat capacities.

Table 8.1 The thermal properties of rocks (weighted average)

Rock composition	Thermal conductivity K_t/K_f, $Wm^{-1}K^{-1}$	Heat capacity C_t/C_f, $MJm^{-3}K^{-1}$	Latent heat Q , MJm^{-3}
Alluvial sands with sandy loam and loam interbeds	1.6/1.8	2.1/1.68	83.8
Sandstone with argillite interbeds	2.7/2.7	1.05/0.85	12.6

8.5 Results of Modeling

Superimposing the 300- and 90-year rhythms leaded to a periodic freezing up and thawing of rocks with a period close to 300 years. The 90-year rhythm, however, made the situation more complicated and caused the duration of the freezing-thawing cycle to deviate from 300 years. Besides, the duration of freezing and thawing periods varied from cycle to cycle. Thus, a thawing period varied from 137 to 208 years (instead of 150 years for a complete 300-year rhythm). A period of total variations amounted to 900 years, i.e. each period included three waves of cooling and warming and three cycles of freezing and thawing, respectively (Figure 8.1).

8.5.1 Climatic Changes and Permafrost Dynamics

The freeze-thaw problem was solved with three upper boundary conditions, a 90-year period cycle, a 300-year period cycle, and the superposition of these fluctuations. Data analysis show the following results (Figure 8.1). The sinusoidal temperature variations with a period of 90 years (Figure 8.1C) forms a layer of permafrost with a thickness of 9.3 m within the alluvial sand. The rate of freeze-thaw was about 0.25 m/year. The lower boundary of permafrost was located at a depth of approximately 9 m through a period of 30 to 35 years. At the 90-year time interval, there was no permafrost for 17.5 years.

Fluctuations of temperature with 300-year period caused perennial freezing down to the 29 m depth in the first part of the domain (the frozen layer included 10 m of alluvial sands and 19 m of sandstones). In the second part of the domain, these fluctuations of temperature caused perennial freezing down to the 15 m depth (Figure 8.1B). The freezing rate of alluvial sands was about 0.14 m/year. The rate for freezing of sandstones was approximately 0.3 m/year. In the first part of the domain, the lower boundary of permafrost was located at a depth of 29 m during 50 to 60 years. In the

second part of the domain, the lower boundary of permafrost was located at a depth of 15 m during 75 to 80 years.

Superposition of the temperature fluctuations with 90- and 300-year periods resulted in a new 900-year period of temperature variations at the ground surface (Figure 8.1). During this 900-year period, the temperature fluctuations caused three cycles of warming-cooling. The duration of these warming-cooling cycles are 277 years, 346 years and 277 years.

During the first cycle (279 years), there was a time of warming at about 138 years, with two temperature maxima of 3.0°C and with one minimum of 0°C in the middle of the warming period. At the cooling interval (141 years), there were two temperature minima, one at the beginning of the interval (-2.4°C), and the other at the end (-3.7°C). In the middle of the cooling interval, there was one maximum with a temperature not greater than 0°C. During the second cycle (364 years), there was a time of warming (208 years) with three temperature maxima of 1.4°C, 3.8°C, and 1.1°C and two temperature minima (-0.6°C and -1.2°C). At the time of cooling (138 years), there were two temperature minima (-3.7°C and -1.9°C) and one maximum (0.6°C). During the third cycle, there was a time of warming (137 years), with two maxima (3.6°C and 3.0°C) and one minimum (-0.4°C). At the time following cooling (140 years), there were two minima (-3.8°C and -2.4°C) and one temperature maximum (0°C).

The formation and dynamics of permafrost caused by the temperature fluctuations were different with respect to different cycles. As shown in Figure 8.1A, simple stable conditions of freeze-thaw occurred during the first cycle. The maximum thickness of permafrost here was near 45 m. Duration of the permafrost existence was about 140 years. During the period of warming, completely thawed soils existed continuously during a 55-year period.

Dynamics of freezing are defined by the time of the surface temperature minima. First minimum (related to temperature fluctuations with a 90-year period)

caused the rapid freezing of alluvial sands to the depth of 8 m. After that, the rate of freezing reduced and the permafrost lower boundary lowered by 2 m during the next 30 years. At that time, the surface temperature was near 0°C. The next 90 years of cooling (coinciding with the minimum of the 300-years rhythm) caused the freezing of the sandstones to the depth of 45 m.

The warming, related to temperature maximum of the 90-year rhythm, caused the thawing of soils from the top and bottom. This was the beginning of the second warming-cooling cycle. As indicated in Figure 8.1A, the thawing from above (during 115 years) was completed at the depth of 30 m in the sandstones. The rate of thawing was influenced by the soil properties and temperature fluctuations at the surface. During the first 20 years, the thawing rate of alluvial sands was about 0.3 m/year; the depth of thawing reached 7.5 m. During the next 60 years, the thawing front actually remains stationary. At the same time, the surface temperature fell to -0.6°C and remained negative for almost 30 years. The short-term permafrost with a thickness of about 3 m was forming. The existence of short-term permafrost caused an actual invariable location of the lower permafrost layer during 30 years. After thawing of short-term permafrost, the thawing of soils from above proceeded with a rate of about 0.1 m/year. It ends with the merger of the upper and lower fronts. After the end of thawing the short-term permafrost with 6 m thickness was formed again and existed for 60 years.

At the end of the second cycle, the depth of permafrost was 27 m. The surface temperature within the cold part of the second cycle was positive during 23 years and the talik with thickness near 3 m existed over the permafrost table.

The third cycle began with thawing of permafrost from above and from below, conditioned by positive surface temperatures. During 70 years, the section consisted of completely thawed soils. However, at the beginning of this time interval, short-term permafrost was formed with a thickness of about 2 m and remained frozen for about 20

years. During the last part of the third cycle, there was permafrost for 140 years, with a maximum depth here of 41 m.

Analysis of the processes in the second part of the domain (with 50 m thickness of alluvial sands) showed that the lower boundary of permafrost was much more stable in time. This was due to the fact that the latent heat of phase changes in alluvial sands was almost seven times greater than in sandstones.

8.5.2 Two-dimensional Temperature Field Dynamics

The application of a two-dimensional numerical model allows the characterization of the anomalies in the temperature field dynamics as a result of the temperature cyclic variations at the ground surface. Let us analyze in detail the dynamics of the permafrost boundaries and temperature field during one such cycle. The freezing half-period may be divided into two stages. At the first stage a temperature field in the first and second blocks differed very little from a one-dimensional field, with temperature differences not exceeding 0.1°C at the same depth in different part of the massif (Figure 8.2A). The temperature field isolines and the boundary of the phase division were actually parallel to each other and to the ground surface.

The permafrost temperature increased with depth almost linearly. The gradient decreased with depth in the thawed zone, reaching the geothermal gradient 0.01 Km^{-1} at the lower boundary of the domain. The first stage was over when the freezing boundary reached the interface between sands and sandstones in an uplifted block of the massif (at the depth of 10 m).

From this moment, the second freezing stage started and the rates of the freezing front advancing deep into the massif differed for the uplifted and subsided blocks. Since Q in sandstones was nearly an order lower than that in sands, the freezing front in an uplifted block moved faster. This leaded to the formation of a scarp

in the lower boundary of permafrost, and the temperature field became laterally inhomogeneous (two-dimensional in this case). The difference in front position increased with time and the developing scarp grew and became steeper (Figure 8.2B). Temperature field isolines repeated a curve of the phase front smoothing it to a certain extent. This, by the way, defined the subsequent evolution of the scarp.

Thus, the configurations of the temperature field and freezing front was a reverse bend with respect to the lithological scarp. The sharpness of this bend and its prominence downward was a characteristic feature of this period of the second stage. The bend protruded 20-25 m away from a lithological contact towards the subsided block filled in with alluvial sands and remained there until the rocks completely thawed (Figure 8.2E). The shape and position of the bend can be explained by the lateral cooling effect of the of the uplifted block where soils were freezing faster. The bend was convex in shape, the convexity being directed towards freezing.

At the end of second stage of freezing when the surface temperature rise close to 0°C, the temperature field in the frozen zone equalized, the bend in temperature field and in the lower permafrost boundary were smoothed and the delineation became less sharp. Thus, if the width of the scarp at the lower permafrost boundary had been 10-15 m, it became now at least 75 m (Figure 8.2C). The amplitude increased (from 10-15 m at the beginning of the second stage to 30-35 m at the end). The middle part of the bend practically coincided with the lithological interface. The temperature field isolines smoothly repeated the position of the phase boundaries. Both the boundary and isolines were slightly convex downward, though in the upper part of permafrost the isolines acquired some upward convexity. Variations in the temperature field at this stage of freezing can be explained by a temperature rise on the ground surface. The colder uplifted and the warmer subsided blocks affected each other in this situation. If the cooling effect of an uplifted block was preserved in the upper part of the scarp, the warming effect of the subsided block effected the lower part quite noticeably. This completing stage directly preceded a half-period of permafrost thawing.

A thawing half-period started when the surface temperature became positive after a stage of "one-dimensional" thawing, when a one-dimensional temperature field was formed in the upper thawed section (Figure 8.2D).

Intensive permafrost thawing from the surface is characteristic of the middle and short-period temperature variations. This leaded to the formation of a relic permafrost layer, the upper boundary of which was at the first stage parallel to the ground surface. The temperature field in this layer rapidly became homogeneous with values close to 0°C. The frozen rocks slowly thaw from below simultaneously. The scarp at the lower boundary was preserved, but its convexity was directed upward (Figure 8.2D).

When the thawing front descended lower than 10 m, i.e. when the sandstones began to thaw in the uplifted block, again a scarp protruded downward was formed in the configuration of the upper front, reversed to the lithological scarp. Its sharp outlines contrasted with the smoothed ones in the permafrost lower boundary (Figure 8.2E). The temperature field isolines in the thawed zone repeated the shape of phase boundary.

Further thawing leaded to a disconnection of relic permafrost occurring at different depth in uplifted and subsided blocks (Figure 8.2F). The formation of a through talik in the zone of a lithological interface can be explained by the temperature field configuration at that time, which is characterized by the highest concentration of the heat flow lines in the lithological scarp.

In spite of a fall in the temperature remaining positive on the surface, permafrost degradation continued. The first to thaw completely were the relic frozen sandstones in an uplifted block. The last permafrost in the subsided block sands disappeared somewhat later (in 20-40 years). Intensive smoothing of the temperature field in the rocks occurred after the complete thawing of permafrost. For a long time, however, it still retained the features inherited from the preceding temporal interval, when relic permafrost was present in the section (Figure 8.3). The temperature field

became practically one-dimensional again when a new freezing half-period began and a permafrost started to form from the surface.

The process of perennial freezing and thawing caused by variations with a period much longer than that considered above has its own peculiarities. The first stage of freezing at the initial phase of the long-term process (with 40000-years period) proceed exactly the way which was described above. A two-dimensional temperature field was formed with an expressed step in the lower boundary of the permafrost opposite to the lithological scarp. Essential differences occurred at the concluding stage of the freezing half-period (when the temperature on the surface while remaining negative tended to be 0°C). The differences are manifested best during a thawing half-period. At this time the duration of the process (we consider a period of 40 000 years) makes the geothermal flow leading to permafrost bottom more important. A numerical experiments showed that the permafrost formed due to a long period rhythms thawed from below to a considerable extent (>50% of the thickness), whereas due to short period rhythms (with 90- and 300-years periods) the permafrost thawed mainly from above (Figure 8.2). Noticeable thawing from below in the last case only occurred for a short time interval coinciding with the beginning of thawing from above. This went on until the temperature gradient in the thawed underlying rocks near the lower permafrost boundary, distorted by the preceding freezing, decreased to the value of the normal geothermal gradient (Figure 2). For a 300-year variations the lower boundary of permafrost began to rise only upon thawing of rocks from above, in case of variations with 40000-year period the temperature at the ground surface increased so slowly that the lower permafrost boundary began to rise almost simultaneously with the temperature rise at the surface and well before the beginning of thawing from above.

It takes about 120-130 years from the moment of the temperature starting to rise at the permafrost bottom to the total rock thawing for a 300-year rhythm. A layer of 4-5 m may thaw during this time interval under the most favorable conditions, which

amounts to not more than 10% of total permafrost thickness. In an unfavorable case thawing from below may be limited by 1-1.5 m for this time interval. The picture is quite different for a 40000-year rhythm. Thawing from below in this case lasts 8000-9000 years. A layer of 100 m and more can thaw from below for this time interval. Active thawing from below with a higher rate in an uplifted block of the rocks composed mainly of sandstones leaded to the following results (Figure 8.4). At the moment when positive temperatures began at the surface, sandstones in uplifted andsubsided blocks were thawed. The lower boundary of permafrost located near the lithological interface between sands and sandstones and a bend was thus formed at this boundary which coincided with the lithological scarp. Calculations showed that permafrost thaw completely in a subsided block in about 1700 years at the depth of 32 m. The maximum permafrost thickness during the period of 40000 years was about 150 m.

Thus, the process of permafrost thawing and the structure of the temperature field formed depend on the period of the temperature variations at the ground surface which caused this thawing. Primarily it refers to a proportion between thawing from below and above. This leads to differences in the configuration of a two-dimensional temperature field formed in inhomogeneous rocks during the degradation of permafrost of different ages. These differences may serve as a diagnostic parameter in the determination of the permafrost age by a two-dimensional configurations of their boundaries and the observed temperature fields.

A similar scarp in the permafrost lower boundary was formed and varied when the rocks were homogeneous and represented by sands, for example, but the temperature distribution at the ground surface was not homogeneous. We considered two-dimensional temperature distribution over the surface, which implies a neighborhood of two different types of landscapes with different mean annual surface temperature (in the left part of the domain average temperature over a 300-year period was -1°C, in the right part it was 0°C), but with similar amplitudes of 2°C and periods

of temperature variations of 300 years. In this case a step was observed in the temperature field and in the configuration of permafrost boundaries at transition from the left to the right parts of domain (Figure 8.5). This step was the steepest at the stage of progressive freezing and had the largest amplitude at that time. At the thawing stage, it became less sharp. The temperature field smoothed and the step flattened in the way it did in case of lithological inhomogeneties (compare Figures 8.2 and 8.5). The transition zone widened and the lower boundary of permafrost smoothly passed over from the left more frozen part of the domain to the right warmer one.

8.6 Conclusions

Superimposing the 300- and 90-year rhythms leaded to a periodic freezing up and thawing of rocks with a period close to 300 years. The 90-year rhythm, however, made the situation more complicated and caused the duration of the freezing-thawing cycle to deviate from 300 years. Besides, the duration of freezing and thawing periods varied from cycle to cycle. Thus, a thawing period varied from 137 to 208 years (instead of 150 years for a complete 300-year rhythm). A period of total variations amounted to 900 years, i.e. each period included three waves of cooling and warming and three cycles of freezing and thawing, respectively.

Temperature fluctuations with period of 90 years did not lead to deep freezing of the ground (less than 10 m) and did not penetrate in the southern permafrost region at great depth (less than 40-50 m). A 300-years fluctuations leaded to greater depth of the freezing (about 30 m in this case). Superposition of both of these fluctuations created a more complex distribution of the temperature field and of its dynamics. Cooling periods varied in duration when permafrost exist; therefore, the thickness of permafrost during each period was also different. Maximum thickness occurred when the minima of both rhythms coincided. The thickness of permafrost exceeded 43 m, i.e. more than 10 m greater than the maximum depth of freezing by the 300-year

fluctuation alone. Superposition of the fluctuations also leaded to complex alternation of short-term permafrost and of the shallow taliks near the ground surface.

The process of permafrost thawing and the structure of the temperature field formed depend on the period of the temperature variations at the ground surface which caused this thawing. Primarily it refers to a proportion between thawing from below and above. This leads to differences in the configuration of a two-dimensional temperature field formed in inhomogeneous rocks during the degradation of permafrost of different ages. These differences may serve as a diagnostic parameter in the determination of the permafrost age by a two-dimensional configurations of their boundaries and the observed temperature fields.

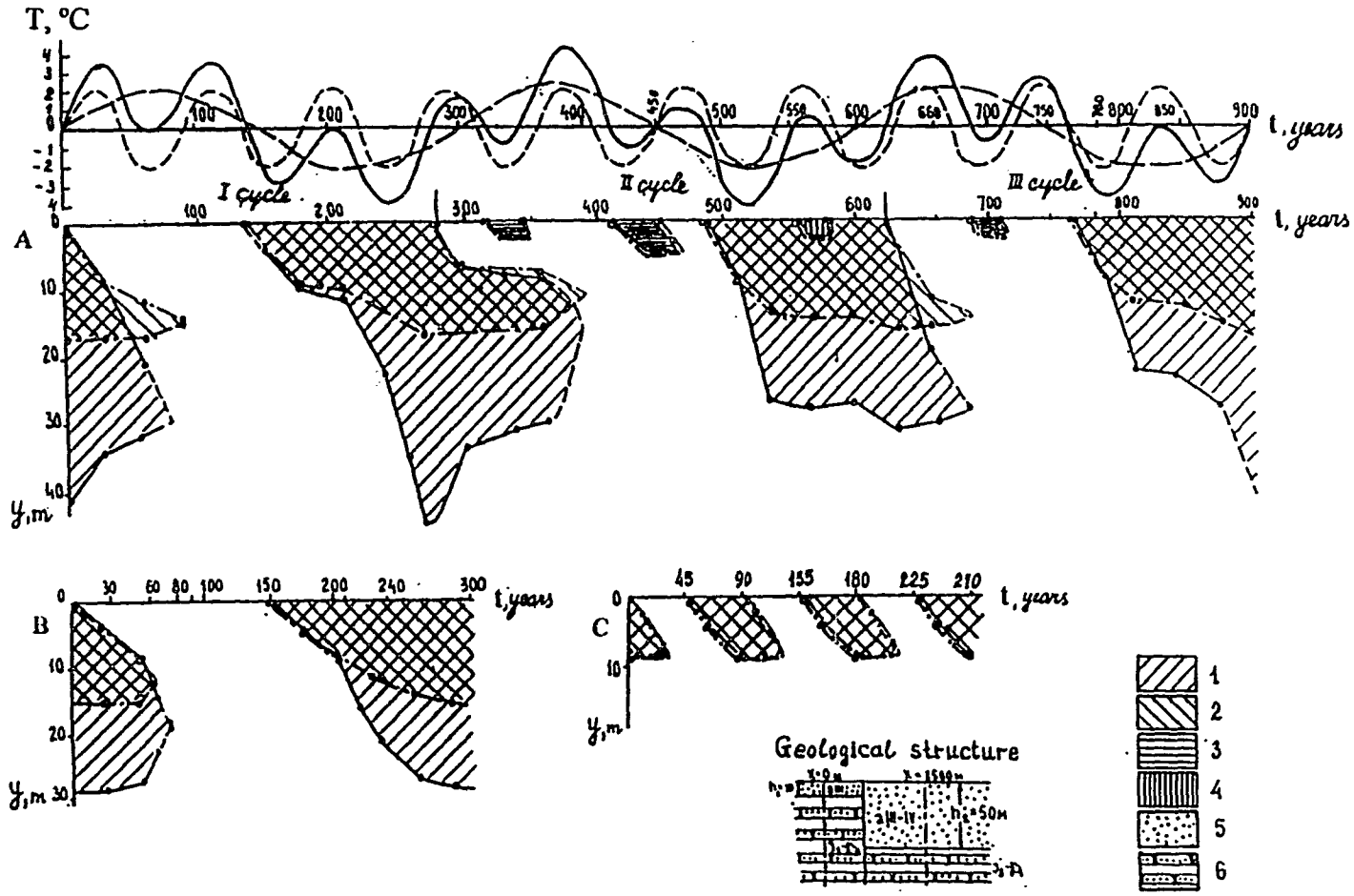

Figure 8.1 Dynamics of freezing-thawing of soils under the superposition of temperature fluctuations at the Earth's surface with 300- and 90-year periods (A) under temperature fluctuations with a 300-year period (B) under fluctuation with 90-year periods (C). The behavior of the surface temperature is shown in the upper graph. The computation results are given for two parts of the domain: 1) permafrost in the first part; 2) permafrost in the second part; 3) short-term permafrost; 4) talik, which gives discontinuous permafrost; 5) sands; 6) sandstones.

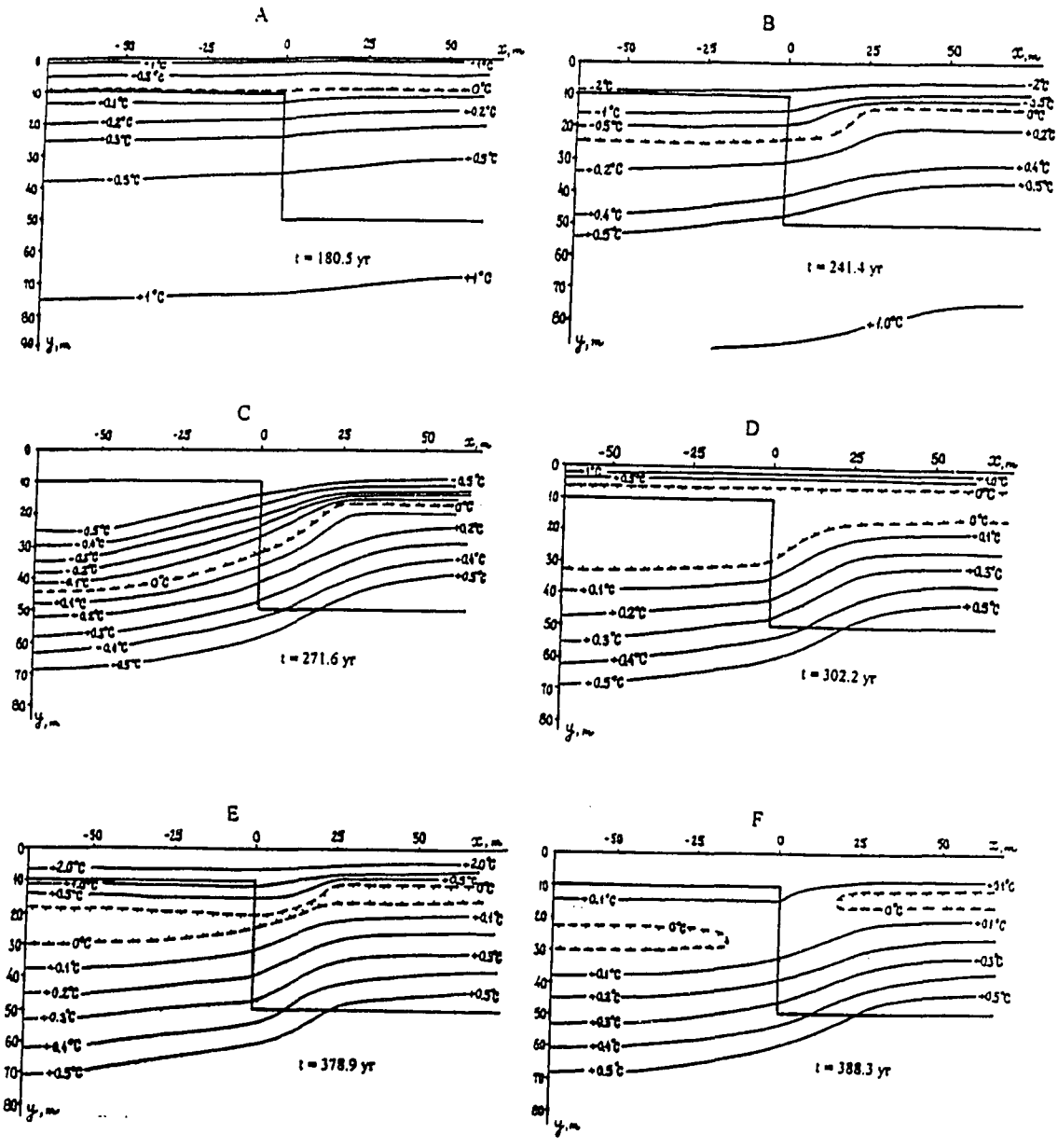

Figure 8.2 Temperature fields in an inhomogeneous rocks corresponding to different phases of variations in the ground surface temperature (see Figure 8.1)

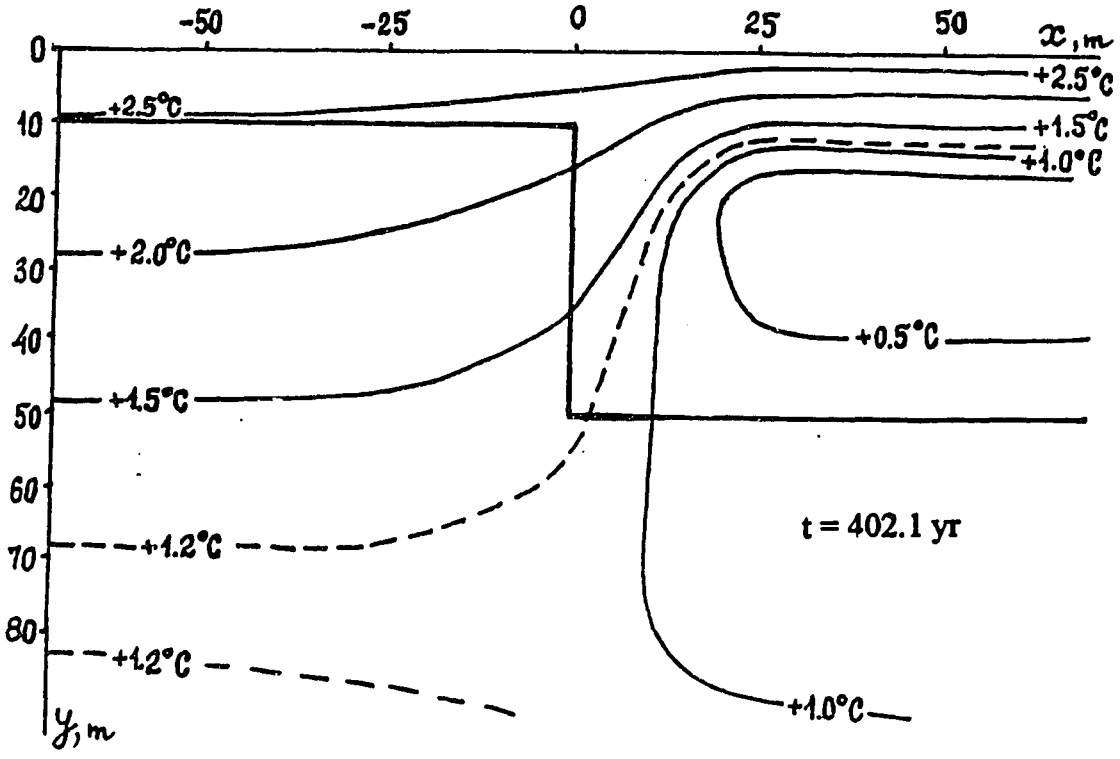

Figure 8.3 Temperature fields in an inhomogeneous rocks corresponding to final phase in the freezing-thawing cycle.

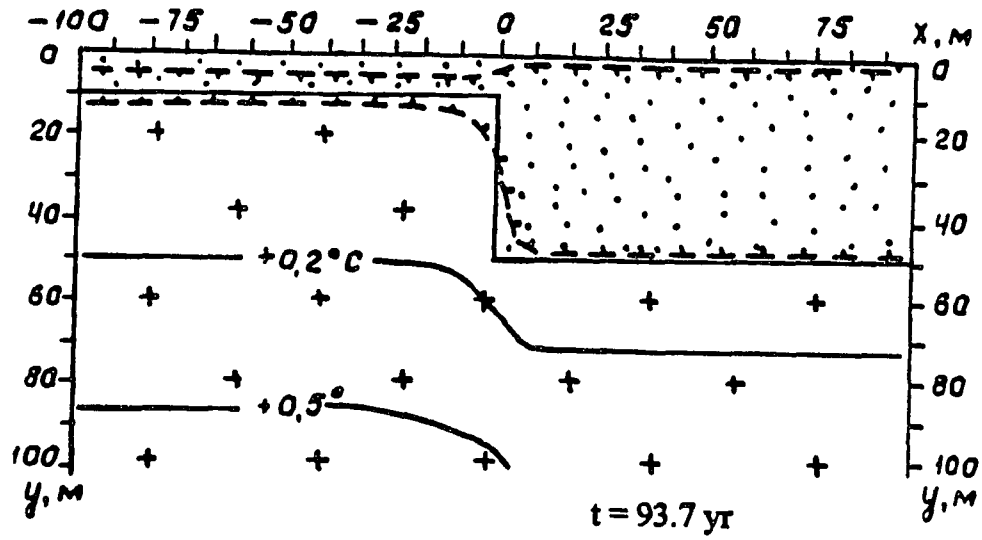

Figure 8.4 The position of the upper and lower boundaries of permafrost and isotherms in inhomogeneous rocks for a moment of time t = 93.7 years of 40000-year cycle in the temperature variations at the ground surface.

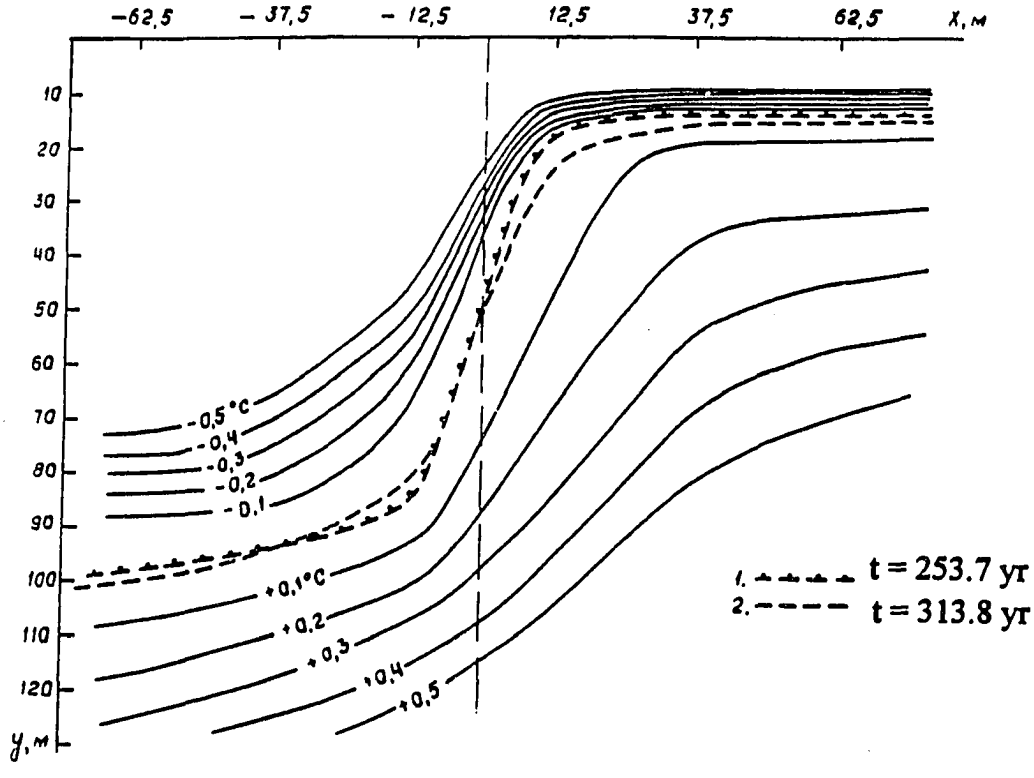

Figure 8.5 The position of the lower boundary of permafrost and configuration of the temperature field in case of inhomogeneous temperature conditions at the ground surface for t = 253.7 years (1) and for t = 313.8 years (2) of the 300-years cycle.

CHAPTER 9

Summary

This thesis presents the results of an extensive examination of the reaction of the active layer and permafrost on different time scales to climatic variations. Changes in climate were treated in these studies neither as sudden step changes from one stable conditions to another nor as permanent one-direction trends, but as a continuously changing process, which can be described in the first approximation as a superposition of a number of distinct cyclic variations with their own periods, phases and amplitudes. The periods of such variations vary from 11 years to hundreds of thousand years.

The reaction of permafrost to climatic changes was studied separately for long-term variations (Milankovich' rhythms) and for short-period fluctuations (with periods of 300 90 and 11 years). This approach allowed quantitative estimates of the amplitudes of the Milankovich' rhythms for several main regions in the Russian permafrost zone, which were not covered by the Late Pleistocene ice sheets. According to the solutions obtained, the amplitude of the 41 ka rhythm decreases from 8-9.5°C in the European North down to 2.5°C in the Far East. The amplitude of the 21 ka rhythm increases from 1°C in northern West Siberia to 1.5-2°C in the Transbaikal region. The total range of climatic variations and the time of their maximum manifestation varies accordingly. Thus, in northern West Siberia (the Ob' River basin) where the amplitude of the 41, 21, and 11 ka rhythms equals 7.2°C, 1.2°C, and 0.5°C, respectively, the total amplitude of temperature variations reaches 16°C and the Holocene thermal maximum dates around 4.5-6.5 ka ago. In the Transbaikal region, where the least difference between the 41 ka and 21 ka rhythms and 11 ka rhythm is practically lacking, the summary total amplitude of climatic variations is twice as small and the Holocene thermal maximum has the earliest dating from 10-11 to 8 ka ago. The curves obtained confirm the known facts on the rise in the amplitude of climatic changes from southeastern to northwestern Russia, as well as the

Holocene thermal maximum lagging behind in the same direction (Khotinsky, 1977). The earlier terms of the thermal maximum in East Siberia, as compared with the European North and West Siberia, can be explained by the laws governing the changes in individual rhythm amplitudes in these regions.

These curves were used as a upper boundary conditions for the numerical modeling of the permafrost dynamics during the Late Pleistocene through the Holocene. The results of modeling explained the two-layer permafrost vertical structure which is common in some regions within the Russian permafrost zone (north of the European part of Russia, north of West Siberia, intermontane depressions in the Transbaikal region and others). One of the paleoclimatic curves (for the south of East Siberia) was used with modifications for the determining permafrost dynamics in the Alaskan Arctic (Osterkamp and Gosink, 1991).

For engineering applications, it is more important to understand the dynamics of the permafrost and its temperature field at specific sites through relatively short time intervals (from ten to one hundred years). The depth of such changes may be relatively small (not more than 50-100 meters). The amplitudes of such short-term changes usually do not exceed 1-2°C, hence their influence on permafrost will be different for the areas with continuous and discontinuous permafrost.

Analyses of air, active layer and near-surface permafrost temperatures (1987 through 1992) allowed a determination of some important features of the spatial and temporal variability of the ground temperature regime and the active layer thicknesses. These measurements were made on a transect southward from Prudhoe Bay, Alaska, which included three sites; one near the coast (West Dock), one 16 km inland (Deadhorse Airport), and one 63 km inland (Franklin Bluffs).

The mean annual air temperatures (MAAT) were almost identical for all three sites: -12.6°C (West Dock), -12.9°C (Deadhorse), and -12.5°C (Franklin Bluffs). Amplitude of annual air temperature increased from the coast (17.2°C for West Dock) inland (20.8°C for Franklin Bluffs). The range of interannual variations of the MAAT was

practically the same for different sites: 3.2°C for West Dock, 2.8°C for Deadhorse, and 2.9°C for Franklin Bluffs. Mean annual ground surface and permafrost surface temperatures (MAGST and MAPST) also had large interannual variations. For the two coastal sites (West Dock and Deadhorse) the range of variations was almost the same as for MAAT (3.6°C for both West Dock and Deadhorse). For Franklin Bluffs the variations of MAGST and MAPST were only about half of MAAT (1.4°C for MAGST and 1.7°C for MAPST). Spatial gradients in MAGST and MAPST were large (about 0.1°C per km) between West Dock and Deadhorse and small between Deadhorse and Franklin Bluffs (about 0.01°C per km). Comparison of the monthly mean ground surface temperatures for Deadhorse and West Dock showed that in May, June and July these temperatures differed less than 0.2°C. The difference reached its maximum in December (6.75°C). During the rest of the winter months the difference was still large. The contribution of the four "summer" months (May-August) to the total 2.5°C MAGST difference was less than 0.1°C and can be explained by slightly warmer summer temperature at the Deadhorse site. This shows that the snow cover played the most important role in temporal and spatial variations of the ground temperatures.

The range of MAGST and MAPST provided large variability in active layer thicknesses. The mean value for the whole period of measurements increased from the coast (35.5 cm at West Dock) to inland (53 cm at Deadhorse, 62 cm at Franklin Bluffs). Interannual changes were also very significant. Active layer thicknesses range from 21 to 46 cm at West Dock, 42 to 69 cm at Deadhorse and 57 to 71.5 cm at Franklin Bluffs. Active layer thicknesses have changed systematically from 1986 to present. At the West dock site, they changed by a factor of two. Maximum thickness occurred at all sites in 1989 and our recent data indicate a broad minimum 1992 until 1994.

Since trace gas emissions from the tundra depend on the temperatures, active layer thicknesses and water table levels among other factors, then these results would seem to suggest systematic changes in the emissions. Indeed the tundra appears to have recently changed from a sink to a source of CO_2. If the observed changes in active layer

thicknesses are part of a cycle then this would imply a reversal of this result in the near future.

The same measured temperature data along with the annual temperature measurements in boreholes (60 to 70 m) during 1983-1995 at the same sites were used for the detail numerical modeling of the active layer thawing and freezing and permafrost temperature dynamics. As a preliminary step, three numerical models for the ground thermal regime calculations (Goodrich, Guymon/Hromadka, and Seregina models) based on different numerical methods and different treatment of freezing and thawing were compared with each other, with analytical solutions, and with measured temperature data, to validate these models and justify their use in our investigations.

Comparison with the Neumann solution in the case with no unfrozen water in the soils shows differences of typically less than 0.15°C between calculated temperatures, using different models and a wide variety of the length of the time and space steps. However, for the case of rapidly changing temperatures at the ground surface, the models using large time and depth steps could not accurately reproduce the temperature field dynamics in the active layer and near-surface permafrost. This means that the good agreement with Neumann solution is a necessary condition but not a sufficient one to justify the use of the models in calculations of the real temperature fields.

In the Goodrich model, time steps not longer than 1 hour and depth steps in the upper 1 m not larger than 0.02 m have to be used to reproduce the thermal regime with reasonable (within 0.3-0.4°C) accuracy. Using the Guymon/Hromadka model, the same accuracy can be obtained with 1 hour time steps and 0.1 m space steps within the upper 1 m depth or 1 day time steps and 0.01 m space steps. However, the use of larger steps does not necessarily decrease the time of calculations compared to the Goodrich model. In simulations of the real conditions at the West Dock site in 1987 with small time and space steps, the results of the calculations of the daily temperatures using both models differed by only 0.02 ^{0}C for the whole year for 18 depths from 0.02 to 0.87 m, except for one day just after freeze-up, when the difference reached 0.35°C at the depth of 0.17 m.

The RMS deviations between the results of these two models for whole year and for all depths was 0.012°C.

For the case with unfrozen water in the frozen soils, the results of calculations using a modified Goodrich and the Guymon/Hromadka models were compared with an analytical solution and found to agree within 0.02°C.

Finite element Guymon/Hromadka thermal model was applied to simulate the processes of seasonal thawing and freezing and temperature field dynamics in the active layer and near-surface permafrost. Measured temperatures at 0.02 m were used for the upper boundary conditions. The model simulates the process of thawing very well (both thawing front and temperature field). However, to obtain good agreement (0.1-0.3^{0}C) with measured data it was necessary to vary the thawed thermal conductivity of the organic soil (upper 0.15-0.3 m) within 70% of mean values each summer. The most likely cause of these variations was the average moisture content changes from summer to summer.

Significant discrepancies between measured and calculated temperatures (up to 2^{0}C and more) appeared during cooling of the active layer after freeze-up. In the model, calculated temperatures decreased sharply in two days after freeze-up and the temperature profiles became almost linear within the upper 1 m , while the measured temperatures decreased very slowly for seven to ten days or more after freeze-up and the temperature profiles kept a parabolic form with a maximum in temperature near the depth where freeze-up (closure) occurred. These large errors appear to be associated with the presence of a significant amount of unfrozen water in the cooling active layer.

To estimate the temperatures when unfrozen water becomes an important factor in the temperature field dynamics, a series of calculations were made for all sites using a model with no unfrozen water. The differences between calculated and measured temperatures became noticeable when initial temperatures at the active layer base were around -9°C for the West Dock and Deadhorse sites and -3°C for Franklin Bluffs.

The most appropriate phase composition (unfrozen water content) curves for each site and for different depths were found by trial and error (i.e. those that produced the smallest differences between calculated and measured temperature profiles). For the two sites in the Prudhoe Bay region (West Dock and Deadhorse) and for Barrow, the agreement between calculated and measured data lasted for one or two weeks and then the calculated temperatures again became too cold compared to measurements. To re-establish agreement it was necessary to modify the form of unfrozen water content curves when temperatures at the permafrost surface became colder than -6°C (West Dock and Barrow) to -7°C (Deadhorse).

Results of modeling for all four sites show that a layer with large unfrozen water content existed during the freeze-up of the active layer near the depth where freeze-up occurred. For the Deadhorse site, this layer continued from the ground surface to the depth of 0.3 m in 1987 and 0.36 m in 1991. For Franklin Bluff in 1987, for West Dock in 1988, and for Barrow in 1993 the thickness of this layer was 0.1 m in the depth intervals between 0.2 and 0.3 m at Franklin Bluff, between 0.15 and 0.25 m at West Dock, and between 0.21 and 0.31 m at Barrow. The curves of unfrozen water content as a function of temperature for this layer show unexpectedly large values of unfrozen water at low temperatures.

The presence of a large amount of unfrozen water in soils magnifies the heat fluxes into and out of ground, because the phase changes in unfrozen water occur not only within the active layer, but also in near-surface permafrost. Unfrozen water also influences the duration of the periods with enlarged heat fluxes in the seasonal cycles.

Daily temperatures during 1986-1993 for all depths from 0.72 m down to 55 m were reconstructed from the available data. The temperature profiles (1986) were used as initial conditions and the measured daily temperatures at 0.72 m were used as the upper boundary conditions and the temperature profiles (1987-1993) were used to validate the results of calculations. Mean annual temperature profiles for 1987-1992 years show significant interannual variations within the upper 30-40 m which are in good agreement

with published data (Osterkamp et al., 1994). The measured (1983-1995) data show that, for the 10 to 11 year cycle, cooling of the permafrost began prior to 1983 with the warming part of the cycle beginning in the middle 1980s. This is consistent with the U.S.G.S. data (Lachenbruch and Marshall, 1986) indicating that their reported cooling was part of a natural cycle and not primarily associated with the disturbance at the ground surface caused by drilling.

The means of the measured temperature profiles below the 20 m depth show a curvature toward warmer temperatures suggesting climatic fluctuations, a cycle or a longer-term warming trend. While these time series of permafrost temperatures are too short to distinguish between these alternatives, it is important to do so because of their possible relationship with the predicted climatic warming.

A numerical permafrost temperatures model was developed for the southern Siberia region to study the influence of short-term rhythmic climatic variations on the dynamics of permafrost. Superimposing the 300- and 90-year temperature rhythms at the ground surface lead to periodic freezing and thawing of rocks in the area near the southern limits of permafrost with a period close to 300 years. The 90-year rhythm, however, made the situation more complicated and caused the duration of the freezing-thawing cycle to deviate from 300 years. Besides, the duration of freezing and thawing periods varied from cycle to cycle. The results of modeling showed that the two-dimensional temperature field along some profiles (particularly at sites with complex geological structures) contain much more information about past permafrost dynamics than temperature profiles from single boreholes. The joint use of both the field temperature data along profiles, and numerical modeling can provide a more reasonable explanation of present permafrost structure and more accurate forecast of permafrost changes in the future.

REFERENCES CITED

Alexiades, V. and Solomon, A. D. (1993). *Mathematical Modeling of Melting and Freezing Processes*. Hemisphere Publishing Corporation, Washington (323 pp.).

Anderson, D. M., Tice, A. R., and McKim, H. L. (1973). The unfrozen water and the apparent specific heat capacity of frozen soils. In *North American Contribution, Second International Conference on Permafrost*, Yakutsk, U.S.S.R., Washington, D.C.: National Academy of Science, pp. 289-295.

Anderson, D. M., and Tice, A. R. (1973). The unfrozen interfacial phase in frozen water systems. In *Ecological Studies: Analysis and Synthesis*. New York: Springer-Verlag, vol. 4, 107-124.

Aziz, A., and Lunardini, V. J. (1992). Assessment of methods to predict the thickness of the active layer in permafrost regions. *Proceedings OMAE 1992*, Paper No. OMAE-92-209, Calgary, Canada.

Aziz, A., and Lunardini, V. J. (1993). Temperature variations in the active layer of permafrost. In *Proceedings of the Sixth International Conference on Permafrost*, Beijing, China, vol. 1, pp. 17-23.

Balobaev, V. T. (1991). *Geothermy of the frozen zone of lithosphere, Northern Asia* (in Russian). Nauka, Novosibirsk (193 pp.).

Balobaev, V. T. and Pavlov, A. V. (1983). Effects of climatic changes and anthropogenic factors on cryolithozone dynamics. In *Problemy geokriologii* (in Russian). Nauka, Moscow, pp. 184-194.

Banin, A. and Anderson, D. M. (1974). Effects of salt concentration changes during freezing on the unfrozen water content of porous materials. *Water Resources Research*, **10**(1), 124-128.

Barry, R. G., Armstrong, R. L., Krenke, A. N., and Kadomtseva, T. G. (1994). Cryospheric indices of Global Change. Final report, NSF grant SES-91-12420, *NOAA* (25 pp.).

Belova, V. A. (1985). *Vegetation and Climate of the Southeast Siberia During the Cenozoic* (in Russian), Nauka, Novosibirsk (158 pp.).

Beltrami, H. and Taylor, A. E. (1994). Records of climatic change in the Canadian Arctic: combination of geothermal and oxygen isotope data yields high resolution ground temperature histories. *EOS*, Transactions, American Geophysical Union, 75(44), p. 75.

Black, P. B. and Tice, A. R. (1988). Comparison of soil freezing curve and soil water curve data for Windsor sandy loam. *USA Cold Regions Research and Engineering Laboratory*, CRREL Report 88-16.

Bonan, G. B. (1989). Environmental factors and ecological processes controlling vegetation patterns in boreal forests. *Landscape Ecology*, **3**, 111-130.

Bonan, G. B. (1991). A biophysical surface energy budget analysis of soil temperature in the boreal forests on interior Alaska. *Water Resources Research*, 27(5), 767-781.

Bonan, G. B., Pollard, D., and Thompson, S. L. (1993). Influence of subgrid-scale heterogeneity in leaf area index, stomatal resistance, and soil moisture on grid-scale land-atmosphere interactions. *Journal of Climate*, **6**, 1882- 1897.

Braley, W. A. and Zarling, J. P. (1990). Multilayer user-friendly thermal model in 1 dimension. Report No. FNWA-AK-RD-90-02, *Alaska Department of Transportation and Public Facilities* (67 pp.).

Brown, J. (1969). Ionic concentration gradients in permafrost, Barrow, Alaska. *CRREL Research Report*, 272, U.S. Army Cold Region Research and Engineering Laboratory, Hanover, N. H. (24 pp.).

Brown, J. (1975). Ecological investigations of the tundra biome in the Prudhoe Bay region, Alaska. *Biological Papers of the University of Alaska*, Special Report No. 2, UAF (215 pp.).

Brown, J. and Johnson, P.L. (1965). *Pedo-ecological Investigations, Barrow, ALaska.* Cold Regions Research and Engineering Laboratory, CRREL Technical Report 159, Hanover, NH (32 pp.).

Brown, J., and Kreig, R. A., eds. (1983). Guidebook to permafrost and related features along the Elliott and Dalton Highways, Fox to Prudhoe Bay, Alaska. *Fourth International Conference on Permafrost*, 18 - 22 July 1983, University of Alaska, Fairbanks, Alaska Division of Geological and Geophysical Surveys (230 pp.).

Brown, J, Nelson, F., and Shur, Y. (1994). Active layer fluctuations: a multi-decade record, Barrow, Alaska, *EOS*, Transactions, American Geophysical Union, vol. 75, p.86 (abst.).

Brown, R. J. E. (1978). Influence of climate and terrain on ground temperature in the continuous permafrost zone of northern Manitoba and Keewatin district, Canada. In *Proceedings of the Third International Conference on Permafrost*, Edmonton, Canada, vol. 1, pp. 15- 21.

Burn, C. R. and Smith, C. A. S. (1988). Observations of the "thermal offset" in near-surface mean annual ground temperatures at several sites near Mayo, Yukon Territory, Canada. *Arctic*, vol. 41, No. 2, pp. 99-104.

Burn, C. R. and Smith, M. W. (1993). Issues in Canadian permafrost research. *Progress in Physical Geography* **17** (2), 156- 172.

Calkin, P. E. (1988). Holocene glaciation of Alaska (and adjoining Yukon Territory, Canada). *Quaternary Scientific Review*, 7, 159-184.

Carslaw, H. S. and Jaeger, J. C. (1959). *Conduction of heat in solids*, second edition. Oxford University Press, Ely House, London (510 pp.).

Clow, G. D., Lachenbruch, A. H. and McKay, C. P. (1991). Investigation of borehole temperature data for recent climate changes: Examples from Alaskan Arctic and Antarctica. In: *Proceedings of the International Conference on the Role of Polar Regions in Global Change*, June 11-15, 1990, Geophysical Institute, University of Alaska, Fairbanks, vol. 2, p. 533.

Clow, G. D. and Saltus, R. W. (1994). USGS program for reconstruction of climate variations in the Alaskan Arctic from borehole temperature measurements - current progress and plans. *EOS*, Transactions, American Geophysical Union, vol.75, p.85 (abst.).

Cohen, J. and Rind, D. (1991). The effect of snow cover on the climate. *Journal of Climate*, **4**, 689- 706.

Currie, R. G. (1993). Luni-solar 18.6 and solar cycle 10-11 year signals in USA air temperature records. *International Journal of Climatology*, **13**, 31-50.

Desrochers D. T. and Granberg, H. B. (1988). Schefferville snow - ground interface temperatures. In *Proceedings of the Fifth International Conference on Permafrost*, Trondheim, Norway, vol. 1, pp. 159- 164.

Dickinson, R. E., Henderson-Sellers, A., Kennedy, P. J. and Wilson, M. F. (1986). Biosphere-atmosphere transfer scheme (BATS) for the NCAR Community Climate Model. *NCAR Technical Note* NCAR/TN-275+STR (69 pp.).

Ershov, E. D., Akimov, Yu. P. and Cheverev, V. G. (1979). *Phase Composition of Moisture in the Frozen Ground* (in Russian). Moscow State University Press, Moscow.

Esch, D. C. and Osterkamp, T. E. (1990). Cold regions engineering: Climatic concerns for Alaska. *Journal of Cold Regions Engineering*, **4**(1), 6- 14.

Everett, K. R., Landforms, in Walker, D. A., Everett, K. R., Webber, P. J. and Brown, J., eds. (1980). Geobotanical atlas of the Prudhoe Bay region, Alaska. *US Army Corps of Engineers*, CRREL, Hanover, New Hampshire, CRREL Report 80-14, pp. 14-19.

Everett, K. R. (1994). Long-term active layer response to industrial disturbances at Prudhoe Bay, Alaska. *EOS*, Transactions, American Geophysical Union, vol.75, p.76 (abst.).

Everett, K. R. and Nelson, F. E. (1994). Active layer/landscape interactions: a retrospective and contemporary regional approach in Arctic Alaska. *1994 Progress Report*. NSF grant number OPP-9318528 (9 pp.).

Garagulya, L. S., Romanovsky, V. E. and Seregina, N. V. (1995). Modeling temperature fields during nonhomogeneous rock freezing and thawing. In *Russian Geocryological Research*, Russian Academy of Science, Moscow, vol. 1, pp. 34-42.

Giorgi, F. (1995). Perspectives for regional earth system modeling. *Global and Planetary Change*, **10**, 23- 42.

Giorgi, F., Marinucci, M. R., and Bates, G. T. (1993). Development of a second generation regional climate model (RegCM2). Part I: Boundary layer and radiative transfer processes. *Monthly Weather Review*, **121**, 2794- 2813.

Gold, L. W. (1967). Influence of surface conditions on ground temperature. *Canadian Journal of Earth Sciences*, **4**, 199- 208.

Goodrich, L. E. (1976). *A numerical model for assessing the influence of snow cover on the ground thermal regime*. Ph.D. Thesis, McGill University, Montreal (410 pp.).

Goodrich, L. E. (1978a). Some results of a numerical study of ground thermal regimes. In *Proceedings of the Third International Conference on Permafrost*, Ottawa, National Research Council of Canada, vol. 1, pp. 29-34.

Goodrich, L. E. (1978b). Efficient numerical technique for one-dimensional thermal problems with phase change. *International Journal of Heat and Mass Transfer*, **21**, 615-621.

Goodrich, L. E. (1982a). The influence of snow cover on the ground thermal regime. *Canadian Geotechnical Journal*, **19**, 421- 432.

Goodrich, L. E. (1982b). *An Introductory Review of Numerical Methods for Ground Thermal Regime Calculations*. DBR Paper No. 1061, Division of Building Research, National Research Council of Canada, Ottawa (33 pp.).

Gordienko, F. G., Kotlyakov, V. M., Korotkevitch, Ye. S., Barkov, N. I. and Nikolaev, S. D. (1983). New results of the isotopic oxygen investigations in the ice cores from the Vostok station to the depth 1412 m (in Russian). In *Materiali Glyaciologicheskich Issledovanii. Khronica, obsugdeniya*. Vol. 46, pp. 168-170.

Gosink, J. P., Kawasaki, K., Osterkamp, T. E., and Holty, J. (1988). Heat and moisture transport during annual freezing and thawing. In *Proceedings of the Fifth International Conference on Permafrost*, Trondheim, Norway, vol. 1, pp. 355-360.

Gosink, J. P., and T. E. Osterkamp (1990). Models for permafrost thickness variation in response to changes in paleoclimate. In *Proceedings of the Fifth Canadian Permafrost Conference* , University of Laval, Quebec, Canada, pp. 191-198.

Gravis, G. F., Moskalenko, N. G. and Pavlov, A. V. (1988). Perennial changes in natural complexes of the cryolithozone. In: *Proceedings of the Fifth International Conference on Permafrost*, Trondheim, Norway, vol. 1, pp. 165-169.

Guymon, G. L., and Hromadka, T. V. (1977). Finite element model of transient heat conduction with isothermal phase change (two and three dimensional). *Corps of Engineers, US Army*, CRREL *Special Report*, 77-38, Hanover, New Hampshire (163 pp.).

Guymon, G. L., Hromadka, T. V., and Berg, R. L. (1980). A one dimensional frost heave model based upon simulation of simultaneous heat and water flux. *Cold Regions Science and Technology*, **3**, 253 - 262.

Guymon, G. L., Hromadka, T. V., and Berg, R. L. (1984). Two-dimensional model of coupled heat and moisture transport in frost-heaving soils. *Journal of Energy Resources Technology*, **106**, 336-343.

Haeberli, W., Cheng, G., Gorbunov, A. P. and Harris, S. A. (1993). Mountain permafrost and climatic change. *Permafrost and Periglacial Processes*, **4**: 165-174.

Harris, S. A. (1990). Long - term air and ground temperature records from the Canadian Cordillera and the probable effects of moisture changes. In *Proceedings of the Fifth Canadian Permafrost Conference*, Laval University, Quebec, Canada, pp. 151- 157.

Haugen, R. K. (1982). *Climate of remote areas in north-central Alaska, 1975-1979 summary*. CRREL Report 82-35.

Hewitson, B. (1994). Regional climates in the GISS general circulation model: surface air temperature. *Journal of Climate*, **7**, 283- 303.

Hewitson, B. and Crane, R. G. (1992). Regional climates in the GISS global circulation model: synoptic-scale circulation. *Journal of Climate*, **5**, 1002-1011.

Hinkel, K. M., Outcalt, S. I. and Nelson, F. E. (1990). Temperature variation and apparent thermal diffusivity in the refreezing active layer, Toolik Lake, Alaska. *Permafrost and Periglacial Processes*, **1**: 265-274.

Hinkel, K. M. and Outcalt, S. I. (1994). Identification of heat-transfer processes during soil cooling, freezing, and thaw in Central Alaska. *Permafrost and Periglacial Processes*, **5**, 217-235.

Hinkel, K. M. and Nicholas, J. R. J. (1995). Active layer thaw rate at a boreal forest site in Central Alaska, U.S.A. *Arctic and Alpine Research*, **27**(1), 72-80.

Hinzman, L. D., Kane, D. L., Gieck, R. E. and Everett K. R. (1991). Hydrologic and t hermal properties of the active layer in the Alaskan Arctic. *Cold Region Science and Technology*, *19*, 95 - 110.

Hinzman, L. D., Kane, D. L. and Everett, K. R. (1993). Hillslope hydrology in arctic setting. In *Proceedings of the Sixth International Conference on Permafrost*, Beijing, China, vol. 1, pp. 267-271.

Hoffman, P. A. and Osterkamp, T. E. (1986). Bar graphs of climatological data for Alaskan stations: Temperature, snowfall, and thawing and freezing degree days for 1949-1982. Contract Rept. 84 NX 203 F 23181, *ADOPFT*, Fairbanks, AK.

Hromadka, T. V., Guymon, G. L., and Berg, R. L. (1981). Some approaches to modeling phase change in freezing soil. *Cold Regions Science and Technology*, 4, 137 - 140.

Hubrechts, Ph., de Nooze, P. and Decleir, H. (1989). Numerical modeling of glacier d'Argentiere and its historic front variations. In J. Oerlemans (ed.), *Glacier fluctuations and climatic change*, by Kluwer Academic Publishers, pp. 373-389.

Imbrie, J. and Imbrie, K. P. (1986). *Ice ages*. Harvard University Press, Cambridge, Massachusetts and London, England (224 pp.).

Judge, A. S. (1975). *Geothermal studies in the Mackenzie valley by the Earth Physics Branch*. Geothermal Service of Canada, Earth Physics Branch, Energy, Mines and Resources, Canada, Geothermal Series No. 2 (12 pp.).

Kane, D. L., Hinzman, L. D. and Zarling, J. P. (1991). Thermal response of the active layer to climatic warming in a permafrost environment. *Cold Regions Science and Technology*, **19**, 110.

Kawasaki, K., Osterkamp, T. E., and Gosink, J. P. (1982). A preliminary evaluation of numerical models suitable for thermal analysis of roadways and airstrips, Report No. AK-RD-82-22, State of Alaska, Dept. of Transportation and Public Facilities.

Kazantsev, V.V. (1994). Is the thermal regime of permafrost determined by solar rhythms? *Cold Regions Science and Technology*, **23**, 93 - 98.

Khotinsky, N. A. (1977). *The Holocene of the Northern Eurasia* (in Russian). Nauka, Moscow (197 pp.).

Kolchugina, T. P. and Vinson, T. S. (1993). Climate warming and the carbon cycle in the permafrost zone of the former Soviet Union. *Permafrost and Periglacial Processes*, **4**, 149- 163.

Kovalenko, V. D., Kizim, L. D., Pashestyuk, A. M. and Nikolaev, V. G. (1987). Study of causes of climatic variability . In *Agroclimatic Resources of Siberia* (in Russian). VASKHNIL SO AN SSSR, Novosibirsk, pp. 103-113.

Kudryavtsev, V. A., Garagula, L. S., Kondrat'yeva, K. A. and Melamed V. G. (1974). *Osnovy merzlotnogo prognoza* (in Russian). MGU (431 pp.) [CRREL Translation: V. A. Kudryavtsev et al., *Fundamentals of Frost Forecasting in Geological Engineering Investigations*, CRREL Draft Translation 606, 1977, 489 pp.]

Kudryavtsev, V. A., Dostovalov, B. N., Romanovsky, N. N., Kondrat'yeva, K. A. and Melamed V. G. (1978). *Geocryology*(in Russian). Moscow University Press (464 pp.).

Kudryavtsev, V. A. (editor) (1981). *Permafrost (short edition)* (in Russian). MSU Press (240 pp.).

Lachenbruch, A. H. (1959). *Periodic heat flow in a stratified medium with application to permafrost problems*, US Geol. Surv. Bull., 1083-A.

Lachenbruch, A. H. (1994). *Permafrost, the active layer, and changing climate*. U. S. Geological Survey, Open-File Report 94-694 (43 pp.).

Lachenbruch, A. H., Sass, J. H., Marshall, B. V., and Moses, T. H. (1982). Permafrost, heat flow and the geothermal regime at Prudhoe Bay, Alaska. *Journal of Geophysical Research*, 87, (B11), 9301-9316.

Lachenbruch, A. H. and Marshall, B. V. (1986). Changing climate: Geothermal evidence from permafrost in the Alaskan Arctic. *Science*, **234**, 689- 696.

Lachenbruch, A. H., Cladouhos, T. T. and Saltus, R. W. (1988). Permafrost temperature and the changing climate. In: *Proceedings of the Fifth International Conference on Permafrost*, Trondheim, Norway, vol. 3, pp. 9-17.

Lovell, C. W. (1957). Temperature effects on phase composition and strength of partially-frozen soil. In *Highway Research Board Bulletin*, 168, pp. 74-95.

Lukyanov, V. S. and Golovko, M. D. (1957). *Calculations of the Active Layer Thickness* (in Russian). Transgeldorizdat, Moscow.

Luthin, J. N. and Guymon, G. L. (1974). Soil moisture-vegetation-temperature relationships in central Alaska. *Journal of Hydrology*, **23**, 233-46.

Lynch, A. H., Chapman, W., Walsh, J. E., and Weller, G. (1995). Development of a regional climate model of the Western Arctic. *Journal of Climate*, Vol. 8, No. 6, pp. 1555-1570.

Majorowicz, J. A. and Judge, A. (1994). Climate induced ground warming at the southern margins of permafrost. *EOS*, Transactions, American Geophysical Union, 75(44), p. 84.

Manabe, S. and Wetherald, R. T. (1975). The effects of doubling the CO_2 concentration on the climate of a general circulation model. *Journal of Atmospheric Science*, 32: 3-15.

Marshall, S., Roads, J. O., and Glatzmaier, G. (1994). Snow Hydrology in a General Circulation Model. *Journal of Climate*, 7, 1251- 1269.

Marshall, S. and Oglesby, R. J. (1994). An improved snow hydrology for GCMs. Part 1: snow cover fraction, albedo, grain size, and age. *Climate Dynamics*, **10**: 21-37.

Maximov, Ye. V. (1972). *The Problem of the Earth Glaciations and Rhythms in Nature* (in Russian). Nauka, Leningrad (296 pp.).

Maximova , L. N. and Romanovsky, V. E. (1985). Climatic changes and some features of the permafrost dynamics during the Holocene within the territory of the USSR. In *Geokriologicheskie issledovaniya* (in Russian). Moscow State University Press, Moscow, pp. 45-57.

Maximova, L. N. and Romanovsky, V. E. (1986). Climatic changes and some features of the permafrost dynamics during the Holocene within the territory of the USSR (in Russian). In *Geokriologicheskie issledovaniya*. Moscow State University Press, Moscow, pp. 45-57.

Maximova, L. N. and Romanovsky, V. E. (1988). A hypothesis of the Holocene permafrost evolution. In *Proceedings of the Fifth International Conference on Permafrost*, Trondheim, Norway, vol. 2, pp. 102-106.

McGaw, R. W., Outcalt, S. I. and Ng, E. (1978). Thermal properties and regime of wet tundra soils at Barrow, Alaska. *In Proceedings of the Third International Conference on Permafrost*, Edmonton, Canada, vol. 1, pp. 48- 53.

Melamed, V. G. (1980). *Heat and Mass Exchange in Soils With the Latent Heat of Phase Changes* (in Russian). Nauka, Moscow (228 pp.).

Meyermanov, A. M. (1986). *Stefan Problem* (in Russian). Nauka, Novosibirsk (239 pp.).

Moiseenko, B. D. and Samarsky, A. A. (1965). An economical scheme of through calculation for a multi-dimensional Stefan's problem (in Russian). *Vichislitelnaya Mathematica i Mathematicheskaya Phisika*, vol. 5, No. 5, pp. 816-827.

Muller, S. W. (1947). *Permafrost or Permanently Frozen Ground and Related Engineering Problems*. J. W. Edwards, Ann Arbor, Mich. (231 pp.).

Nakano, Y. and Brown, J. (1971). Effect of a freezing zone of finite width on the thermal regime of soils. *Water Resources Research*, 7(5), 1226-1233.

Nakano, Y. and Brown, J. (1972). Mathematical modeling and validation of the thermal regimes in tundra soils, Barrow, Alaska. *Arctic and Alpine Research*, 4(1), 19-38.

Nelson, F. E., Outcalt, S. I., Hinkel, K. M., Murray, D. F. and Murray, B. M. (1988). Microtopographic thermal contrasts, northern Alaska. *In Proceedings of the Fifth International Conference on Permafrost*, Trondheim, Norway, vol. 1, pp. 819-823.

Nelson, F. E., Lachenbruch, A. H., Woo, M. K., Koster, E. A., Osterkamp, T. E., Gavrilova, M. K. and Chang, G. O. (1993). Permafrost and changing climate. In *Proceedings of the Sixth International Conference on Permafrost*, Beijing, China, vol. 2, pp. 987- 1005.

Nersesova, Z. A. and Tutunov, I. A. (1957). Physical and chemical processes in the frozen ground (in Russian). In *Materials of the Laboratory Investigations of the Frozen Ground*, Academy of Science of the U.S.S.R., Moscow.

Nicholson, F. H. and Granberg, H. B. (1973). Permafrost and snow cover relationships near Schefferville. *In Proceedings of the Second International Conference on Permafrost*, Yakutsk, USSR, North American Contribution, Washington DC: National Academy of Science, pp. 151-158.

Nicholson, F. H. (1978). Permafrost modification by changing the natural energy budget. In *Proceedings of the Third International Conference on Permafrost*, Edmonton, Canada, vol. 1, pp. 61 - 67.

Oechel, W. C., Hastings, S. J., Vourlitis, G., Jenkins, M., Riechers, G. and Grulke, N. (1993). Recent change of Arctic tundra ecosystems from a net carbon dioxide sink to a source. *Nature*, vol. 361, pp. 520-523.

Oechel, W. C. and Vourlitis, G. L. (1994). The effect of climate change on land-atmosphere feedbacks in arctic tundra regions. *Tree*, vol. 9, no. 9, pp. 324-329.

Osterkamp, T. E. (1982). Potential impact of a warmer climate on permafrost in Alaska. In *Proceedings of the Conference on the Potential Effects of Carbon Dioxide - Induced Climatic Changes in Alaska*, Miscellaneous Publication 83-1, SALRM, University of Alaska, Fairbanks, Alaska, pp. 106-113.

Osterkamp, T. E. (1985). *Temperature measurements in permafrost*. Report FHWA-AK-RD-85-11, Alaska DOTPF, Fairbanks, AK (87 pp.).

Osterkamp, T. E. (1987). Freezing and thawing of soils and permafrost containing unfrozen water or brine. *Water Resources Research*, 23(12), 2279-2285.

Osterkamp, T. E. (1994). Evidence for warming and thawing of discontinuous permafrost in Alaska. *EOS*, Transactions, American Geophysical Union, 75(44), p. 85.

Osterkamp, T. E. and Lachenbruch, A. H. (1990).Thermal regime of permafrost in Alaska and predicted global warming. *Journal of Cold Regions Engineering*, 4(1), 38-42 .

Osterkamp, T. E., Zhang, T., Fei, T. and Gosink, J. P. (1990). Permafrost temperatures in shallow boreholes along a north-south transect of Alaska, *EOS*, Transactions, American Geophysical Union, vol. 71(43), p.1603 (abst.).

Osterkamp, T. E., and J. P. Gosink (1991). Variations in permafrost thickness in response to changes in paleoclimate. *Journal of Geophysical Research*, 94(B3), 4423-4434.

Osterkamp, T. E., Zhang, T. and Romanovsky, V. E. (1994). Evidence for a cyclic variation of permafrost temperatures in northern Alaska. *Permafrost and Periglacial Processes*, 5, 137-144.

Osterkamp, T. E. and Romanovsky, V. E. (1996). Characteristics of Changing Permafrost Temperatures in the Alaskan Arctic, U.S.A. *Arctic and Alpine Research* (in press).

Osterkamp, T. E. and Romanovsky, V. E. (unpublished). Freeze-up of the Active Layer on the Coastal Plain in the Alaskan Arctic. *Permafrost and Periglacial Processes.*

Outcalt, S. I., Nelson, F. E., and Hinkel, K. M. (1990). The zero-curtain effect: heat and mass transfer across an isothermal region in freezing soil. *Water Resources Research*, 26(7), 1509-1516.

Pavlov, A. V. (1976). *Heat transfer of the soil and atmosphere at northern and temporal latitudes*. CRREL draft translation 511, Hanover, NH: Cold Regions Research and Engineering Laboratory (298 pp.).

Pavlov, A. V. (1980). *Calculation and regulation of the soil freezing regime* (in Russian). Nauka, Novosibirsk (240 pp.).

Pavlov, A. V. (1994). Current changes of climate and permafrost in the Arctic and Sub-Arctic of Russia. *Permafrost and Periglacial Processes*, 5: 101-110.

Pollard, D. and Thompson, S. L. (1995). Use of a land-surface-transfer scheme (LSX) in a global climate model: the response to doubling stomatal resistance. *Global and Planetary Change*, 10, 129- 161.

Porkhaev, G. V. (1970). *The Thermal Interaction Between Buildings and Engineering Constructions and Permafrost* (in Russian). Nauka, Moscow (208 pp.).

Rawlinson, S. E. (editor) (1983). Guidebook to permafrost and related features, Prudhoe Bay, Alaska. *Fourth International Conference on Permafrost*, 18-22 July 1983, University of Alaska, Fairbanks (177 pp.).

Roman, L. T. and Konovalov, A. A. (1984). Thermal properties of the peaty soils and peat. In E. D. Ershov (editor) *Thermal Properties of the Earth Materials* (in Russian). Moscow State University Press, Moscow, pp. 128-136.

Romanovsky, V. E. (1987). Approximate calculation of the insulation effect of the snow cover. In *Geokriologicheskie Issledovania* (in Russian), MGU Press, vol. 23, pp. 145- 157.

Romanovsky, V. E. (1989). A method for calculation of the thermal offset within the stratiform active layer. In *Geokriologicheskie Issledovanija* (in Russian), MSU Press, vol. 24, pp. 237-243.

Romanovsky, V. E., Maximova, L. N. and Seregina, N. V.(1991a). Paleotemperature Reconstruction for Freeze-Thaw Processes During the Late Pleistocene Through the Holocene. In *Proceedings of the International Conference on the Role of Polar Regions in Global Change*, June 11-15, 1990, Geophysical Institute, University of Alaska, Fairbanks, vol. 2, pp. 537-542.

Romanovsky, V. E., Garagula, L. S. and Seregina N. V. (1991b). Freezing and Thawing of Soils Under the Influence of 300- and 90-Year Periods of Temperature Fluctuation. In *Proceedings of the International Conference on the Role of Polar Regions in Global Change*, University of Alaska, Fairbanks, vol. 2, pp. 543-548.

Romanovsky, V. E. and Maximova, L. N. (1991). *Analysis of the time sequences in the temperature variations at the ground and permafrost surfaces to discover periodical components* (in Russian). Final Report 3.1.4.-5, to the Program No. 18 "Global Change of the Environment and Climate" of the State Science and Technology Committee of the USSR, Moscow (48 pp.).

Romanovsky, V. E. and Osterkamp, T. E. (1994). Temporal and spatial behavior of the active layer in the northern Alaska: 1986-1993. *EOS*, Transactions, American Geophysical Union, vol.75, p.86 (abst.).

Romanovsky, V. E. and Osterkamp, T. E. (1995a). Interannual variations of the thermal regime of the active layer and near-surface permafrost in Northern Alaska. *Permafrost and Periglacial Processes*, **6**(4) , 313-335.

Romanovsky, V. E. and Osterkamp, T. E. (1995b). Modeling of the permafrost temperature dynamics and active layer thawing and freezing at Prudhoe Bay, Alaska. *EOS*, Transactions, American Geophysical Union, 76(46), 237-238 (abst.).

Romanovsky, V. E. and Osterkamp, T. E. (1996). Thawing of the active layer on the coastal plain of the Alaskan Arctic. *Permafrost and Periglacial Processes* (submitted).

Rouse, W. R. (1984). Microclimate of Arctic tree line. 2. Soil microclimate of tundra and forest. *Water Resources* Research, **20**, 67-73.

Rozanov, M. I. (1987). Parameters of annual tree rings as informational basis for long-term prediction of bioecological resources. In *Agroclimatic Resources of Siberia* (in Russian). VASKHNIL SO AN SSSR, Novosibirsk, pp. 80-102.

Safanda, J., Cermak, C., Pollack, H. N. and Chapman, D. S. (1994). Past millennium climate trend inferred from borehole temperatures: examples from central Europe and Russia. *EOS*, Transactions, American Geophysical Union, 75(44), p. 76.

Selkregg, L. L. (1975). *Alaska regional profiles: Arctic region.* Anchorage, University of Alaska, Arctic Environmental Information and Data Center, vol. 2 (218 pp.).

Seregina, N. V. (1989). Some of the mathematical models used in Geocryology and methods of their numerical solution (in Russian). In *Geocryological Investigations*. Moscow State University Press, Moscow, pp. 243-246.

Sergin, S. Ya. (1975). The ground surface temperatures during the coldest and warmest periods of the late Quaternary time (in Russian). In *Izvestiya AN SSSR, ser. geogr.*, 3, pp. 37-48.

Shnitnikov, A. V. (1957). *Variability of the General Humidity of the Northern Hemisphere Mainlands* (in Russian). AN SSSR Press, Moscow-Leningrad (337 pp.).

Shur, Iu. L. (1988). *Upper horizon of permafrost and thermokarst* (in Russian). Nauka, Novosibirsk (214 pp.).

Shur, Iu. L., Nelson, F. E., Brown, J., and Hinkel, K. M. (1995). Active layer freezeback at Barrow, Alaska. *EOS*, Transactions, American Geophysical Union, 76(46), 244.

Smirnova, N. N. and Artushina, V. I. (1984). Thermal conductivity of soils as a function of their moisture content and density. In E. D. Ershov (editor) *Thermal Properties of the Earth Materials* (in Russian). Moscow State University Press, Moscow, p. 87-93.

Smith, M. W. (1975). Microclimatic influences on ground temperatures and permafrost distribution, Mackenzie Delta, Northwest Territories. *Canadian Journal of Earth Sciences*, 12 (1), 421-438.

Smith, M. W. (1976). *Permafrost in the Mackenzie delta, Northwest Territories.* Geological Survey of Canada, Paper 75 - 28.

Smith, M. W. (1993). Climatic change and permafrost. *In Canada's Cold Environments* (edited by H. M. French and O. Slaymaker), pp. 290-311.

Smith, M. W. and Riseborough, D. W. (1983). Permafrost sensitivity to climate change. In *Proceedings of the Fourth International Conference on Permafrost*, Fairbanks, Alaska, pp. 1178- 83.

Sturm, M. and Holmgren, J. (1994). Effects of microtopography on texture, temperature and heat flow in Arctic and Sub-Arctic snow. *Annals of Glaciology*, 19, 63- 68.

Sumgin, M. I., Kachurin, S. P., Tolstikhin, N. I., and Tumel', V. F. (1940). *General Geocryology* (in Russian). Academy of Science of the USSR, Moscow (240 pp.).

Tice, A. R., Burrous, C. M., and Anderson, D. M. (1978). Determination of unfrozen water in frozen soil by pulsed nuclear magnetic resonance. In *Proceedings of the Third International Conference on Permafrost, Edmonton, Alberta, Canada*, National Research Council of Canada, vol. 1, pp. 149-155.

Tice, A. R., Black, P. B., and Berg, R. L. (1988). Unfrozen water contents of undisturbed and remolded Alaskan silt as determined by nuclear magnetic resonance. *USA Cold Regions Research and Engineering Laboratory*, CRREL Report 88-19 (17 pp.).

Tikhonov, A. N. and Samarsky, A. A. (1966). *Mathematical Physics* (in Russian). Nauka, Moscow (367 pp.).

Tipenko, G. S. (1987). Analytical methods to solve the heat exchange problems in geocryology. In L. S. Garagula (editor) *The Usage of Mathematical Methods in Geocryology* (in Russian), Moscow State University Press, Moscow, pp. 38-79.

Tsytovich, N. A. (1973). *Mechanics of the Frozen Ground* (in Russian). Vischaya Shkola, Moscow.

Uspensky, A. V. (red.) (1975). *Methods of Solution of Boundary and Reverse Problems of Heat Conductivity* (in Russian). Moscow State University Press, Moscow (151 pp.).

Verseghy, D. L. (1991). Class - a Canadian land surface scheme for GCMs. I. Soil model. *International Journal of Climatology*, **11**, 111- 133.

Verseghy, D. L., McFarlane, N. A., and Lazare, M. (1993). Class - a Canadian land surface scheme for GCMs, II. Vegetation model and coupled runs. *International Journal of Climatology*, **13**, 347- 370.

Waelboeck, C. (1993). Climate-soil processes in the presence of permafrost: a systems modelling approach. *Ecological Modelling*, **69**, 185-225.

Wang, B. and French, H. M. (1994). Climate controls and high-altitude permafrost, Qinghai-Xizang (Tibet) Plateau, China. *Permafrost and Periglacial Processes*, **5**: 87-100.

Washburn, A. L. (1980). *Geocryology*. John Wiley and Sons, NY (406 pp.).

Yendrikhinsky, A. S. (1982). Main geological events in the southern Siberia during the late Pleistocene through Holocene (in Russian). In *Pozdniy pleistotsen i golotsen yuga Vostochnoi Sibiri*. Nauka, Novosibirsk, pp. 6-35.

Zamana, L. V. (1980). Relic permafrost layers in the northern parts of the Baikal rift zone depressions (in Russian). In *Geokriologicheskie usloviya zony BAM*. Permafrost Institute Press, Yakutsk, pp. 31-37.

Zarling, J. P. (1987). Approximate solution to the Neumann problem. *1987 International Symposium on Cold Region Heat Transfer*. New York: American Society of Mechanical Engineering, pp. 47- 57.

Zhang, T. (1993). *Climate, seasonal snow cover and permafrost temperatures in Alaska north of the Brooks range*. Ph.D. Thesis, University of Alaska, Fairbanks (232 pp.).

Zhang, T. and Osterkamp, T. E. (1993a). Climate and permafrost temperatures in Alaska north of the Brooks Range. *EOS*, Transactions, American Geophysical Union, vol. 74(16), p. 89 (abst.).

Zhang, T. and Osterkamp, T. E. (1993b). Changing climate and permafrost temperatures in the Alaskan Arctic. *In Proceedings of the Sixth International Conference on Permafrost*, Beijing, China, vol. 1, pp. 783-788.

Zhang, T., Osterkamp, T. E. and Stamnes, K. (submitted). Influence of the depth hoar layer of the seasonal snow cover on the ground thermal regime. *Water Resources Research*.

Zubakov, V. A. (1986). *The Global Climatic Events During the Pleistocene* (in Russian). Gidrometeoizdat, Leningrad (286 pp.).